Supercritical carbon dioxide spray drying for the production of stable dried protein formulations

Nuchuchua, O.

Cover Page

Universiteit Leiden

The handle http://hdl.handle.net/1887/46172 holds various files of this Leiden University dissertation.

Author: Nuchuchua, O.
Title: Supercritical carbon dioxide spray drying for the production of stable dried protein formulations
Issue Date: 2017-02-23

Supercritical carbon dioxide spray drying
for the production of stable dried protein formulations

Onanong Nuchuchua

อรอนงค์ หนูชูเชื้อ

Supercritical carbon dioxide spray drying
for the production of stable dried protein formulations

Proefschrift

Ter verkrijging van

de graad van Doctor aan de Universiteit Leiden,

op gezag van Rector Magnificus Prof. Mr. C.J.J.M. Stolker,

volgens besluit van het College voor Promoties

te verdedigen op donderdag 23 Februari 2017

klokke 15:00 uur

door

Onanong Nuchuchua

Geboren te Bangkok (Thailand)

in 1982

Table of Contents

CHAPTER 1

General introduction

1. Protein dehydration

Therapeutic proteins and vaccines prepared in a liquid dosage form may be sensitive to stress, often undergoing physical and chemical degradation, such as deamidation, oxidation and aggregation in response to pH, temperature, agitation and surface adsorption [1, 2]. This instability of liquid protein formulations may negatively impact the safety and efficacy upon administration. In contrast, a dried protein is generally more stable because of the lack of water for reactant mobilization [2]. Thus, protein dehydration is a means for developing stable protein/vaccine formulations with prolonged shelf-life, as compared to liquid protein formulations.

The most commonly used protein drying methods are lyophilization and spray-drying [3, 4]. For lyophilization, protein formulations are frozen and the water is removed by sublimation at low pressure [4]. In the case of conventional spray-drying, a protein solution is atomized via a nozzle, and dried using heated air in a spraying tower [5]. In order to maintain the desired stability, and correspondingly the protein activity, the residual water content in dried protein formulations should generally be no more than 3% (w/w). Lyophilization and spray-drying methods are used to prepare commercially available pharmaceuticals and biologics, such as peptides [6], hormones [7-9], enzymes [10], blood plasma [11], DNA [12], inactivated viruses in vaccines [13, 14] and proteins [15-17]. However, both processes are not without their limitations; lyophilization is costly and time consuming, and the freezing and drying steps can lead to the denaturation and aggregation of proteins [18], while the combination or individual effect of heat and the air/water interface in conventional hot air spray-drying method may destabilize proteins [19-21].

An alternative to these drying methods is to use supercritical carbon dioxide (scCO$_2$), where high pressure CO$_2$ is used as the drying medium. CO$_2$ is non-toxic, non-flammable, inexpensive, readily available and recyclable [22], and is a supercritical fluid above 75.8 bar and 31.5 °C (Fig. 1). It is possible to tune the density, and thus the solvent power, of the scCO$_2$ by changing pressure and temperature [23]. It has previously been shown that scCO$_2$ spray drying can be used to prepare proteins powders from formulations containing immunoglobulin G, insulin, lysozyme, or myoglobin [24, 25]. One of the major benefits of drying processes with scCO$_2$ is that the dehydration can be carried out at ambient temperature, thereby avoiding the thermal denaturation of protein. In this thesis, spraying a protein formulation into scCO$_2$ has been investigated as a protein dehydration process.
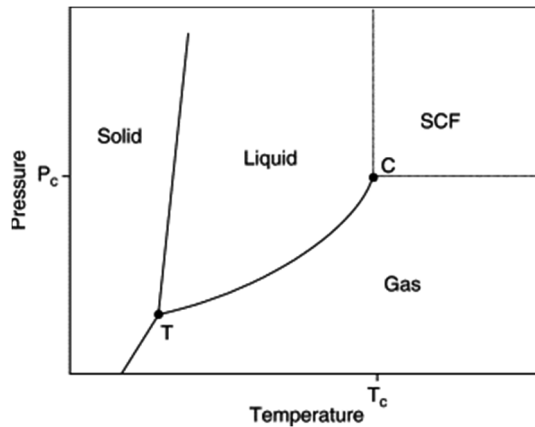
Fig. 1   Phase diagram, as a function of pressure (P) and temperature (T), of a substance that can occur as a supercritical fluid (SCF). Supercritical CO_2 occurs above the critical point (C), i.e., where pressure and temperature are ≥ 75.8 bar and ≥ 31.5 °C. The picture is taken from Nalawade et al. [38].

2.   Supercritical carbon dioxide spray drying methods for proteins

With the supercritical CO_2 spray drying process, a protein formulation filled in a high pressure syringe pump is atomized by the CO_2 via a nozzle at a constant flow rate into a drying vessel filled with $scCO_2$ [26] (as shown in Fig. 2). The water removal from the atomized droplets is carried out in the vessel by mass transfer between water and CO_2 phases at a constant operating pressure and temperature. The atomization process influences the rate of water evaporation upon drying and the particle size of the resulting protein powder. For a batch process, the dried protein products are collected on a filter after the depressurization of the vessel. Powdered products of model proteins such as lysozyme [27], myoglobin [28] and immunoglobulin G [28] have already been prepared in order to evaluate the dehydration method by the $scCO_2$ spray drying process. However, in some cases, the $scCO_2$ spray drying could destabilize proteins or induce the formation of aggregates.

As the solubility of water is low in $scCO_2$, modifiers (such as dimethyl sulfoxide (DMSO) [29], DMFA [28], ethanol [28], methanol [30], ethyl acetate [28], dichloromethane (DCM) and 1,1,1,3,3,3-hexafluoro-2-propanol (HFIP) [31]) have been added to the $scCO_2$ to enhance the drying kinetics. In a previous drying study, ethanol was used to enhance the solubility of water in $scCO_2$ when spray drying protein-trehalose

formulations. However, residual ethanol was found in the resultant CO_2-dried powder, which may lead to destabilization of the proteins, as detected by changes in protein structure and an increase in aggregate formation [32]. To eliminate the ethanol, a secondary drying step, such as vacuum drying, was required [33]. For these reasons, the use of organic solvents in CO_2 spray drying is not desired.
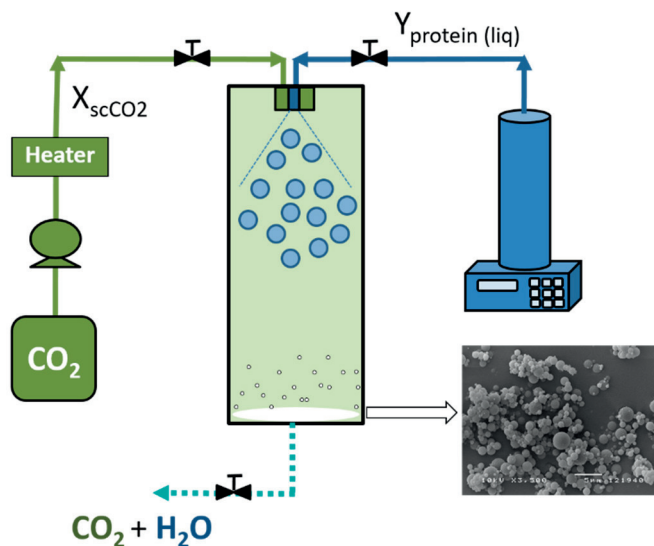
Fig. 2 Schematic set-up of the CO_2 spray dryers used in this study. P and T are the abbreviations of pressure and temperature, while X_{scCO2} and $Y_{protein(liq)}$ indicate the flows of scCO$_2$ and liquid protein formulation.

3. The challenge of supercritical drying methods and the choice of excipients on protein integrity

In contrast with numerous studies about harmful effects of lyophilization and conventional spray drying on protein structure [34-36], there is only limited information available in the public domain about the effects of scCO$_2$ drying methods on the stability of proteins, both during processing and storage. Since the drying process using scCO$_2$ fundamentally differs from freeze-drying and spray drying, the detrimental effects on protein integrity may also be different. The main factors of scCO$_2$ drying, such as pressure, temperature, atomization,

acidification, flow rates of carbon dioxide or protein solution, may affect the stability of proteins.

From previous studies, it has been observed that $scCO_2$ drying affects the structure and bioactivity of excipient-free protein formulations [32, 33]. Upon reconstitution of the dried products, the bioactivities of lysozyme [37] and lactate dehydrogenase [37] had decreased as compared to their original solutions. Moreover, changes in the protein structures were found, with one study showing a decrease in the α-helix content or an increase in the β-sheet structure of lysozyme [29]. For $scCO_2$ spray dried myoglobin (with or without a sugar excipient), no changes in the secondary structure were observed after the drying process, although there was a decrease in the heme-myoglobin interaction as well as the formation of insoluble myoglobin residues [26]. In this case, adding a sugar excipient helped stabilizing the protein [26].

When freeze-drying proteins, formulation excipients (e.g., buffer, sugar and surfactant) are often used to stabilize the protein during drying [3]. For example, trehalose is an osmolyte that can form H-bonds with a protein molecule, helping to maintain the structure and functionality of the protein when it is subjected to chemical and/or thermal stress, dehydration and freeze damage from ice crystal formation during freeze-drying [3]. For $scCO_2$ spray drying, the processing conditions are very different compared to freeze drying, and may therefore require different excipients and formulations to achieve the same protein stability. To date, however, the efficacy of protein stabilizers during $scCO_2$ spray drying has yet to be fully elucidated. Moreover, the complexity of the pressurization system and the properties of $scCO_2$ (e.g., atomizing $scCO_2$ and $scCO_2$ drying medium) make it difficult to study the influences of $scCO_2$ spray drying parameters on protein integrity. However, through a systematic study of the processing parameters, it may be possible to better understand the $scCO_2$ spray drying mechanisms and the role of formulation excipients in maintaining the protein integrity, making it ultimately possible to tune the processing conditions in order to prepare stable dried protein formulations.

4. Aims of thesis

The main goals of this thesis are to understand the $scCO_2$ spray drying mechanisms and parameters that influence the stability of proteins, to evaluate the excipients to stabilize protein formulations during $scCO_2$ spray drying, and to study the scalability of the $scCO_2$ spray drying process. For this study, lysozyme and myoglobin were used as model proteins. More specifically, the detailed aims are as follows:

- To study the $scCO_2$ spray drying parameters (i.e., pressure, protein solution and CO_2 flow rate, feed volume) without the use of organic solvents, in order to produce dried protein formulations with minimal residual water content in a single drying step

- To evaluate the scalability of the $scCO_2$ spray drying process

- To gain fundamental insight into the effect of the CO_2 spray drying parameters at sub- and supercritical conditions (65-130 bar and 25-50°C) on the stability of myoglobin

- To understand the effect of the CO_2/water interface and pH shift on heme destabilization and aggregation in myoglobin solutions using a gas bubbling method at atmospheric conditions.

- To evaluate the influence of pharmaceutical excipients on the stability of myoglobin in terms of heme binding and aggregation during $scCO_2$ spray drying

5.   Outline of the thesis

Particle characterization methods are important for evaluating the properties of drug-containing particles engineered by $scCO_2$ processes, in order to ensure that they exhibit the desired characteristics for drug delivery. **Chapter 2** is a review of the particle characterization techniques most commonly used in evaluating particles produced by $scCO_2$ technology.

As the use of organic solvents in $scCO_2$ was previously shown to affect protein integrity, a single-step organic solvent free $scCO_2$ spray drying process is investigated in **Chapter 3**, with the aim to produce a dried protein powder with a target residual water content of max. 3% (w/w). The residual water content of the powdered product is studied as a function of pressure, volume of protein feed solution, and the flow rates of both the CO_2 and the protein solution. The study is carried out by using lysozyme as a protein model. The best processing conditions are further used to prepare dried formulations of other model proteins, including a-lactalbumin, a-chymotrypsinogen A and a monoclonal antibody. In addition, the scalability of the $scCO_2$ spray drying process is evaluated by simply controlling the atomization by maintaining the same gas-to-liquid mass ratio on each scale.

Even when using the best conditions obtained in Chapter 3, $scCO_2$ spray drying without organic solvent still resulted in the destabilization of the model protein myoglobin, as was seen from the partial loss of heme and the formation of protein aggregates. The study of **Chapter 4** aims to reveal the influence of the critical parameters associated with the $scCO_2$ spray drying process, such as pressure, temperature, pressurized CO_2 and the combined spraying and drying steps, on myoglobin's structural integrity. In relation to this, **Chapter 5** shows the effect of acidification and the CO_2/water interface on myoglobin stability using a gas bubbling method under atmospheric conditions. The results are compared to those obtained with N_2 gas bubbling, which has been used as a control, to study the influence of gas/water interface on proteins without lowering the pH. Building upon the results from Chapters 4 and 5, **Chapter 6** demonstrates the effect of pharmaceutical excipients on myoglobin, for further development of stable dried myoglobin formulations prepared via $scCO_2$ spray drying. Finally, the overall results are summarized and the main conclusions and prospects are discussed in **Chapter 7**.

References

[1]   M.C. Manning, D.K. Chou, B.M. Murphy, R.W. Payne, D.S. Katayama, Stability of Protein Pharmaceuticals: An Update. Pharm Res, 20 (2010) 544-575.

[2]   M.C. Manning, K. Patel, R.T. Borchardt, Stability of Protein Pharmaceuticals, Pharm Res, 6 (1989) 903-918.

[3]   J. Carpenter, Rational design of stable lyophilized protein formulations, Protein Sci, 13 (2004) 54-54.

[4]   W. Wang, Lyophilization and development of solid protein pharmaceuticals, Int J Pharm, 203 (2000) 1-60.

[5]   Y.F. Maa, P.A.T. Nguyen, S.W. Hsu, Spray-drying of air-liquid interface sensitive recombinant human growth hormone, J Pharm Sci, 87 (1998) 152-159.

[6]   M. Irngartinger, V. Camuglia, M. Damm, J. Goede, H.W. Frijlink, Pulmonary delivery of therapeutic peptides via dry powder inhalation: effects of micronisation and manufacturing, Eur J Pharm and Biopharm, 58 (2004) 7-14.

[7]   C. Srinivasan, A. Siddiqui, M. Korang-Yeboah, M.A. Khan, Stability characterization and appearance of particulates in a lyophilized formulation of a model peptide hormone-human secretin, Int J Pharm, 481 (2015) 104-113.

[8]   M.S. Salnikova, C.R. Middaugh, J.H. Rytting, Stability of lyophilized human growth hormone, Int J Pharm, 358 (2008) 108-113.

[9]   N.R. Rabbani, P.C. Seville, The influence of formulation components on the aerosolisation properties of spray-dried powders, J Control Release, 110 (2005) 130-140.

[10]   B.S. Selivanov, Stabilization of cellulases using spray drying, Eng Life Sci, 5 (2005) 78-80.

[11]   Z.Z. Nurgalieva, R. Almuchambetova, A. Machmudova, D. Kapsultanova, M.S. Osato, J. Peacock, R.P. Zoltek, P.A. Marchildon, D.Y. Graham, A. Zhangabylov, Use of a dry-plasma collection device to overcome problems with storage and transportation of blood samples for epidemiology studies in developing countries, Clin Diagn Lab Immunol, 7 (2000) 882-884.

[12]   B.F. Oliveira, M.H.A. Santana, M.I. Re, Spray-dried chitosan microspheres as a pDNA carrier, Dry Technol, 24 (2006) 373-382.

[13]   B. Peeters, W.F. Tonnis, S. Murugappan, P. Rottier, G. Koch, H.W. Frijlink, A. Huckriede, W.L. Hinrichs, Pulmonary immunization of chickens using non-adjuvanted spray-freeze dried whole inactivated virus vaccine completely protects against highly pathogenic H5N1 avian influenza virus, Vaccine, 32 (2014) 6445-6450.

[14]   D. Chen, S. Kapre, A. Goel, K. Suresh, S. Beri, J. Hickling, J. Jensen, M. Lal, J.M. Preaud, M. Laforce, D. Kristensen, Thermostable formulations of a hepatitis B vaccine and a meningitis A polysaccharide conjugate vaccine produced by a spray drying method, Vaccine, 28 (2010) 5093-5099.

[15]   Y.F. Maa, S.J. Prestrelski, Biopharmaceutical powders: particle formation and formulation considerations, Curr Pharm Biotechnol, 1 (2000) 283-302.

[16]   M.T. Cicerone, M.J. Pikal, K.K. Qian, Stabilization of proteins in solid form, Adv Drug Deliver Rev, 93 (2015) 14-24.

[17]   S.D. Webb, J.L. Cleland, J.F. Carpenter, T.W. Randolph, Effects of annealing lyophilized and spray-lyophilized formulations of recombinant human interferon-gamma, J Pharm Sci, 92 (2003) 715-729.

[18]   I. Roy, M.N. Gupta, Freeze-drying of proteins: some emerging concerns, Biotechnol Appl Biochem, 39 (2004) 165-177.

[19]   Z.S. Yu, K.P. Johnston, R.O. Williams, Spray freezing into liquid versus spray-freeze drying: Influence of atomization on protein aggregation and biological activity, Eur J Pharm Sci, 27 (2006) 9-18.

[20]   S.D. Webb, S.L. Golledge, J.L. Cleland, J.F. Carpenter, T.W. Randolph, Surface adsorption of recombinant human interferon-gamma in lyophilized and spray-lyophilized formulations, J Pharm Sci, 91 (2002) 1474-1487.

[21]   M. Dissanayake, S. Liyanaarachchi, T. Vasiljevic, Functional properties of whey proteins microparticulated at low pH, J Dairy Sci, 95 (2012) 1667-1679.

[22]   J.M. DeSimone, Practical approaches to green solvents, Science, 297 (2002) 799-803.

[23]   T.A. Hoefling, R.R. Beitle, R.M. Enick, E.J. Beckman, Design and Synthesis of Highly CO_2-Soluble Surfactants and Chelating-Agents, Fluid Phase Equilibria, 83 (1993) 203-212.

[24]   S.P. Cape, J.A. Villa, E.T.S. Huang, T. Yang, J.F. Carpenter, R.E. Sievers, Preparation of active proteins, vaccines and pharmaceuticals as fine powders using supercritical or near-critical fluids, Pharm Res, 25 (2008) 1967-90.

[25]   N. Jovanović, A. Bouchard, G.W. Hofland, G.J. Witkamp, D.J. Crommelin, W. Jiskoot, Stabilization of IgG by supercritical fluid drying: Optimization of formulation and process parameters, Eur J Pharm Biopharm, 68 (2008) 183-190.

[26]   N. Jovanović, A. Bouchard, G.W. Hofland, G.J. Witkamp, D.J. Crommelin, W. Jiskoot, Distinct effects of sucrose and trehalose on protein stability during supercritical fluid drying and freeze-drying, Eur J Pharm Sci, 27 (2006) 336-45.

[27]   G. Muhrer, M. Mazzotti, Precipitation of lysozyme nanoparticles from dimethyl sulfoxide using carbon dioxide as antisolvent, Biotechnol Prog, 19 (2003) 549-56.

[28]   R. Thiering, F. Dehghani, A. Dillow, N.R. Foster, Solvent effects on the controlled dense gas precipitation of model proteins, J Chem Technol Biotechnol, 75 (2000) 42-53.

[29]   M.A. Winters, B.L. Knutson, P.G. Debenedetti, H.G. Sparks, T.M. Przybycien, C.L. Stevenson, S.J. Prestrelski, Precipitation of proteins in supercritical carbon dioxide, J Pharm Sci, 85 (1996) 586-594.

[30]   R. Thiering, F. Dehghani, A. Dillow, N.R. Foster, The influence of operating conditions on the dense gas precipitation of model proteins, J Chem Technol Biotechnol, 75 (2000) 29-41.

[31]   N. Elvassore, A. Bertucco, P. Caliceti, Production of insulin-loaded poly(ethylene glycol)/poly(l-lactide) (PEG/PLA) nanoparticles by gas antisolvent techniques, J Pharm Sci, 90 (2001) 1628-1636.

[32]   N. Jovanović , A. Bouchard , M. Sutter , M. Van Speybroeck, G.W. Hofland, G.J. Witkamp, D.J. Crommelin, W. Jiskoot, Stable sugar-based protein formulations by supercritical fluid drying. Int J Pharm, 346 (2008) 102-108.

[33]   A. Bouchard, N. Jovanović, G.W. Hofland, W. Jiskoot, E. Mendes, D.J.A. Crommelin, G.J. Witkamp, Supercritical fluid drying of carbohydrates: Selection of suitable excipients and process conditions, Eur J Pharm Biopharm, 68 (2008) 781-794.

[34]   M.J. Pikal, D. Rigsbee, M.J. Akers, Solid State Chemistry of Proteins IV. What is the Meaning of Thermal Denaturation in Freeze Dried Proteins?, J Pharm Sci, 98 (2009) 1387-1399.

[35]   M.J. Pikal, D. Rigsbee, M.L. Roy, Solid State Stability of Proteins III: Calorimetric (DSC) and Spectroscopic (FTIR) Characterization of Thermal Denaturation in Freeze Dried Human Growth Hormone (hGH), J Pharm Sci, 97 (2008) 5122-5131.

[36]   A.M. Abdul-Fattah, D. Lechuga-Ballesteros, D.S. Kalonia, M.J. Pikal, The impact of drying method and formulation on the physical properties and stability of methionyl human growth hormone in the amorphous solid state, J Pharm Sci, 97 (2008) 163-184.

[37]   S.P. Sellers, G.S. Clark, R.E. Sievers, J.F. Carpenter, Dry powders of stable protein formulations from aqueous solutions prepared using supercritical CO_2-assisted aerosolization, J Pharm Sci, 90 (2001) 785-97.

[38]   P. Sameer, F.P. Nalawade, L.P.B.M. Janssen, Supercritical carbon dioxide as a green solvent for processing polymer melts: Processing aspects and applications. Prog Polym Sci, 31 (2006) 19–43.

CHAPTER 2

Characterization of drug delivery particles produced by supercritical carbon dioxide technologies

Onanong Nuchuchua[1], M. Reza Nejadnik[1], Sebastiaan C Goulooze[2], Nataša Jovanović Lješković[3], Hayley Ann Every[4], Wim Jiskoot[1]

[1] Division of Drug Delivery Technology, Cluster Biotherapeutics, Leiden Academic Centre for Drug Research (LACDR), Leiden University, The Netherlands
[2] Division of Pharmacology, Leiden Academic Centre for Drug Research (LACDR), Leiden, The Netherlands
[3] Department of Pharmaceutics, Utrecht Institute for Pharmaceutical Sciences, Utrecht, The Netherlands
[4] FeyeCon Development & Implementation B.V., Weesp, The Netherlands

Abstract

This review focuses on characterization methods for drug/excipient particles produced with supercritical CO_2 (scCO_2) particle engineering technologies. Proper characterization of particles can guide optimization of their production process and provide an indication of their *in vivo* behavior. In particular, characterization techniques for particle size distribution and morphology, drug loading and release, structure of matrix components, biotherapeutic activity, porosity analysis, particle surface, surface charge, toxicology/biocompatibility and residual solvent/water analysis, are discussed. Moreover, we discuss particle analytical techniques that are not commonly used in the scCO_2 research field but are of potential use for pharmaceutically relevant scCO_2-engineered particles. These techniques often work synergistically in particle characterization by mutually supporting the interpretation of their outcomes, which is crucial to efficiently develop a successful production process of drug/excipient particles.

1.　Introduction

Therapeutic agents, such as small molecules, proteins and vaccines are often formulated in a matrix that may consist of biopolymers, sugars, polysaccharides, porous materials (e.g., silica) or inorganic compounds. The preparation of these matrices in particle form has been shown to improve drug delivery in several ways, e.g., by allowing the use of less invasive administration routes, improving drug stability, controlling the release profile, increasing bioavailability and/or selectively targeting of particular tissues or cell types [1-3]. Some pharmaceutical particle products have already obtained market approval and are currently used in established treatments of diseases [4]. One example is an anticancer agent, formulated as paclitaxel/albumin nanoparticles with improved solubility and delivery of the drug into endothelial cells when compared to traditional paclitaxel formulations [5].

Various characteristics of the particles have been shown to greatly influence the performance of the particulate formulation. Particle size, among others, is of significance in the process of drug administration, where typically particles with a size range between 0.1-0.3 µm are used for intravenous (IV) delivery, 10-200 µm for subcutaneous or intramuscular delivery [6], 1-5 µm for pulmonary delivery and 0.1-100 µm for oral delivery [7]. In most cases, particles have to reach their target site through the blood circulation system. After entering the vascular bed, particles can escape from the circulation through openings, also called fenestrations, of the endothelial barrier. The size limits of these openings for different organs has been summarized elsewhere and is a contributing factor to the typical particle size dependent biodistribution of particles in the body. Although it is roughly said that particles have to be smaller than 150 nanometer to cross the endothelial barrier, there are several reports that indicate penetration of particles much larger than the limits of these opening [8]. These observations have mainly to do with pathological conditions where the vasculature and the fenestrations undergo changes in size and allow penetration of larger particles. For instance nanoparticles as large as a couple of hundred nanometer in diameter have been used to target tumor cells [9, 10]. In a different area of application, the particle size is a critical factor in induction of immunogenicity in vaccine delivery systems [11, 12]. Briefly, nanoparticles target the CD8$^+$ T cell responses and dendritic cells while microparticles (2-3 µm) activate macrophages. Size is just one attribute of particle characteristics and there is a vast amount of information concerning the relevance of other properties of particles in various pharmaceutical applications.

The above-mentioned relations between the particle characteristics and their window of potential function indicate that, regardless of the application, the engineering of particles for drug delivery requires comprehensive characterization of the physical, chemical and biological attributes of the particles. A good characterization provides required data for understanding the property-function relations and for the optimization of particle production processes and therapeutic efficacy. Thus, careful selection of characterization techniques is crucial for the development of stable and effective drug delivery particles.

Particle preparation for pharmaceutical applications is typically carried out by conventional techniques, such as milling, solvent evaporation and spray drying [13], or relatively new methods such as supercritical carbon dioxide technology, cryogenic technologies, and nanomilling [14]. Milling involves the use of a mechanical force to break up a material into smaller particles, typically in the range of 1-100 μm. While such methods are inexpensive, the particle size and homogeneity that can be achieved are often limited [15]. Particle formation by solvent evaporation is a simple method for preparing particles over a broad size range. However, residual solvents can remain in the particles [16], which may lead to cytotoxicity upon administration. Spray drying produces powder product by atomizing a solution to form droplets that are subsequently dried by hot air. While it is a fast and easily scalable process that is capable of achieving narrow particle size distributions in the range of 0.1 to 1000 μm, the high temperatures needed for drying can lead to degradation of biological compounds [17-19]. Cryogenic technologies, such as freeze drying, rely on sublimation to produce dried products. They are considered to be a mild process and are generally used for the dehydration of biotherapeutics. However, the particle size of freeze-dried products is not well-controlled. Moreover, such methods are energy intensive and time consuming [20].

Among these techniques, the use of supercritical CO_2 (scCO_2) to create multicomponent drug/excipients particles is of particular interest for several reasons [21]. ScCO_2 has a relatively mild critical pressure (7.4 MPa) and temperature (301.4 K), allowing processing of thermolabile substances at desirable temperatures [22-24]. It is also inexpensive, nontoxic and relatively inert [25].

Moreover, scCO_2 technology can be used to process a broad range of drug formulations from a variety of materials with controlled size distributions and specific particle morphologies [21, 26-29], in particular to develop drug carrier systems [26, 30, 31] and to improve drug

bioavailability [32]. A review article of Campardelli et al. [31] introduced several $scCO_2$-based particle production techniques that allow for preparation of solid nanoparticles, nanostructured and nanoporous microparticles, and nanoporous materials. The literature cited in this review demonstrates that there is a large, heterogeneous array of particles for pharmaceutical applications that have been engineered by using $scCO_2$ technology [33]. These particles have been characterized by various techniques and literature data show that the methods used to characterize drug/excipient particles are numerous and aiming for a broad range of properties, while no standard testing procedure has been implemented (Table 1 and Fig. 1). Moreover, it is apparent from these articles that the influence of the processing conditions in $scCO_2$ processes on the resultant particle characteristics is not well understood, compared to conventional particle production methods.

The aim of this review is to discuss the strategies and methods used for the characterization of $scCO_2$-produced drug-containing particles. In particular, the techniques are categorized with respect to their targeted properties, i.e., particle size distribution and morphology, drug loading and release, structure of matrix components, biotherapeutic activity, surface chemistry, porosity, surface charge, toxicology/biocompatibility and residual solvent/water. This review will take into consideration the strengths and weaknesses of each characterization technique, and also include a list of methods that may potentially be useful as additional characterization methods for particles produced with $scCO_2$ technology. Table 2 summarizes techniques that have been used to characterize particles prepared by $scCO_2$ technologies (indicated by an asterisk when such a technique is used in one of the cited articles in Table 1) as well as techniques that have been used for particles prepared with other methods and can be useful for characterizing drug-containing particles engineered by $scCO_2$ technologies. In the review of each technique special attention will be paid to highlighting the way characterization can help improving the production and application of particulate drug delivery systems.
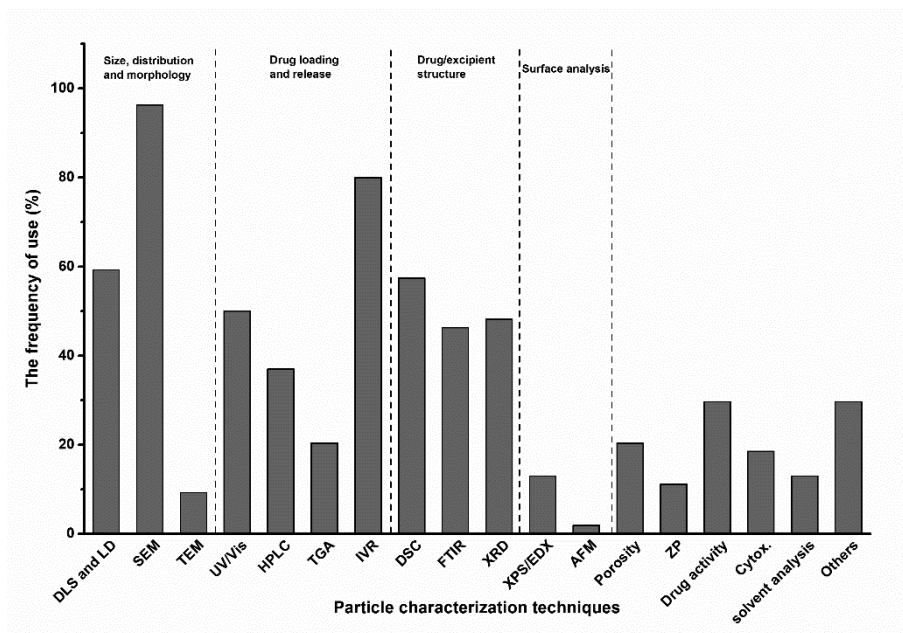
Fig. 1 The frequency of use of particle characterization techniques used in scCO$_2$ technology. Abbreviations; **AFM** (Atomic force microscopy), **Cytox** (Cytotoxicity by in vitro and in vivo assay), **DLS and LS** (dynamic light scattering and laser diffraction), **DSC** (Differential scanning calorimetry), **EDX** (Energy dispersion X-ray spectroscopy), **FTIR** (Fourier transform infrared spectroscopy), **HPLC** (high performance liquid chromatography with UV detector), **IVR** (*In vitro* release and dissolution study), **Porosity** (Brunauer-Emmett-Teller surface area analysis and Barrett-Joyner-Halenda determination, N$_2$ absorption and pore size distribution), **SEM** (Scanning electron microscopy), **Solvent analysis** (Gas chromatography), **TGA** (Thermogravimetric analysis), **TEM** (Transmission electron microscopy), **UV/Vis** (UV/Vis spectroscopy), **XPS** (X-ray photoelectron spectroscopy), **XRD** (X-ray diffraction), and **ZP** (Zeta potential measurement).

Table 1. Particle characterization techniques used in the field of scCO$_2$ techniques.

Particle constituents	Role CO$_2$ (production technique)	Particle size distribution, morphology				Drug loading and release				Structure of drug/excipient			Surface chemistry	Refs.
		LS/LD	SEM	TEM	NTA/MFI	UV/Vis	TGA	IVR	HPLC/UV	DSC	FTIR	XRD	XPS/EDX	
Retinyl palmitate, PLA	Solvent (RESOLV)	•	•			•								[84]
Fenofibrate, PLGA	Solvent (RESOLV)	•	•							•		•		[148]
Naproxen, PLA	Solvent (RESS)	SMPS	•								•			[118]
Prednisolone, PEG, SDS	Non-solvent (ASES)	•	•											[171]
Lysozyme, PLA, ammonium bicarbonate	Non-solvent (emulsion-combined PCA)	•	•			•	•	•		•	•			[64]
Methotrexate, PLA	Non-solvent (emulsion-combined PCA)	•	•			•		•		•	•	•		[65]
Curcumin, PLGA	Non-solvent (fluidization-assisted SAS)	•	•			•		•		•				[79]
5-fluorouracil, PLA-PEG, PEG	Non-solvent (reverse emulsion SEDS)	•	•				•	•	•		•			[63]
Azacitidine, PLA	Non-solvent (SAS)		•					•	•	•				[172]
Gentamicin, PVP/MA	Non-solvent (SAS)		•								•			[114]
Nilotinib, HPMCP	Non-solvent (SAS)	•	•					•	•	•		•		[130]
Paracetamol, PLA	Non-solvent (SAS)		•	•				•		•		•		[13]
Paracetamol, PLA	Non-solvent (SAS)		•				•	•					•	[173]
Dutasteride, HP-β-CD	Non-solvent (SAS)	•	•						•			•		[174]

Drug, carrier	Method											Ref.
Cilostazol and one of (Poloxamer 188, Poloxamer 407, TPGS 1000, Gelucire® 44/14, Gelucire ® 50/13)	Non-solvent (SAS)	•								•		[175]
Amoxicillin, ethyl-cellulose	Non-solvent (SAS)	•	•		•	•	•	•	•	•		[137]
Camptothecin, folic acid conjugated dextran	Non-solvent (SAS)	•	•		•	•	•	•	•	•		[176]
Diflunisal, PVP	Non-solvent (SAS)	•	•		•	•	•	•	•		•	[132]
Quercetin, poloxamer 407	Non-solvent (SAS)	•	•		•	•	•	•	•	•		[156]
10-hydroxycamptothecin, PLA	Non-solvent (SAS)			•	•	•	•	•	•			[131]
Lysozyme, CaCO₃	Non-solvent (SAS)	•	• OM			•	•		•			[150]
Viscumin, PLA	Non-solvent (ultrasound-assisted SAS)		•		•					•		[177]
Curcumin, PLGA	Non-solvent (ultrasound-assisted SAS)	•	•		•		•	•	•			[178]
Rifampicin, lactose	Non-solvent (SAS-DEM)	•	•		•	•	•	•	•	•		[49]
Nevirapine, lactose,	Non-solvent (SAS-DEM)	•	•		•	•	•	•	•			[51]

Material	Method										Ref
microcrystalline cellulose											
Itraconazole, lactose	**Non-solvent (SAS-DEM)**	LO	•				•	•		•	[50]
Paclitaxel, PLA	**Non-solvent (SAS-EM)**	•	•			•	•	•	•	•	[48]
One of (piroxicam and diclophenac), PLGA	**Non-solvent (SFEE)**	•	•	•		•			•	•	[43]
Insulin, PLGA	**Non-solvent (SFEE)**	• (OM)	•			•	•	•		•	[44]
Piroxicam, PLGA	**Non-solvent (SFEE)**	• (OM)	•	•	•	•			•	•	[39]
Hydrocortison, PLGA	**Non-solvent (SFEE)**	• (OM)	•		•	•	•			•	[42]
Rhodamine, hollow gold nanoshells, PLA	**Non-solvent (SFEE)**	•	•	•	•	•	•		•	•	[135]
Morphine, PLA-PEG-PLA	**Non-solvent (SEDS)**	•	•	•		•	•	•	•	•	[179]
Indomethacin, Fe₃O₄, PLA	**Non-solvent (SEDS)**	•	•		•	•	•		•	•	[85]
Paclitaxel, PLA	**Non-solvent (SEDS)**	•	•	•	•	•	•	•	•	•	[89]
Indomethacin, PLA, PLGA	**Non-solvent (SEDS)**	•	•	•	•	•	•		•	•	[110]
Amoxicillin, chitosan	**Non-solvent (SEDS)**	•	•	•	•	•	•		•	•	[111]
Puerarin, PLA	**Non-solvent (SpEDS)**	•	•		•	•	•		•	•	[61]
5-fluorouracil, SiO₂, PLA	**Non-solvent (SpEDS)**	•	•		•	•			•	•	[62]
Methotrexate, PLA-PEG-PLA	**Non-solvent (SpEDS)**	•	•	•	•	•			•	•	[60]

Compound, carrier	Method										Ref.
Methotrexate, Fe₃O₄, PLA-PEG-PLA	**Non-solvent** (SpEDS)	•		•	•	•	•	•	•		[88]
Fenofibrate, SBA-15	**Solvent/ non-solvent** scCO₂-assisted impregnation	•		•	•	•	•	•	•	•	[134]
Fenofibrate, SBA-15	**Solvent/ non-solvent** scCO₂-assisted impregnation			•	•	•	•	•	•	•	[124]
Metronidazole, melanin	**Solvent/ non-solvent** scCO₂-assisted impregnation	•		•		•	•			•	[180]
Ibuprofen, DMAEMA-based molecularly imprinted polymers	**Solvent/ non-solvent** scCO₂-assisted impregnation	•				•					[181]
Ibuprofen, MCM-41	**Solvent/ non-solvent** scCO₂-assisted impregnation	•		•	•	•	•	•			[120]
Fenofibrate, Neusilin UFL2	**Solute** Melt-adsorption	•				SEC	•	•	•		[59]
Tetanus Toxoid, PLA	**Solute** PGSS	•	•			•	•				[53]
hGH, PLA, PLGA	**Solute** PGSS	•	•			SEC	•	•			[54]
BSA (bovine serum albumin), one of (PLA, PLA-PEG copolymers)	**Solute** PGSS	•	•	•		•	•	•			[55]
S-(+)-ibuprofen, one or	**Solute** PGSS	•	•			•	•	•			[182]

Material	Role										Ref.
several of (Pluronic® F127, Pluronic® L64, Gelucire®, glyceryl monostearat e)											
Gentamicin, dextran	**Atomization aid** SAA	•				•	•	•	•	•	[74]
Gentamicin, heat denatured albumin	**Atomization aid** SAA	•				•	•	•	•	•	[75]
Lyosozyme, myoglobin, trehalose, sucrose	**Atomization aid**	•				•		•	•		[67, 116]
Polyclonal human serum IgG, trehalose, cyclodextrin	**Atomization aid**								•		[117]
Lysozyme, α-lactalbumin, α-chymotrypsin ogen A, monoclonal antibody, myoglobin Trehalose	**Atomization aid**	•	•	•	•		SEC	•			[68, 69]
Piroxicam, PVP	**Other** Polymerization medium/solvent	•		•		•			•	•	[183]

Table 1. Particle characterization techniques used in the field of scCO$_2$ techniques (continue).

Particle constituents	Role CO$_2$ (production technique)	Porosity	Surface charge	Drug activity	Toxicology	Residual solvent and water content	Other properties*	Refs.
		BET and BJH/N$_2$ absorption/Pore size distribution	ZP		In vitro and In vivo	GC and Karl Fischer method		
Retinyl palmitate, PLA	**Solvent** (RESOLV)							[84]
Fenofibrate, PLGA	**Solvent** (RESOLV)		●					[148]
Naproxen, PLA	**Solvent** (RESS)							[118]
Prednisolone, PEG, SDS	**Non-solvent** (ASES)							[171]
Lysozyme, PLA, ammonium bicarbonate	**Non-solvent** (emulsion-combined PCA)	HPMIP		●			●	[64]
Methotrexate, PLA	**Non-solvent** (emulsion-combined PCA)	HPMIP		●	●	●	●	[65]
Curcumin, PLGA	**Non-solvent** (fluidization-assisted SAS)							[79]
5-fluorouracil, PLA-PEG, PEG	**Non-solvent** (reverse emulsion SEDS)			●	●			[63]
Azacitidine, PLA	**Non-solvent** (SAS)							[172]
Gentamicin, PVP/MA	**Non-solvent** (SAS)			●	●		●	[114]
Nilotinib, HPMCP	**Non-solvent** (SAS)		●	●		●	●	[130]
Paracetamol, PLA	**Non-solvent** (SAS)							[13]
Paracetamol, PLA	**Non-solvent** (SAS)		●					[173]
Dutasteride, HP-β-CD	**Non-solvent** (SAS)	●		●			●	[174]
Cilostazol and one of	**Non-solvent** (SAS)	●				●	●	[175]

Materials	Method					Ref.
(Poloxamer 188, Poloxamer 407, TPGS 1000, Gelucire® 44/14, Gelucire® 50/13)						
Amoxicillin, ethyl-cellulose	**Non-solvent** (SAS)					[137]
Camptothecin, folic acid conjugated dextran	**Non-solvent** (SAS)					[176]
Diflunisal, PVP	**Non-solvent** (SAS)					[132]
Quercetin, poloxamer 407	**Non-solvent** (SAS)			•		[156]
10-hydroxycamptothecin, PLA	**Non-solvent** (SAS)					[131]
Lysozyme, CaCO₃	**Non-solvent** (SAS)		•	•		[150]
Viscumin, PLA	**Non-solvent** (ultrasound-assisted SAS)			•		[177]
Curcumin, PLGA	**Non-solvent** (ultrasound-assisted SAS)					[178]
Rifampicin, lactose	**Non-solvent** (SAS-DEM)					[49]
Nevirapine, lactose, microcrystalline cellulose	**Non-solvent** (SAS-DEM)					[51]
Itraconazole, lactose	**Non-solvent** (SAS-DEM)	•				[50]
Paclitaxel, PLA	**Non-solvent** (SAS-EM)					[48]
One of (piroxicam and diclophenac), PLGA	**Non-solvent** (SFEE)				•	[43]

Substance, Carrier	Method							Ref.
Insulin, PLGA	**Non-solvent** (SFEE)			•				[44]
Piroxicam, PLGA	**Non-solvent** (SFEE)		•		•			[39]
Hydrocortison, PLGA	**Non-solvent** (SFEE)		•					[42]
Rhodamine, hollow gold nanoshells, PLA	**Non-solvent** (SFEE)							[135]
Morphine, PLA-PEG-PLA	**Non-solvent** (SEDS)	•						[179]
Indomethacin, Fe_3O_4, PLA	**Non-solvent** (SEDS)	•		•				[85]
Paclitaxel, PLA	**Non-solvent** (SEDS)			•		•		[89]
Indomethacin, PLA, PLGA	**Non-solvent** (SEDS)	•		•				[110]
Amoxicillin, chitosan	**Non-solvent** (SEDS)	•		•				[111]
Puerarin, PLA	**Non-solvent** (SpEDS)							[61]
5-fluorouracil, SiO_2, PLA	**Non-solvent** (SpEDS)							[62]
Methotrexate, PLA-PEG-PLA	**Non-solvent** (SpEDS)							[60]
Methotrexate, Fe_3O_4, PLA-PEG-PLA	**Non-solvent** (SpEDS)	•	•	•				[88]
Fenofibrate, SBA-15	**Solvent/ non-solvent** scCO$_2$-assisted impregnation						•	[134]
Fenofibrate, SBA-15	**Solvent/ non-solvent** scCO$_2$-assisted impregnation						•	[124]
Metronidazole, melanin	**Solvent/ non-solvent** scCO$_2$-assisted impregnation	•						[180]

Material						Technique	Ref
Ibuprofen, DMAEMA-based molecularly imprinted polymers	•		•		•	•	**Solvent/ non-solvent** scCO₂-assisted impregnation	[181]
Ibuprofen, MCM-41	•						**Solvent/ non-solvent** scCO₂-assisted impregnation	[120]
Fenofibrate, Neusilin UFL2	•			•			**Solute** Melt-adsorption	[59]
Tetanus Toxoid, PLA				•		•	**Solute** PGSS	[53]
hGH, PLA, PLGA				•		•	**Solute** PGSS	[54]
BSA (bovine serum albumin), one of (PLA, PLA-PEG copolymers)							**Solute** PGSS	[55]
S-(+)-ibuprofen, one or several of (Pluronic® F127, Pluronic® L64, Gelucire®, glyceryl monostearate)							**Solute** PGSS	[182]
Gentamicin, dextran				•		•	**Atomization aid** SAA	[74]
Gentamicin, heat denatured albumin							**Atomization aid** SAA	[75]
Lyosozyme, myoglobin, trehalose, sucrose	•	•		•		•	**Atomization aid**	[67, 116]
Polyclonal human serum						•	**Atomization aid**	[117]

	IgG, trehalose, cyclodextrin				
Atomization aid	Lysozyme, α-lactalbumin, α-chymotrypsinogen A, monoclonal antibody, myoglobin Trehalose	•		•	•
					[68, 69]
Other Polymerization medium/solvent	Piroxicam, PVP				[183]

BET/BJH (Brunauer-Emmett-Teller surface area analysis and Barrett-Joyner-Halenda determination), **DSC** (Differential scanning calorimetry), **EDX** (Energy dispersion X-ray spectroscopy), **FTIR** (Fourier transform infrared spectroscopy), **GC** (Gas chromatography), **HPLC/UV** (high performance liquid chromatography with UV detector), **HPMIP** (High-pressure mercury intrusion porosimetry), **IVR** (In vitro release and dissolution study), **LD** (Laser diffraction), **LS** (Light scattering techniques), **LO** (Light obscuration), **MFI** (Flow-imaging microscopy), **NTA** (Nanoparticle tracking analysis), **OM** (Optical microscopy), **Others** (mucoadhesion, particle stability, residual water/organic content determination, protein structure analysis), **SEC** (Size exclusion chromatography), **SEM** (Scanning electron microscopy), **SMPS** (Scanning mobility particle sizer), **TEM** (Transmission electron microscopy), **TGA** (Thermogravimetric analysis), **UV/Vis** (UV/Vis spectroscopy), **XRD** (X-ray diffraction), **XPS** (X-ray photoelectron spectroscopy), **ZP** (Zeta potential measurement).

2.   Supercritical carbon dioxide-mediated particle engineering

2.1. scCO$_2$ as a solvent

Several methods use scCO$_2$ as a solvent for drug and/or excipient, and rely on a reduction in pressure to induce particle formation. The first method of this category is often referred to as the Rapid Expansion of Supercritical Solutions (RESS) technique [34]. After the constituents are dissolved in scCO$_2$, the mixture is depressurized over a nozzle. The resulting expansion of scCO$_2$ reduces its solvation power, leading to supersaturation of the mixture and precipitation of the solute to form particles. The use of this technique is often limited, as scCO$_2$ remains a poor solvent for most of the polymers and pharmaceutical compounds, making RESS-like processes a less viable option for the production of particles containing them [33].

One way to overcome the limited solubility is by using an organic co-solvent, which can be added to increase the solubility of drug or polymer in the scCO$_2$. However, when working with organic solvents, there is the risk that some solvent remains in the particles, therefore requiring additional drying steps to remove it. Moreover, the solvent may also cause particle agglomeration [33]. Variations of the RESS method include a non-solvent RESS process (RESS-N), which relies on the differences in solubility of an excipient and drug in scCO$_2$ to promote the precipitation of the excipient on the already prepared drug particles to create microparticles with a core-shell structure [35-37], and the spraying of the supercritical solution into a liquid solvent (RESOLV), to obtain a suspension of micro- or nanosized particles [33, 38].

The second technique that makes use of scCO$_2$ as a solvent is scCO$_2$-assisted impregnation. When a saturated solution of drug in scCO$_2$ is brought into contact with insoluble excipient particles, the drug can be loaded into the particles by two mechanisms [39]. In the first approach, rapid depressurization of the scCO$_2$/drug solution allows for the drug to be deposited inside the particles, which often consist of a polymer or silica matrix. During such a process, it is possible that the drug can deposit outside the excipient particles, leading to an inhomogeneous mixture of drug and excipient molecules. The second mechanism involves drug adsorption by the excipient, which relies on an interaction (e.g., H-bonding) between the solid excipient particles and the drug [39]. When the excipient is a polymer, scCO$_2$ serves not only as a solvent for the drug, but also promotes diffusion of the scCO$_2$ solution into the polymer matrix by swelling of the polymer[40].

In the third method, that is Supercritical Fluid Emulsion Extraction (SFEE) technique, a $scCO_2$ solvent can be used to dissolve and extract the organic phase of an emulsion. In this case, the drug and other particle constituents are dissolved in the organic phase of a traditional oil-in-water emulsion and $scCO_2$ is a non-solvent for the particle constituents that can extract the organic solvent very rapidly and efficiently. The extraction of the organic phase will produce an aqueous suspension of microparticles, which can subsequently be filtered and dried to obtain a powder. One of the benefits of SFEE is that the particle size can be controlled by manipulating the size of the droplets in the emulsion [41]. In addition, the aqueous phase is supposed to prevent agglomeration [41]. This method was originally developed by Shekunov et al. [42] for the preparation of pure nanoparticles of cholesterol acetate, griseofulvin and megestrol. It has also been used to create drug/polymer particles with Eudragit® and poly(lactic-co-glycolic acid)(PLGA) [41, 43-46].

2.2. $scCO_2$ as a non-solvent

The fact that most drugs and polymers have a poor solubility in $scCO_2$ can also be exploited in particle formation techniques, where the $scCO_2$ is then used as an anti-solvent. In processes like Supercritical Anti-Solvent (SAS) and Precipitation with Compressed Anti-solvent (PCA), a solution of drug and excipients is sprayed into a precipitation chamber containing $scCO_2$ [47]. As the $scCO_2$ dissolves into the sprayed droplets, the solubility of the constituents in the droplet decreases, leading to the precipitation of micro- or nanosized particles [48]. These anti-solvent processes often lead to very small (down to nm size range) particles, as the rapid precipitation limits the possibility for the particles to grow. However, an additional organic solvent is often employed in anti-solvent processes to enhance the mass transfer between $scCO_2$ and drug/excipient solution, leading to remaining of a residual organic solvent content in particles [47], which may cause cytotoxicity upon drug administration.

Several modifications of the $scCO_2$ anti-solvent process have been developed, to improve the atomization and to create particles with narrower size distributions. Chattopadhyay et al. [49] developed the Supercritical Anti-Solvent with Enhanced Mass Transfer (SAS-EM) process, where an atomizing tip with ultrasonic frequency is used to improve mass transfer between $scCO_2$ and the drug/excipient solution. The same technique was used by Lee et al. [50] to produce microparticles of paclitaxel and poly L-lactic acid (PLA). In a variation of this method called the Supercritical Anti-Solvent Drug-Excipient Mixing (SAS-DEM)

process, a drug solution is sprayed into a suspension of excipients in $scCO_2$. This causes the drug to precipitate in composite particles containing the excipient. This method is used to avoid agglomeration of drug particles and improve the dissolution rate by increasing the surface area [51-53].

2.3. $scCO_2$ as a solute

$scCO_2$ can dissolve in many polymeric matrices, causing swelling and lowering of the glass transition temperature [47]. This behavior is exploited in the Particles from Gas Saturated Solutions (PGSS) process, as it allows for intimate mixing of a molten polymer and an (insoluble) drug. Subsequent rapid depressurization of the $scCO_2$ saturated molten mixture over a nozzle causes a rapid and homogeneous cooling of the sample, which induces precipitation of solid drug/polymer particles [54]. This method has been used recently to make protein/polymer particles with several different polymers such as PLGA, PLA and copolymers of PLA and polyethylene glycol (PEG) [55-57]. In addition, the PGSS technique has been used to prepare protein-loaded lipid-based particles with a high protein loading and a controlled released profile [33, 58]. In this case, the technique has been referred to as Gas-Assisted Melting Atomization (GAMA). Despite the ability of the process in producing particles, it has been reported that the PGSS process is disadvantageous for preparation of particles in the submicron size range [59].

Moreover, $scCO_2$ can help to improve a traditional hot-melting dispersion method for manufacturing micronized particles, by lowering the melting temperature of dispersed active agents [60]. As shown in a study by Cha et al. [61], the suppression in melting by the supercritical allows for intimate mixing between a molten drug (fenofibrate) and a mesoporous carrier (magnesium aluminometasilicate, Neusilin UFL2) at only 50 °C, in contrast to the hot-melting method, which was conducted at 90 °C.

2.4. $scCO_2$ as a drying medium

In a commonly used technique called Solution-Enhanced Dispersion by $ScCO_2$ (SEDS), the solution is mixed with $scCO_2$ prior to spraying through a coaxial nozzle [33]. This increases the mass transfer between the sprayed solution and $scCO_2$, reducing both the drying time and the extent of particle agglomeration. Alternatively, a similar $scCO_2$/solution mixture can be sprayed into a liquid phase, to create a dispersion as in the case of Suspension Enhanced Dispersion by $scCO_2$ (SpEDS) [62-64]. Another modification of the SEDS technique was developed by Zhang et al. [65]: the reverse-emulsion-Solution Enhanced

Dispersion by $scCO_2$ (reverse emulsion-SEDS), in which an oil-in-water emulsion containing both drug (5-fluorouracil) and polymer was dried using an SEDS-like process. However, the emulsion sprayed into the $scCO_2$ medium was not treated with $scCO_2$ prior to spraying. The reverse emulsion-SEDS is also comparable to the emulsion-combined PCA [66, 67].

Similar to the SEDS process, $scCO_2$ is used as a low temperature drying medium, which is particularly beneficial for thermolabile substances [68]. In the $scCO_2$ spray drying process, a protein formulation is pumped into the drying system, where it is atomized by the $scCO_2$ via a nozzle into a drying vessel filled with $scCO_2$ [69]. The water removal from the atomized droplets is carried out in the vessel by mass transfer between water and $scCO_2$ phases. The $scCO_2$ spray drying has been used to prepare dried formulations of lysozyme [69], myoglobin [69, 70] and immunoglobulin G [71] in our laboratories. The two other techniques in this category are $scCO_2$ assisted atomization (SAA) and carbon dioxide-assisted nebulization with a bubble dryer (CAN-BD) [72, 73]. In both cases, $scCO_2$ is mixed with a solution of the drug/polymer prior to spraying, to create either an emulsion or a solution. The emulsion/solution is then sprayed into a vessel at lower pressure, where the expansion of $scCO_2$ facilitates the formation of microdroplets, allowing for fast drying (several ms) despite the low temperatures (32 - 52 °C) [74, 75]. The SAA technique has been used recently to create gentamicin/albumin particles and gentamicin/alginate/pectin particles [76, 77]. SAA and CAN-BD processes are similar to PGSS drying for preparing particles of β-carotenoid in lecithin as described by Paz et al. [78]. It has been suggested that proteins can suffer from an acidification by CO_2, however, a suitable buffer can control the pH of protein formulations during $scCO_2$ drying processes [70].

3.   Particle characterization

The order of the presentation of particle characterization techniques that are discussed in this review paper is based on the frequency of their use for the analysis of $scCO_2$ engineered particles. As presented in Fig. 1, more that 50% of the analyses by particle characterization methods have aimed for investigating one of these three categories of properties: 1) particle size distribution and morphology, 2) drug loading and release and 3) drug and excipient structure. Other properties such as surface chemistry and charge, *in vitro* and *in vivo* drug activity and efficacy, toxicology and others have been less studied.

3.1. Particle size distribution and morphology

3.1.1.   Dynamic light scattering (DLS) and laser diffraction (LD)

Dynamic light scattering (DLS) or photon correlation spectroscopy measures the variation of the intensity of scattered light over time to determine the diffusion coefficient and therewith the average equivalent-sphere hydrodynamic diameter of particles in a suspension [79, 80]. This technique can measure particle size in the range of about 1-1000 nm. DLS measurements are easy to perform and this technique is quite common due to the availability of the necessary equipment in most laboratories. However, small traces of large particles and agglomerates can skew the results, because they scatter light more efficiently than smaller particles do [8].

DLS analysis was applied to study the effects of the production parameters of the SAS process with ultrasonic vibration to prepare uniform PLGA-coated curcumin nanoparticles in the range of 40-63 nm. The results showed that low power of the ultrasonication (60 W) resulted in poor mixing of pure curcumin particles, whereas curcumin aggregation occurred with a high ultrasonic power (420 W) [81]. Another study by Zhang et al. [65] used DLS to determine influences of operating parameters of a reverse-emulsion SEDS process on the particle size distribution of 5-fluorouracil (an antitumor drug) loaded in a copolymer PLA/PEG. The results suggested that the nanoparticles with a narrow size distribution were obtained when the pressure of the SEDS process was high, but the operational temperature and solution flow rate were low. In this study, the DLS results were supported by the images from scanning electron microscopy (SEM).

Laser diffraction (LD), similar to DLS, is based on analysis of the scattered light. It is in principle a commonly used static light scattering method in which particle sizes are determined based on an intensity of scattered light as a function of scattering angle. LD is suitable for measurement of the particle size in the range of submicron to millimeter. LD has been used in studies of Kang et al. [66] and Chen et al. [67] to observe drug-loaded, porous PLA microparticles prepared by PCA process. The particles were designed for pulmonary drug delivery. In theory, inhaled drug/excipient particles should have an aerodynamic diameter (aerodynamic diameter is a function of geometric size and particle density) in a range of 1-5 μm to reach the alveolar airways [82]. The results of the LD measurement suggested that the geometric particle sizes of drug-loaded porous microparticles were about 10-20 μm. However, due to the porosity of particles resulting in a lower density, the aerodynamic diameter of drug-loaded PLA porous microparticles was

about 3 μm [66, 67]. Therefore, porous particles with a geometric size greater than 10 μm may have a desired aerodynamic size due to the low mass densities of particles [83, 84].

3.1.2. Scanning electron microscopy (SEM)

SEM is used to visualize the morphology or shape of particles in a dry state. SEM uses a focused beam of electrons to scan the sample. Various types of signals (secondary or back-scattered electrons and X-rays) coming from the sample can be detected to create an image, or gain information about the elemental composition of the surface. The resolution of a SEM image can be as small as 1 nm [85], while at the lowest magnification particles as large as hundreds of microns can be imaged. Based on SEM images, Sane and Limtrakul [86] showed that PLA nanoparticles loaded with a model drug (retinyl palmitate) from RESOLV process were different in size due to presence or absence of a component of retinyl palmitate and excipients in the precipitating solution. SEM also gave clear images of the agglomerates of retinyl palmitate/PLA nanoparticles. However, particles seen in SEM images are dry and therefore their size can be smaller than their hydrodynamic diameter determined from DLS or some other light interaction methods [86]. Moreover, SEM images can be also used for estimation of particle porosity and the elemental analysis of a particle surface [41, 52, 87], as explained below.

3.1.3. Transmission electron microscopy (TEM)

Using TEM, particles with a size range of 1 nm - 5 μm can be imaged [88]. The intensity of electrons after interacting to a specimen is detected at the other side of the sample, and then used to create a sample image [89]. Although better resolutions can be achieved with TEM (0.1 nm) than with SEM, the sample preparation tends to be more complex. TEM is also used to visualize the distribution of the constituents in particles and distribution of particles after uptake [13, 90, 91]. It is noteworthy that the use of a focused electron beam in TEM may damage the structure of material samples during the imaging.

A few examples of TEM for particle engineered by $scCO_2$ processes are available (see Table 1). TEM micrographs have been used to observe the internal structure of particles, e.g., to evaluate whether there are pores or localized structures in particles that indicate effective loading with a drug. Kalani and Yunus [13] showed the 15.5 nm thickness of a PLA outer shell filled with paracetamol inside, after coprecipitating in antisolvent CO_2 process. In addition, the TEM can be coupled with energy dispersion X-ray spectroscopy in order to analyze presence of

elements from a drug and excipient in nanoparticles prepared by Suspension-Enhanced Dispersion by Supercritical CO_2 (SpEDS), which is a modified version of the SEDS process mentioned in section 2.4 [90].

3.1.4.   Optical microscopy (OM)

The use of visible light to magnify an object by an objective and eyepiece lens is probably the oldest particle characterization technique for micron sized particles. OM has been applied for observing the formation of the $water_1$/oil/$water_2$ emulsion of drug/PLGA microspheres [41, 44]. The primary $water_1$/oil emulsion consisted of a water phase (a drug suspension in a solution of polyvinyl alcohol (PVA) in ethanol or DMSO) in an oil phase (PLGA in ethyl acetate), while the secondary $water_2$ solution was ethyl acetate-saturated aqueous PVA solution. The emulsion was later introduced into the supercritical fluid emulsion extraction (SFEE). After depressurization, the microspheres were formed while residual organic solvents in the $water_1$/oil/$water_2$ emulsion were extracted. The images of OM can be used for simple and fast screening of emulsion droplet formation. However, other techniques such as SEM or TEM may be required to observe more details of particle morphology [41, 44].

3.1.5.   Nanoparticle tracking analysis (NTA)

NTA analyzes particles in liquid solutions using the visualization of the light scattered by single particles and tracking of the Brownian motion of those particles. The instrument consists of a laser light scattering microscope with a charge-coupled device (CCD) camera, which enables the visualization and recording of the movement of nanoparticles in suspension, and a software, which will track and identify individual nanoparticles moving under Brownian motion and relates the movement to a particle size according to the Stokes-Einstein equation. This technique is suitable for particle sizes between 30 and 1000 nm, and particle concentrations in the range of 10^7–10^9/ml [92]. The measurement requires a small amount of a sample solution (less than 1 ml).

In a study of Nuchuchua et al. [71], NTA was used to determine of the nanoparticle size distribution and concentration in the reconstituted samples of dried protein/trehalose formulations prepared by $scCO_2$ spray drying. This study allowed for detection of nanoparticles in reconstitutions that could be protein aggregates. These results also led to further studies on the optimization of formulations in order to minimize the aggregation of proteins induced by $scCO_2$ spray drying [71].

3.1.6. Fluid imaging technology

Depending on the design and flow cell characteristics, fluid imaging microscopy (also called flow imaging microscopy) measures particles in range of 1 to hundreds of µm. Flow imaging microscopy methods capture picture frames when a solution stream (containing particles) passes through a flow cell centered in the field of-view of a custom magnification system having a well characterized and extended depth-of-field. The images are analyzed to collect data with respect to count, size, concentration, as well as other aspects like shape and contrast parameters [93-95].

ScCO$_2$ spray drying processing parameters such as pressure, temperature, pressurized CO$_2$ and spray drying, were studied with respect to their effects on myoglobin aggregation. By fluid imaging microscopy, the formation of myoglobin aggregates was observed in the range of larger than 1 µm after the myoglobin/trehalose formulation was incubated in the pressurized CO$_2$ (65-130 bar and 25-50°C) without spray drying. The aggregation was explained to have been induced by CO$_2$ acidification as the pH of the myoglobin formulation was decreased from 6.2 to about 5 [70]. This study is among the few that raised awareness that the scCO$_2$ processing under uncontrolled conditions may destabilize proteins. In other research studies on scCO$_2$ particle formation, biodegradable particles containing biologics were successfully analyzed by flow imaging microscopy [56, 57].

3.1.7. Light obscuration (LO)

Light obscuration is the blockage of light by particles in a suspension, when particles pass through the lit pathway. Analysis of the shadow of particles allows for extracting particle size distribution and concentration. This technique is able to measure particle sizes in the range of 1-200 µm. LO is currently, besides optical microscopy, the listed technique in the US and European pharmacopeias for giving specifications of sub-visible particle concentration in parenteral solutions [96-98]. LO, however, would give an inaccurate estimation of particle sizes and concentrations where there is a low optical contrast or small difference in the refractive index of the particles and the suspending fluid [93]. Despite the attractive features, LO has not been a frequently used particle characterization method in the area of particle engineering by scCO$_2$ techniques. In the single example included in Table 1, Sathigari et al. [52] obtained the particle size distribution of antifungal itraconazole microflakes with and without additives by LO and SEM. However, the average particle size from LO was smaller than the estimated average size derived from SEM images. As shown by the

images, the itraconazole without additives had more of a rectangular shape, while the itraconazole with additives formed the spherical cluster of rectangular shape, called microflakes. This study showed that LO has limitations in analyzing non-spherical particles.

3.1.8. *Scanning mobility particle sizer spectrometry (SMPS)*

Scanning mobility particle sizer spectrometry (SMPS) is typically used for measuring aerosols in the range of 2.5-1000 nm [99, 100]. The particles are brought to a bipolar charger to create electrical charges on particles, which are then separated in an electrical field in a differential mobility analyzer (DMA). The separation is by means of their electrical mobility (depending on particle diameter and charge). SMPS is particularly useful for determining size of particles in a solid dosage form, which is applicable to determine particles for inhaled drugs [101] and other powdered products [100].

SMPS was integrated in a RESS setup to monitor the size of naproxen-loaded PLA particles during the expansion in an aerosol phase. The particle size distribution was obtained and related to the particle production time in the RESS process. Pure naproxen particles showed an increase in the median diameter with increasing the processing time, whereas the naproxen-PLA did not. This implied that PLA helps to reduce the agglomeration of naproxen [46]. In this case, the in situ SMPS in the RESS process assisted to determine the particle size distribution before the end of the particle preparation process.

3.1.9. *Flow field-flow fractionation (Flow FFF)*

Flow field-flow fractionation (flow FFF) has become an interesting analytical separation technique used as a standard method for size characterization of protein aggregates and high molecular weight polymers (>10 MDa) as well as nano- and micro-sized particles. The separation is based on variations in the diffusion coefficient, described in the Stokes-Einstein equation, as a function of diameter, temperature and viscosity of samples [47]. Many operation setups have been developed such as symmetrical and asymmetrical parallel plate flow channels [48-51], trapezoidal asymmetrical parallel plate flow FFF [52-54] and circular hollow fiber flow FFF [55]. The underlying principle of the technique, however, remains the same.

Trapezoidal asymmetrical parallel plate flow FFF is a standard commercially available asymmetrical parallel plate flow FFF (AF4) [47]. In brief, the particles are introduced into a separation chamber on the top of a membrane near the inlet of the channel flow medium. Particles

are pushed and concentrated on the membrane by means of a cross flow. The different diffusion coefficient of particles allows the small particles which diffuse back faster to be rearranged on top of the larger ones. When the secondary flow in the direction of channel is introduced, the small particle sizes will be firstly eluted at the channel outlet, followed by the larger particles due to gradient flow speed that is faster in the center and slower towards the edges of the channel.

AF4 coupling with a refractometer, UV/Vis and fluorescence spectrophotometers and a multi-angle light scattering detector allows for determining the size and concentration of particles [92]. As shown by a study of Müller et al. [102], TiO_2 nanoparticles in a sunscreen were investigated for the labelling of nanoparticle-containing consumer products with respect to the EU regulation on cosmetics and food. Before analyzing the TiO_2 nanoparticles, a $scCO_2$ extraction process was chosen instead of using a solvent extraction method to remove lipid components in a sunscreen. Using the AF4 method, the UV detector was used to determine the concentration of TiO_2 nanoparticles while the light scattering detection module gave information concerning the nanoparticle size. The results showed that the size and concentration of the TiO_2 nanoparticles in the sunscreen were comparable to that of the unformulated nanoparticles. An aggregation of TiO_2 nanoparticles was also observed by the AF4 technique. Despite its capacity, particularly the wide size range of detection, the AF4 method has not been used to characterize $scCO_2$-engineered particles.

3.1.10. Disc centrifugal sedimentation

With this technique particles are separated based on settling velocity upon a rotation of a disc centrifuge plate [103, 104]. This method is used for nanoparticle characterization. To determine the size, particles are introduced into a rotating disc, which is filled with a slight density gradient fluid for stabilization with respect to the sedimentation velocity. Upon centrifugation, particles are spun out through the fluid and detected by light attenuation. This settling velocity can be correlated to the size of the particles. The rheological properties of the fluid (density, viscosity) are calculated using polyvinyl chloride standard particles with known density and hydrodynamic diameter. This method has been shown to be able to distinguish small differences in the size of nanoparticles in a dispersion, which is quite challenging for many other techniques such as DLS[105].

3.1.11. Tunable resistive pulse sensing (TRPS)

This technique measures the mobility of individual particles. The system is composed of a tunable membrane with an orifice (a sensing zone), the two sides of which are covered with an electrolyte solution. An electrical current is applied to both sides of the electrolyte solution. When particles are introduced at one side and pass through the orifice; the electrical current of the system will be temporarily changed giving a signal of short-lived electrical impedance for each particle. The height of the signal represents the particle size, whereas the frequency of the signals is a measure of the concentration of particles. The flow of particles through the orifice is controlled by a vacuum unit. Due to the electrophoretic mobility, this technique can also perform zeta potential measurements using Smoluchowski's approximation [106, 107]. TRPS is applicable to measure submicron-sized particles, such as 100-400 nm liposomes [108], 570 nm conductive polymer microgels [109], 1 µm magnetic spheres and aggregates [110] and emulsions less than 1 µm size [106]. Although TRPS has not been used to analyze particles prepared by scCO$_2$ processes, it is may be a promising method to determine individual particles in a suspension.

3.2. Drug loading and release

Drug loading is a process to incorporate drugs into carriers, dependent on the physicochemical properties of drugs and excipients. Incorporation process is based on several mechanisms of interactions between the drugs and the carrier such as hydrogen bonding, ionic interaction, dipole interaction, physical entrapment, precipitation, covalent bonding or surface absorption [111]. Typically in order to measure the total amount of drug in the particles, drug/excipient particles are often dissolved in an aqueous medium or organic solvent and the amount of the drug in the solution is measured by using a variety of techniques that will be discussed below [112, 113].

Drug release is a reverse process of detachment of the drug from carriers, to be ready for pharmacological action. A study of drug release can provide information of drug-excipient interactions and a prediction of *in vivo* behavior [111]. By using in vitro drug release tests, the particle production process can be optimized to achieve the desired release characteristics before *in vivo* pharmacokinetic tests are performed. In addition, *in vitro* results can guide certain aspects of the design of *in vivo* studies, such as sampling times [51]. In a typical *in vitro* release study, a separation of the drug from a particle matrix is needed. Often this separation is achieved by means of dialysis. A dialysis membrane will separate particles from released drug that can diffuse through the

membrane into a release medium [114]. The release medium is collected at time intervals and analyzed by a selection of techniques that allow precise determination of the drug concentration. Use of centrifugation and filtering is also common for separation of the released drug from the particles. *In vitro* drug release is usually measured in physiological buffers at the physiological temperature (37°C) [115]. Phosphate-buffered saline (PBS), with a pH of 6.8 or 7.2, is the most commonly used dissolution buffer for $scCO_2$ engineered particles (Table 1). Simulated gastric or intestinal fluid has also been used as a dissolution medium when the purpose is oral delivery. Sometimes additional reagents such as surfactants (e.g., polysorbate 20, polysorbate 80 or sodium dodecyl sulfate) or bacteriostatic agents are added to the dissolution medium to prevent surface adsorption of the released drug or to hinder bacterial growth in long-term release experiments [116, 117].

For preparation of controlled release particles by $scCO_2$ processes, various carriers have been used such as 1-vinyl-2-pyrolidone, dextran, PLA, PLGA and PEG (Table 1). Often the drug release mechanisms are complicated, for instance, for PLGA particles drug release involves drug diffusion through water-filled pores and a polymer, osmotic pumping, and polymer erosion. A drug release mechanism could be predicted by the release profiles in the so-called phase I, II and III. In the tri-phasic profile, phase I is a burst release due to the attribution of drugs on the surface of particle, followed by a slow release profile (phase II) of drug diffusion through matrix pores with the beginning of PLGA degradation. Phase III is a second burst release after the PLGA erosion [44-46]. Drug loaded PLGA microspheres showed differences in tri-phasic release profiles of phase I, II and III, depended on particle size, morphology and drug loading [44-46, 55-57]. An example study of Porta et al. [46] prepared insulin-loaded PLGA microspheres by a double emulsion method with $scCO_2$ solvent extraction. The results showed that the size of PLGA microparticles did not influence the loading degree but had great effects on the release of insulin particularly on the first day of the experiment.

3.2.1. UV/Vis and fluorescence spectrophotometry and liquid chromatography

UV/Vis and fluorescence spectroscopy are common techniques for quantifying the drug loading in the particles and released drugs (see Table 1 and Fig. 1). Whereas UV/Vis spectroscopy is more straightforward, fluorescence spectroscopy may be a preferred choice in cases where the sensitivity of UV/Vis is not sufficient or when excipients have UV absorbance and interfere with the UV signal. For that purpose

the drug is sometimes labelled with a fluorescence tag in order to have a stronger and more selective signal. In addition, there are a variety of biochemical assays in which interaction of secondary molecules with the drug results in a color change that is detectable by UV or fluorescence signals. In another widely used approach, UV and/or fluorescence detection coupled to the liquid chromatography are employed for determination of the loading and release. Liquid chromatography allows for separation of the drug from excipients, leading to enhanced selectivity. Moreover, concentrating the drug component in chromatography technique may increase sensitivity.   As seen in Table 1, the application of UV/Vis and liquid chromatography is very broad for determining various categories of drug compounds, such as proteins [69, 70, 118, 119], nonsteroidal anti-inflammatory drugs [41, 87, 120] and many others [81].

3.2.2. Thermogravimetric analysis (TGA)

Another method that has been used to study the drug loading is TGA. During a typical TGA analysis, a sample is gradually heated, while continuously being weighed, thereby measuring the weight gain/loss as function of the temperature. Mass loss may result from solvent evaporation, dehydration or degradation of the drug or excipients [121]. TGA can be used to quantify inorganic components in particles by performing the analysis up to a temperature at which drugs or other constituents are degraded. For example, in a study by Li-Hong et al. [122], where ibuprofen was loaded into silica microparticles with the assistance of $scCO_2$, the TGA curve associated with ibuprofen evaporation was found at an elevated temperature (150-250 °C) in the loaded silica microparticles. This study allowed for determination of the ibuprofen loading degree in the silica particles, showing that an increase in operating pressures of the $scCO_2$ impregnation process resulted in an increase in the degree of ibuprofen loading in silica microparticles.

3.3. Structure of drug/excipient components

Particles made by $scCO_2$ are drug/excipient complexes prepared with different drug depositions or encapsulation approaches that can result in chemical and/or physical changes in the native structure of the original components. Below we discuss methods to determine the structure of drug/excipient components after particle engineering processes by $scCO_2$.

3.3.1. Differential scanning calorimetry (DSC)

DSC allows for the identification of the temperatures at which thermal transitions like melting, glass transition and degradation occur [123]. The most common use of DSC in $scCO_2$ particle characterization is to compare the thermal characteristics of particles produced with $scCO_2$ technology with those of the individual components and/or physical mixtures. The absence of a melting and/or crystallization transition in a DSC thermogram may indicate that the material is in an amorphous state. The formation of particles exhibiting a disordered structure of drug and excipient, mostly results in an apparent increase in solubility, dissolution rate and oral bioavailability [124].

Additionally, a DSC thermogram can be used to indicate the presence of a molecular interaction between certain particle constituents. In a study by Kang et al. [112], after indomethacin was loaded in a polymeric matrix by using a SED process, the glass transition temperatures of the excipients and the melting point of the drug were lower than those of the physical mixture, indicative of a molecular interaction between the drug and the polymers. In another study by Cha et al. [61], the area under the melting peak in the thermogram was used to quantify the fraction of crystalline drug (fenofibrate) in particles prepared by a melt-absorption method using $scCO_2$. In this study, some level of disorder in the final product was desired in order to promote drug dissolution rate and bioavailability. DSC could therefore be used to optimize the production process by comparing crystallinity of particles produced with different techniques and under different conditions.

3.3.2. Spectroscopic methods

3.3.2.1. Fourier-transform infrared spectroscopy (FTIR)

Infrared (IR) spectroscopy exploits the fact that certain chemical groups absorb IR light at characteristic wavelengths, depending on inter- and intramolecular interactions [125]. Comparing the FTIR spectra of the pure materials with that of a particulate formulation can confirm the presence of intended constituents in the particles. In addition, the technique can be used to show (the absence of) molecular interactions between the constituents within a particle. Peak shifts in the spectrum of the particles indicate a molecular interaction or other changes in the bond associated with the peak.

After the particle formation by a SEDS process, no molecular interactions between puerarin and PLA was found. The FTIR signals were identical to those associated with the original structure of both

components [63]. In addition, FTIR analysis supported a release study of puerarin from PLA particles by indicating that a representative peak of puerarin component completely disappeared after puerarin was released for 48 hours from microparticles [63]. Similar release studies were observed in the cases of 5-fluorouracil-SiO_2-PLA and methotrexate in multilayer PLA microspheres, obtained from SAS and SED processes [62, 64], respectively. These results suggested the physical co-precipitation of drug/excipient by the $scCO_2$ processes. In another study, a complex of fenofibrate and mesoporous silica (SBA-15) was prepared by the $scCO_2$-assisted impregnation and studied by FTIR. FTIR spectra revealed a shift in the peak associated with the silanol group of the silica constituent of the particle, which the authors ascribed to hydrogen bonding between the carbonyl group of the drug (fenofibrate) and the silanol group in the silica. This molecular interaction between drug and excipient indicated an effective loading of fenofibrate into the silica carrier [126]. In the work of Jovanović et al. [118], lysozyme formulations with and without sugar excipient were dried using a $scCO_2$ spray drying process. The structure of α-helix and intermolecular β-sheet of the reconstituted lysozyme was determined using FTIR. A decrease in the α-helix content (representing lysozyme destabilization) and an increase in the β-sheet content (indicating the formation of protein aggregates) were found in the case of lysozyme formulation without sugar. The results demonstrate the stabilizing effect of sugar on the protein during the $scCO_2$ spray drying process.

3.3.2.2.   *Fluorescence spectroscopy*

Fluorescence spectroscopy is a light interaction technique used for the detection of fluorophores (fluorescent molecules), which absorb electromagnetic radiation with a specific energy (called the excitation wavelength) and emit the energy at a specific wavelength called the emission wavelength [127]. For protein research, tryptophan residues are often selectively excited at 295 nm, because their emission intensity and wavelength maximum are strongly dependent on their local environment, and thus can be used to probe changes in protein conformation [70, 128]. Intrinsic tryptophan fluorescence emission spectra of polyclonal IgG were similar before and after exposure of the protein to a $scCO_2$ spray drying process, suggesting that its tertiary structure was fully preserved [119]). Fluorescence spectroscopy was used to determine the heme loss of myoglobin after $scCO_2$ spray drying. Basically, the tryptophan residues in myoglobin are quenched by heme, giving a low fluorescence intensity for native myoglobin. However, the $scCO_2$ spray dried myoglobin showed an increase in the fluorescence

intensity, specifically suggesting that the heme was partially removed from myoglobin during the $sccO_2$ spray drying process [69, 70].

3.3.2.3.   *Circular dichroism spectroscopy*

Another spectroscopic method is circular dichroism (CD), which is used to determine the chirality of chemical compounds, which give unequal absorption of left-handed and right-handed polarized light [129]. CD is a useful technique to determine the secondary structure of proteins in the far-UV wavelength range (190-250 nm), and the tertiary structure in the near-UV wavelength range (250-350 nm) as well as the specific binding properties of proteins (e.g., ligand binding) [69-71, 130, 131]. For a series of $scCO_2$ spray dried protein formulations based on lysozyme, a-lactalbumin, a-chymotrypsinogen A and monoclonal antibody, no changes in the Far-UV CD or Near-UV CD spectra were observed compared to the untreated formulations [71]. This suggests that there is no change in the secondary or tertiary structures of these proteins after $scCO_2$ spray drying. In a case study of myoglobin, however, the visible CD signal from the bound heme group at 409 nm was decreased after the $scCO_2$ spray drying process, while the far-UV signal of myoglobin was not altered when compared to the untreated myoglobin, suggesting that the heme binding site was altered, which could be due to the loss or dislocation of the heme group during the $scCO_2$ spray drying process [69, 70].

3.3.3. X-ray diffraction (XRD)

X-ray powder diffraction is used for characterization of the crystallinity in solid materials. For a crystalline material, sharp X-ray diffraction peaks will be visible, which are absent in an amorphous material. This technique has been used for $scCO_2$ particle characterization. The absence of sharp peaks observed in the spectrum of the particles indicated absence of the crystalline state in the nilotinib (tyrosine kinase inhibitor)/hydroxypropyl methylcellulose hybrid nanoparticles prepared by the $scCO_2$ anti-solvent process. The amorphous structure was shown to lead to an improvement in several properties such as desired dissolution rate of nilotinib, improved GI absorption and bioavailability in male beagle dogs [132]. XRD was also used to study the crystallinity of sugar excipients in a $scCO_2$ spray dried protein formulation. Immediately after spray drying, the X-ray diffraction peaks of sucrose were absent, but were later detected after 1 month storage at 4 °C [118]. The presence of a crystalline state is in many cases undesirable, as it can be an indication that the drug and other excipients are not molecularly dispersed. Presence of crystalline structure in the drug or excipients may suggest that the drug is locally

deposited on the surface of microparticles (rather than being mixed). For example, the incomplete encapsulation of 10-hydroxycamptothecin in PLA by a scCO$_2$ anti-solvent process led to appearance of clear peaks form the crystalline structure of the 10-hydroxycamptothecin [133]. In a different study, the polymorphism of the anti-inflammatory drug diflunisal was observed by XRD, after its precipitation in polyvinylpyrrolidone in a scCO$_2$ anti-solvent process. The polymorphism of diflunisal influenced its dissolution [134].

3.4. Particle surface analysis

3.4.1.Energy dispersion X-ray spectroscopy (EDX)

When a sample is irradiated with an electron beam, electrons present in the sample can be displaced from their electron shell. When this 'vacancy' in the electron shell is filled by an electron from a higher energy electron shell, X-rays are emitted to release excess energy. The energy of these X-rays is characteristic for the element from which they are emitted, which is exploited in the EDX to investigate the elemental composition of a sample [135].

By combining this technique with SEM, a presence of a discriminating element (that is present in one particle constituent, but not in others) can be visualized within the SEM/EDX image. In several studies this method has been used to investigate the distribution of the drug within particles, or to confirm that drug/polymer particles were produced. In a study by Kalani et al. [13], the absence of chlorine in a final product confirmed the successful elimination of the chlorinated solvent used during SAS process. Della Porta et al. [41, 45] showed the distribution of piroxicam or diclophenac sodium on a PLGA matrix after scCO$_2$ processes, by analyzing the distribution of the sulfur atom of piroxicam and the chlorine atom of diclophenac sodium. The SEM/EDX images showed low intensity of fenofibrate's chloride atom when fenofibrate was successfully impregnated in mesoporous silica using the scCO$_2$ loading process, compared to its physical mixture [136]. A similar result was found when fenofibrate was distributed into the pores of Neusilin® UFL2 (magnesium aluminometasilicate) [61]. Moreover, the group of Compardelli et al. [137] coupled EDX analysis to TEM to analyze hollow gold nanoparticles (HGNs) in PLA nanospheres, which were used to encapsulate rhodamine using a non-solvent CO$_2$ process. The EDX spectrum presented the composition of gold (the Au peak), and also the residual impurity of cobalt and chlorine from the synthesis of HGNs.

3.4.2. X-ray photoelectron spectroscopy (XPS)

XPS is used to measure the elemental composition of the particle surface. The technique is comparable to EDX, but the sample irradiation occurs with X-rays instead of an electron beam. In XPS, the electrons displaced by the X-rays (photoelectrons) are detected. The energy of the photoelectrons are characteristic for the elements emitting them and the number of photoelectrons emitted is directly proportional to the abundance of an element [138]. The biggest difference between the application of EDX and XPS is that XPS measures the elemental composition of the particle surface at its outermost layer up to tens of nm in depth whereas EDX provides elemental information from a depth of hundreds of nm to a couple of µm. The chance that photoelectrons escape the sample decreases exponentially with increasing depth. XPS was used by Montes et al. [139] to demonstrate that a shell was actually in place in particles that had a core-shell structure. In this study, using a SAS process to encapsulate amoxicillin in ethyl cellulose particles, UV/Vis spectrophotometry gave about 35-50% loading efficiency of amoxicillin. However, the photoelectrons emission of the nitrogen atom in amoxicillin was not found on the particle surface by XPS, suggesting that the amoxicillin was located in the core surrounded by the ethyl cellulose shell. In a study by Chen et al. [87], XPS was used to investigate the localization of Fe_3O_4 nanoparticles within PLA-magnetic microparticles, which were prepared using the Suspension-Enhanced Dispersion by supercritical CO_2 (SpEDS) process. The authors concluded that the nanoparticles were successfully encapsulated inside the microparticles, rather than adhering to the surface.

3.4.3. Atomic force microscopy (AFM)

AFM is used for studying the topography of a particle surface. AFM analysis is based on the interaction force between a tiny tip (usually made from silica or silicon nitride) on a cantilever and the sample when the tip is dragged on a sample surface. The interaction results in the deflection of the cantilever that is reflecting a laser light to a photo diode detector. The deflection data is therefore recorded and turned into a constructed image on the operating computer during measuring. AFM is mostly used to create high-resolution images in the nano-scale range [140]. The drug loading in particles may change a particle surface as found in a study of Della Porta et al. [45] where they studied the surface roughness of drug/PLGA microsphere particles produced by a $scCO_2$ technique and an emulsion method. The surface of drug/PLGA particles from both preparation methods was moderately wrinkled,

whereas that of the pure PLGA particles was smooth, indicating that the wrinkles on particle's surface may be related to the drug dispersion in the PLGA polymer.

3.5. Porosity analysis

3.5.1. Brunauer-Emmett-Teller (BET) surface area analysis and Barrett-Joyner-Halenda (BJH) pore size and volume analysis

In pharmaceutics, a porous drug carrier such as mesoporous silica and magnesium aluminometasilicate, provides a high surface area to increase drug loading capacity [61, 141, 142]. Porous particles are characterized in terms of surface area and porosity analysis before loading drugs in order to check pore availability. After filling with drugs, the surface area and porosity of the particles are normally decreased. The analysis of gas adsorption is a widely used characterization technique for porous materials [143]. The measurement is commonly conducted at -196 °C, the gas molecules (typically N_2) are allowed to absorb as a monolayer on the free surface of the particles. A rise in pressure leads to complete gas filling into pores. Changes pressure and analysis of the adsorption phenomena can be used to calculate the surface area and pore size and volume distributions by using theoretical equations by Brunauer-Emmett-Teller (BET) and Barrett-Joyner-Halenda (BJH), respectively [144, 145]. However, the gas absorption would be influenced by a heterogeneous surface of the particles [143].

Neusilin UFL2 is a fine porous powder of magnesium aluminometasilicate used for drug absorption. Cha et al. [61] used the above-mentioned method to analyze the surface area and pore size distribution of Neusilin UFL2 excipients. The specific surface area and total pore volume of Neusilin UFL2 decreased with an increasing fenofibrate-to-Neusilin UFL2 ratio. As compared to hot-melt adsorption and solvent evaporation methods, the supercritical CO_2 method facilitated complete pore filling of fenofibrate into the pores of Neusilin UFL2. Similar results were obtained by Ahern et al. [136] and Li-hong et al. [122] who reported a reduction of the pore volumes of silica microspheres after drug loading processes with $scCO_2$.

3.5.2. High-pressure mercury intrusion porosimetry (HPMIP)

In a typical intrusion porosimetry, a non-wetting liquid is intruded into a porous material at high pressure. Mercury is the most commonly used substance for this application due to its non-wetting properties on solid surfaces. An external pressure is used to force mercury into the

pores, to overcome the surface tension of the liquid and the angle of contact with the solid surface. The employed pressure and volume of mercury after intrusion and extrusion is used to determine the pore size and volume network, pore size distribution, density and particle size. [146]. This technique can be applied for pore sizes between 3.5 nm and 500 μm [146]. For HPMIP to be effective, the pore structure needs to be accessible via the surface of the particle, and also interconnected. Usually HPMIP shows smaller pore sizes compared with SEM or optical micrographs [146].

In recent studies [66, 67], solid microspheres of lysozyme/PLA with ammonium bicarbonate (used to make pores) were formed by the PCA process. In order to obtain porous microparticles, the ammonium bicarbonate was eliminated in a vacuum step and HPMIP and SEM were used to determine the porosity of particles, which was then used to evaluate their potential aerodynamic behavior. The result showed that an increase in particle porosity led to a decrease in a density of particles, which in turn influenced the aerodynamic behaviour [66, 67].

3.6. Surface charge

The zeta potential is a measure of the surface charge of particles in a suspension [147]. More specifically, it is the average electrostatic potential between the slipping plane of a particle and a point in the fluid phase (away from the particle) [148]. Zeta potential is not measured directly, but theoretical models are used to calculate it [149].

Zeta potential is often used to predict the colloidal stability of drug-loaded particles produced by $scCO_2$ processes [91, 132, 150]. A large absolute zeta potential will result in repulsion between particles, which increases the colloidal stability of suspensions by reducing agglomeration [151]. Absolute zeta potentials above 30 mV are generally required for sufficient electrostatic stabilization, although steric stabilization can supplement a relatively low electrostatic stabilization. The zeta potential was used as an indicator to evaluate incorporation of positively-charged lysozyme in negatively-charged $CaCO_3$ particles during a $scCO_2$ process. The results showed that the negative zeta potential of $CaCO_3$ particles was decreased when lysozyme was incorporated into the particles [152].

A particle's zeta potential also may affect its pharmacokinetics, mucoadhesion and toxicity, but these aspects have not been addressed in studies dealing with $scCO_2$ engineered particles presented in Table 1. Zeta potential has been manipulated to achieve a desired targeting or biodistribution. Chitosan, a deacetylated derivative from a

naturally occurring polysaccharide, can be used to produce particles with a positive zeta potential [153]. This positive charge gives the particles mucoadhesive properties where the negative charge of the mucus and mucosal surface promote electrostatic interaction with the particles [153, 154]. Zeta potential has also been reported to affect protein adsorption; for instance, positive zeta potentials result in more adsorption of bovine serum albumin, which has a negative zeta potential at pH 7.4 [9, 155, 156]. The cytotoxicity of nanoparticles has also been related to their surface charge; positively charged particles tend to be more cytotoxic in non-phagocytic cells and could cause membrane damage. Negatively charged particles are more likely to cause intracellular damage and apoptosis [157].

3.7. Biotherapeutic activity and efficacy

A major goal in clinical pharmacology is to understand the dose-effect of designed drugs on biotherapeutic efficacy. The intrinsic activity has to do with the determination of biological responses regarding to an affinity of drug binding to a receptor, while the potency is related to the amount of drug required to give a therapeutic effect. For drug delivery applications, it has been suggested that particle formation by $scCO_2$ processes can improve biotherapeutic efficacy, drug targeting or reduce drug toxicity. However, as shown in this review paper, most of the studies so far are mainly focused on optimizing conditions for the preparation of drug/excipient nano- and microparticles for an application and only a limited number of studies go beyond particle preparation. The testing of drug activities in these papers are mostly carried out by *in vitro* methods that are related to the original activities of model drugs such as enzyme activity [66, 152], antioxidant property [158], antibacterial activity [76] and cell culture based assays (e.g., cell proliferation and antitumor activity) [91, 112] [67]. In addition, a few cited articles show that nano- and microparticles engineered by $scCO_2$ technology are applicable to vaccine and therapeutic protein delivery. For these specific applications, animal models (e.g., rats, rabbits and monkeys) are used to observe drug bioavailability after intravenous, oral, subcutaneous, and pulmonary administration. Drug levels and therapeutic efficacy in biological systems are usually determined by withdrawing blood serum from the animals [55, 65]. Particle based formulations often show improved biotherapeutic efficacy and bioavailability with the effect of a sustained drug release. For instance, a single shot tetanus toxoid/PLGA microparticles from the PGSS (NanoMix™) process was able to maintain the antigen activity for five months and potentially repeat the stimulation of antigen presenting cells that, in turn, could lead to the elimination of the need for booster

dosage of the vaccine [55]. In another example, 5-fluorouracil-loaded PLA-PEG/PEG nanoparticles prepared using the reverse emulsion-SEDS process showed a prolonged drug release and half-life, as well as an increase in diffusion into a tumor tissue. Compared to the non-particulate 5-fluorouracil, the nanoparticles improved an inhibition rate on tumor cells and increased the lifespan by a factor two [65].

3.8. Toxicology

In vitro experiments are important for the initial toxicological studies of micro/nanoparticles because they can provide mechanistic information and are inexpensive compared to animal studies [159, 160]. There are several *in vitro* assays for cytotoxicity, which can measure cell viability or test for a certain mechanism of toxicity [161]. Cell viability assays evaluate toxicity of particles by monitoring processes like membrane integrity, metabolic activity and DNA synthesis. Mechanistic assays monitor specific types of toxicity, such as DNA damage or oxidative stress. However, the absorption/emission spectra and light scattering of nanoparticles can in some cases result in false positive/negative signals in colorimetric assays [159]. In other cases particles interfere with the assay though unintended chemical reactions with reagents; for instance, several types of particles have been shown to interfere with the MTT assay, by reducing the tetrazolium salt to the product, resulting in a reported cell viability of over 100% [161]. Therefore, it is important to confirm absence of interference of a particle with the *in vitro* toxicology assay in order to ensure that the results are valid [162].

Zhang et al. [65] observed an *in vivo* hepatotoxicity on rats after administering 5-fluorouracil-loaded PLA-PEG/PEG nanoparticles prepared by a reverse emulsion-SEDS process. The liver cells stained with haemotoxylin and eosin dyes were investigated by using electron microscopy. The nanoparticles from the $scCO_2$ process showed no harmful drug hepatotoxicity on rats comparable to the untreated group.

3.9. Residual solvent and water content analysis

Organic solvents are occasionally used in $scCO_2$ particle engineering techniques or during preparation of emulsion samples. Residual solvents in the final product may cause toxicity and therefore certain limits for residuals in the pharmaceuticals have been proposed by the ICH harmonized guideline Q3C (R5) [101]. Residual organic solvents can be analyzed by the static head-space method of gas chromatography (GC). The sample is incubated at relative high temperature to allow the evaporation of solvents as a gas phase, which will be separated in a stationary column. Generally speaking $scCO_2$

techniques usually help to remove residual organic solvents because of solubility of organic solvents in $scCO_2$. After the depressurization process, the solvent concentration in particle products is often less than other conventional encapsulation methods [18, 21, 33, 81, 102].

The residual water content of dried particles has been shown to influence the stability of the particles and also that of incorporated biopharmaceuticals during storage. [71, 163] A common method to determine the residual water content is Karl Fischer titration [71]. Alternatively, TGA can be used to determine the amount of residual moisture and/or solvent in a sample by monitoring the weight loss when the sample is heated. For example, TGA coupled with FTIR was used by Bouchard et al. [164] in order to determine the amount of residual water and ethanol in $scCO_2$ dried protein formulations.

3.10.   Other specific properties

The particle characterization techniques described above may not be exhaustive and other characterization techniques may be needed, depending on the type or the functionality of particles. An example of a drug delivery functionality is mucoadhesion, which can be desired if the target tissue is one with a mucosal surface, such as targets in respiratory and gastrointestinal systems [165], or when systemic effects following mucosal administration are the aim [166]. In a study by Patel et al. [113], an *ex vivo* wash off test was performed after applying microparticles to a piece of rat stomach mucosa. This allowed the authors to evaluate mucoadhesion, prior to any *in vivo* experiments.

Another example of particles that require additional characterization are magnetic particles. Magnetic particles can be used as an MRI contrasting agent, but could also be guided to the target tissue with a magnetic field [167]. In two $scCO_2$ particle engineering studies, particles were created containing Fe_3O_4, a drug and a polymer [87, 90]. The saturation magnetization of the particles was measured by a vibrating sample magnetometer, to confirm that particles with desirable magnetic properties were successfully created.

4.   Summarizing discussion

The analysis of the information gathered in this review (Fig. 1) indicates that when particle products are obtained, normally, particle size and morphology are investigated as key properties that points to the success of the particle preparation process [11]. Concerning this class of properties, it is noteworthy that, often, a single characterization method

is unable to provide a full picture with respect to the size and morphology. For instance, although light scattering methods such as dynamic light scattering (DLS) and laser diffraction (LD) are often chosen to obtain information about particle size and size distribution, these methods have serious shortcomings especially when the analyzed sample has a wide size distribution [92]. Moreover, DLS and LD do not give information about the number of particles. In addition, the particle size is usually presented in the form of an average diameter, however, many particles are produced in asymmetric shapes with different ratios of horizontal and vertical projections. Shape factor often causes considerable disagreements between measured average diameter and real size for a range of particle size analyzers. As a result, to improve the reliability of particle size determination, it would be recommendable to use a couple of techniques that use different physical principles (so called orthogonal methods), such that method specific limitations do not compromise the overall picture [168]. In this context it is recommendable to use one of the imaging-based techniques, to give information about the size, shape and other general aspects at the same time [8].

Furthermore, the drug loading degree and *in vitro* drug release are among the most studied parameters that help understanding the quantity and quality of drug incorporation in a particulate system. However, it is important to realize, that the other properties may be determining parameters for pharmaceutically relevant particles, particularly because the scCO$_2$ processes may change the structure of drugs and carriers. For instance, Keles et al. [169] found that scCO$_2$ enhanced the hydrolysis of PLGA (that was used as a matrix carrier for the drug), thereby creating a porous structure when the ratio of lactide to glycolide was low. Similarly, the particle formation process may also lead to the degradation of active ingredients, such as protein drugs that have been shown to undergo destabilization by CO$_2$ acidification [70]. Other processing parameters in scCO$_2$ technologies may also cause degradation (e.g., structural change, loss of activity and aggregation) of proteins.

Therefore, analysis of the drug/excipient structure is the next widely studied category of properties in particles prepared with scCO$_2$ technologies. Considering the susceptibility of biopharmaceuticals to degradation and also the fast growth of this group of drugs in modern medicine, special consideration regarding the characterization of particles that carry these drugs will be underway. A number of studies have used analytical techniques (such as UV/Vis spectroscopy, circular dichroism, fluorescence spectroscopy, size-exclusion chromatography and flow-imaging microscopy) for mere purpose of characterization of

protein structure and aggregation [70, 71]. These tools were also able to characterize typical $scCO_2$ dried proteins such as lysozyme, a-lactalbumin, a-chymotrypsinogen A, monoclonal antibody and myoglobin [70, 71]. Considering that it is difficult to recommend a set of standard analytical techniques for determining protein integrity due to the diversity and specificity of each protein as well as the type of particles, the selection of techniques is based on the product of interest. Numerous fundamental techniques for characterization of therapeutic proteins are summarized and explained elsewhere [170, 171].

Following these principal properties, surface chemistry of the particles as well as surface charge are among the ones that have been addressed in the $scCO_2$ literature. Some important properties such as porosity of particles, pharmacological activity and cytotoxicity are also studied although less frequently. Some other parameters such as storage stability of the $scCO_2$-engineered particles have not been addressed despite the fact that insufficient stability can hinder the applicability of particles for drug delivery applications [172].

Observed differences in the frequency of use of particle characterization techniques are in principle related to how basic the properties are and for what purpose they are prepared. We cannot rule out the possibility that it may also depend on less scientific factors such as the straightforwardness of a certain characterization or availability of equipment in the workplaces. In addition, availability of knowledge concerning the relations between a certain property and function would result in an incentive for in-depth characterization in that area. For instance, recent knowledge concerning the stability issues associated with biopharmaceuticals has led to extra attention to the use of methods that address those. Overall, establishment of a good scientific ground for preparation of particles with desired size and loading properties would make room for more thorough characterization with respect to other potentially relevant properties such as bioactivity, toxicology, clinical trials and long-term particle stability.

Table 2. Particle characterization techniques used and potentially useful in scCO$_2$ technologies for particle engineering.

Particle characterization technique	Principle	Applicability limits and other considerations
1. Particle size distribution and morphology		
Dynamic light scattering (DLS)*	Relates the variation of the light scattering signal coming from particles in a suspension to their Brownian motion and size (random particle movements are related to particle size, viscosity, and temperature)	For particles in the range of 5-1000 nm, For liquid samples and particles in a suspension, Difficult to analyze polydisperse samples, No concentration information, No shape information
Laser diffraction (LD)*	Analysis of the scattering of static light by particles in a suspension at multiple angles	For particles in the submicron to millimetre size range, Liquid sample, Requires large amount of sample, No concentration information, No shape information
Scanning electron microscopy (SEM)*	Electron beam interacts with the surface and backscattered or secondary electrons coming out of the surface is detected. This information is used to reconstruct an image	For particles in the range of a few nm up to a hundreds of μm, For dried particles, Low throughput analysis, Needs sample treatment such as applying a conductive coating, No information about concentration, Very informative about the shape and features of the particles

Technique	Principle	Characteristics
Transmission electron microscopy (TEM)*	Electron beam interacts with the thin sample and electrons coming out of the other side of the thin sample are detected. This information is used to reconstruct an image	For particles in the range of a few nm up to a hundreds of μm, For dried particles, Low throughput analysis, No information about concentration, Very informative about the shape and features of the particles
Optical microscopy (OM)*	Magnification by use of an object and an eye lens	For particles in the range of a μm to hundreds of μm, Suitable for both liquid and dry samples, Low throughput analysis, No information about concentration, Very informative about the shape and features of the particles
Nanoparticle tracking analysis (NTA)*	Tracking of light scattering signal coming from individual particles in a suspension and relating the movement of particles to the size	For particles in the range of 20-1000 nm, For liquid samples and particle in a suspension, Multiple parameter settings during video recording and particle analysis, Provides concentration information, No shape information
Fluid imaging microscopy*	Particle suspension flowed in a narrow chamber and imaged	For particles in the range of a μm to hundreds of μm, Liquid sample, Provides concentration information, Very informative about the shape and features of the particles

Light obscuration (LO)*	Blocking of light by particles in a suspension and analysis of the shadow to get information about the size	For particles in the range of a μm to hundreds of μm, Liquid sample, Provides concentration information, Sensitive to presence of translucent particles, No shape information
Scanning mobility particle sizer spectroscopy (SMPS)*	Particles charged and their mobility analyzed and related to the size	For particles in the range of 2-1000 nm, For dry particles, No shape information
Flow field-flow fractionation (Flow FFF)	Separation of particles in a flow channel as a result of size dependent diffusion properties	For particles in the range of nm to a few μm, For liquid samples, Optimization for each sample required, No shape information
Disc centrifugal sedimentation	Analysis of the sedimentation velocity of particles under centrifugation	For particles in the range of a few nm to hundreds of nm, Liquid sample, Need for optimization of the fluid density gradient, Size determination depending on calibration particles, No direct concentration information
Tunable resistive pulse sensing (TRPS)	Particles passing a narrow pore influence the baseline electrical resistance between the two sides. This resistance is proportional to the size of particles	For particles in the nm size range or μm size range depending on the type of membranes and the pore size, Liquid sample, Baseline signal is sensitive to small changes

		in the environment and is difficult to stabilize
2. Drug loading and release		
UV/Vis and fluorescence spectroscopy*	Analysis of the interaction of light with the drug at a certain wavelength in the UV/Vis range and relating it to the concentration of the drug	Straightforward and reliable for determining the concentration of drugs. Liquid sample. The detection limit may be relatively high for some samples. Interference by scattered light from particles/separation needed
Chromatography tools* (e.g. liquid chromatography)	Separation of the drug in a column and measuring the concentration of it using a range of detectors such as UV and fluorescence detectors	Suitable for concentration measurements, Liquid sample, Allowing for detection of relatively smaller amounts due to concentrating and purifying in the separation phase, Provides information about other separated components, Separation phase and elution medium have to optimized, Sensitive to blockage of columns
Thermogravimetric analysis*	Follows the degradation of components when temperature is increased and relates it to their amount	Suitable for measuring the amount of components and carriers Depending on their reaction to heating, Dry sample
3. Structure of drug/excipient components		
Differential scanning calorimetry (DSC)*	Thermoanalytical technique for monitoring thermal events during	Suitable for obtaining information on sample crystallinity, glass transition temperature, melting point,

	heating to detect the changes in material phases	liquid and dry samples, Needs background info about the behavior of the individual components
Spectroscopic methods; - Fourier transform infrared spectroscopy (FTIR)*	Follows absorption of infrared light and relates it to the vibration status of certain chemical groups	Provides information about the chemical groups and their interaction with their environment, For dry or liquid sample, Needs sample preparation, Allows for protein structure analysis, No quantitative analysis
- Fluorescence spectroscopy*	Absorption and emission of the specific wavelength of light	Fluorophores, Liquid sample with an adequate concentration, Should know the maximum absorption and emission of light for the given fluorophore
- Circular dichroism (CD)*	Unequal absorption of left-handed and right-handed polarized light of a chiral compound. The sinusoidal wave is as a result of such two different signals of the polarized light.	Chiral compounds, Determining protein secondary and tertiary structures and specific binding property of proteins, Liquid sample should be freshly prepared, Known concentration and cuvette size are needed for the calculation of the CD signal
X-ray diffraction*	Diffraction patterns of X-ray interacting with the material analyzed and related to the order of atoms in the material	Suitable for analysis of sample crystallinity, For dry sample, Allows for determination of percentage

		crystallinity, Requires vast background knowledge on the diffraction patterns of potential components
4. Surface chemistry		
Energy dispersion X-ray spectroscopy (EDX)*	Irradiation of samples with an electron beam results in emission of X-ray due to jump of electrons from one energy band to another, the energy of these X-rays is characteristic for the element from which they are emitted	Suitable for elemental analysis at the surface of the material, For dry sample just as used for SEM, The signal is from a depth of a few hundred nm to a couple of μm, Allows for mapping of the elements on the surface, Not sensitive for light elements
X-ray photoelectron spectroscopy (XPS)*	Irradiating samples with X-ray and analysis of photoelectrons emitted from the surface, the amount and energy of the electrons give information about the abundance and type of the elements	Suitable for chemical analysis of the surface, Dry sample, Information form the outermost layer of the surface (depth of 0 – 10 nm)
Atomic force microscopy (AFM)*	Scanning of the surface of the sample with a fine tip and following the movements of the tip due to the feeling of the topographical features of the surface	Suitable for analysis of the surface topography, For solid surfaces either dry or fixed in situ, Provides a topographical map at the nanoscale, Can give information about the type of material in phase mode, Particularly suitable for composites
5. Porosity analysis		

Brunauer-Emmett-Teller (BET) Surface Area Analysis and Barrett-Joyner-Halenda (BJH) determination*	Analysis of gas pressure and gas adsorption to the surfaces of the pores, relating them to the total surface area and therewith amount and characteristics of the pores	Suitable for determination of the porosity of samples, Sample has to be dry, Particle agglomeration may lead to false impressions, Sensitive to modelling errors
High-pressure mercury intrusion porosimeter (HPMIP) *	Insertion of mercury into a porous material by pressure	Suitable for determination of pore diameter, pore volume and pore distribution, Dry sample, Not suitable for closed pores, Toxic mercury waste
6. Surface charge		
Zeta potential measurement (ZP)*	analysis of electrophoretic mobility (laser Doppler electrophoresis) of particles in a suspension	Measurement of zeta potential, Liquid sample, Zeta potential depends on pH and ionic strength of the buffer used
7. Biotherapeutic activity and efficacy		
In vitro activity assay*	Depending on the active compound, e.g., analysis of enzyme activity, antibacterial assay, antitumor activity, antioxidative activity	Difficult to model the physiological environment, Potential interference of excipients with the assays
In vivo study*	Testing of the drug delivery system in animal models; e.g., subcutaneous, IV, oral administration	Can observe bioavailability, pharmacokinetic study, biodistribution, efficacy, Complex animal model development, Expensive and laborious, May not correlate with human data

8. Toxicology		
In vitro cell-based assays*	Drug toxicity to cells; i.e., tumor cells, immune cells, fibroblast and other cells	Difficult to model the physiological environment, Potential interference of excipients with the assays
In vivo animal studies*	Drug toxicity evaluated in animal models	Expensive and laborious, May not correlate with human data
9. Residual solvent and water content analysis		
Gas chromatography (GC)*	Solvent evaporation and separation monitored	Measurement of residual solvent content, Liquid or dry samples, Challenges for less volatile substances
Karl Fischer titration*	The amount of residual water content in dry samples by titration of other compounds and colorimetric or volumetric detection of reactions	Suitable for determination of the residual water content in dried particles
10. Other specific properties		
Mucoadhesion*	The adhesion of a material on mucosal surface studied by a range of in vitro procedures	Suitable for studying interaction of particles with mucus, Difficult to model the mucus
Magnetic measurement*	Analysis of the behavior of particles in a magnetic field	Suitable for analysis of targeting with an external magnetic field, Magnetic particles are normally good contrast agents for imaging

*Used in scCO$_2$ particle engineering

Abbreviations of scCO$_2$ engineering processes

Supercritical carbon dioxide (supercritical CO$_2$ or scCO$_2$)

Rapid Expansion of Supercritical Solutions (RESS)

Non-solvent RESS process (RESS-N)

Supercritical solution into a liquid solvent (RESOLV)

Aerosol Solvent Extraction System (ASES)

Supercritical Fluid Emulsion Extraction (SFEE)

Supercritical Anti-Solvent (SAS)

Precipitation with Compressed Anti-solvent (PCA)

Supercritical Anti-Solvent with Enhanced Mass Transfer (SAS-EM)

Supercritical Anti-Solvent Drug-Excipient Mixing (SAS-DEM)

Particles from Gas Saturated Solutions (PGSS)

Gas-Assisted Melting Atomization (GAMA)

Solution-Enhanced Dispersion by ScCO$_2$ (SEDS)

Suspension Enhanced Dispersion by scCO$_2$ (SpEDS)

Reverse-emulsion-Solution Enhanced Dispersion by scCO$_2$ (reverse emulsion-SEDS)

ScCO$_2$ assisted atomization (SAA)

Carbon dioxide-assisted nebulization with a bubble dryer (CAN-BD)

References

[1]   O. C. Farokhzad, R. Langer, Impact of nanotechnology on drug delivery, ACS Nano, 3 (2009) 16-20.

[2]   A.H. Chow, H.H. Tong, P. Chattopadhyay, B.Y. Shekunov, Particle engineering for pulmonary drug delivery, Pharm Res, 24 (2007) 411-37.

[3]   M. Manzano, V. Aina, C.O. Areán, F. Balas, V. Cauda, M. Colilla, M.R. Delgado, M. Vallet-Regí, Studies on MCM-41 mesoporous silica for drug delivery: Effect on particle morphology and amine functionalization, Chem Eng J, 137 (2008) 30-37.

[4]   M.L. Etheridge, S.A. Campbell, A.G. Erdman, C.L. Haynes, S.M. Wolf, J. McCullough, The big picture on nanomedicine: the state of investigational and approved nanomedicine products. Nanomedicine, 9 (2013) 1-14.

[5]   A. L. Vasilakes, T.D. Dziubla, P.P. Wattamwar, Polymeric Nanoparticles. In Engineering Polymer Systems for Improved Drug Delivery, R.A. Bader and D.A. Putnam, Editors. 2014, John Wiley & Sons. p. 117-148.

[6]   S.P. Schwendeman, R.B. Shah, B.A. Bailey, A.S. Schwendeman, Injectable controlled release depots for large molecules. J Control Release, 190 (2014) 240-53.

[7]   P. York, U.B. Kompella, B.Y. Shekunov, Supercritical Fluid Technology for Product Development. Vol. 138. 2004, New York: CRC Press.

[8]   M. Gaumet, A. Vargas, R. Gurny, F. Delie, Nanoparticles for drug delivery: The need for precision in reporting particle size parameters, Eur J Pharm Biopharm, 69 (2008) 1-9.

[9]   F. Alexis, E. Pridgen, L.K. Molnar, O.C. Farokhzad, Factors affecting the clearance and biodistribution of polymeric nanoparticles, Mol Pharm, 5 (2008) 505-515.

[10]   Greish, K., Enhanced permeability and retention of macromolecular drugs in solid tumors: a royal gate for targeted anticancer nanomedicines, J Drug Target, 15 (2007) 457-64.

[11]   B. Slutter, W. Jiskoot, Sizing the optimal dimensions of a vaccine delivery system: a particulate matter, Expert Opin Drug Deliv, 13 (2016) 167-70.

[12]   N. Benne, J. van Duijn, J. Kuiper, W. Jiskoot, B. Slütter, Orchestrating immune responses: How size, shape and rigidity affect the immunogenicity of particulate vaccines. J Controll Release, 234 (2016) 124-34.

[13]   M. Kalani, R. Yunus, Effect of supercritical fluid density on nanoencapsulated drug particle size using the supercritical antisolvent method, Int J Nanomedicine, 7 (2012) 2165-72.

[14]   B.B. Kale, N.H. Aloorkar, S.M. Deshmukh, S.P. Sulake, P.V. Humbe, P.P. Mane, Recent advancements in prticle engineering techniques for pharmaceutical applications, Indo Am J Pharm Res, 4 (2014) 2027-49.

[15]   R.T.Y. Lim, W.K. Ng, E. Widjaja, R.B.H. Tan, Comparison of the physical stability and physicochemical properties of amorphous indomethacin prepared by co-milling and supercritical anti-solvent co-precipitation, J Supercrit Fluids, 79 (2013) 186-201.

[16]   M. Tabbakhian, F. Hasanzadeh, N. Tavakoli, Z. Jamshidian, Dissolution enhancement of glibenclamide by solid dispersion: solvent evaporation versus a supercritical fluid-based solvent -antisolvent technique, Res Pharm Sci, 9 (2014) 337-50.

[17]   Z. S. Yu, K. P. Johnston, R. O. Williams, Spray freezing into liquid versus spray-freeze drying: Influence of atomization on protein aggregation and biological activity, Eur J Pharm Sci, 27 (2006) 9-18.

[18]   S.D. Webb, S.L. Golledge, J.L. Cleland, J.F. Carpenter, T.W. Randolph, Surface adsorption of recombinant human interferon-gamma in lyophilized and spray-lyophilized formulations, J Pharm Sci, 91 (2002) 1474-87.

[19]   M. Dissanayake, S. Liyanaarachchi, T. Vasiljevic, Functional properties of whey proteins microparticulated at low pH, J Dairy Sci, 95 (2012) 1667-79.

[20]   I. Roy, M.N. Gupta, Freeze-drying of proteins: some emerging concerns, Biotechnol Appl Biochem, 39 (2004) 165-177.

[21]   A. Tabernero, E.M. Martín del Valle, and M.A. Galán, Supercritical fluids for pharmaceutical particle engineering: Methods, basic fundamentals and modelling, Chem Eng Process, 60 (2012) 9-25.

[22]   M. D. Louey, M. Van Oort, A.J. Hickey, Aerosol dispersion of respirable particles in narrow size distributions produced by jet-milling and spray-drying techniques, Pharmaceut Res, 21 (2004) 1200-6.

[23]   T. L. Rogers, K.P. Johnston, and R.O. Williams 3rd, Solution-based particle formation of pharmaceutical powders by supercritical or compressed fluid CO_2 and cryogenic spray-freezing technologies, Drug Dev Ind Pharm, 27 (2001) 1003-15.

[24]   S.A. Shoyele, S. Cawthorne, Particle engineering techniques for inhaled biopharmaceuticals, Adv Drug Deliv Rev, 58 (2006) 1009-29.

[25]   E. Del Valle, M. Galan, Supercritical Fluid technique for particle engineering: Drug delivery applications, Rev Chem Eng, 21 (2005) 33-69.

[26]   E. Reverchon, R. Adami, G. Caputo, I. De Marco, Spherical microparticles production by supercritical antisolvent precipitation: Interpretation of results, J Supercrit Fluids, 47 (2008) 70-84.

[27]   E. Reverchon, Supercritical antisolvent precipitation of micro- and nano-particles. J Supercrit Fluids, 15 (1999) 1-21.

[28]   A. Martin and M.J. Cocero, Micronization processes with supercritical fluids: fundamentals and mechanisms, Adv Drug Deliv Rev, 60 (2008) 339-50.

[29]   A. Martin, and M.J. Cocero, Precipitation processes with supercritical fluids: patents review, Recent Pat Eng, 2 (2008) 9-20.

[30]   N. Esfandiari, Production of micro and nano particles of pharmaceutical by supercritical carbon dioxide, J Supercrit Fluids, 100 (2015) 129-41.

[31]   R. Campardelli, L. Baldino, E. Reverchon, Supercritical fluids applications in nanomedicine, J Supercrit Fluids, 101 (2015) 193-214.

[32]   P. Khadka, J. Ro, H. Kim, I. Kim, J. T. Kim, H. Kim, J. M. Cho, G. Yun, J. Lee, Pharmaceutical particle technologies: An approach to improve drug solubility, dissolution and bioavailability, Asian J Pharm Sci, 9 (2014) 304–16.

[33]   E. Elizondo, J. Veciana, N. Ventosa, Nanostructuring molecular materials as particles and vesicles for drug delivery, using compressed and supercritical fluids. Nanomedicine, 7 (2012) 1391-408.

[34]   P.G. Debenedetti, J.W. Tom, X. Kwauk, S.-D. Yeo, Rapid expansion of supercritical solutions (RESS): fundamentals and applications, Fluid Phase Equilib, 82 (1993) 311-21.

[35]   K. Matsuyama, K. Mishima, H. Umemoto, S. Yamaguchi, Environmentally benign formation of polymeric microspheres by rapid expansion of supercritical carbon dioxide solution with a nonsolvent, Environ Sci Technol, 35 (2001) 4149-55.

[36]   K. Matsuyama, K. Mishima, K.-I. Hayashi, H. Ishikawa, H. Matsuyama, T. Harada, Formation of microcapsules of medicines by the rapid expansion of a supercritical solution with a nonsolvent, J Appl Polym Sci, 89 (2003) 742-52.

[37]   K. Mishima, K. Matsuyama, D. Tanabe, S Yamauchi, T.J. Young, K.P. Johnston, Microencapsulation of proteins by rapid expansion of supercritical solution with a nonsolvent, Aiche Journal, 46(2000) 857-65.

[38]   Y.P. Sun, M.J. Meziani, P. Pathak, L. Qu, Polymeric nanoparticles from rapid expansion of supercritical fluid solution, Chem-Euro J, 11 (2005) 1366-73.

[39]   S. G. Kazarian, G.G. Martirosyan, Spectroscopy of polymer/drug formulations processed with supercritical fluids: in situ ATR-IR and Raman study of impregnation of ibuprofen into PVP, Int J Pharm, 232 (2002) 81-90.

[40]   A.R. Berens, G.S. Huvard, R.W. Korsmeyer, F.W. Kunig, Application of Compressed Carbon-Dioxide in the Incorporation of Additives into Polymers, J Appl Polym Sci, 46 (1992) 231-42.

[41]   G. Della Porta, E. Reverchon, Nanostructured microspheres produced by supercritical fluid extraction of emulsions. Biotechnol Bioeng, 100 (2008) 1020-33.

[42]   B.Y. Shekunov, P. Chattopadhyay, J. Seitzinger, R. Huff, Nanoparticles of poorly water-soluble drugs prepared by supercritical fluid extraction of emulsions, Pharmaceut Res, 23 (2006) 196-204.

[43]   P. Chattopadhyay, R. Huff, B. Shekunov, Drug encapsulation using supercritical fluid extraction of emulsions, J Pharm Sci, 95 (2006) 667-79.

[44]   N .Falco, E. Reverchon, G. Della Porta, Injectable PLGA/hydrocortisone formulation produced by continuous supercritical emulsion extraction, Int J Pharm, 441 (2013) 589-97.

[45]   G. Della Porta, N. Falco, E. Reverchon, NSAID drugs release from injectable microspheres produced by supercritical fluid emulsion extraction, J Pharm Sci, 99 (2010) 1484-99.

[46]   G.D. Porta, N. Falco, E. Giordano, E. Reverchon, PLGA microspheres by Supercritical Emulsion Extraction: a study on insulin release in myoblast culture, J Biomater Sci Polym Ed, 24 (2013) 1831-47.

[47] M. Kalani, R. Yunus, Application of supercritical antisolvent method in drug encapsulation: a review, Int J Nanomedicine, 6 (2011) 1429-42.

[48] S. Palakodaty, P. York, Phase behavioral effects on particle formation processes using supercritical fluids. Pharmaceut Res, 16 (1999) 976-85.

[49] P. Chattopadhyay, R. Gupta, Production of griseofulvin nanoparticles using supercritical CO_2 antisolvent with enhanced mass transfer, International Journal of Pharmaceutics, 228 (2001) 19-31.

[50] L. Lee, C. Wang, K. Smith, Supercritical antisolvent production of biodegradable micro- and nanoparticles for controlled delivery of paclitaxel, J Control Release, 125 (2008) 96-106.

[51] C.A. Ober, L. Kalombo, H. Swai, R. B. Gupta, Preparation of rifampicin/lactose microparticle composites by a supercritical antisolvent-drug excipient mixing technique for inhalation delivery, Powder Technol, 236 (2013) 132-38.

[52] S.K. Sathigari, C.A. Ober, G.P. Sanganwar, R.B. Gupta, R.J. Babu, Single-Step Preparation and Deagglomeration of Itraconazole Microflakes by Supercritical Antisolvent Method for Dissolution Enhancement, J Pharm Sci, 100 (2011) 2952-65.

[53] G.P. Sanganwar, S. Sathigari, R.J. Babu, R.B. Gupta, Simultaneous production and co-mixing of microparticles of nevirapine with excipients by supercritical antisolvent method for dissolution enhancement, Eur J Pharm Sci, 39 (2010) 164-74.

[54] Z. Knez, E. Weidner, Particles formation and particle design using supercritical fluids, Curr. Opin. Solid State Mater. Sci., 7 (2003) 353-61.

[55] A. Baxendale, P. van Hooff, L.G. Durrant, I. Spendlove, S.M. Howdle, H.M. Woods, M.J. Whitaker, O.R. Davies, A. Naylor, A.L. Lewis, L. Illum, Single shot tetanus vaccine manufactured by a supercritical fluid encapsulation technology, Int J Pharm, 413 (2011) 147-54.

[56] F. Jordan, A. Naylor, C.A. Kelly, S.M. Howdle, A. Lewis, L. Illum, Sustained release hGH microsphere formulation produced by a novel supercritical fluid technology: in vivo studies, J Control Release, 141 (2010) 153-60.

[57] D.R. Perinelli, G. Bonacucina, M. Cespi, A. Naylor, M. Whitaker, G.F. Palmieri, G. Giorgioni, L. Casettari, Evaluation of P(L)LA-PEG-P(L)LA as processing aid for biodegradable particles from gas saturated solutions (PGSS) process, Int J Pharm, 468 (2014) 250-7.

[58] S. Salmaso, N. Elvassore, A. Bertucco, P. Caliceti, Production of Solid Lipid Submicron Particles for Protein Delivery Using a Novel Supercritical Gas-Assisted Melting Atomization Process, J Pharm Sci, 98 (2009) 640-50.

[59] T.K. Fahim, I.S.M. Zaidul, M.R. Abu Bakar, U.M. Salim, M.B. Awang, F. Sahena, K.C.A. Jalal, K.M. Sharif, M.H. Sohrab, Particle formation and micronization using non-conventional techniques-review, Chem Eng Process, 86 (2014) 47-52.

[60] R. Dohrn, E. Bertakis, O. Behrend, E. Voutsas, D. Tassios, Melting point depression by using supercritical CO_2 for a novel melt dispersion micronization process, J Mol Liq, 131 (2007) 53-9.

[61]   K.H. Cha, K.J. Cho, M.S. Kim, J.S. Kim, H.J. Park, J. Park, W. Cho, J.S. Park, S.J. Hwang, Enhancement of the dissolution rate and bioavailability of fenofibrate by a melt-adsorption method using supercritical carbon dioxide, Int J Nanomedicine, 7 (2012) 5565-75.

[62]   A.Z. Chen, G.Y. Wang, S.B. Wang, L. Li, Y.G. Liu, C. Zhao, Formation of methotrexate-PLLA-PEG-PLLA composite microspheres by microencapsulation through a process of suspension-enhanced dispersion by supercritical CO_2, Int J Nanomedicine, 7 (2012) 3013-22.

[63]   A.-Z. Chen, Y. Li, F.-T. Chau, T.-Y. Lau, J.-Y. Hu, Z. Zhao, D. K.-W. Mok, Microencapsulation of puerarin nanoparticles by poly(l-lactide) in a supercritical CO_2 process, Acta Biomater, 5 (2009) 2913-9.

[64]   A.Z. Chen, Y. Li, D. Chen, J.Y. Hu, Development of core-shell microcapsules by a novel supercritical CO_2 process, J Mater Sci Mater Med, 20 (2009) 751-8.

[65]   C. Zhang, G. Li, Y. Wang, F. Cui, J. Zhang, Q. Huang, Preparation and characterization of 5-fluorouracil-loaded PLLA-PEG/PEG nanoparticles by a novel supercritical CO_2 technique, Int J Pharm, 436 (2012) 272-81.

[66]   Y.-Q. Kang, C. Zhao, A.-Z. Chen, S.-B. Wang, Y.-G. Liu, W.-G. Wu, X.-Q. Su, Study of lysozyme-loaded poly-L-lactide (PLLA) porous microparticles in a compressed CO_2 antisolvent process, Materials, 6 (2013) 3571-83.

[67]   A.-Z. Chen, C. Zhao, S.-B. Wang, Y.-G. Liu, D.-L. Lin, Generation of porous poly-L-lactide microspheres by emulsion-combined precipitation with a compressed CO_2 antisolvent process, J Mater Chem B, 1 (2013) 2967-75.

[68]   A. Nunes, C. Duarte, Dense CO_2 as a Solute, Co-Solute or Co-Solvent in Particle Formation Processes: A Review, Materials, 4 (2011) 2017-41.

[69]   N. Jovanović, A. Bouchard, G.W. Hofland, G.J. Witkamp, D.J. Crommelin, W. Jiskoot, Distinct effects of sucrose and trehalose on protein stability during supercritical fluid drying and freeze-drying, Eur J Pharm Sci, 27 (2006) 336-45.

[70]   O. Nuchuchua, H.A. Every, W. Jiskoot, Critical processing parameters of carbon dioxide spray drying for the production of dried protein formulations: A study with myoglobin, Eur J Pharm Biopharm, 103 (2016) 200-9.

[71]   O. Nuchuchua, G. Hofland, H.A. Every, W. Jiskoot, Scalable organic solvent free supercritical fluid spray drying process for producing dry protein formulations, Eur J Pharm Biopharm, 88 (2014) 919-30.

[72]   E. Reverchon, Supercritical-assisted atomization to produce micro- and/or nanoparticles of controlled size and distribution, Ind Eng Chem Res, 41 (2002) 2405-11.

[73]   E. Reverchon, R. Adami, S. Cardea, G. D. Porta, Supercritical fluids processing of polymers for pharmaceutical and medical applications, J Supercrit Fluids, 47 (2009) 484-92.

[74]   R. Sievers, Formation of aqueous small droplet aerosols assisted by supercritical carbon dioxide, Aerosol Sci Technol, 30 (1999) 3-15.

[75]   S.P. Cape, J.A. Villa, E.T.S. Huang, T.-H. Yang, J.F. Carpenter, R.E. Sievers, Preparation of active proteins, vaccines and pharmaceuticals as fine powders using supercritical or near-critical fluids, Pharm Res, 25 (2008) 1967-90.

[76]   R.P. Aquino, G. Auriemma, T. Mencherini, P. Russo, A. Porta, R. Adami, S. Liparoti, G. Della Porta, E. Reverchon, P. Del Gaudio, Design and production of gentamicin/dextrans microparticles by supercritical assisted atomisation for the treatment of wound bacterial infections, Int J Pharm, 440 (2013) 188-94.

[77]   G. Della Porta, R. Adami, P. Del Gaudio, L. Prota, R. Aquino, E. Reverchon, Albumin/gentamicin microspheres produced by supercritical assisted atomization: optimization of size, drug loading and release, J Pharm Sci, 99 (2010) 4720-9.

[78]   E. de Paz, A. Martin, M.J. Cocero, Formulation of beta-carotene with soybean lecithin by PGSS (Particles from Gas Saturated Solutions)-drying, J Supercrit Fluids, 72 (2012) 125-33.

[79]   K. Schmitz, Basic Concepts of Light Scattering. In Introduction to Dynamic Light Scattering by Macromolecules, 2012, Elsevier. p. 11-42.

[80]   B. J. Berne, R. Pecora, Dynamic Light Scattering: With Applications to Chemistry, Biology, and Physics. 2013, New York: Courier Dover Publications.

[81]   F. Zabihi, N. Xin, S. Li, J. Jia, T. Cheng, Y. Zhao, Polymeric coating of fluidizing nano-curcumin via anti-solvent supercritical method for sustained release, J Supercrit Fluids, 89 (2014) 99-105.

[82]   D. Traini, D. Traini, Inhalation drug delivery, in: P. Colombo, D. Traini, F. Buttini (Eds.), Inhalation Drug Delivery: Techniques and Products, John Wiley & Sons, Ltd., West Sussex, UK, 2013, pp. 1-10.

[83]   D.A. Edwards, D. Chen, J. Wang, A. Ben-Jebria, 1998. Controlled-release inhalation aerosols. In: Respiratory drug delivery VI. Hilton Head, SC: Interpharm Press, Inc, 187-192.

[84]   C.J. Musante, J.D. Schroeter, J.A. Rosati, T.M. Crowder, A.J. Hickey, T.B. Martonen, Factors affecting the deposition of inhaled porous drug particles, J Pharm Sci, 91 (2002) 1590-600.

[85]   K. D. Vernon-Parry, Scanning Electron Microscopy: an introduction, III-Vs Review, 13 (2000) 40-4.

[86]   A. Sane, J. Limtrakul, Formation of retinyl palmitate-loaded poly(L-lactide) nanoparticles using rapid expansion of supercritical solutions into liquid solvents (RESOLV), J Supercrit Fluids, 51 (2009) 230-37.

[87]   A.Z. Chen, Y.Q. Kang, X.M. Pu, G.F. Yin, Y. Li, J.Y. Hu, Development of Fe_3O_4-poly(L-lactide) magnetic microparticles in supercritical CO_2, J Colloid Interface Sci, 330 (2009) 317-22.

[88]   H. G. Merkus, in: Henk G. Merkus (Eds.), Particle Size Measurements Fundamentals, Practice, Quality, Springer Science+Business Media B.V., Netherlands, 2009, pp. 210.

[89]   L. Reimer and H. Kohl, Transmission Electron Microscopy: Physics of Image Formation. 5 ed. 2008: Springer-Verlag New York Inc.

[90]   A.-Z. Chen, L. Li, S.-B. Wang, X.-F. Lin, Y.-G. Liu, C. Zhao, G.-Y. Wang, Z. Zhao, Study of Fe_3O_4–PLLA–PEG–PLLA magnetic microspheres based on supercritical CO_2: Preparation, physicochemical characterization, and drug loading investigation, J Supercrit Fluids, 67 (2012) 139-48.

[91]   Y. Kang, J. Wu, G. Yin, Z. Huang, X. Liao, Y. Yao, P. Ouyang, H. Wang, Q. Yang, Characterization and biological evaluation of paclitaxel-loaded poly(L-lactic acid) microparticles prepared by supercritical CO_2, Langmuir, 24 (2008) 7432-41.

[92]   V. Filipe, A. Hawe, W. Jiskoot, Critical evaluation of Nanoparticle Tracking Analysis (NTA) by NanoSight for the measurement of nanoparticles and protein aggregates, Pharm Res, 27 (2010) 796-810.

[93]   D.K. Sharma, D. King, P. Oma, C. Merchant, Micro-flow imaging: flow microscopy applied to sub-visible particulate analysis in protein formulations, AAPS J, 12 (2010) 455-64.

[94]   D. Weinbuch, S. Zölls, M. Wiggenhorn, W. Friess, G. Winter, W. Jiskoot, A. Hawe, Micro-flow imaging and resonant mass measurement (Archimedes)--complementary methods to quantitatively differentiate protein particles and silicone oil droplets, J Pharm Sci, 102 (2013) 2152-65.

[95]   S. Zölls, D. Weinbuch, M. Wiggenhorn, G. Winter, W. Friess, W. Jiskoot, A. Hawe, Flow imaging microscopy for protein particle analysis--a comparative evaluation of four different analytical instruments, AAPS J, 15 (2013) 1200-11.

[96]   J.F. Carpenter, T.W. Randolph, W. Jiskoot, D.J. Crommelin, C.R. Middaugh, G. Winter, Y.X. Fan, S. Kirshner, D. Verthelyi, S. Kozlowski, K.A. Clouse, P.G. Swann, A. Rosenberg, B. Cherney, Overlooking subvisible particles in therapeutic protein products: gaps that may compromise product quality, J Pharm Sci, 98 (2009) 1201-5.

[97]   S.K. Singh, N. Afonina, M. Awwad, K. Bechtold-Peters, J.T. Blue, D. Chou, M. Cromwell, H.J. Krause, H.C. Mahler, B.K. Meyer, L. Narhi, D.P. Nesta, T. Spitznagel, An industry perspective on the monitoring of subvisible particles as a quality attribute for protein therapeutics, J Pharm Sci, 99 (2010) 3302-21.

[98]   A. Hawe, F. Schaubhut, R. Geidobler, M. Wiggenhorn, W. Friess, M. Rast, C. de Muynck, G. Winter, Pharmaceutical feasibility of sub-visible particle analysis in parenterals with reduced volume light obscuration methods, Eur J Pharm Biopharm, 85 (2013) 1084-7.

[99]   J.G. Watson, J.C. Chow, D.A. Sodeman, D.H. Lowenthal, M.-C.O. Chang, K. Park, X. Wang, Comparison of four scanning mobility particle sizers at the Fresno Supersite, Particuology, 9 (2011) 204-9.

[100]   T. Amodeo, C. Dutouquet, O.L. Bihan, M. Attoui, E. Frejafon, On-line determination of nanometric and sub-micrometric particle physicochemical characteristics using spectral imaging-aided Laser-Induced Breakdown Spectroscopy coupled with a Scanning Mobility Particle Sizer, Spectrochim Acta Part B At Spectrosc, 64 (2009) 1141-52.

[101]   J. Löndahl, W. Möller, J.H. Pagels, W.G. Kreyling, E. Swietlicki, O. Schmid, Measurement techniques for respiratory tract deposition of airborne nanoparticles: a critical review, J Aerosol Med Pulm Drug Deliv, 27 (2014) 229-54.

[102]   D. Müller, S. Cattaneo, F. Meier, R. Welz, T. de Vries, M. Portugal-Cohen, D.C. Antonio, C. Cascio, L. Calzolai, D. Gilliland, A. de Mello, Inverse supercritical fluid extraction as a sample preparation method for the analysis of the nanoparticle content in sunscreen agents, J Chromatogr A, 1440 (2016) 31-6.

[103]   M. Nadler, T. Mahrholz, U. Riedel, C. Schilde, A. Kwade, Preparation of colloidal carbon nanotube dispersions and their characterization using a disc centrifuge, Carbon, 46 (2008) 1384-92.

[104]   A. Neumann, W. Hoyer, M.W. Wolff, U. Reichl, A. Pfitzner, B. Roth, New method for density determination of nanoparticles using a CPS disc centrifuge (TM), Colloids Surf B Biointerfaces, 104 (2013) 27-31.

[105]   H. Fissan, S. Ristig, H. Kaminski, C. Asbach, M. Epple, Comparison of different characterization methods for nanoparticle dispersions before and after aerosolization, Anal Methods, 6 (2014) 7324-34.

[106]   J.A. Somerville, G.R. Willmott, J. Eldridge, M. Griffiths, K.M. McGrath, Size and charge characterization of a submicrometre oil-in-water emulsion using resistive pulse sensing with tunable pores, J Colloid Interface Sci, 394 (2013) 243-51.

[107]   R. B. Schoch, J.Y. Han, P. Renaud, Transport phenomena in nanofluidics, Rev Mod Phys, 80 (2008) 839-83.

[108]   L. Yang, M.F. Broom, I.G. Tucker, Characterization of a nanoparticulate drug delivery system using scanning ion occlusion sensing, Pharm Res, 29 (2012) 2578-86.

[109]   A. Deric, Holden, G.H., L. Andrew Lyon, H. S. White, Resistive pulse analysis of microgel deformation during nanopore translocation, J Phys Chem C, 115 (2011) 2999-3004.

[110]   G. R. Willmott, M. Platt, G.U. Lee, Resistive pulse sensing of magnetic beads and supraparticle structures using tunable pores, Biomicrofluidics, 6 (2012) 014103.

[111]   A. Villiers, M. M. de Villiers, Drug Loading into and in vitro Release from Nanosized Drug Delivery Systems. In Nanotechnology in Drug Delivery, 2008, American Association of Pharmaceutical Scientists, pp.129-155. 40, no.

[112]   Y. Kang, J. Wu, G. Yin, Z. Huang, Y. Yao, X. Liao, A. Chen, X. Pu, L. Liao, Preparation, characterization and in vitro cytotoxicity of indomethacin-loaded PLLA/PLGA microparticles using supercritical CO_2 technique, Eur J Pharm Biopharm, 70 (2008) 85-97.

[113]   J. Patel, P. Patil, Preparation and characterization of amoxicillin mucoadhesive microparticles using solution-enhanced dispersion by supercritical CO_2. J Microencapsul, 29 (2012) 398-408.

[114]   C. Washington, Evaluation of Non-Sink Dialysis Methods for the Measurement of Drug Release from Colloids - Effects of Drug Partition, Int J Pharm, 56 (1989) 71-74.

[115]   S. S. D'Souza, P.P. DeLuca, Methods to assess in vitro drug release from injectable polymeric particulate systems, Pharm Res, 23 (2006) 460-74.

[116]   E. Elizondo, S. Sala, E. Imbuluzqueta, D. González, M.J. Blanco-Prieto, C. Gamazo, N. Ventosa, J. Veciana, High loading of gentamicin in bioadhesive PVM/MA nanostructured microparticles using compressed carbon-dioxide, Pharm Res, 28 (2011) 309-21.

[117]   S. Ravi, K.K. Peh, Y. Darwis, B.K. Murthy, T.R. Singh, C. Mallikarjun, Development and characterization of polymeric microspheres for controlled release protein loaded drug delivery system, Indian J Pharm Sci, 70 (2008) 303-9.

[118]   N. Jovanović, A. Bouchard, M. Sutter, M. Van Speybroeck, G.W. Hofland, G.J. Witkamp, D.J. Crommelin, W. Jiskoot, Stable sugar-based protein formulations by supercritical fluid drying, Int J Pharm, 346 (2008) 102-8.

[119]   N. Jovanović, A. Bouchard, G.W. Hofland, G.J. Witkamp, D.J. Crommelin, W. Jiskoot, Stabilization of IgG by supercritical fluid drying: optimization of formulation and process parameters, Eur J Pharm Biopharm, 68 (2008) 183-90.

[120]   M. Gadermann, S. Kular, A.H. Al-Marzouqi, R. Signorell, Formation of naproxen-polylactic acid nanoparticles from supercritical solutions and their characterization in the aerosol phase, Phys Chem Chem Phys, 11 (2009) 7861-8.

[121]   M. E. Brown, Introduction to Thermal Analysis: Techniques and Applications. 2001: Springer Science & Business Media. 264.

[122]   W. Li-Hong, C. Xin, X. Hui, Z. Li-Li, H. Jing, Z. Mei-Juan, L. Jie, L. Yi, L. Jin-Wen, Z. Wei, C. Gang, A novel strategy to design sustained-release poorly water-soluble drug mesoporous silica microparticles based on supercritical fluid technique, Int J Pharm, 454 (2013) 135-42.

[123]   P. Gill, T.T. Moghadam, B. Ranjbar, Differential scanning calorimetry techniques: applications in biology and nanoscience, J Biomol Tech, 21 (2010) 167-93.

[124]   M. Zhang, H. Li, B. Lang, K. O'Donnell, H. Zhang, Z. Wang, Y. Dong, C. Wu, R.O. Williams 3rd, Formulation and delivery of improved amorphous fenofibrate solid dispersions prepared by thin film freezing, Eur J Pharm Biopharm, 82 (2012) 534-44.

[125]   F. Rouessac, A. Rouessac, Infrared Spectroscopy, in Chemical Analysis: Modern Instrumentation Methods and Techniques. 2007, John Wiley & Sons Ltd. p. 207-40.

[126]   R. J. Ahern, A. M. Crean, K. B. Ryan, The influence of supercritical carbon dioxide (SC-CO$_2$) processing conditions on drug loading and physicochemical properties, Int J Pharm, 439 (2012) 92-9.

[127]   A. B. Ghisaidoobe, S.J. Chung, Intrinsic tryptophan fluorescence in the detection and analysis of proteins: a focus on Forster resonance energy transfer techniques, Int J Mol Sci, 15 (2014) 22518-38.

[128]   W. Jiskoot, A. J. W. G. Visser, J. N. Herron, M. Sutter, Fluorescence spectroscopy. In: Methods for Structural Analysis of Protein Pharmaceuticals (W. Jiskoot and D.J.A. Crommelin, Eds.), AAPS Press, Arlington, VA, 2005: p. 27-82.

[129]   N. J. Greenfield, Using circular dichroism spectra to estimate protein secondary structure, Nat Protoc, 6 (2006) 2876-90.

[130]   A. Rodger, R. Marrington, D. Roper, S. Windsor, Circular dichroism spectroscopy for the study of protein-ligand interactions, Methods Mol Biol, 305 (2005) 343-64.

[131]   M. Bloemendal, W. Jiskoot, Circular dichroism spectroscopy. In: Methods for Structural Analysis of Protein Pharmaceuticals (W. Jiskoot and D.J.A. Crommelin, Eds.). AAPS Press, Arlington, VA, 2005: p. 83-130.

[132]   G. Jesson, M. Brisander, P. Andersson, M. Demirbüker, H. Derand, H. Lennernäs, M. Malmsten, Carbon dioxide-mediated generation of hybrid nanoparticles for improved bioavailability of protein kinase inhibitors, Pharm Res, 31 (2014) 694-705.

[133] W. Wang, G. Liu, J. Wu, Y. Jiang, Co-precipitation of 10-hydroxycamptothecin and poly (L-lactic acid) by supercritical CO_2 anti-solvent process using dichloromethane/ethanol co-solvent, J Supercrit Fluids, 74 (2013) 137-44.

[134] F. Zahran, A. Cabañas, J.A.R. Cheda, J.A.R. Renuncio, C. Pando, Dissolution rate enhancement of the anti-inflammatory drug diflunisal by coprecipitation with a biocompatible polymer using carbon dioxide as a supercritical fluid antisolvent, J Supercrit Fluids, 88 (2014) 56-65.

[135] J.B. Hall, M.A. Dobrovolskaia, A.K. Patri, S.E. McNeil, Characterization of nanoparticles for therapeutics, Nanomedicine, 2 (2007) 789-803.

[136] R.J. Ahern, J.P. Hanrahan, J.M. Tobin, K.B. Ryan, A.M. Crean, Comparison of fenofibrate-mesoporous silica drug-loading processes for enhanced drug delivery, Eur J Pharm Sci, 50 (2013) 400-9.

[137] R. Campardelli, G.D. Porta, L. Gomez, S. Irusta, E. Reverchon, J. Santamaria, Au-PLA nanocomposites for photothermally controlled drug delivery, J Mater Chem B, 2 (2014) 409-17.

[138] P. M. A. Sherwoord, Auger and X-Ray Photoelectron Spectroscopy, in Handbook of Nanophase Materials, A. Goldstein, Editor. 1997, CRC Press. p. 337-43.

[139] A. Montes, E. Baldauf, M.D. Gordillo, C.M. Pereyra, E.J. Martínez de la Ossa, Polymer encapsulation of amoxicillin microparticles by SAS process, J Microencapsul, 31 (2014) 16-22.

[140] Y. Seo, W. Jhe, Atomic force microscopy and spectroscopy, Reports on Progress in Physics, 71 (2008).

[141] G. Ahuja, K. Pathak, Porous carriers for controlled/modulated drug delivery, Indian J Pharm Sci, 71 (2009) 599-607.

[142] V. Mamaeva, J.M. Rosenholm, L.T. Bate-Eya, L. Bergman, E. Peuhu, A. Duchanoy, L.E. Fortelius, S. Landor, D.M. Toivola, M. Lindén, C. Sahlgren, Mesoporous Silica Nanoparticles as Drug Delivery Systems for Targeted Inhibition of Notch Signaling in Cancer, Mol Ther, 19 (2011) 1538-46.

[143] K. Sing, The use of nitrogen adsorption for the characterization of porous materials, Colloid Surface A, 187 (2001) 3-9.

[144] S. Brunauer, P.H. Emmett, E. Teller, Adsorption of Gases in Multimolecular Layers, J Am Chem Soc, 60 (1938) 309-19.

[145] E. Barrett, L. Joyner, P. Halenda, The determination of pore volume and area distributions in porous substances. 1. Computations from nitrogen isotherms, J Am Chem Soc, 73 (1951) 373-80.

[146] H. Giesche, Mercury porosimetry: A general (practical) overview, Part Part Syst Charact, 23 (2006) 9–19.

[147] B. Kirby, E. Hasselbrink, Zeta potential of microfluidic substrates: 1. Theory, experimental techniques, and effects on separations, Electrophoresis, 25 (2004) 187-202.

[148] L. Rabinovich-Guilatt, P. Couvreur, G. Lambert, D. Goldstein, S. Benita, C. Dubernet, Extensive surface studies help to analyze zeta potential data: the case of cationic emulsions, Chem Phys Lipids, 131 (2004) 1-13.

[149]   R. Hidalgoalvarez, On the conversion of experimental electrokinetic data into double-layer characteristics in solid-liquid interfaces. In Advances in Colloid and Interface Science. 1991. p. 217-341.

[150]   S. Dalvi, M. Azad, R. Dave, Precipitation and stabilization of ultrafine particles of Fenofibrate in aqueous suspensions by RESOLV, Powder Technol, 236 (2013) 75-84.

[151]   R. Muller, C. Jacobs, O. Kayser, Nanosuspensions as particulate drug formulations in therapy Rationale for development and what we can expect for the future, Adv Drug Deliver Rev, 47 (2001) 3-19.

[152]   L.N. Hassani, F. Hindré, T. Beuvier, B. Calvignac, N. Lautram, A. Gibaud, F. Boury, Lysozyme encapsulation into nanostructured $CaCO_3$ microparticles using a supercritical CO_2 process and comparison with the normal route, J Mater Chem B, 1 (2013) 4011-19.

[153]   I. Sogias, A. Williams, V. Khutoryanskiy, Why is chitosan mucoadhesive?, Biomacromolecules, 9 (2008) 1837-42.

[154]   M. Bogatai, T. Vovk, M. Kerec, A. Dimnik, I. Grabnar, A. Mrhar, The correlation between zeta potential and mucoadhesion strength on pig vesical mucosa, Biol Pharm Bull, 26 (2003) 743-746.

[155]   S. Patil, A. Sandberg, E. Heckert, W. Self, S. Seal, Protein adsorption and cellular uptake of cerium oxide nanoparticles as a function of zeta potential, Biomaterials, 28 (2007) 4600-07.

[156]   S. Salgin, U. Salgin, S. Bahadir, Zeta Potentials and Isoelectric Points of Biomolecules: The Effects of Ion Types and Ionic Strengths, Int J Electrochem Sci, 7 (2012) 12404-14.

[157]   E. Frohlich, The role of surface charge in cellular uptake and cytotoxicity of medical nanoparticles, Int J Nanomedicine, 7 (2012) 5577-91.

[158]   M. Fraile, R. Buratto, B. Gómez, Á. Martín, M.J. Cocero, Enhanced Delivery of Quercetin by Encapsulation in Poloxamers by Supercritical Antisolvent Process, Ind Eng Chem Res, 53 (2014) 4318-27.

[159]   A. Sharma, S. Madhunapantula, G. Robertson, Toxicological considerations when creating nanoparticle-based drugs and drug delivery systems, Expert Opin Drug Metab Toxicol, 8 (2012) 47-69.

[160]   N. Lewinski, V. Colvin, R. Drezek, Cytotoxicity of nanoparticles, Small, 4 (2008) 26-49.

[161]   B.J. Marquis, S.A. Love, K.L. Braun, C.L. Haynes, Analytical methods to assess nanoparticle toxicity, Analyst, 134 (2009) 425-39.

[162]   A.L. Holder, R. Goth-Goldstein, D. Lucas, C.P. Koshland, Particle-Induced Artifacts in the MTT and LDH Viability Assays, Chem Res Toxicol, 25 (2012) 1885-92.

[163]   W. Abdelwahed, G. Degobert, S. Stainmesse, H. Fessi, Freeze-drying of nanoparticles: Formulation, process and storage considerations, Adv Drug Deliver Rev, 58 (2006) 1688-713.

[164]   A. Bouchard, N. Jovanović, G.W. Hofland, W. Jiskoot, E. Mendes, D.J.A. Crommelin, G.-J. Witkamp, Supercritical fluid drying of carbohydrates: selection

of suitable excipients and process conditions, Eur J Pharm Biopharm, 68 (2008) 781-94.

[165] R. Shaikh, T.R.R. Singh, M.J. Garland, A.D. Woolfson, R.F. Donnelly, Mucoadhesive drug delivery systems, J Pharm Bioallied Sci, 3 (2011) 89-100.

[166] M. Amidi, E. Mastrobattista, W. Jiskoot, W.E. Hennink, Chitosan-based delivery systems for protein therapeutics and antigens, Adv Drug Deliv Rev, 62 (2010) 59-82.

[167] M. Arruebo, R. Fernández-Pacheco, M.R. Ibarra, J. Santamaría , Magnetic nanoparticles for drug delivery, Nano Today, 2 (2007) 22-32.

[168] A. Bootz, V. Vogel, D. Schubert, J. Kreuter, Comparison of scanning electron microscopy, dynamic light scattering and analytical ultracentrifugation for the sizing of poly(butyl cyanoacrylate) nanoparticles, Eur J Pharm Biopharm, 57 (2004) 369-75.

[169] H. Keles, A. Naylor, F. Clegg, C. Sammon, Investigation of factors influencing the hydrolytic degradation of single PLGA microparticles, Polym Degrad Stab, 119 (2015) 228-41.

[170] W. Jiskoot, D. Crommelin, (Eds.), Methods for Structural analysis of Protein Pharmaceuticals, American Association of Pharmaceutical Scientists, USA 2005.

[171] H.-C. Mahler, W. Jiskoot, Analysis of Aggregates and Particles in Protein Pharmaceuticals, John Wiley & Sons, Inc., New Jersey, 2012.

[172] J. das Neves, M. Amiji, M.F. Bahia, B. Sarmento, Assessing the physical-chemical properties and stability of dapivirine-loaded polymeric nanoparticles, Int J Pharm, 456 (2013) 307-14.

[173] K. Moribe, M. Fukino, Y. Tozuka, K. Higashi, K. Yamamoto, Prednisolone multicomponent nanoparticle preparation by aerosol solvent extraction system, Int J Pharm, 380 (2009) 201-5.

[174] A. Argemí, A. Vega, P. Subra-Paternault, J. Saurina, Characterization of azacytidine/poly(L-lactic) acid particles prepared by supercritical antisolvent precipitation, J Pharm Biomed Anal, 50 (2009) 847-52.

[175] M. Kalani, R. Yunus, N. Abdullah, Optimizing supercritical antisolvent process parameters to minimize the particle size of paracetamol nanoencapsulated in L-polylactide, Int J Nanomedicine, 6 (2011) 1101-5.

[176] M. S. Kim, Influence of hydrophilic additives on the supersaturation and bioavailability of dutasteride-loaded hydroxypropyl-β-cyclodextrin nanostructures, Int J Nanomedicine, 8 (2013) 2029-39.

[177] M. Kim, J. Kim, S. Hwang, Enhancement of Wettability and Dissolution Properties of Cilostazol Using the Supercritical Antisolvent Process: Effect of Various Additives, Chem Pharm Bull, 58 (2010) 230-3.

[178] Y. Zu, D. Wang, X. Zhao, R. Jiang, Q. Zhang, D. Zhao, Y. Li, B. Zu, Z. Sun, A novel preparation method for camptothecin (CPT) loaded folic acid conjugated dextran tumor-targeted nanoparticles, Int J Mol Sci, 12 (2011) 4237-49.

[179] E.S. Kolotova, S.G. Egorova, A.A. Ramonova, S.E. Bogorodski, V.K. Popov, I.I. Agapov, M.P. Kirpichnikov, Cytotoxic and Immunochemical Properties of

Viscumin Encapsulated in Polylactide Microparticles, Acta Naturae, 4 (2012) 101-6.

[180]   F. Zabihi, N. Xin, J. Jia, T. Chen, Y. Zhao, High Yield and High Loading Preparation of Curcumin-PLGA Nanoparticles Using a Modified Supercritical Antisolvent Technique, Ind Eng Chem Res, 53 (2014) 6569-74.

[181]   F. Chen, G. Yin, X. Liao, Y. Yang, Z. Huang, J. Gu, Y. Yao, X. Chen, H. Gao, Preparation, characterization and in vitro release properties of morphine-loaded PLLA-PEG-PLLA microparticles via solution enhanced dispersion by supercritical fluids, J Mater Sci Mater Med, 24 (2013) 1693-705.

[182]   M. Araújo, R. Viveiros, T.R. Correia, I.J. Correia, V.D. Bonifácio, T. Casimiro, A. Aguiar-Ricardo, Natural melanin: a potential pH-responsive drug release device, Int J Pharm, 469 (2014) 140-5.

[183]   M.S. da Silva, R. Viveiros, P.I. Morgado, A. Aguiar-Ricardo, I.J. Correia, T. Casimiro, Development of 2-(dimethylamino)ethyl methacrylate-based molecular recognition devices for controlled drug delivery using supercritical fluid technology, Int J Pharm, 416 (2011) 61-8.

[184]   M. Fraile, ÿ. Martín, D. Deodato, S. Rodriguez-Rojo, I.D. Nogueira, A.L. Simplício, M.J. Cocero, C.M.M. Duarte, Production of new hybrid systems for drug delivery by PGSS (Particles from Gas Saturated Solutions) process, J Supercrit Fluids, 81 (2013) 226-35.

[185]   A. Galia, O. Scialdone, G. Filardo, T. Spanò, A one-pot method to enhance dissolution rate of low solubility drug molecules using dispersion polymerization in supercritical carbon dioxide, Int J Pharm, 377 (2009) 60-9.

CHAPTER 3

Scalable organic solvent free supercritical fluid spray drying process for producing dry protein formulations

O Nuchuchua[1], H A Every[2], G W Hofland[2], W Jiskoot[1]

[1] Division of Drug Delivery Technology, Leiden Academic Centre for Drug Research (LACDR), Leiden University, The Netherlands

[2] FeyeCon Development & Implementation B.V., Weesp,

The Netherlands

Abstract

In this study, we evaluated the influence of supercritical carbon dioxide ($scCO_2$) spray drying conditions, in the absence of organic solvent, on the ability to produce dry protein/trehalose formulations at 1:10 and 1:4 (w/w) ratios. When using a 4L drying vessel, we found that decreasing the solution flow rate and solution volume, or increasing the $scCO_2$ flow rate resulted in a significant reduction in the residual water content in dried products (Karl Fischer titration). The best conditions were then used to evaluate the ability to scale the $scCO_2$ spray drying process from 4L to 10L chamber. The ratio of $scCO_2$ and solution flow rate was kept constant. The products on both scales exhibited similar residual moisture contents, particle morphologies (SEM), and glass transition temperatures (DSC). After reconstitution, the lysozyme activity (enzymatic assay) and structure (circular dichroism, HP-SEC) were fully preserved, but the sub-visible particle content was slightly increased (flow imaging microscopy, nanoparticle tracking analysis). Furthermore, the drying condition was applicable to other proteins resulting in products of similar quality as the lysozyme formulations. In conclusion, we established $scCO_2$ spray drying processing conditions for protein formulations without an organic solvent that holds promise for the industrial production of dry protein formulations.

1. Introduction

Proteins are structurally unstable during purification, processing and storage [1-5]. Several physical and chemical degradation processes can lead to loss of native protein structure and aggregation [6, 7], which can negatively impact the safety and efficacy of therapeutic protein products. In order to improve their shelf-life, therapeutic proteins are often formulated in the solid state in the presence of sugars (e.g., sucrose, trehalose) [8-10] and stored below the glass transition temperature of the formulation [11, 12]. The amount of water present in dry protein formulations has a significant impact on their stability [5, 13, 14]. In such cases, the remaining water may result from bound, surface and/or trapped water, and is different for each protein product [5]. For most freeze-dried protein products, 1% to 3% residual moisture should be low enough to maintain the chemical and/or conformational stability, and therefore the potency of the product over time. This range is consistent with the regulations published in Title 21 of the Code of Federal Regulations for Food and Drugs (1990), which proposes that the maximum residual moisture content should be no greater than 3%. However, since the influence of water on the stability is largely dependent on the type of protein as well as its formulation, the optimal residual moisture level needs to be determined for each protein product.

The number of available methods for drying protein products is limited. While lyophilization is commonly used in industry for the preparation of dry therapeutic protein formulations, spray drying techniques have generated a lot of interest [15-18]. Among the available drying technologies, supercritical carbon dioxide (scCO$_2$) spray drying processes have been found to be advantageous for protein drying due to fast drying times and mild processing conditions at near ambient temperatures (>30°C). Moreover, carbon dioxide is inexpensive, non-toxic and can be recycled. Protein powder production by different scCO$_2$ processing methods has been reported previously [19-26]. In this process, a liquid solution (feed solution, containing protein and/or sugars) and scCO$_2$ pass through a two-fluid nozzle, where the feed solution is atomized by the scCO$_2$ stream. The liquid drops are dried as the result of extraction of water and anti-solvent precipitation of protein and excipients [24, 27]. The finished products can be made in the form of a powder, granules or agglomerates [28]. By controlling the atomizing gas/solution flow rates, nozzle sizes and solution concentrations, free-flowing and uniform spherical particles with a distinct particle size distribution can be prepared [29].

Since the solubility of water in $scCO_2$ is rather limited (about 0.2% (w/w) at 130 bar, 37°C), organic solvents, such as ethanol, have been added to the $scCO_2$ phase to enhance the water solubility and thereby facilitate the drying process [22, 30]. However, organic solvents may perturb the native protein structure and organic solvent residues can be entrapped in the dry products [23], which may compromise their stability. Furthermore, the removal of residual organic solvent typically requires an additional drying step. In order to avoid the use of organic solvents and to design a single-step drying process to meet the criteria of residual moisture content, the drying conditions should be adjusted to compensate for the reduced water uptake in $scCO_2$. In a previous paper we showed that dry protein/trehalose formulations could be produced by supercritical carbon dioxide ($scCO_2$) spray drying without the use of organic solvents, but the residual moisture content for the obtained powders was still relatively high and a secondary (vacuum) drying step was used to reduce it [31]. From this, it can be concluded that the processing conditions were not yet optimal for the production of protein powders and that further investigation was required to determine whether a stable product could be achieved in a single drying step by simply adjusting the processing parameters.

Understanding the operating window of the process is an important consideration for upscaling and subsequent commercialization, as this determines the production capacity and associated operating costs. Up to now, the relationship between the $scCO_2$ processing parameters (such as pressure, solution and $scCO_2$ flow rates) and the residual moisture content of supercritically dried products has not been quantified. Thus, the first aim of this study was to evaluate the influence of the $scCO_2$ processing conditions, in the absence of organic solvent, on the ability to produce dried protein formulations with minimal residual water content in a single drying step.

Although the initial tests were performed on the lab scale, it is also important to understand the ability to scale $scCO_2$ spray drying. Up-scaling is required for production of protein formulations for commercial applications, whereas downscaling can be beneficial when researching expensive active pharmaceutical ingredients. Hot-air spray drying is considered a scalable process [32] that has previously been shown to depend on several aspects, namely 1) atomization, 2) mixing of droplets and drying gas, 3) drying kinetics and residence time and 4) product collection [32]. It is anticipated that these same aspects are relevant in $scCO_2$ spray drying as well. Ideally, all four criteria should be optimized in order to maintain geometric, kinematic and dynamic similarity of the process between the different scales. However, the atomization is of key importance, as it also influences all the other aspects of the drying

process. Thus it is anticipated that by controlling the droplet size via atomization, it is possible to achieve the same product quality on different processing scales, as demonstrated in a hot-air spray drying study [33]. The criteria for up-scaling and down-scaling of the $scCO_2$ spray drying have not yet been established. While it is anticipated that the scaling of the $scCO_2$ process would involve similar aspects to hot-air spray drying, as mentioned above, it is also recognized that there are fundamental differences between the two processes, such as temperature profiles within the vessel and the water uptake capacity of the drying medium. Nevertheless, the ability to control the droplet break-up via atomization will also be an important aspect in $scCO_2$ drying, in order to ensure that a dry powder product is obtained. Thus, the second aim of this research was to evaluate the feasibility to scale the $scCO_2$ spray drying process by simply controlling the atomization by maintaining the same gas-to-liquid mass ratio (GLR) on each scale.

In this study, lysozyme has been chosen as a model protein and trehalose as an excipient in amounts based on previous studies [25, 26, 34]. Dry products were characterized for residual moisture content, particle morphology and glass transition temperature, and reconstituted powders for protein integrity and aggregation. To evaluate the general applicability of the drying process, the best processing conditions determined for the lysozyme/trehalose formulation were used to prepare dried formulations of α-lactalbumin, α-chymotrypsinogen A, and monoclonal IgG. These formulations were also characterized for residual moisture content, protein integrity and aggregation.

2. Materials and Methods

2.1. Preparation and characterization of feed solutions

Liquid formulations were composed of hen egg white lysozyme (70000 U/mg, Sigma-Aldrich, St. Louis, USA) with/without trehalose (Sigma-Aldrich, St. Louis, USA) in deionized water. In addition to lysozyme, similar solutions were also prepared with a monoclonal human IgG used in previous studies [35, 36], α-chymotrypsinogen A from bovine pancreas and α-lactalbumin type III from bovine milk, both purchased from Sigma-Aldrich, St. Louis, USA. The solutions were prepared at 5% solids content according to Table 1. The density of the liquid formulations was analyzed gravimetrically, by weighing the solution upon filling a 25 ml volumetric flask. The kinematic viscosity was determined using an Ostwald viscometer (SI Analytics GmbH, Mainz, Germany). The surface tension was measured by the capillary rise method (Surface tension apparatus, KIMBLE CHASE, New York, USA). Each sample was measured in triplicate

at room temperature (22 °C). All liquid formulations were filtered through a 0.22 μm cellulose filter before the measurements and spray drying experiments.

Table 1. Composition and physical properties of the aqueous feed solutions.

Lysozyme/ trehalose (w/w ratio)	Total solids conc. (% w/w)	Lysozyme conc. (% w/w)	Trehalose conc. (% w/w)	Density* (g/cm^3)	Viscosity* (mPa.s)	Surface tension** (dynes/cm)
0:1	5	0	5.00	1.015	1.03	73.61 ± 1.44
1:10	5	0.45	4.55	1.014	1.05	72.10 ± 0.10
1:4	5	1.00	4.00	1.015	1.06	70.96 ± 0.83

* n = 3 (standard deviation < 0.001), experiments were done at 22 °C, ** Measured surface tension of water was 73.47 ± 0.41 dynes/cm at 22 °C.

2.2. Supercritical carbon dioxide spray-drying processing conditions

Carbon dioxide (grade 3.5) was obtained from Linde Gas (Schiedam, The Netherlands). The drying experiments were carried out at different production scales, involving 1L, 4L and 10L drying chambers. The geometric sizes of the different drying chambers and nozzles are shown in Table 2. The general set-up has been explained in detail by Bouchard et al. [30]. Briefly, the scCO$_2$ was supplied by a diaphragm pump (Lewa, Leonberg, Germany) and the formulation solution was fed by a syringe pump (Isco, Lincoln, USA). They were then fed together through a coaxial converging nozzle (Spraying Systems Co. B.V., Ridderkerk, The Netherlands) into a vessel containing scCO$_2$ [22].

Table 2. Geometry of drying chambers and nozzles used for the different production scales.

Drying chamber	Diameter (cm)	Length (cm)	Nozzle diameter (D)	
			D_{Liquid} (cm)	D_{CO_2} (cm)
1L	6.5	25	0.04	0.16
4L	10	50	0.04	0.16
10L	13	75	0.04	0.24

A 4L batch production scale unit (Separex, F54250 Champigneulles, France) was used for initially optimizing the spraying conditions, which are summarized in Table 3. The experimental variables were pressure (E, H), scCO$_2$ flow rate (A, B), solution volume (D, E, F) and solution flow rate (B, C, E, G). Once the solution was sprayed, the resultant powdered product was flushed with fresh scCO$_2$ for 30 minutes before harvesting, to remove excess water from the spray-drying vessel.

All products were collected by a filter paper (Whatman® qualitative filter paper, Grade 1, 25 mm diameter, Diegem, Belgium) at the bottom part of the drying chamber.

The conditions that gave rise to the lowest residual moisture content on the 4L system were then scaled accordingly and evaluated on 1L and 10L scales (Table 3). For these experiments, the temperature and pressure were kept constant at 130 bar and 37°C, respectively. The powder was stored in a desiccator at room temperature (22°C) before further analysis.

Table 3. Spraying conditions used for the different production scales.

Conditions*	Pressure (bar)	Feed rate (g/min)	scCO$_2$ flow (g/min)	GLR** (x10^3)	Feed volume (g)
4L production scale					
A	130	0.1	208	2.08	15
B	130	0.1	500	5	15
C	130	0.2	500	2.5	15
D	130	0.3	500	1.67	7.5
E	130	0.3	500	1.67	15
F	130	0.3	500	1.67	30
G	130	0.5	500	1	15
H	180	0.3	500	1.67	15
1L production scale					
I	130	0.04	208	5	15
J	130	0.08	208	2.5	15
K	130	0.13	208	1.67	15
L	130	0.21	208	1	15
10L production scale					
M	130	1	5000	5	150
N	130	2	5000	2.5	150
O	130	3	5000	1.67	150
P	130	5	5000	1	150

*Effect of pressure: E, H, Effect of scCO₂ rate: A, B, Effect of feed volume: D, E, F, Effect of feed rate: B, C, E, G. All conditions were carried out at 37 °C.,**GLR is the atomization mass ratio of gas-to-liquid through a nozzle, where gas refers to $scCO_2$ in this study.

2.3. Powder characterization

2.3.1. Residual moisture content

The residual moisture content of dried powders was measured in triplicate with a Karl-Fischer coulometer (Metrohm 756F, Herisau, Switzerland) as per the manufacturer's instructions. 10 mg of powder, accurately weighed, was added to 1 ml of methanol and left for at least 30 min. 100 µl of the mixture was then injected into the sample chamber for analysis. Residual moisture contents were calculated from three different spray-dried batches at any given spray-drying condition, and expressed as a percentage of the sample weight (% w/w) with the standard errors.

2.3.2. Scanning electron microscopy

The morphology of the particles was examined by using a scanning electron microscope (Jeol JSM-5400, Tokyo, Japan). Particles were fixed to the specimen holder with conductive double sided tape before sputtering with a thin layer of gold. The power and magnification were 10 kV and 3,500 fold, respectively. In order to determine the particle size, the diameter of forty of the perfectly spherical microparticles was measured relative to the scale bar in each picture. The average particle sizes were presented with the standard errors.

2.3.3. Differential scanning calorimetry

Differential scanning calorimetry (DSC) was performed with a Polymer Laboratories DSC (PL-DSC, TA instrument, USA) by using a method reported by Pikal et al. [14]. Briefly, powdered samples of approximately 5-6 mg were pressed into hermetically sealed pans. The samples were first heated at 10 °C/min until the T_g was found and then super-cooled to -20 °C at 100 °C/min. The samples were then subjected to a second heating scan at 10 °C/min until 200 °C. The glass transition temperature (T_g) is observed as a step transition in the heat capacity as a function of temperature, as the material changes from the glassy to rubbery state. For the dry sample formulations, the T_g is reported as the

mid-point relative to the onset and offset temperature of this step transition.

2.4. Protein analysis

2.4.1. Protein content

About 5 and 11 mg of dry formulation 1:4 and 1:10, accurately weighed, were dissolved in 1 ml of water. Owing to the amorphous state of the powders, the samples dissolved immediately to form an aqueous solution, which was gently mixed by hand before experiments. The protein concentration in solution was theoretically 1 mg/ml and the solution was subsequently diluted to approximately 0.1 mg/ml prior to measurement. The protein content was then determined by using a UV spectrophotometer (Agilent 8453, Agilent Technologies, Santa Clara, USA) at 280 nm, using extinction coefficients of 2.64, 2.01, 2.00 and 1.69 ml cm^{-1} mg^{-1} for lysozyme [37], α-lactalbumin [38], α-chymotrypsinogen A [39], and monoclonal IgG [36], respectively.

2.4.2. Lysozyme activity assay

The enzymatic activity of lysozyme in scCO$_2$ processed powder was determined using a bacteriolysis assay based on the decrease in optical density of a *Micrococcus lysodeikticus* suspension at 450 nm (Agilent 8453, Agilent Technologies, Santa Clara, USA). Five microliters of 0.01 mg/ml lysozyme was added to 200 μl of 0.2 mg/ml of *M. lysodeikticus*. The reaction was carried out in 66 mM phosphate buffer, pH 6.2. Native lysozyme and blank buffer were used as a positive and negative control, respectively, as described elsewhere [34].

2.4.3. Circular dichroism spectroscopy

In order to study the structure of processed proteins, far-UV (190–260 nm) and near-UV (250–320 nm) circular dichroism (CD) spectroscopy measurements (J-810 Spectropolarimeter, JASCO Inc., Easton, USA) were performed at 25 °C, using a 0.1-cm and a 1-cm quartz cuvette, respectively. Parameters were set at a sensitivity of 100 mdeg, with a data pitch of 10 nm, a bandwidth of 2 nm, a scanning speed of 100 nm. Samples were freshly prepared in 66 mM phosphate buffer (PB) at pH 6.2 with a lysozyme concentration of 0.2 and 1 mg/ml for far-UV and near-UV CD measurements, respectively. CD spectra of six

sequential measurements were averaged and corrected for the blank (PB). The CD signals were converted to molar ellipticity per amino acid residue ([θ]).

2.4.4. High performance size-exclusion chromatography

Samples (50 µl of 1 mg/ml protein concentration) were analyzed by high performance size-exclusion chromatography (HP-SEC) with a Discovery® BIO Gel Filtration column (300 Å pore size) (Sigma-Aldrich, St. Louis, USA) and Super SW guard column (Sigma Aldrich). A 515 HPLC pump and 717 Plus autosampler (Waters, Milford, USA) were operated at a flow rate of 0.7 ml/min. The mobile phase consisted of 100 mM sodium phosphate buffer, 200 mM sodium chloride, 0.05% (w/v) sodium azide and 0.1% (w/v) SDS at a pH of 7.2 and was filtered through a 0.2 um filter prior to use. Chromatograms were recorded with an SPD-6AV UV detector (Shimadzu, Tokyo, Japan) at a wavelength of 280 nm.

2.4.5. Nanoparticle tracking analysis

Sub-micron particles were studied by nanoparticle tracking analysis (NTA). Dry powder formulations were redissolved in deionized water at 5% by weight of solid, the same as the concentration of the liquid formulations before scCO$_2$ processing. NTA measurements were performed with a NanoSight LM20 (NanoSight, Amesbury, UK), equipped with a 640-nm laser. The samples were injected in the sample chamber with sterile syringes (BD Discardit II, New Jersey, USA). All measurements were performed at 22 °C. The software used for capturing and analyzing the data is the NTA 2.0 Build 127. The samples were measured for 100 s with manual shutter and gain adjustments [40]. The "single shutter and gain mode" was used to capture images of the protein aggregates. The mean arithmetic size was calculated by using the NTA software. Each sample was measured in triplicate.

2.4.6. Flow imaging microscopy

Protein formulations (5% solid content) were dissolved in deionized water and sub-visible microparticles were determined by flow imaging microscopy using an MFI5200 instrument (Protein Simple, California, USA). The measurements were controlled by MVAS software version 1.3. One milliliter of solution was introduced into a flow-cell with a dimension of 100 and 1016 µm in depth and diameter, respectively.

The sample stream, at a flow rate of 6 ml/min, passed through a flow-cell illuminated by a blue LED. Images of the particles were captured by an optical camera. Pictures were the resolution of 1280x1024 pixels. The data were analyzed by MVAS software (Release 1.3). Total particle concentrations are reported for particle sizes larger than 1, 10, and 25 µm.

3. Results

3.1. Optimization of the spraying conditions to minimize the water content

The first step was to study the processing conditions in order to achieve a dried powder protein formulation with minimal residual moisture content without the use of organic co-solvents. For these experiments, we used the 4L drying chamber. Spray drying parameters such as pressure, $scCO_2$ flow rate, solution volume and flow rate, were varied in this study (see Table 3). Trehalose solution alone was used to evaluate the spraying conditions, because it is a hygroscopic material and the main component in the dried protein formulations.

Increasing the operating pressure from 130 (E) to 180 (H) bar did not show a significant effect on the residual moisture content, which was found to be 3.67±0.04 % and 3.40±0.70%, respectively. Thus, a pressure of 130 bar was used in the subsequent experiments.

Under condition E, dried powder was harvested with and without a post-drying process, and the residual moisture contents measured immediately. Dried products without post-drying presented comparatively high residual water contents (4.81±0.08%). Thus, the post-drying for half an hour was consistently used in all other experiments.

The residual moisture content was found to increase when the $scCO_2$ flow rate was decreased. The spraying condition B ($scCO_2$ flow rate 500 g/min) and A (208 g/min) yielded a residual moisture content of 2.38±0.12% and 3.50±0.38%, respectively. Therefore, the $scCO_2$ flow rate was kept at 500 g/min for the subsequent tests, which is the maximum flow rate for the 4L drying chamber.

Different solution volumes were studied and found to significantly influence the residual moisture content, as shown in Fig. 1a. Upon spraying 30 g of sample (F), the residual moisture content was about 6.40±0.38%. When the feed volume was decreased to 15 g and 7.5 g (E and D, respectively), the water content also decreased and approached a value of approximately 4%. Furthermore, the solution flow

rate was varied from 0.1 to 0.5 g/min (condition B, C, E, G) and its effect on the residual moisture content is demonstrated in Fig. 1b. The moisture content was decreased from about 3.67% to 2.48% when the feed rate was reduced from 0.3 g/min to 0.2 g/min. A further reduction of the solution flow rate to 0.1 g/min did not significantly affect the residual moisture content (2.38%). Conversely, no dried products were obtained when a solution flow rate of 0.5 g/min was applied.
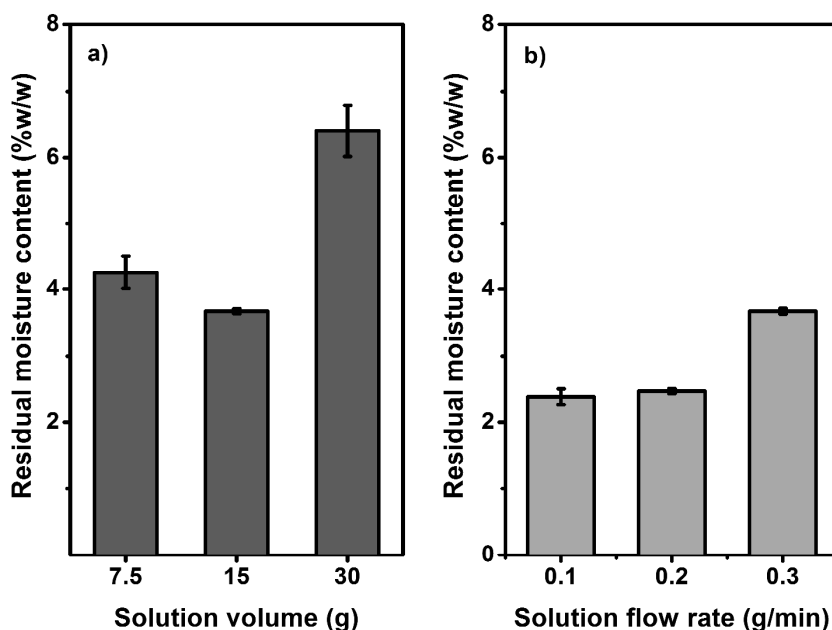
Fig. 1 Effect of a) feed solution volume (feed rate: 0.3 g/min) and b) feed rate (feed volume: 15 g) of an aqueous 5% (w/w) trehalose solution with 500 g/min CO_2 flow on the residual moisture content of the obtained powder, using the 4L drying chamber (conditions D, E, F and B, C, E; see Table 3).

From the above-mentioned results, it is apparent that the lowest residual moisture content (2.38±0.12%) in the dried formulations was obtained under condition B (see Table 3), corresponding to a feed volume and rate of 15 ml and 0.1 g/min, respectively, and a CO_2 flow rate of 500 g/min (thus, a gas/liquid mass ratio (GLR) of 5000), with a post drying time of half an hour. When applying these conditions to lysozyme formulations, containing lysozyme and trehalose in a 1:4 and 1:10 (w/w) ratio (Table 1), dry powder products were obtained with a similar residual

moisture content of 2.47±0.12 and 2.68±0.08%, respectively (Table 4). Further analysis of the products is reported in section 3.3.

Table 4. Characteristics of powdered products produced at two different production scales.

Formulation	Moisture content (%by weight)	T_g (°C)	Lysozyme content (%by weight)		Lysozyme activity (%)	Average size of dried particles** (μm)
			Theoretical	Experimental		
Condition B*						
0:1	2.38± 0.12	70.21± 1.57	-	-	-	0.99 ± 0.45
1:10	2.68± 0.08	72.04± 3.54	9	10.46 ± 0.00	102.86± 1.92	1.11 ± 0.79
1:4	2.47± 0.12	72.22± 1.30	20	28.75 ± 0.01	102.27± 0.65	1.29 ± 0.56
Condition M*						
0:1	2.46± 0.12	73.74± 4.15	-	-	-	1.04 ± 0.35
1:10	2.37± 0.20	70.45± 3.02	9	11.77 ± 0.00	100.55± 2.55	1.08 ± 0.50
1:4	2.62± 0.13	73.22± 0.96	20	22.82 ± 0.02	102.44± 4.38	1.25 ± 0.59

*See Table 3, **n = 40

3.2. Scalability of the scCO₂ spray drying process

The scalability of the developed process was tested by using drying chambers of 1L, 4L and 10L scale. For each system, the maximum scCO₂ flow rates used were 208, 500, and 5000 g/min, respectively. The geometry of vessels and the size of the nozzles are listed in Table 2. The diameter of the scCO₂ nozzle on 10L scale was bigger than that of others to allow for the higher scCO₂ flow rate. Notably, dried lysozyme/trehalose formulations could not be produced under any condition in the 1L vessel.

In the up-scaling study, four gas-to-liquid mass ratios (GLR 5000, 2500, 1670 and 1000) were applied on both 4L and 10L scale (Table 3, conditions B, C, E, G and M, N, O, P). Fig. 2 shows the residual moisture content in trehalose powders as a function of GLR for both scales. Increasing the GLR significantly reduced the residual moisture content for both scales, from about 4% to 2.4%. For a GLR of 1000, no dry powders could be produced; instead a dried thin film was obtained on the paper filter.

Dry formulations 1:4 and 1:10 of lysozyme and trehalose have been produced under conditions B and M on 4L and 10L scales

(corresponding to a GLR of 5000, Table 3). The residual moisture contents of dried lysozyme formulations were comparable to those of the dried pure trehalose (Table 4).
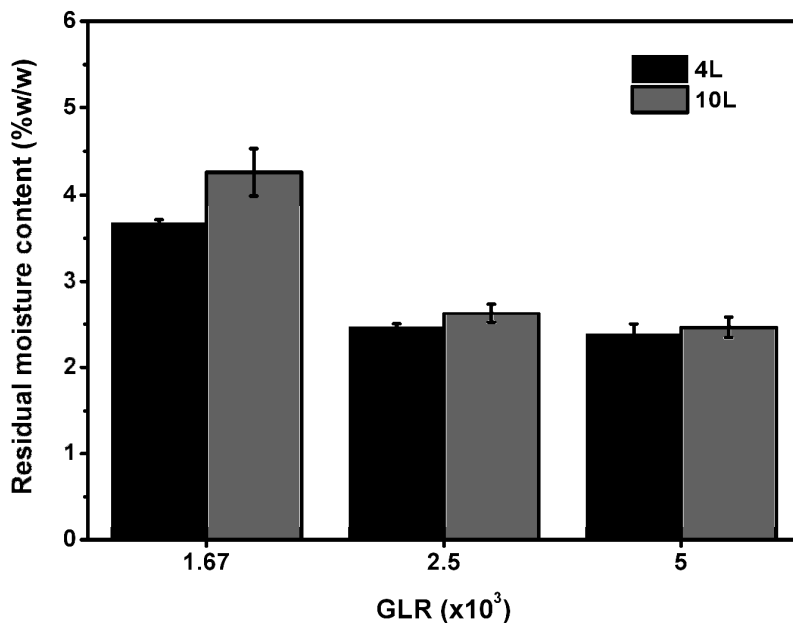
Fig. 2 Effect of the gas-to-liquid ratio (GLR) on the residual moisture content of the obtained trehalose powders, using the 4L (black) and 10L (gray) drying chambers (conditions B, C, E and conditions M, N, O, respectively; see Table 3).

3.3. Product characterization

3.3.1. Glass transition temperature

The glass transition temperature (T_g) of the dried formulations produced under conditions B and M was determined by DSC. T_g values of about 70-74 °C were observed, independent of formulation composition and production scale (Table 4).

3.3.2. Particle morphology

The morphology of the dry powder formulations was observed by scanning electron microscopy. Fig. 3 shows the trehalose powders prepared with different feed rates on 4L and 10L scales. The same GLR for different production scales gives particles that are visually very similar; they were 1-5 µm in range and appeared visually agglomerated. Fig. 4 presents the particle morphology of dry lysozyme/trehalose formulations (1:4 and 1:10), which show a dimpled surface. The average particle sizes of dry products produced by different drying chambers, but with the same GLR (5000), were determined relative to the standard scale bar in their SEM pictures, as reported in Table 4. The average sizes of dried lysozyme formulation particles on the 4L scale were similar to those of the 10L scale products.

3.3.3. Protein integrity after drying

In order to evaluate the protein integrity in the dry powder formulations immediately after the production day, the lysozyme content, activity, structure and aggregate content were analyzed after reconstitution in ultrapure water. No insoluble residues were visually observed for any of the solutions. The enzymatic activity of the reconstituted lysozyme formulations was fully recovered (Table 4). Results of far-UV and near-UV spectroscopy suggested that both the secondary and tertiary structure of lysozyme was totally preserved after processing (Fig. 5). Moreover, HP-SEC indicated that drying had not induced any lysozyme aggregation or fragmentation (Fig. 6). However, nanoparticle tracking analysis (NTA) and flow imaging microscopy indicated an increase in the number of nanoparticles and microparticles (Fig. 7 and 8) as compared to liquid formulations of lysozyme before the drying process. Upon increasing the lysozyme content, the number of particles increased. Surprisingly, particles were also detected for the pure trehalose formulation. Nanoparticle formation was more pronounced for powders produced in the 4L drying chamber compared to the 10L vessel (Fig. 7b and c). The size distributions were similar, with most of the particles in the range of 100 to 400 nm.

In contrast to the nanoparticle counts, the total microparticle counts in dried samples produced in the 10L vessel were higher than those of the 4L scale, as shown in Fig. 8. In addition, formulation 1:4 contained a higher microparticle load than formulation 1:10. The majority of the detected particles had a size between 1 and 10 µm (Table 5).
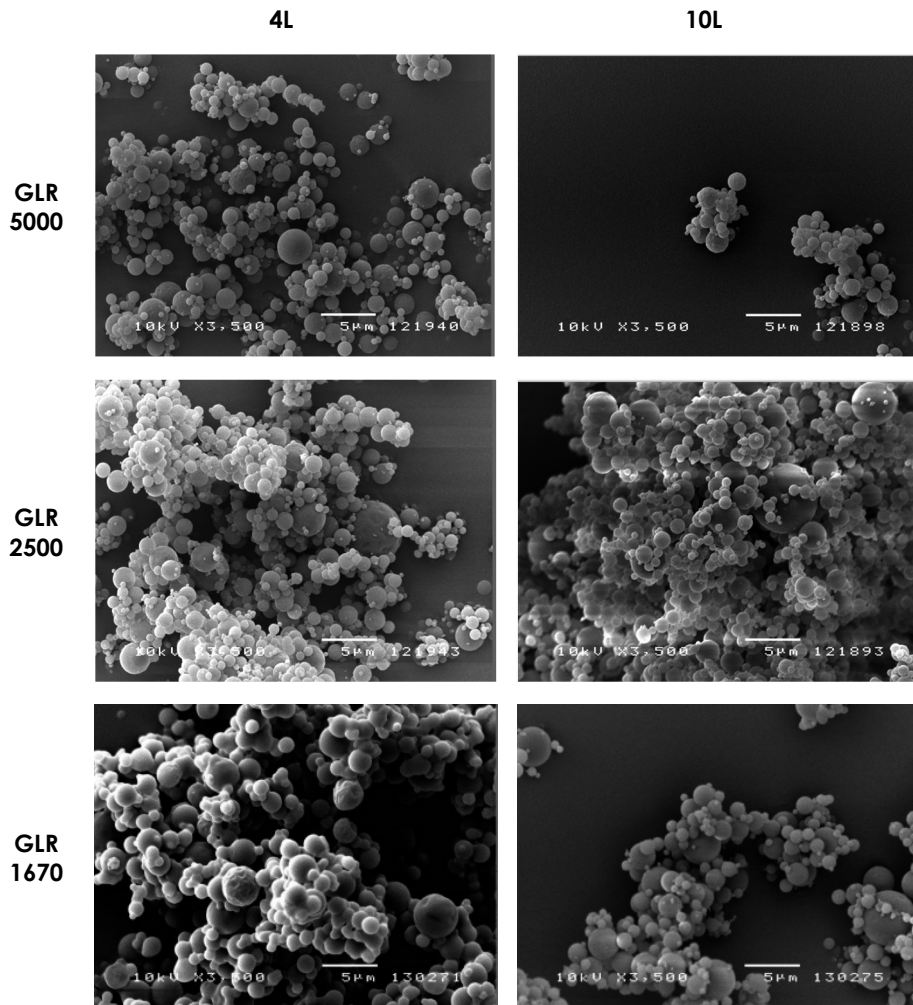
Fig. 3 Particle morphology of trehalose produced in the 4L (left panel) and the 10L (right panel) drying chambers. GLR are indicated for each spraying condition. The spraying conditions are B, C, E and M, N, O at the 4L and 10L scale, respectively (see Table 3).
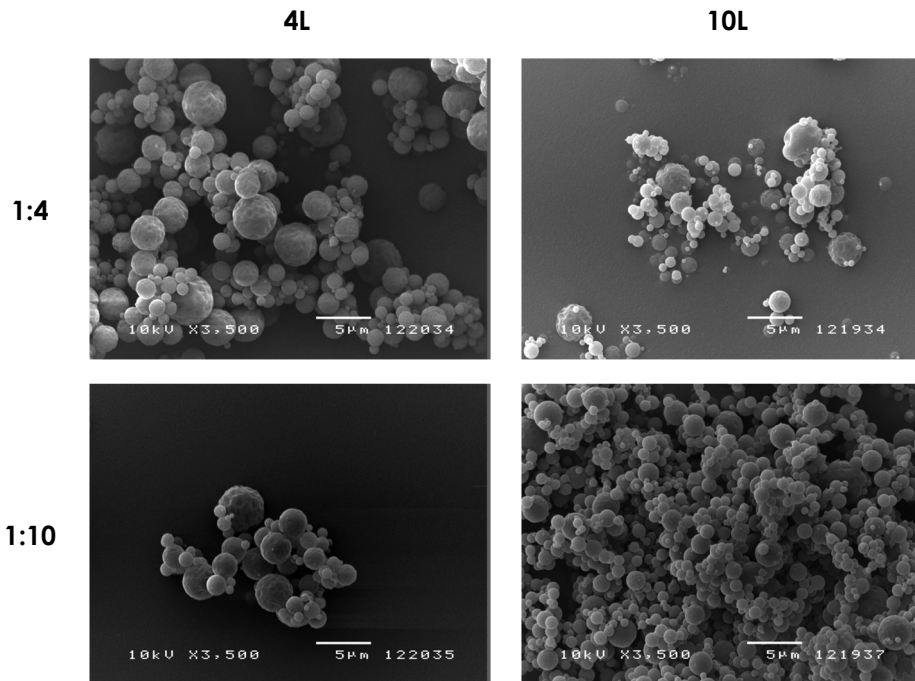
Fig. 4 Particle morphology of dried formulations of 1:4 and 1:10 of lysozyme and trehalose produced in the 4L (left panel) and 10L (right panel) drying chambers with condition B and M (see Table 3) at GLR 5000.
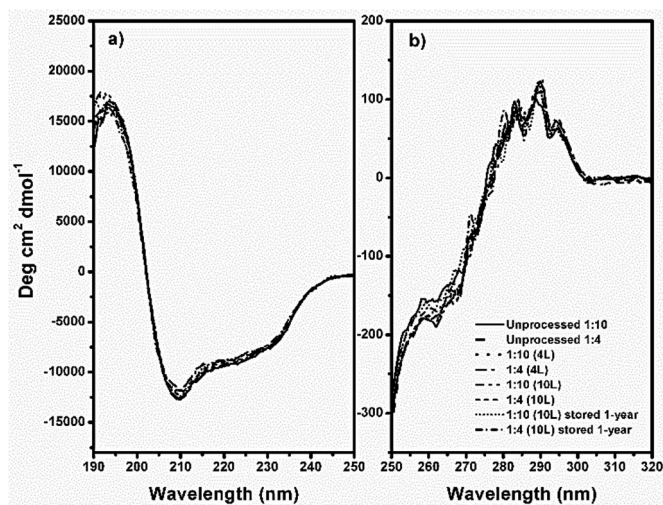
Fig. 5 Far-UV (a) and near-UV (b) circular dichroism spectra of lysozyme formulations with trehalose (1:10 and 1:4) before and after drying in the 4L (condition B) and 10L (condition M) drying chambers on the production day (see Table 3), and after one-year storage. Dried formulations were reconstituted in water prior to analysis. Unprocessed lysozyme of formulation 1:10 and 1:4 was used as a control.
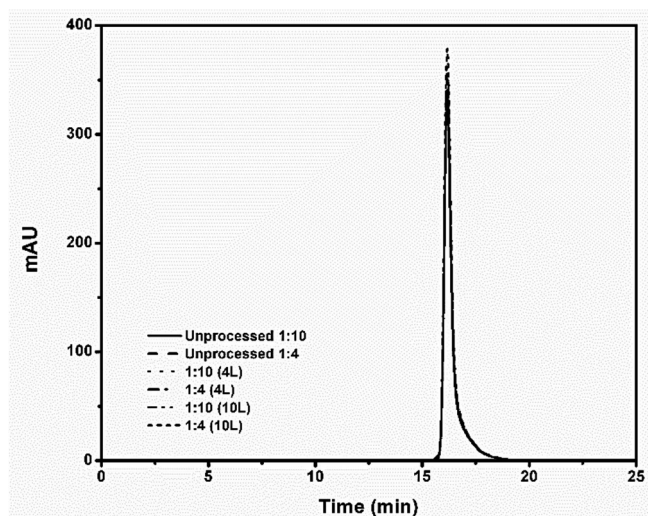
Fig. 6 High performance size-exclusion chromatograms of lysozyme before and after drying in the 4L and 10L drying chambers by condition B and M (see Table 3), respectively. Dried formulations were reconstituted in water prior to analysis. Unprocessed lysozyme of formulation 1:10 and 1:4 was used as a control.

3.3.4. Protein integrity after drying and storage

Dried protein formulations were stored in a desiccator at room temperature for a year, after which the protein activity and structure were analyzed. The lysozyme activity of formulation 1:4 dropped to 86.73±2.30%, whereas the lysozyme activity of formulation 1:10 was preserved during storage (105.63±2.38%). Moreover, the secondary and tertiary structure of lysozyme in both formulations was fully maintained, as observed by circular dichroism (Fig. 5a, b). In addition, the nanoparticle and microparticle contents in reconstituted solutions were not significantly different, compared to the results obtained immediately after the production day (Fig. 7 and 8).
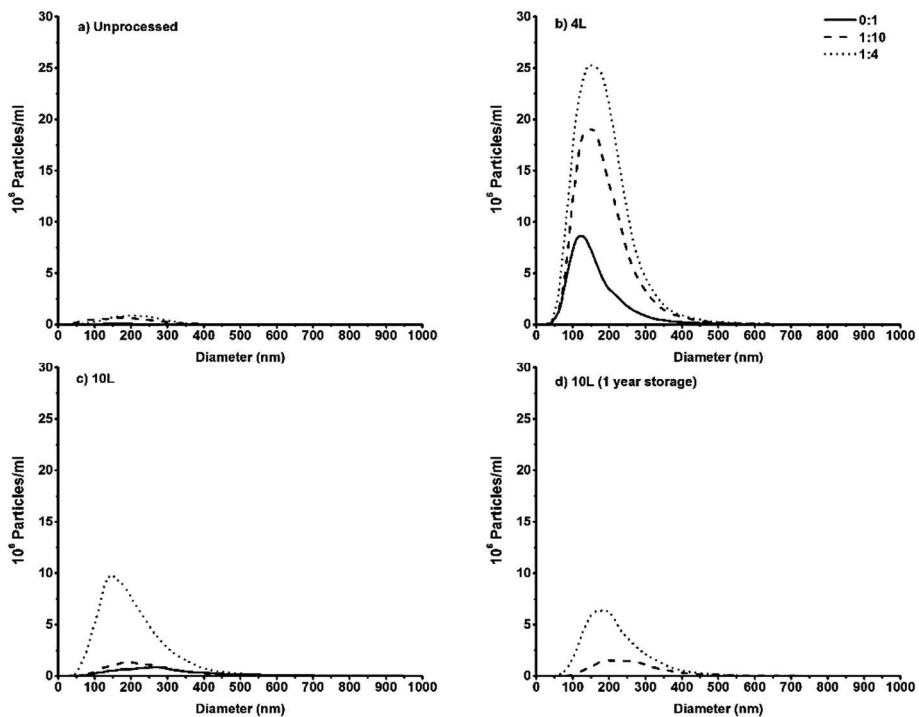
Fig. 7 Number of sub-micron particles detected by NTA. Lysozyme formulations with trehalose (0:1, 1:10 and 1:4) were analyzed before (a) and after drying in the 4L (b) and 10L (c) drying chambers on the production day. The formulations 1:10 and 1:4 produced at 10L scale were also analyzed after one-year storage (d). Dried formulations were produced by using conditions B and M, respectively, and reconstituted in water prior to analysis.
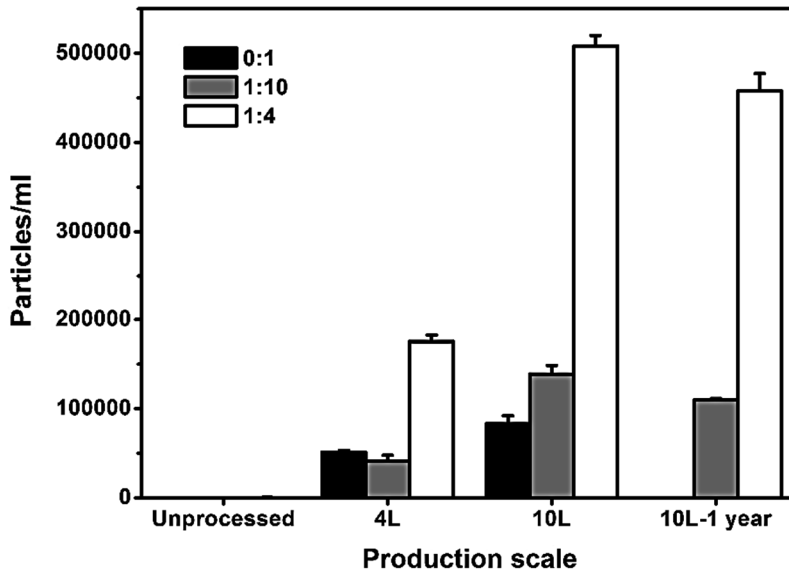
Fig. 8 Total number of sub-visible particles ($\geq 1\ \mu m$) detected by flow imaging microscopy. Lysozyme formulations with trehalose (0:1, 1:10 and 1:4) were analyzed before and after drying in the 4L and 10L drying chambers on the production day. The formulations 1:10 and 1:4 produced at 10L scale were also analyzed after one-year storage. Dried formulations were produced by using conditions B and M, respectively, and reconstituted in water prior to analysis.

Table 5.   Number of sub-visible particles (per ml) in formulations before drying and after reconstitution of dried powders by MFI.*

Formulations	Before drying	4L**	10L***
Number of particles (> 1 μm)			
0:1	86 ± 16	51315 ± 2032	83122 ± 8829
1:10	138 ± 11	41438 ± 6483	139029 ± 9344
1:4	360 ± 61	175259± 7388	508466 ± 11737
Number of particles (> 10 μm)			
0:1	1.39 ± 1.29	135 ± 56	620 ± 103
1:10	2.49 ± 2.10	502 ± 162	899 ± 10
1:4	5.16 ± 1.37	722 ± 139	2793 ± 512
Number of particles (> 25 μm)			
0:1	0	3.28 ± 5.67	39.3 ± 16.2
1:10	0.55 ± 0.95	18.6 ± 9.6	20.1 ± 4.1
1:4	0.42 ± 0.74	12.0 ± 5.3	165 ± 86

* Values represent mean ± standard deviation (n = 3), ** Spraying condition B (see Table 3), *** Spraying condition M (see Table 3)

3.3.5. Applicability of the developed method to other proteins

Three other proteins, α-lactalbumin, α-chymotrypsinogen A, and monoclonal IgG, were substituted for lysozyme in the 1:10 formulation and dried at 4L scale following condition B (see Table 3). The powdered products were similar in appearance to the corresponding dry lysozyme formulation. It was observed that the residual water contents were constant at 2.65%, 2.42%, and 2.41% for the formulations of α-lactalbumin, α-chymotrypsinogen A, and IgG, respectively. Upon reconstitution of the protein formulations in ultrapure water, UV-Vis analysis of these solutions showed that the protein contents were fully recovered for all formulations except IgG, where only 75% of the protein was detected in the reconstituted solution. The secondary structures of processed α-lactalbumin, α-chymotrypsinogen A, and IgG were not changed (Fig. 9), and their tertiary structures were fully preserved according to near-UV circular dichroism spectroscopy (data not shown). HP-SEC did not reveal any protein aggregation or fragmentation peaks in case of α-lactalbumin, α-chymotrypsinogen A, and IgG. However, a decrease in the monomer recovery was observed for α-lactalbumin and IgG, as shown in Fig. 9.

The number of microparticles detected by flow imaging microscopy for each of the protein formulations is reported in Table 6. For processed α-lactalbumin, the microparticle concentrations were very similar to those of the corresponding lysozyme formulation (cf. Table 5). However, the microparticle concentrations for α-chymotrypsinogen A and IgG were more than one order of magnitude higher than those for lysozyme and α-lactalbumin.

With respect to the nanoparticle content, NTA showed that the scCO$_2$ dried α-lactalbumin, chymotrypsinogen A, and IgG formulations contained higher particle concentrations than the respective unprocessed protein solutions (Fig. 9). Nevertheless, the nanoparticle concentrations for all of these processed formulations were considerably lower than those of the processed lysozyme formulations (cf. Fig. 7). For IgG, the particle size distribution was slightly shifted to larger particles. For α-chymotrypsinogen A, the presence of large particles (>1 μm) caused interference in the light scattering in the NTA technique [40], which gave rise to a strong erroneous signal in the size range below 100 nm (Fig. 9).
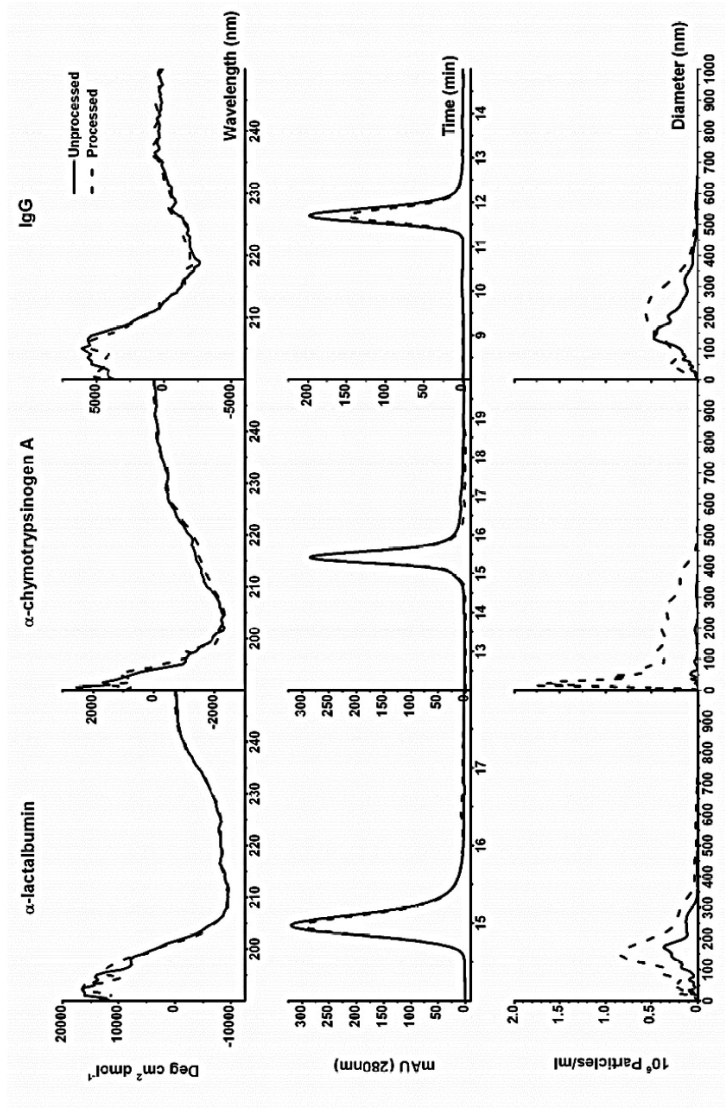
Fig. 9 Far-UV circular dichroism spectra (upper graphs), high performance size-exclusion chromatograms (middle graphs), and NTA results (lower graphs) of α-lactalbumin, α-chymotrypsinogen A, and monoclonal IgG formulation with trehalose (1:10 (w/w)) analyzed before (solid lines) and after drying and reconstitution (dotted lines). Dried formulations were produced by using conditions B (see Table 3).

Chapter 3

Table 6. Residual water content, protein recovery and number of sub-visible microparticles/ml in 1:10 (w/w) protein/trehalose formulations before drying and after reconstitution of dried powders.

1:10 w/w protein/trehalose formulations	Residual water content (% w/w)	Protein recovery** (%)	Micro-flow imaging (particles/ml)***		
			≥ 1 μm	≥ 10 μm	≥ 25 μm
Unprocessed					
α-lactalbumin A	NA***	NA	3981 ± 574	105 ± 15	34 ± 8
α-chymotrypsinogen A	NA	NA	11832 ± 2065	400 ± 61	44 ± 7
Monoclonal IgG	NA	NA	640 ± 246	33 ± 9	6 ± 1
*scCO$_2$ drying processed**					
α-lactalbumin A	2.65 ± 0.47	96.98 ± 4.70	37005 ± 3142	182 ± 5	18 ± 5
α-chymotrypsinogen A	2.42 ± 0.29	101.22 ± 8.11	1466708 ± 16484	33118 ± 1891	3201 ± 162
Monoclonal IgG	2.41 ± 0.21	75.60 ± 1.45	981835 ± 24496	23724 ± 3122	1004 ± 135

Spraying condition B (see Table 3), ** Absorbance at 280 nm, *** Values represent mean ± standard deviation (n = 3), NA = Not applicable

4. Discussion

4.1. Evaluation of the spraying conditions in order to minimize the water content

The present study clearly shows that the residual moisture content depends on the spraying conditions, in particular the carbon dioxide and solution flow rates, and solution volume. However, pressure is not expected to have a significant influence, as the solubility of water in $scCO_2$ is only slightly higher when pressure is increased (0.185 % (w/w) at 130 bar compared to 0.209 % (w/w) at 180 bar) [41].

Trehalose alone was used in the initial experiments; due to their hygroscopicity, the drying of sugars is more complicated than drying proteins alone. The ability to produce free-flowing sugar powders is strongly dependent on both the temperature and relatively humidity (RH) of the drying medium. If the atomized droplets are unable to dry sufficiently during the spray drying process, the particles will tend to collide and stick to one another, which is referred to as stickiness [42]. For low-molecular-weight materials such as mono- and discaccharides, the glass transition temperature (T_g) is a good approximation for the stickiness temperature [43]. The glass transition temperature of sugars is strongly influenced by the water activity (RH). Exposure of trehalose to increasing RH results in a reduction in T_g from 120°C at 0% to 37°C at 40%RH [44]. Consequently, if the RH in the vessel is too high, then the T_g will be lower than the processing temperature, thus leading to increased stickiness and product collapse. Based on the results from Heljo et al. [44], it is anticipated that a free-flowing trehalose powder will only be obtained if the RH does not exceed 40% under the current processing conditions.

During the spray drying process, the relative humidity in the drying vessel tends to increase upon feeding of the aqueous solution. However, there is also continuous flow of the $scCO_2$ during spraying that removes the water from the vessel. The rate of water removal (and by association, the water accumulation) will depend on the mass transfer of water from the sprayed solution to the $scCO_2$ phase, and will be influenced by the relative flow rates of both the aqueous solution and carbon dioxide. For a given $scCO_2$ flow rate, it is possible to determine the time taken for $scCO_2$ in the vessel to be refreshed, referred to here as the regeneration time. In the case of the 4L vessel (3080 g CO_2), the regeneration time is 6.16 minutes for a $scCO_2$ flow rate of 500g/min (3080 g CO_2/500 g/min). Therefore, in order to avoid excessive water accumulation during spraying, the solution flow rate should be such that

most of the water is removed during the time taken to regenerate the $scCO_2$.

The water saturation limit in $scCO_2$ at 130 bar and 37°C is 0.185% (w/w). Under these conditions, the 4L vessel contains 3080 g of carbon dioxide, which would require 5.69 g of water to reach water saturation (100% RH) under static conditions. In order to limit the RH to 40%, the amount of water in $scCO_2$ should not exceed 2.27 g during the entire spraying process in order to obtain dry products. Based on the $scCO_2$ regeneration times, it is possible to calculate the maximum solution flow rate required to avoid accumulating this amount of water in the vessel. For a $scCO_2$ flow rate of 500 g/min, the solution flow rate should be less than 0.37 g/min (max 2.27 g water is fed into the vessel during 6.16 min). In the case of lower $scCO_2$ flow rates, this maximum solution flow rate will also be reduced. In this study, the results showed that the residual moisture contents of the dry powders were significantly higher in the case of 0.3 g/min solution flow rate, while 0.1 and 0.2 g/min gave very similar results. Furthermore, a dried product was not obtained when 0.5 g/min solution flow rate was used in the process. These results are consistent with the above calculations, and confirm that the appropriate solution flow rate is less than 0.3 g/min under these conditions. However, it should be noted that these calculations are based on equilibrium conditions, and have not taken into consideration the accumulation of water over longer periods of time.

A similar increase in the residual moisture content was also observed when the volume of solution was increased. A solution volume of 30 g fed at 0.3 g/min resulted in a high residual moisture content in the dry product, as clearly shown in Fig. 2. For solution volumes of 7.5 and 15 g, the residual moisture contents decreased and were constant. Thus, it is apparent that the solution volume (and correspondingly the spraying time) is also an important factor in minimizing the water accumulation in the vessel.

Based on these results, it appears that the residual moisture content in the trehalose powders is dependent on the water accumulation, and by association the relative humidity in the spraying vessel. An increase in the amount of solution sprayed and/or the solution flow rate will result in faster accumulation of water. It is hypothesized that during the course of spraying, the water accumulation affects the drying process, thus limiting the removal of the water from the sprayed droplets. The resultant powder products will subsequently contain higher residual moisture contents with increasing solution volume.

In this study, the lowest moisture contents of about 2.38-2.46% were obtained when 15 g of solution was sprayed with a solution flow rate of 0.2 g/min or less and maximum carbon dioxide flow rate with half an hour of post-drying time. Around 2.5% moisture content, the glass transition temperature of lysozyme/trehalose formulations was about 70 °C. There was no clear relationship between the formulation composition and the resultant glass transition temperature. In conclusion, the $scCO_2$ spray drying process was able to produce dry products with low moisture content, which were within the range of standard moisture contents for freeze-dried products.

4.2. Evaluation of the scalability of the spray drying process

Having established the influence of the processing conditions on the residual moisture content, the next step was to evaluate whether it is possible to obtain the same products upon scaling the process. The scalability of the $scCO_2$ spray drying process was investigated for three different scales (1L, 4L and 10L), with the coaxial nozzle dimensions as shown in Table 2. The basic settings used for each system were based on the best conditions determined for the 4L scale. As mentioned earlier, the ability to obtain the spray-dried products depends on four factors; atomization, mixing of droplets and drying gas, drying kinetics and residence time, and product collection [32]. In this study, we found that a constant GLR was feasible for up-scaling the $scCO_2$ spray drying method, but the vessel dimension is also an important factor to obtain a powdered product.

4.2.1. Effect of GLR

Upon scaling, maintaining the original droplet size via the atomization process is of key importance, to ensure that the particle size and product quality are the same. In case of a two-fluid nozzle, the droplet size can be controlled by varying the GLR through the nozzle [32]. Since the physical properties of the lysozyme solutions were not significantly different in terms of viscosity, density, and surface tension (see Table 1), the droplet break-up is expected to be the same for each solution.

For a GLR of 5000, spray-dried products of lysozyme/trehalose formulations (1:4 and 1:10) contained about 2.5% residual water on both the 4L and 10L scales. Moreover, when comparing the microparticle sizes of the dried formulations prepared on both scales, the results were

also very similar, as can be seen in the SEM pictures. This is consistent with the previous study [30], where it has been reported that for GLR values greater than 10, the droplet size is constant.

To sum up, our study showed that it is feasible to scale up $scCO_2$ spray drying by maintaining the same GLR. The quality of the final products was found to be the same for both the 4L and 10L scale.

4.2.2 Effect of vessel dimensions

In the case of the 4L setup, it was shown that the ability to dry the protein formulation was dependent on the accumulated water, and correspondingly the relative humidity (RH), in the vessel. As mentioned earlier, for trehalose particles, the relative humidity in the vessel should not exceed 40% [44], on all scales. In the case of the 1L scale, it was not possible to obtain dry trehalose powders. For this setup, the vessel contains 750 g of carbon dioxide at 130 bar and 37°C. Under these conditions, only 0.56 g of water is required to achieve 40% RH and the regeneration time of carbon dioxide is also quite short (3.6 minutes for a CO_2 flow rate of 208 g/min). However, even when spraying at 0.13 g/min, the time taken to accumulate 0.56 g of water in the vessel is longer than the regeneration time (4.3 min vs 3.6 min). Thus, the relative humidity should be below the critical limit. Consequently, the inability to obtain a dry powder in this case does not appear to be due to the water accumulation in the vessel.

The other factor to take into consideration is whether there is sufficient drying time for the droplets, which will depend on the dimensions of the vessel. In the case of the 4L and 10L vessels, the ratios of length and diameter (L/D) are 5 and 5.77 respectively (see Table 2), whereas the L/D ratio for the 1L drying chamber is 3.8, which is notably lower. Based on these results, as well as data reported in the literature, it is recommended that the L/D ratio should be higher than 5 for a spray drying method in order to obtain a dry powder product [45].

4.3 Protein integrity

4.3.1 Lysozyme

In this study, the lysozyme/trehalose formulations were composed of 80.0-90.9% trehalose by weight. The trehalose serves to protect lysozyme integrity, thus minimizing the formation of larger structures (e.g., dimer, trimer). In this study, the lysozyme activity and

structure was fully retained after reconstitution of the processed materials (Fig 5, Table 4) and only lysozyme monomer was observed by size exclusion chromatography (Fig. 6). Perez-Moral et al. [46] have demonstrated that increasing the percentage of trehalose or sucrose in a freeze-dried formulation inhibited the thermal aggregation of β-lactoglobulin. A significant decrease in β-lactoglobulin dimers was observed when the amount of sugar was greater than 50% in the formulations.

While the reconstituted solutions showed no visible insoluble residues (no optical density at 350 nm), they were also analyzed for sub-visible particles, the results of which are shown in Fig. 7 and 8. The numbers of sub-visible particles in protein formulations are considered important quality attributes [47]. According to the US and European pharmacopeias, there is a limit to the number of sub-visible microparticles that may be present in a protein solution, when observed by light obscuration (LO). Briefly, parenteral therapeutic proteins should contain fewer than 6000 particles/ml larger than 10 µm and 600 particles/ml larger than 25 µm using the LO method, which reports the concentration and size of particles in liquid samples in the range of 1-600 µm. For this study, we have used flow imaging microscopy, where the particles in the range of 1-400 µm are captured in individual photographs. The number of particles above 1 µm, 10 µm and 25 µm for each sample are reported in Table 5, and in all cases are within the above-mentioned limits.

In order to observe the particle concentration and size in the range of 30-1000 nm, NTA was used. With NTA, the individual particles are tracked by Brownian motion. Although there are currently no regulations concerning particles that are less than 1 µm in size, the results from the NTA can provide information regarding the protein aggregation in the sub-micron size range [40].

While the pathway of protein aggregation is presently unclear, induced conditions, such as heat stress or pH shift, enable the smaller aggregates to agglomerate and present larger particles. This has been observed in the case of conventional spray drying, where increasing the temperature induced changes in the secondary structure and aggregation of an immunoglobulin (IgG) [17].

It should be noted that in this study, a significantly large number of particles were detected in the dried pure trehalose after reconstitution. So, it appears that the observed particles are not the result of protein aggregation alone but may also be due to contamination. This is highly likely as the products were not prepared in

a clean room facility. Moreover, the negligible loss of monomer in HP-SEC (Fig. 6) indicates that the level of proteinaceous particles was very low.

In order to evaluate the stability of the protein formulations, the dry samples produced on the 10L scale were stored in a desiccator at room temperature (22°C) for 1 year. After this time, the formulation 1:10 retained full preservation of the lysozyme activity and structure. The number of particles in range of nanometer and micrometer after redissolving in pure water was not significantly different when compared to the freshly prepared products. For the formulation 1:4, however, a decrease in lysozyme activity was found. Consequently, it appears that in the case of the formulation 1:4 that there is insufficient trehalose to protect the protein from degradation during storage. These results suggest that the stability of the protein is not only dependent on the residual moisture content, but also the formulation composition.

4.3.2 Applicability of the developed method to other proteins

In order to gain insight into the applicability of the $scCO_2$ drying process for other proteins, the best drying conditions found for lysozyme were used to prepare dried powders of α-lactalbumin, α-chymotrypsinogen A, and monoclonal IgG. The same formulation as implemented for lyosozyme was also used for these proteins. Although no attempt was made to optimize the formulation for the specific proteins, in terms of the residual moisture content, protein structure and aggregation, the results for these three proteins were comparable with those of the processed lysozyme.

The sub-visible particle content of the processed α-lactalbumin formulation was comparable to that of lysozyme. However, a large increase of sub-visible microparticles was found for the α-chymotrypsinogen A and monoclonal IgG formulations. This could be due to the non-GMP environment and the suboptimal formulation of each protein. For instance, inclusion of a buffer in the formulation was shown to increase the recovery of soluble polyclonal IgG after $scCO_2$-processing [26], likely because it limited CO_2-mediated acidification during the drying process. Therefore, we expect that the loss of soluble protein and the formation of sub-visible particles, as observed for some of the protein formulations, can be inhibited by tailoring the formulation to the needs of each protein. To this end, the mutual influence of processing and formulation effects on protein stability should be studied. This was beyond the scope of the present study, but is currently under investigation.

5. Conclusion

Lysozyme/trehalose formulations in a solid state were prepared by an organic solvent-free $scCO_2$ spray drying process. In this study, we found a strong relationship between the residual water content and processing parameters. In order to minimize the amount of moisture in the powder product, the relative humidity in the drying vessel should be controlled. This was achieved by using low flow rates of solution with a high $scCO_2$ flow rate during the drying process. Furthermore, the feed volume of protein solution should be limited to avoid an increase in the relative humidity inside the drying vessel. Our study also demonstrated the scalability of $scCO_2$ spray drying from 4L to 10L drying chambers, which were able to produce the same quality powdered products in terms of residual moisture content, particle size, and glass transition temperature. The enzymatic activity and structure of the model protein lysozyme were fully preserved in samples produced on both scales. Moreover, in this study, the best condition from the 4L scale was also used to prepare other dry protein formulations in a similar manner.

References

[1]   E.Y. Chi, S. Krishnan, T.W. Randolph, J.F. Carpenter, Physical stability of proteins in aqueous solution: mechanism and driving forces in nonnative protein aggregation, Pharm Res, 20 (2003) 1325-1336.

[2]   M.E. Cromwell, E. Hilario, F. Jacobson, Protein aggregation and bioprocessing, AAPS J, 8 (2006) E572-579.

[3]   C.N. Pace, Conformational stability of globular proteins, Trends Biochem Sci, 15 (1990) 14-17.

[4]   W. Wang, Instability, stabilization, and formulation of liquid protein pharmaceuticals, Int J Pharm, 185 (1999) 129-188.

[5]   J.K. Towns, Moisture-Content in Proteins - Its Effects and Measurement, J Chromatogr A, 705 (1995) 115-127.

[6]   S. Ohtake, Y. Kita, T. Arakawa, Interactions of formulation excipients with proteins in solution and in the dried state, Adv Drug Deliv Rev, 63 (2011) 1053-1073.

[7]   A.S. Rosenberg, Effects of protein aggregates: an immunologic perspective, AAPS J, 8 (2006) E501-507.

[8]   S.P. Cape, J.A. Villa, E.T. Huang, T.H. Yang, J.F. Carpenter, R.E. Sievers, Preparation of active proteins, vaccines and pharmaceuticals as fine powders using supercritical or near-critical fluids, Pharm Res, 25 (2008) 1967-1990.

[9]   H. Okamoto, K. Danjo, Application of supercritical fluid to preparation of powders of high-molecular weight drugs for inhalation, Adv Drug Deliv Rev, 60 (2008) 433-446.

[10]   I. Pasquali, R. Bettini, F. Giordano, Solid-state chemistry and particle engineering with supercritical fluids in pharmaceutics, Eur J Pharm Sci, 27 (2006) 299-310.

[11]   F. Franks, R.H.M. Hatley, S.F. Mathias, Materials Science and the Production of Shelf-Stable Biologicals, Biopharm-Technol Bus, 4 (1991) 38-&.

[12]   B.S. Chang, R.M. Beauvais, A. Dong, J.F. Carpenter, Physical factors affecting the storage stability of freeze-dried interleukin-1 receptor antagonist: glass transition and protein conformation, Arch Biochem Biophys, 331 (1996) 249-258.

[13]   E.D. Breen, J.G. Curley, D.E. Overcashier, C.C. Hsu, S.J. Shire, Effect of moisture on the stability of a lyophilized humanized monoclonal antibody formulation, Pharm Res, 18 (2001) 1345-1353.

[14]   M.J. Pikal, D.R. Rigsbee, M.L. Roy, Solid state chemistry of proteins: I. glass transition behavior in freeze dried disaccharide formulations of human growth hormone (hGH), J Pharm Sci, 96 (2007) 2765-2776.

[15]   H. Yoshii, F. Buche, N. Takeuchi, C. Terrol, M. Ohgawara, T. Furuta, Effects of protein on retention of ADH enzyme activity encapsulated in trehalose matrices by spray drying, J Food Eng, 87 (2008) 34-39.

[16]   A. Ajmer, R. Scherliess, Stabilisation of proteins via mixtures of amino acids during spray drying, Int J Pharm, 463 (2014) 98-107.

[17]   S. Schule, W. Friess, K. Bechtold-Peters, P. Garidel, Conformational analysis of protein secondary structure during spray-drying of antibody/mannitol formulations, Eur J Pharm Biopharm, 65 (2007) 1-9.

[18]   H. Grohganz, Y.Y. Lee, J. Rantanen, M.S. Yang, The influence of lysozyme on mannitol polymorphism in freeze-dried and spray-dried formulations depends on the selection of the drying process, Int J Pharm, 447 (2013) 224-230.

[19]   D.P. Nesta, J.S. Elliott, J.P. Warr, Supercritical fluid precipitation of recombinant human immunoglobulin from aqueous solutions, Biotechnol Bioeng, 67 (2000) 457-464.

[20]   M. Sarkari, I. Darrat, B.L. Knutson, CO_2 and fluorinated solvent-based technologies for protein microparticle precipitation from aqueous solutions, Biotechnol Progr, 19 (2003) 448-454.

[21]   H. Todo, K. Iida, H. Okamoto, K. Danjo, Improvement of insulin absorption from intratracheally administered dry powder prepared by supercritical carbon dioxide process, J Pharm Sci, 92 (2003) 2475-2486.

[22]   A. Bouchard, N. Jovanovic, A.H. de Boer, A. Martin, W. Jiskoot, D.J. Crommelin, G.W. Hofland, G.J. Witkamp, Effect of the spraying conditions and nozzle design on the shape and size distribution of particles obtained with supercritical fluid drying, Eur J Pharm Biopharm, 70 (2008) 389-401.

[23]   A. Bouchard, N. Jovanovic, G.W. Hofland, W. Jiskoot, E. Mendes, D.J. Crommelin, G.J. Witkamp, Supercritical fluid drying of carbohydrates: selection of suitable excipients and process conditions, Eur J Pharm Biopharm, 68 (2008) 781-794.

[24]   A. Bouchard, N. Jovanovic, W. Jiskoot, E. Mendes, G.J. Witkamp, D.J.A. Crommelin, G.W. Hofland, Lysozyme particle formation during supercritical fluid drying: Particle morphology and molecular integrity, J Supercrit Fluid, 40 (2007) 293-   307.

[25]   N. Jovanovic, A. Bouchard, G.W. Hofland, G.J. Witkamp, D.J. Crommelin, W. Jiskoot, Stabilization of proteins in dry powder formulations using supercritical fluid technology, Pharm Res, 21 (2004) 1955-1969.

[26]   N. Jovanovic, A. Bouchard, G.W. Hofland, G.J. Witkamp, D.J. Crommelin, W. Jiskoot, Stabilization of IgG by supercritical fluid drying: optimization of formulation and process parameters, Eur J Pharm Biopharm, 68 (2008) 183-190.

[27]   A. Martin, A. Bouchard, G.W. Hofland, G.J. Witkamp, M.J. Cocero, Mathematical modeling of the mass transfer from aqueous solutions in a supercritical fluid during particle formation, J Supercrit Fluid, 41 (2007) 126-137.

[28]   C.I. Nindo, J. Tang, Refractance window dehydration technology: A novel contact drying method, Dry Technol, 25 (2007) 37-48.

[29]   J.A. Duffie, Marshall Jr., W.R., Factors influencing the properties of spray-dried material (Part I and II), Chem. Eng. Progress, 49 (1953) 417-486.

[30]   A. Bouchard, N. Jovanovic, A. Martin, G.W. Hofland, D.J.A. Crommelin, W. Jiskoot, G.J. Witkamp, Effect of the modifier on the particle formation and crystallisation behaviour during precipitation from aqueous solutions, J Supercrit Fluid, 44 (2008) 409-421.

[31]   N. Jovanović, A. Bouchard, M. Sutter, M. V. Speybroeck, G. W. Hofland, G. J. Witkamp, D. J.A. Crommelin, W. Jiskoot, Stable sugar-based protein formulations by supercritical fluid drying, Int J Pharm, 346 (2007) 102-108.

[32]   K. Masters, Spray drying handbook, 5th ed., Longman Scientific & Technical ;Wiley, Burnt Mill, Harlow, Essex, England, New York, 1991.

[33]   P. Thybo, L. Hovgaard, J.S. Lindelov, A. Brask, S.K. Andersen, Scaling up the spray drying process from pilot to production scale using an atomized droplet size criterion, Pharm Res, 25 (2008) 1610-1620.

[34]   N. Jovanovic, A. Bouchard, G.W. Hofland, G.J. Witkamp, D.J. Crommelin, W. Jiskoot, Distinct effects of sucrose and trehalose on protein stability during supercritical fluid drying and freeze-drying, Eur J Pharm Sci, 27 (2006) 336-345.

[35]   B. Kükrer, V. Filipe, E. van Duijn, P. Kasper, R.J. Vreeken, A.J.R. Heck, W. Jiskoot, Mass spectrometric analysis of intact human monoclonal antibody aggregates fractionated by size-exclusion chromatography, Pharm Res, 27 (2010) 2197–2204.

[36]   V. Filipe, W. Jiskoot, A.H. Basmeleh, A. Halim, H. Schellekens, V. Brinks, Immunogenicity of different stressed IgG monoclonal antibody formulations in immune tolerant transgenic mice, mAbs, 4 (2012) 740-752.

[37]   K.C. Aune, and Tanford C., Thermodynamics of the denaturation of lysozyme by guanidine hydrochloride. I. Dependence on pH at 25°C. Biochemistry, 8 (1969) 4579–4585.

[38]   M. J. Kronman, R. E. Andreotti, Inter- and intramolecular interactions of a-lactalbumin. I. the apparent heterogeneity at acid pH, Biochemistry, 3 (1964) 1145.

[39]   J. A. Beeley, S.M. Stevenson, J.G. Beeley, Polyacrylamide gel isoelectric focusing of proteins: determination of isoelectric points using an antimony electrode, Biochim Biophys Acta, 285 (1972) 293-300.

[40]   V. Filipe, A. Hawe, W. Jiskoot, Critical Evaluation of Nanoparticle Tracking Analysis (NTA) by NanoSight for the Measurement of Nanoparticles and Protein Aggregates, Pharm Res, 27 (2010) 796-810.

[41]   M.B. King, A. Mubarak, J.D. Kim, T.R. Bott, The Mutual Solubilities of Water with Supercritical and Liquid Carbon-Dioxide, J Supercrit Fluid, 5 (1992) 296-302.

[42]   G.E. Downton, J.L. Flores-Luna, C.J. King, Mechanism of stickiness in hygroscopic, amorphous powders, Ind Eng Chem Fund, 21 (1982) 447-451.

[43]   V. Normand, A. Subramaniam, J. Donnelly, P.E. Bouquerand, Spray drying: Thermodynamics and Operating Conditions, Carbohyd Polym, 97 (2013) 489-495.

[44]   V.P. Heljo, A. Nordberg, M. Tenho, T. Virtanen, K. Jouppila, J. Salonen, S.L. Maunu, A.M. Juppo, The effect of water plasticization on the molecular mobility and crystallization tendency of amorphous disaccharides, Pharm Res, 29 (2012) 2684-2697.

[45]   C.A. Rinil Kuriakose, Computational fluid dynamics (CFD) applications in spray drying of food products, Trends Food Sci Tech, 21 (2010) 383-398.

[46]   N. Perez-Moral, C. Adnet, T.R. Noel, R. Parker, The aggregative stability of beta-lactoglobulin in glassy mixtures with sucrose, trehalose and dextran, Eur J Pharm Biopharm, 78 (2011) 264-270.

[47]   J.F. Carpenter, T.W. Randolph, W. Jiskoot, D.J.A. Crommelin, C.R. Middaugh, G. Winter, Y.X. Fan, S. Kirshner, D. Verthelyi, S. Kozlowski, K.A. Clouse, P.G. Swann, A. Rosenberg, B. Cherney, Overlooking subvisible particles in therapeutic protein products: gaps that may compromise product quality, J Pharm Sci, 98 (2009) 1201-1205.

CHAPTER 4

Critical processing parameters of carbon dioxide spray drying for the production of dried protein formulations: a study with myoglobin

O. Nuchuchua[1], H.A. Every[2], W. Jiskoot[1]

[1] Division of Drug Delivery Technology, Leiden Academic Centre for Drug Research (LACDR), Leiden University, The Netherlands

[2] FeyeCon Development & Implementation B.V., Weesp,

The Netherlands

Abstract

The aim of this study was to gain fundamental insight into protein destabilization induced by supercritical CO_2 spray drying processing parameters. Myoglobin was used as a model protein (5 mg/ml with 50 mg/ml trehalose in 10 mM phosphate buffer, pH 6.2). The solution was exposed to sub- and supercritical CO_2 conditions (65-130 bar and 25-50°C), and CO_2 spray drying under those conditions. The heme binding of myoglobin was determined by UV/Vis, fluorescence, and circular dichroism spectroscopy, while myoglobin aggregation was studied by using size-exclusion chromatography and flow imaging microscopy. It was found that pressure and temperature alone did not influence myoglobin's integrity. However, when pressurized CO_2 was introduced into myoglobin solutions at any condition, the pH of the myoglobin formulation shifted to about 5 (measured after depressurization), resulting in heme binding destabilization and aggregation of myoglobin. When exposed to CO_2, these degradation processes were enhanced by increasing temperature. Heme binding destabilization and myoglobin aggregation were also seen after CO_2 spray drying, and to a greater extent. Moreover, the CO_2 spray drying induced the partial loss of heme. In conclusion, pressurized CO_2 destabilizes the myoglobin, leading to heme loss and protein aggregation upon spray drying.

1. Introduction

In previous studies, supercritical carbon dioxide (scCO$_2$) spray drying has been shown to be applicable for drying formulations of several proteins, such as lysozyme, a-lactalbumin, a-chymotrypsinogen A, myoglobin, and monoclonal and polyclonal immunoglobulins. However, depending on the protein and the processing conditions, protein aggregation and denaturation were sometimes observed [1-4]. In particular, myoglobin appeared to be especially sensitive to scCO$_2$ spray drying, as reflected by partial heme loss and the formation of insoluble residues [4]. Moreover, protein powders or protein-containing particles prepared using other supercritical carbon dioxide techniques have also shown instability in protein structure, bioactivity and aggregation, as presented in the review by Cape et al. [5]. Based on these observations, it is apparent that there are some elements of the scCO$_2$ drying processes that compromise the stability of myoglobin.

Myoglobin is a heme protein. The heme group is composed of protoprophyrin IX that surrounds an iron ion, which is embedded in the heme pocket of myoglobin. The heme binding affinity of myoglobin depends on the interactions of the heme group with the proximal histidine and the adjacent hydrophobic amino acids [6, 7]. The covalent bonds between the heme-iron and the imidazole ring of the proximal histidine can destabilize under acidic conditions. Lowering the pH to values in the range of 3.5-4.5 also causes protonation of the proximal histidine buried in the heme pocket, resulting in the unfolding of myoglobin, and a decrease in the heme binding affinity [7, 8]. The heme can actually be extracted in cold acidified organic solvents, such as acetone or methylethylketone, to form the heme-free protein, apomyoglobin [9].

Any changes in heme binding within myoglobin can be detected spectroscopically, as the absorption, fluorescence and circular dichroism (CD) spectra are very sensitive to the heme binding and protein conformation [4, 10-12]. Fig. 1 shows a typical UV/Vis spectrum of a myoglobin/trehalose formulation, with the heme absorption at 409 nm (Soret band) and the protein absorption at 280 nm. The position and shape of the Soret band indicate an oxidized form of myoglobin with Fe(III)protoporphyrin [7]. As was observed in a previous study on scCO$_2$ spray drying of myoglobin, a decrease in the relative intensity of the Soret band (in both UV/Vis and CD spectroscopy) and an increase in the intrinsic fluorescence signal indicate heme loss [4]. However, the factor(s) responsible for the heme loss during the scCO$_2$ spray drying process remained unclear.

The scCO$_2$ spray drying process involves atomization and subsequent drying of a protein solution under pressure with a continuous flow of scCO$_2$. During this process, the protein may undergo irreversible changes in structure and consequently a loss in functionality. Moreover, an aqueous protein formulation may become acidified during spraying, due to the reaction between carbon dioxide (CO$_2$) and water to form carbonic acid [13, 14]. Furthermore, the CO$_2$/water interface after the atomization may induce protein denaturation and aggregation [15, 16]. Given the sensitivity of myoglobin, it is hypothesized that one or more of these factors could account for the destabilization that was previous observed for myoglobin formulated with trehalose at 1:10 weight ratio and 10 mM phosphate buffer at pH 6.2. Therefore, the aim of this study was to gain fundamental insight into the effect of the sub- and supercritical CO$_2$ processing conditions on the stability of myoglobin in that formulation. The individual processing parameters, such as pressure, temperature, exposure to CO$_2$, and CO$_2$ spray drying, were investigated separately. In order to evaluate the influence of each processing parameter on the integrity of myoglobin, UV/Vis spectroscopy, fluorescence spectroscopy, CD spectroscopy, high performance size-exclusion chromatography (HP-SEC), and flow imaging microscopy analyses were used. It is anticipated that by understanding these fundamental process-related factors of scCO$_2$ spray drying on the stability of myoglobin, the conditions and/or the formulation can be optimized, in order to protect proteins against process-induced damage.

2. Materials and Methods

2.1 Preparation of liquid myoglobin formulation

A liquid myoglobin formulation was prepared from 5 mg/ml myoglobin from equine skeletal muscle with 50 mg/ml trehalose in 10 mM sodium phosphate buffer, pH 6.2. All chemicals were obtained from Sigma-Aldrich, St. Louis, USA. The liquid formulation was filtered through a 0.22-µm pore cellulose acetate filter (Millex®-GV, Cork, Ireland) before performing the experiments.

2.2 Experimental conditions

The effects of pressure and temperature on myoglobin stability were studied independently by using a high-pressure vessel (TELEDYNE ISCO, Lincoln, USA). In all cases, the tests were performed using 10 ml of the liquid myoglobin formulation. The effect of temperature was studied under atmospheric pressure at 25, 37, and 50 °C (conditions A, B, and C). The vessel was heated by flowing water from a controlled temperature water bath (Lauda C6, LAUDA-Königshofen, Germany)

through a heating jacket that surrounds the vessel. The effect of pressure was studied at 65 and 130 bar at different temperatures (25, 37, and 50 °C, corresponding to conditions D, E, F, G, H, I). The desired pressure was achieved by reducing the volume of the vessel with a piston. The myoglobin/trehalose formulations were kept under the set conditions for two hours. After completing each experiment, the solutions were removed from the vessel and left for an hour to cool down to room temperature prior to analysis.

The effect of CO_2 on myoglobin stability was studied by incubating 10-ml aliquots of the liquid myoglobin formulation with pressurized CO_2 in the high-pressure vessel. Carbon dioxide (grade 3.5) was obtained from Linde Gas (Schiedam, The Netherlands). The solution was exposed to both subcritical and supercritical CO_2 at 65 and 130 bar and 25, 37, and 50 °C (conditions J, K, L, N, O, and P). The CO_2 was brought to the desired pressure with a separate pump system before being introduced into the incubation vessel. The volume ratio of the liquid myoglobin formulation to CO_2 was fixed at 1:10. After forty-minute incubation time, CO_2 was slowly removed by depressurization to atmospheric pressure. The CO_2-incubated liquid myoglobin formulations were kept at 4 °C for 12 hours before analysis.

In order to exclude the influence of CO_2 density on myoglobin integrity, a series of experiments at a constant CO_2 density of 0.77 g/cm^3 were conducted. The conditions for these tests were 77 bar and 25 °C, 130 bar and 37 °C, and 188 bar and 50 °C (conditions M, O, Q). The incubation time, depressurization rate and storage conditions were the same as for the experiments above.

The effect of CO_2 spray drying was investigated at 65 and 130 bar and 25, 37, and 50 °C (condition R, S, T, U, V, and W). A 4-liter spray drying module (F54250S model from Separex, Champigneulles, France) was used in this study. The drying vessel was filled with the pressurized CO_2 and brought to the desired temperature and pressure before feeding in the liquid myoglobin formulation via a high-pressure syringe pump maintained at 25 °C (TELEDYNE ISCO, Lincoln, USA). The solution was atomized by the pressurized CO_2 stream through a coaxial converging nozzle (Spraying Systems Co. B.V., Ridderkerk, The Netherlands). The diameter of the nozzle orifices was 0.16 cm and 0.04 cm for the CO_2 and the liquid, respectively. The solution and CO_2 flow rates were kept constant at 0.2 and 500 g/min, respectively. The spraying time was 40 minutes, followed by 30 minutes post-drying step with fresh CO_2, to remove any residual moisture from the vessel and consequently the product. After depressurization, the dried myoglobin formulations were collected from a paper filter (Whatman® qualitative filter paper,

Grade 1, 25 mm diameter, Diegem, Belgium). The product was then stored in a desiccator at room temperature prior to analysis. In addition to these experiments, one test was performed at 130 bar and 37 °C without the post drying step, in order to study the effect of post-drying (condition V-).

All experimental conditions are summarized in Table 1. Each experimental condition was repeated three times (n=3).

2.3 Protein analysis

2.3.1 Sample preparation for myoglobin analysis

If necessary, liquid myoglobin formulation samples were diluted in 10 mM phosphate buffer (PB), pH 6.2. For the dried myoglobin/trehalose formulations, an amount of powder corresponding to 5 mg myoglobin and 50 mg trehalose was accurately weighed and dissolved in 1 ml of water, taking into consideration the amount of phosphate salts and the residual water content after spray drying [3]. The powdered products were dissolved overnight at room temperature to complete the dissolution of powders. The solutions were subsequently diluted in 10 mM PB, pH 6.2. The diluted samples were filtered through a 0.22-μm pore cellulose acetate filter (Millex®-GV, Cork, Ireland) before protein structural analysis by UV/Vis, circular dichroism and fluorescence spectroscopy. The sample concentrations for each analysis are mentioned below.

2.3.2 Protein recovery and recovery of bound heme

The protein solutions were diluted to approximately 0.1 mg/ml prior to measurement. The protein content was determined by using a UV spectrophotometer (Agilent 8453, Agilent Technologies, Santa Clara, USA). The spectra were collected from 190 nm to 1000 nm. The myoglobin concentration was calculated using a molar extinction coefficient of 3.45×10^4 $M^{-1}cm^{-1}$ at 280 nm [17]. The absorbance ratio between 409 and 280 nm (A409/A280) from each spectrum represents the absorption of heme group bound to the proximal histidine in the heme pocket of myoglobin [18]. The percentages of protein content recovery of the treated myoglobin (see Eq. 1) were compared to those of the untreated liquid myoglobin formulation at 25°C (condition A).

$$Protein\ recovery(\%) = \left[\frac{A280\ (processed)}{A280\ (nonprocessed)}\right] \times 100 \qquad (Eq.\ 1)$$

Table 1. Experimental conditions and the corresponding protein recovery and heme absorption using UV/Vis spectroscopy.

Conditions[a]	Pressure(bar)	Temperature(°C)	CO_2	CO_2 density (g/cm^3)	Spray drying	Post drying	Protein recovery[e] (%wt)	A409/A280[f]
Effect of temperature[b,g]								
A	atmospheric	25	-	-	-	-	100	5.50 ± 0.03
B	atmospheric	37	-	-	-	-	100.0 ± 4.7	5.47 ± 0.01
C	atmospheric	50	-	-	-	-	104.3 ± 1.4	5.56 ± 0.01
Effects of pressure and temperature[b]								
D	65	25	-	-	-	-	97.1 ± 3.0	5.67 ± 0.01
E	65	37	-	-	-	-	96.0 ± 10.7	5.50 ± 0.01
F	65	50	-	-	-	-	104.6 ± 2.0	5.54 ± 0.01
G	130	25	-	-	-	-	100.1 ± 2.0	5.55 ± 0.01
H	130	37	-	-	-	-	98.1 ± 6.4	5.66 ± 0.00
I	130	50	-	-	-	-	100.2 ± 4.1	5.74 ± 0.01
Effects of carbon dioxide[c]								
J	65	25	+	0.72	-	-	91.1 ± 6.3	5.43 ± 0.12*
K	65	37	+	0.18	-	-	95.2 ± 3.6	5.38 ± 0.15*
L	65	50	+	0.15	-	-	85.6 ± 7.7	4.98 ± 0.52*
M	77	25	+	0.77	-	-	93.4 ± 5.8	5.56 ± 0.04
N	130	25	+	0.86	-	-	94.4 ± 3.2	5.42 ± 0.16*
O	130	37	+	0.77	-	-	95.8 ± 0.6	5.28 ± 0.13*

P	130	50	+	+	0.64	-	-	85.6±0.6	4.99±0.35*
Q	188	50	+	+	0.77	-	-	86.6±5.0	5.26±0.22

Effects of spray drying and post drying[d]

R	65	25	+	+	0.72	+	+	89.0±5.0	5.23±0.10*
S	65	37	+	+	0.18	+	+	85.2±2.0	4.87±0.36*
T	65	50	+	+	0.15	+	+	79.1±0.3	4.44±0.45*
U	130	25	+	+	0.86	+	+	90.4±1.4	5.24±0.17*
V-	130	37	+	+	0.77	+	-	82.7±2.8	5.05±0.12
V	130	37	+	+	0.77	+	+	79.5±1.6	4.93±0.18*
W	130	50	+	+	0.64	+	+	76.2±4.0	4.71±0.20*

[a] Formulation of 5 mg/ml myoglobin and 50 mg/ml trehalose in 10 mM phosphate buffer at pH 6.2 was used for all experiments.
[b] Incubation time was two hours.
[c] The ratio of myoglobin solution to carbon dioxide was 1:10 (v/v), forty-minutes incubation time.
[d] Forty minutes spray drying with (+) and without (-) thirty minutes post drying.
[e] Data were obtained from the absorbance at 280 nm by UV/Vis spectroscopy (see methods).
[f] Data were obtained from the ratio of the absorbances at 409 and 280 nm by UV/Vis spectroscopy (see methods).
[g] Reference solutions.
* A significant reduction (p < 0.05) of A409/A280 ratio found comparing to the untreated samples at conditions A, B, C.

2.3.3 Circular dichroism spectroscopy

In order to study the structure of myoglobin, far-UV (190-250 nm) and near-UV/Vis (350-450 nm) CD spectroscopy measurements (J-810 Spectropolarimeter, JASCO Inc., Easton, USA) were performed at 25 °C. Parameters were set at a sensitivity of 100 mdeg, with a data pitch of 10 nm, a bandwidth of 2 nm, and a scanning speed of 100 nm/min. Samples were freshly prepared with a myoglobin concentration of 0.1 mg/ml and placed in a 0.1-cm and 1-cm quartz cuvette for far-UV CD and near-UV/Vis CD measurements, respectively. CD spectra of six sequential measurements were averaged and corrected for the blank. The CD signals were converted to molar ellipticity per amino acid residue (θ). The signal of the heme specific site at 409 nm of the samples was also compared to that of reference solution (25 °C), and shown as a relative molar ellipticity.

2.3.4 High performance size-exclusion chromatography

Samples (50 μl of 1 mg/ml protein concentration) were analyzed by HP-SEC with a Discovery® BIO Gel Filtration column (300 Å pore size) (Sigma-Aldrich, St. Louis, USA). The mobile phase consisted of 150 mM phosphate buffer, pH 7.0, and was filtered through a 0.2-μm filter prior to use. The flow rate was set at 0.7 ml/min. The chromatograms were recorded by a UV detector (Agilent 1100 VWD, Santa Clara, USA) and a fluorescence detector (Agilent 1200 FLD, Santa Clara, USA). The absorbance of each spectrum at a wavelength of 280 nm was used to calculate the percentages of myoglobin monomer, aggregates, and fragments. The monomer recovery of the CO_2 incubated (conditions J, K, L, N, O, P) and CO_2 spray dried (conditions R, S, T, U, V, W) myoglobin was calculated as percentage of the monomer peak area relative to that of the untreated sample (condition A). The fluorescence emission intensity was collected at 350 nm with the excitation at 295 nm. For each chromatogram, the total peak area of the fluorescence signal intensity was compared to the absorbance at 280 nm, and shown as I_{350}/A_{280}. Apomyoglobin, which lacks the heme group, was used as a control.

2.3.5 Flow imaging microscopy

The presence of sub-visible microparticles was determined by flow imaging microscopy using an MFI5200 instrument (Protein Simple, California, USA). The measurements were controlled and the data analyzed by MVAS software version 1.3. Prior to analysis, the formulations

were diluted to a myoglobin concentration of 1 mg/ml. One milliliter of solution was introduced at a flow rate of 6 ml/min into a flow cell with the dimensions of 100 and 1016 μm in depth and diameter, respectively, illuminated by a blue LED. Images of the particles were captured by an optical camera. Pictures were obtained with a resolution of 1280x1024 pixels. Total particle concentrations are reported for particle sizes larger than 1, 10, 25 and 50 μm.

2.4 Statistical analysis

The data were analyzed by a two-way ANOVA via the GraphPad Prism to test the myoglobin integrity as a function of processing parameters (untreated, pressurized with and without CO_2, CO_2 spray drying) and temperatures/pressures. Values were considered significant when p was less than 0.05. The data of each experimental condition (n=3) are shown as average ± standard deviation.

3. Results and discussion

In a previous study, the destabilization of myoglobin after CO_2 spray drying was observed, as reflected by the presence of insoluble residues and heme loss in the resultant product [4]. However, the drying was carried out in the presence of an organic solvent, which was thought to contribute to the destabilization [4]. Upon repeating these experiments in the absence of organic solvent, however, insoluble residues and heme loss were still detected (unpublished results), which implies that one or more of the other factors within the process also contribute to the destabilization of myoglobin. In order to understand the influence of the CO_2 spray drying processing parameters on the instability of myoglobin, a systematic study of each parameter on the protein's stability was conducted.

The processing parameters related to the CO_2 spray drying were differentiated into four factors: temperature (25-50°C), pressure (atmospheric and 65-130 bar), presence of CO_2, and spray drying in a CO_2 environment at 25-50°C and 65-130 bar. No organic solvents were used in these experiments. Changes in myoglobin structure, in terms of heme loss and protein aggregation, were monitored to explain how these parameters influence myoglobin stability.

To analyze heme-bound myoglobin, UV/Vis analysis was conducted. Myoglobin shows absorption band centered around 409 nm (Fig. 1), related to absorption of the heme group, which indicates the

coordination of heme with the nitrogenous base of the proximal histidine in the heme pocket [18]. The absorption at 280 nm reflects the aromatic amino acid residues the protein. The signal of near-UV/Vis CD at 409 nm (Fig. 2) will shift and/or decrease depending on the heme π-$\pi*$ electronic dipole transition moments with proximal aromatic amino acid residues in the heme pocket of myoglobin [19, 20]. Myoglobin's tryptophan fluorescence signal is highly quenched by the bound heme group [21, 22]. Therefore, any increase in the fluorescence emission intensity (Fig. 3) is directly related to heme loss, leading to an increase in the concentration of apomyoglobin. As shown in the previous study, heme loss from myoglobin was not only accompanied by an increase in the fluorescence emission intensity, but also resulted in a reduced absorbance at 409 nm (presented by the ratio of 409 nm to 280 nm), and molar ellipticity at 409 nm (by near-UV/Vis CD) [4]. In addition, soluble and sub-visible myoglobin aggregates were analyzed by HP-SEC and flow-imaging microscopy, respectively. The results are discussed below.
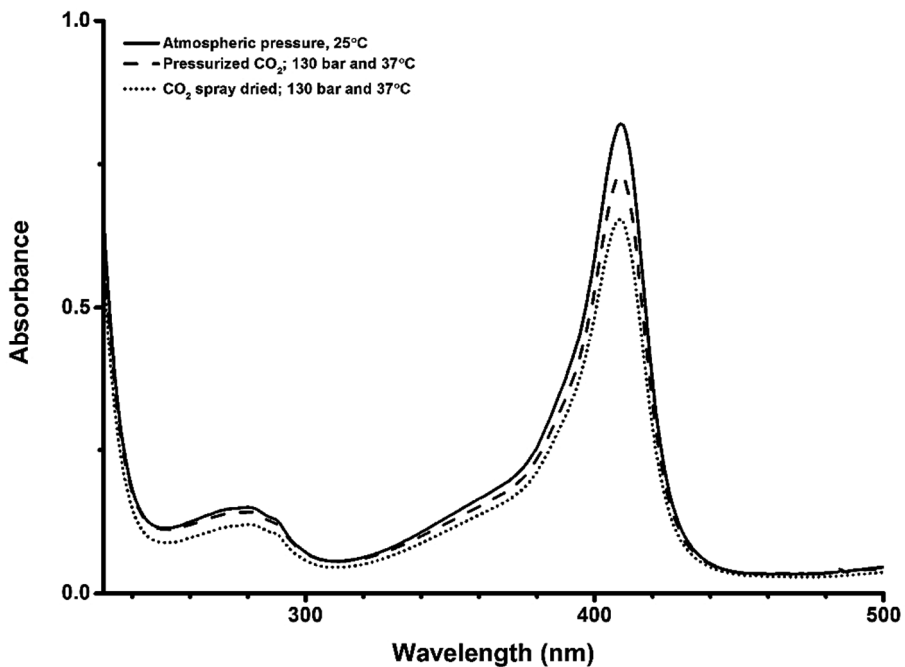
Fig. 1 UV/Vis spectra of CO_2-incubated myoglobin and reconstituted solution of spray dried myoglobin formulations (both conducted at 130 bar and 37 °C, conditions O and V), compared to that of untreated myoglobin formulation (condition A).
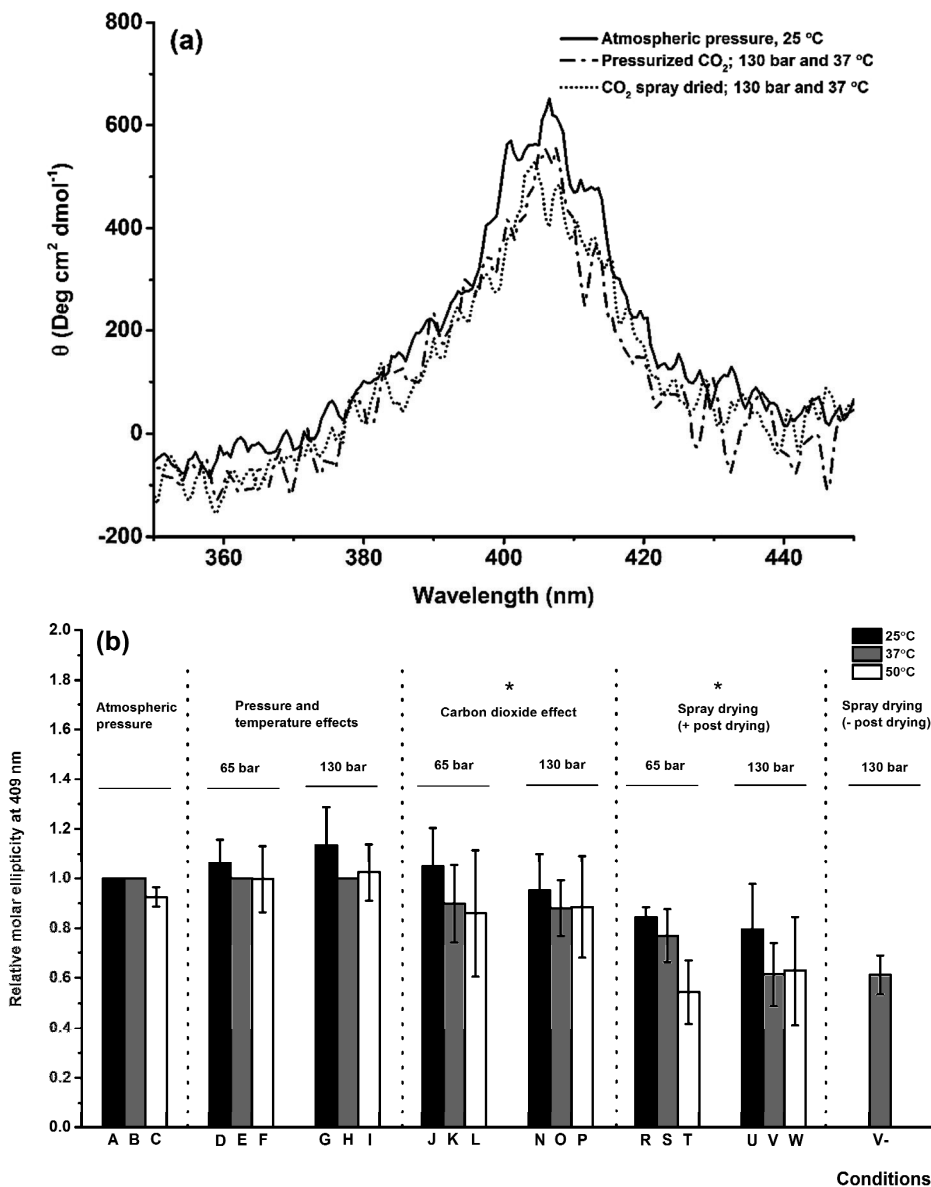
Fig. 2 Near/Vis-CD spectra (**graph a**) of CO_2-incubated myoglobin and reconstituted solution of spray dried myoglobin formulations (both conducted at 130 bar 37 °C), compared to that of untreated myoglobin formulation. Relative molar ellipticity (**graph b**) at the Soret band (409 nm) for myoglobin formulations at atmospheric pressure (conditions A, B, C), pressurized at 65 bar (conditions D, E, F) and 130 bar (conditions G, H, I), CO_2-incubated myoglobin formulations at 65 bar (conditions J,

K, L) and 130 bar (conditions N, O, P) at 1:10 volume ratio of myoglobin formulation to carbon dioxide, and reconstituted spray dried myoglobin formulations with half an hour post drying produced at 65 bar (conditions R, S, T) and 130 bar (conditions U, V, W). The experiments for the atmospheric pressure, 65 and 130 bar were done at 25, 37, and 50 °C. A significant difference (*) in the relative molar ellipticity at the heme specific site found in the experimental group of CO_2 incubation (conditions J, K, L, N, O, P) and CO_2 spray drying (conditions R, S, T, U, V, W), comparing to the untreated samples at conditions A, B, C with *p < 0.05*.

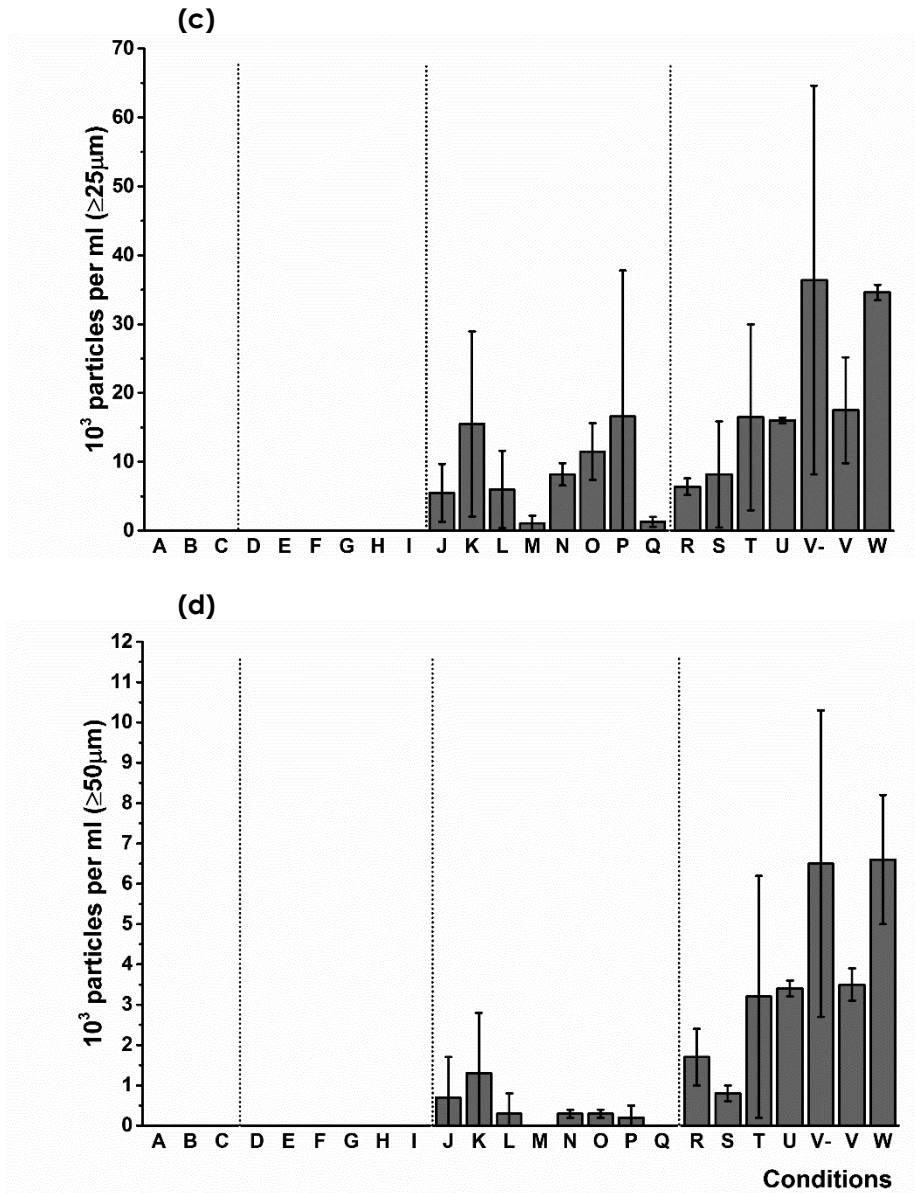### 3.1 Effects of temperature 25-50°C at atmospheric pressure (1 bar) and 65-130 bar without carbon dioxide

The scCO_2 spray drying process takes place under pressurized conditions at a given temperature. It was first necessary to evaluate whether temperature and pressure alone affect myoglobin's structure. Therefore, pressures at 65-130 bar and temperatures at 25-50 °C used for the CO_2 spray drying conditions were studied. The results of protein recovery, the ratio of A409/A280 (Table 1), molar ellipticity (as a measure of myoglobin's secondary structure (data not shown)), circular dichroism at the heme specific site (Fig. 2), and fluorescence intensity (Fig. 3b) indicate that the heme binding site was not perturbed over the pressure and temperature range studied. In addition, the range of pressures and temperatures studied did not induce any myoglobin aggregation, as shown by HP-SEC (Fig. 4) and flow imaging microscopy (Fig. 5, conditions A-I). Both untreated myoglobin and pressurized myoglobin solutions contained very low numbers of sub-visible particles. Therefore, myoglobin was stable under these conditions.

These results are in line with a study by Doster and Gebhardt [23], who found that a myoglobin solution at pH 7 was only denatured when exposed to pressures above 3 kbar, as indicated by the optical spectral properties of the heme group. Under these high-pressure conditions, only 40% of the a-helix structure of myoglobin was recovered.
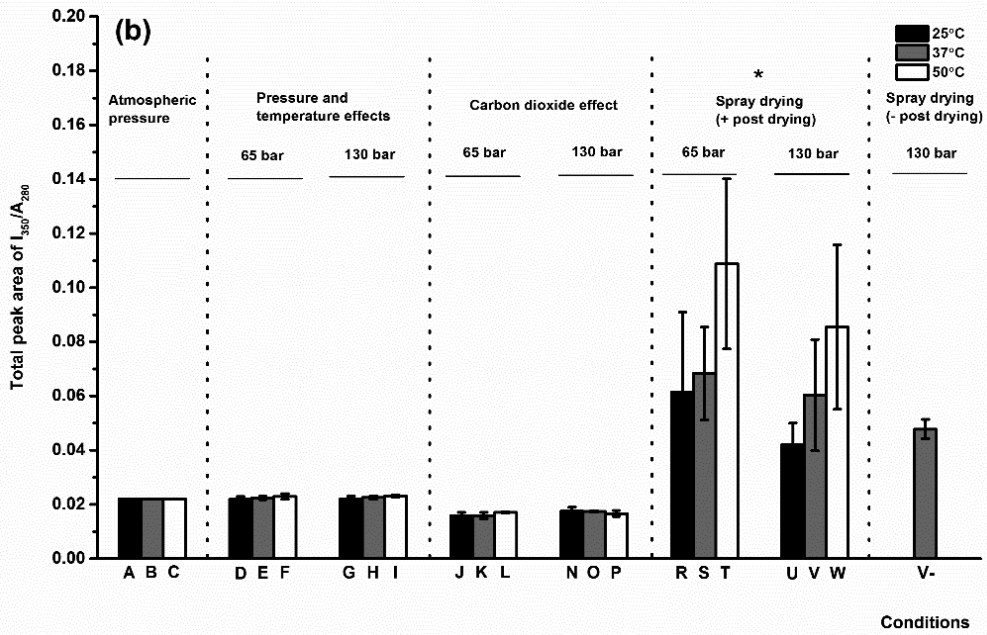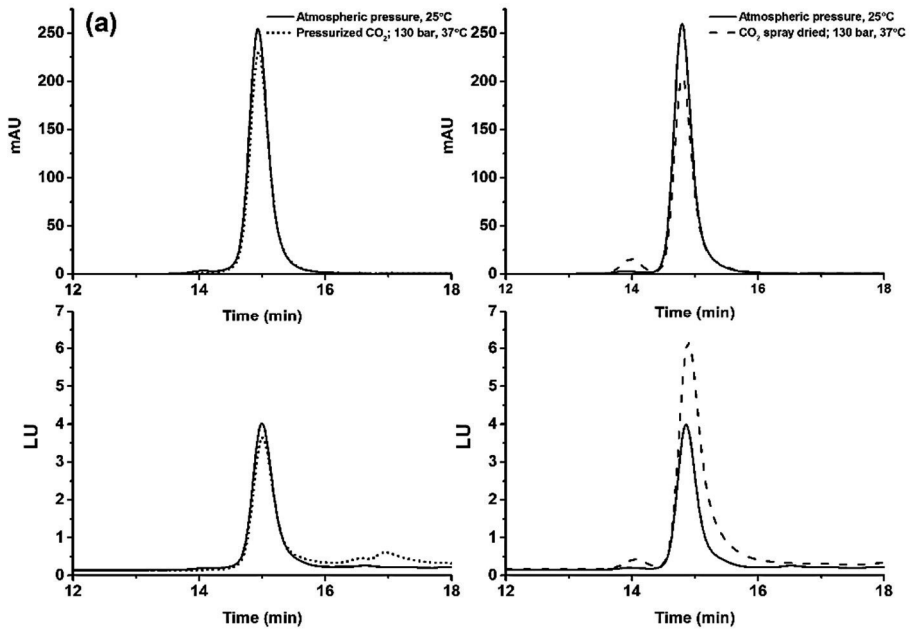
Fig. 3 HP-SEC chromatograms (**graph a**) detected by UV absorption at 280 nm
(upper panels) and fluorescence emission at 350 nm (lower panels) of
CO_2-incubated myoglobin formulation (left panels) and reconstituted
spray dried myoglobin formulation (right panels) conducted at 130 bar 37
°C, compared to untreated myoglobin formulation. mAU =
milliabsorbance unit; LU =luminescence **units**. The relative total peak area
(**graph b**) of the fluorescence emission signal at 350 nm to protein
absorption at 280 nm (I_{350}/A_{280}) for reference myoglobin formulations
(conditions A, B, C), pressurized at 65 bar (conditions D, E, F) and 130 bar
(conditions G, H, I), CO_2-incubated myoglobin formulations under 65 bar
(conditions J, K, L) and 130 bar (conditions N, O, P) at 1:10 volume ratio of
myoglobin formulation to carbon dioxide, and reconstituted spray dried
myoglobin formulations with half an hour post drying produced at 65 bar
(conditions R, S, T) and 130 bar (conditions U, V, W). See Table 1. A
significant difference (*) of the fluorescence intensity found in the
experimental group of spray drying at conditions R, S, T, U, V, W,
comparing to the untreated non-pressurized samples at conditions A, B,
C with $p < 0.05$.
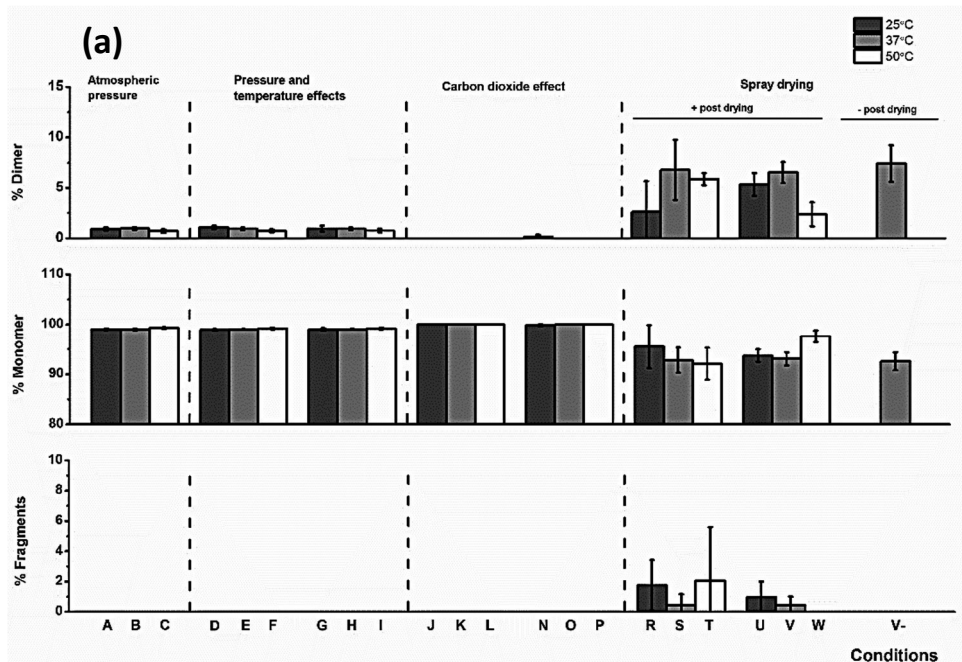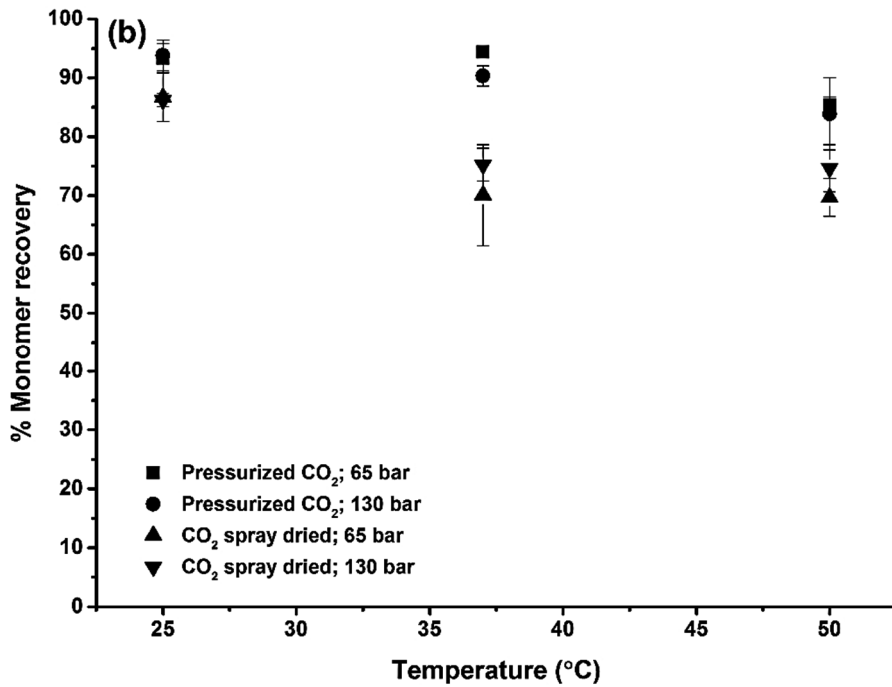
Fig. 4 The percentages of dimer, monomer, and fragments (**graph a**) for reference myoglobin formulations (conditions A, B, C), pressurized at 65 bar (conditions D, E, F) and 130 bar (conditions G, H, I), CO_2-incubated myoglobin formulations at 65 bar (conditions J, K, L) and 130 bar (conditions N, O, P), and reconstituted spray dried myoglobin formulations with post drying produced at 65 bar (conditions R, S, T) and 130 bar (conditions U, V, W), as determined by HP-SEC (absorption at 280 nm). The percentage of monomer recovery (**graph b**) for myoglobin formulations incubated with pressurized CO_2 at 65 bar (conditions J, K, L) and 130 bar (conditions N, O, P), and reconstituted spray dried myoglobin formulations with post drying produced at 65 bar (conditions R, S, T) and 130 bar (conditions U, V, W). See Table 1 for conditions.

(a)

Atmospheric pressure | Pressure and temperature effects | Carbon dioxide incubation | Spray drying

(b)
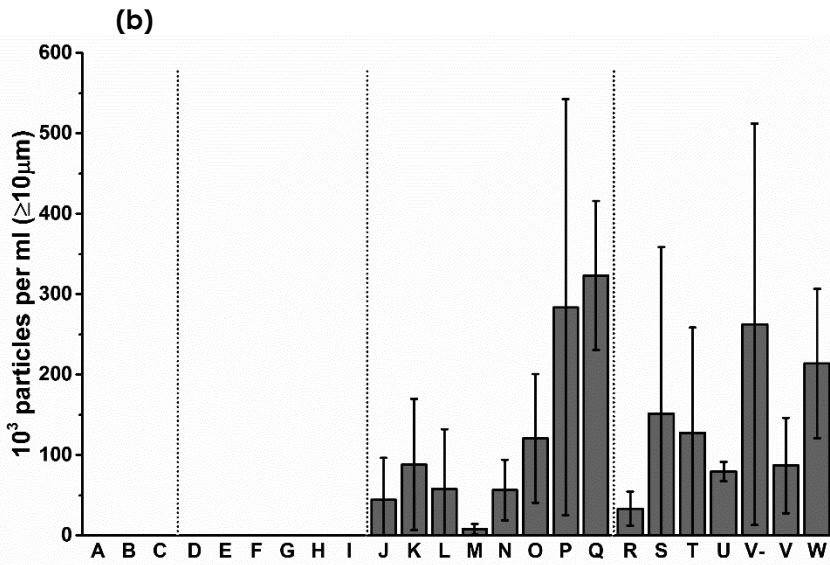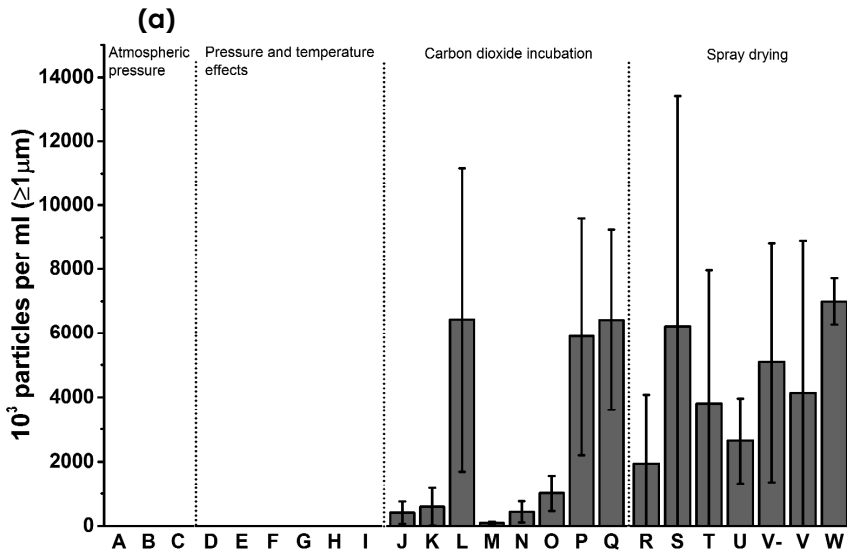
Fig. 5 Particle concentrations larger than 1 μm (a), 10 μm (b), 25 μm (c) and 50 μm (d) in untreated, pressurized without CO_2, pressurized with CO_2 and CO_2 spray drying myoglobin formulations observed by flow imaging microscopy. Volume refers to that of undiluted (reconstituted) liquid myoglobin formulation. See Table 1 for experimental conditions. A significant difference (*) of the particle concentrations (≥ 1 μm) found in the experimental group of CO_2 incubation.

3.2 Effects of carbon dioxide at 65-130 bar and 25-50°C

In scCO$_2$ spray drying, CO$_2$ is responsible for the atomization of the solution as well as being the drying medium. The properties of CO$_2$, such as the density, viscosity and surface tension, depend on the operating pressure and temperature. As myoglobin's integrity was maintained upon varying the pressure and temperature, the next step in this study was to expose the myoglobin solution to CO$_2$. To this end, CO$_2$, at given pressures and temperatures, was introduced into a high-pressure vessel containing the myoglobin formulation. This experiment was designed to simulate the exposure of the protein to the CO$_2$ medium at 65-130 bar and 25-50°C, but without the drying process.

After incubating the myoglobin solutions with pressurized CO$_2$ at sub- and supercritical conditions (65-130 bar 25-50°C), the pH had shifted from 6.2 to approximately 5.1 (Table 2). The shift in the pH is due to the production of carbonic acid from the interaction between the CO$_2$ and the water [13, 14]. Varying the CO$_2$ conditions hardly influenced the final pH of the solution. Furthermore, the original pH (pH 6.2) was not recovered, even 12 hours after completion of the experiment (Table 2). This indicates that the 10 mM phosphate buffer at pH 6.2 is not capable of controlling the pH of the solution upon exposure to pressurized CO$_2$.

Table 2. The pH of the myoglobin formulations after CO$_2$ incubation at 25, 37, 50 °C and 65 bar (conditions J, K, L) and 130 bar (conditions N, O, P). The pH was re-measured 12 hours after depressurization. The untreated myoglobin formulations at 25, 37, 50 °C were used as a control.

Pressure conditions	pH		
	25°C	37°C	50°C
Atmospheric pressure	6.27 ± 0.00	6.26 ± 0.00	6.25 ± 0.00
0 h after depressurization			
65 bar	5.20 ± 0.03	5.31 ± 0.07	5.38 ± 0.06
130 bar	5.17 ± 0.01	5.32 ± 0.05	5.45 ± 0.07
12 h after depressurization			
65 bar	5.43 ± 0.04	5.62 ± 0.01	5.86 ± 0.02
130 bar	5.41 ± 0.01	5.50 ± 0.05	5.94 ± 0.16

As the pH could only be measured after depressurization, it is possible that the myoglobin solution was exposed to even lower pH values during the course of the experiments. Hofland et al. [24] found that casein solutions (120 g in 1 liter water) exposed to pressurized CO_2 showed a pH drop from 6.75 (original pH) to 4.82 upon increasing the pressure from 1 to 25 bar. The pH remained stable at 4.82, even with a further increase in pressure. The pH under pressurized conditions was slightly higher for higher temperatures over a range of 25-50°C. From these observations, it can be concluded that myoglobin is exposed to acidic conditions when it comes in contact with high-pressure CO_2, which may contribute to its destabilization, as discussed below.

In this study, the incubation with pressurized CO_2 was also found to affect the integrity and the recovery of myoglobin, as shown by a decrease in the A409/A280 ratio and the absorbance at 280 nm, respectively (see Fig. 1 and Table 1). A further decrease in the A409/A280 ratio was observed with increasing temperature. These results indicate a change in the heme coordination within the heme pocket. It has previously been shown that a decrease in the pH of a myoglobin solution results in the protonation of the proximal histidine in the heme pocket, which causes the disruption of the iron-histidine bond and a change in the heme absorption spectrum [25, 26]. Thus, it is expected that the affinity of myoglobin for the heme will be reduced after the exposure to low pH induced by the pressurized CO_2. Indeed, Hargrove et al. [27, 28] showed that the heme dissociation from myoglobin at pH 5 was $\geq$100-fold faster than at neutral pH at 37°C, as monitored by changes in the Soret band. Consequently, such conditions may lead to heme dissociation when myoglobin is exposed to pressurized CO_2.

In order to determine whether the structure of myoglobin was influenced by CO_2, CD signals at 409 nm for probing the heme-protein interaction was studied. The relative molar ellipticity decreased after exposure to CO_2, with a greater decrease observed at higher temperatures, suggesting a change in the heme specific binding site. However, the results were not significantly different between 65 and 130 bar at constant temperature (Fig. 2).

In addition, the predominantly a-helical secondary structure of myoglobin, after the CO_2 incubation, did not change under the conditions studied (Fig. 6). In contrast, Ishikawa et al. [29] showed that CO_2 bubbling under pressurized conditions resulted in irreversible unfolding of myoglobin. This was achieved at ambient temperatures. However, it should be noted that these experiments were performed for myoglobin solutions that did not contain any excipient. Moreover, it is

possible that the change in myoglobin structure was influenced by the CO_2/water interface because of the gas bubbling method.
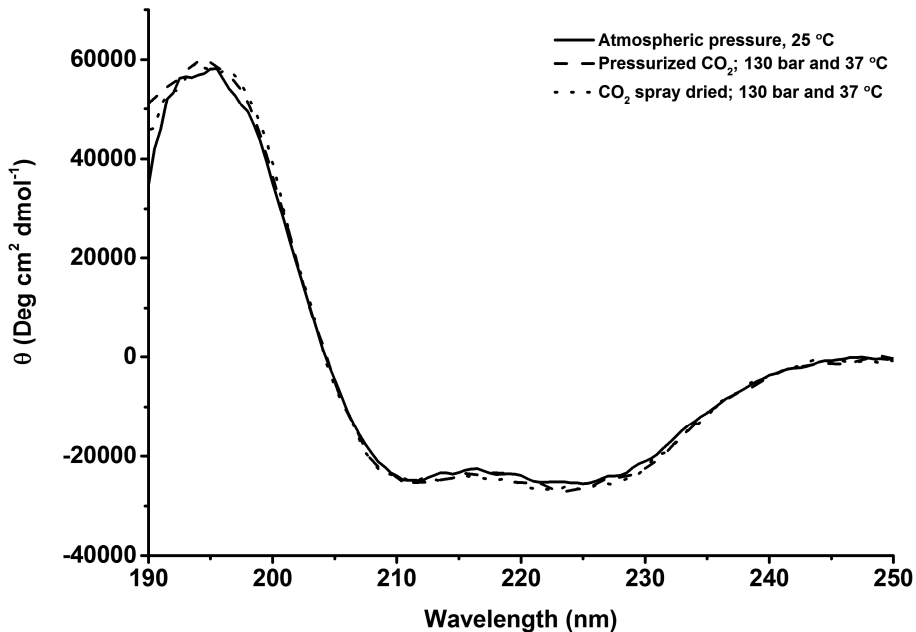

Fig. 6   Far-UV CD spectra of CO_2-incubated myoglobin and reconstituted solution of spray dried myoglobin formulations (both conducted at 130 bar and 37 °C, conditions O and V), compared to that of untreated myoglobin formulation.

The results from UV/Vis and CD spectroscopy showed that the myoglobin structure changes upon increasing temperature. However, the fluorescence intensity of myoglobin after the CO_2 incubation (Fig. 3) gave a constant signal, similar to that of the untreated (conditions A, B, C) and pressurized samples without CO_2 (conditions D, E, F, G, H, I). The ratio between the fluorescence at 350 nm and the absorbance at 280 nm (I_{350}/A_{280}) was determined from the total peak areas observed by HP-SEC. For the samples exposed to elevated temperature and pressure, the ratio of I_{350}/A_{280} was 0.22, and constant in all cases, while apomyoglobin showed a substantially larger I_{350}/A_{280} of 1.19 (not shown). Consequently, the tryptophan fluorescence signal can be used to determine the loss of heme from myoglobin. For the myoglobin

formulations exposed to CO_2, no increase in the fluorescence signal was observed, with the I_{350}/A_{280} values also around 0.22, suggesting that the heme was still embedded in the heme pocket.

Whereas pressure and temperature without CO_2 did not influence the total myoglobin concentration, a decrease in the protein content was found after the CO_2 incubation at higher temperatures (Table 1), with only 85% protein recovery at 65 bar and 130 bar at 50 °C (conditions L and P). This appears to be due to aggregation of myoglobin, because a decrease in the monomer content was found under these conditions (Fig. 4b). Moreover, an increase in concentration of particles larger than 1 µm was observed by flow-imaging microscopy (Fig. 5). Interestingly, the dimer content was decreased after incubation with CO_2 (Fig. 4a). Since no oligomers were detected by HP-SEC and the monomer content was reduced, the dimers proably were converted into micron-sized aggregates. Altogether, from these results it can be concluded that the aggregation is most likely the result of the shift in pH.

For the CO_2 incubation tests, different temperatures and pressures were used, which gave rise to different CO_2 densities. In order to evaluate whether the CO_2 density has an influence on the stability of myoglobin, several conditions were chosen that have the same CO_2 density (0.77 g/cm³, conditions M, O, and Q). As was observed for the CO_2 incubation tests, the results also showed a reduction in the heme absorption and protein content as the processing temperature increased (Table 1). Moreover, these values obtained at the same temperature but different pressure (and therefore different density) are almost the same (Table 1). From this, it can be concluded that changes in the myoglobin integrity can be attributed to the increase in temperature, and not the differences in CO_2 density.

Overall, it can be concluded that exposing the myoglobin formulation to pressurized CO_2 caused acidification, resulting in a change in the heme binding and aggregation of myoglobin (monomer loss and high particle concentrations). However, the heme was not removed, as the tryptophan fluorescence signal did not increase. In addition, the destabilization of myoglobin was promoted by increasing the processing temperature.

3.3 Effects of spray drying using carbon dioxide at 65-130 bar and 25-50°C

Having studied the influence of temperature, pressure and CO_2 exposure, the next series of experiments evaluated the influence of the spraying process on myoglobin integrity.

Upon reconstituting the spray-dried myoglobin, a greater reduction ($p < 0.05$) in heme absorbance was found (decreasing to approximately 85% at both 65 and 130 bar and 50 °C) when compared to the CO_2-incubated myoglobin solutions (as seen in Table 1 and Fig. 1). The reconstituted myoglobin formulation did not show a significant difference in the secondary structure (Fig. 6). However, a further decrease in the molar ellipticity at heme specific site (by CD) was observed with increasing temperature (Fig. 2). However, the data were not significantly different as compared to the CO_2-incubated group. Furthermore, the fluorescence signals also increased significantly, which was not observed in the case of the CO_2-incubated myoglobin solutions (Fig. 3). As an increase in the fluorescence signal corresponds to the formation of apomyoglobin, these results indicate that a partial loss of heme occurs during spray drying, at both subcritical and supercritical CO_2 conditions. In addition, the loss of heme slightly increased with increasing temperature.

Lower protein recoveries were observed for the reconstituted spray dried products with less than 80% recovery at the highest temperatures, as can be seen in Table 1. Furthermore, higher amounts of dimers (2.5-7.5%) and additionally some fragments (0.5-2%) of myoglobin were present after spray drying (Fig. 4a) when compared to the untreated myoglobin formulation (condition A). A further loss of monomer in the reconstituted solutions was also found, when compared to the CO_2-incubated samples (Fig. 4b). The CO_2 spray drying process also induced the formation of larger myoglobin aggregates, as shown in Fig. 5. Moreover, the total particle content was higher in the reconstituted solutions of spray-dried myoglobin powders when compared to the myoglobin solutions incubated with CO_2. In these cases, the sub-visible particles were also larger in diameter (Fig. 5).

Upon reconstitution of the spray-dried myoglobin/trehalose formulation produced at 130 bar and 37°C, the pH was 5.12 ± 0.06. In a similar manner to the CO_2 incubated solutions, these results suggest that the atomized myoglobin solution was acidified by the pressurized CO_2. In addition, it has been observed before that residual CO_2 can be present in powdered products after depressurization [30], which may explain the decrease in the pH upon reconstitution.

In this study, it was concluded that acidification causes a weakening of the heme binding of myoglobin. When this is combined with the spray drying process, some of the myoglobin molecules loose the heme. For the spray drying tests, the spray time was 40 minutes, which was typically followed by 30 minutes of post-drying. One experiment was also conducted without post drying. The results showed that the ratio of A409/A280 and relative molar ellipticity of myoglobin (at the heme specific site) treated with or without the post drying were not significantly different (Table 1 and Fig. 2, condition V and V-). Myoglobin aggregation, with and without the post-drying, were also similar in terms of dimer content and sub-visible particle sizes, as shown in Fig. 4 and Fig. 5. This suggests that the heme removal and myoglobin aggregation occurred during the 40-minute spray drying, when the myoglobin/trehalose formulation is atomized and dehydrated in the pressurized CO_2 environment.

While the acidification by CO_2 mainly affects the heme binding affinity and aggregation, other parameters of the CO_2 spray drying method may interfere with the myoglobin structure. The atomization step subjects the solution to a large CO_2/water interface, which may lead to protein denaturation and aggregation. Moreover, CO_2 is non-polar and therefore the protein may reorient so that the hydrophobic components are exposed to the surface, which may initiate the unfolding of the protein. Any of these factors, combined with the lowering of the heme affinity due to acidification by CO_2, could cause the destabilization of myoglobin, thus leading to the removal of heme and an increase in myoglobin aggregation. However, it is difficult to independently study atomization and drying parameters of the CO_2 spray drying method.

3.4 Effect of protein formulation

It is anticipated that this mechanistic study of the influence of the CO_2 spray drying process on myoglobin destabilization could be useful for the future development of protein formulations for protein drying. What is apparent from this study is that for pH-sensitive proteins like myoglobin, the formulation should be carefully selected to avoid a pH shift during CO_2 spray drying. In order to evaluate this hypothesis, the concentration of the phosphate buffer pH 6.2 was increased up to 150 mM. Under these conditions, it was found that the A409/A280 ratio showed nearly 100% recovery of the heme (CO_2 spray dried at 130 bar and 37°C) (data not shown). Such high buffer concentrations may not be ideal, e.g., when the formulation has to be kept isotonic, but could provide a solution if high-concentration protein formulations are used

that can be diluted before administration. Also, one could use a higher buffer pH than 6.2, such as 7.0, which in particular for phosphate would further increase its buffering capacity.

4. Conclusion

In this study, the influence of the critical CO_2 spray drying processing parameters on the stability of dried myoglobin formulations was investigated. This was done by monitoring the effect of temperature, pressure, contact with CO_2 and the spray drying steps on myoglobin structure. In the range of 65-130 bar and 25-50 °C, pressure and temperature alone did not influence the myoglobin integrity. After incubation with pressurized CO_2, the pH of the myoglobin solution was about 5, which compromised the heme binding in myoglobin and induced myoglobin aggregation. Spray drying with pressurized CO_2 resulted in the loss of heme and a further increase in myoglobin aggregation. Moreover, this was exacerbated by an increase in temperature but not affected by increasing pressure. Overall, the results indicate that exposure of myoglobin to CO_2 destabilizes the myoglobin, which eventually leads to heme loss and protein aggregation during CO_2 spray drying.

References

[1]   N. Jovanović, A. Bouchard, G. W. Hofland, D. J. Crommelin, W. Jiskoot, Stabilization of IgG by supercritical fluid drying: optimization of formulation and process parameters, Eur J Pharm Biopharm, 68 (2008) 183-190.

[2]   N. Jovanović, A. Bouchard, M. Sutter, M. V. Speybroeck, G. W. Hofland, G. Witkamp, D. J. A. Crommelin, W. Jiskoot, Stable sugar-based protein formulations by supercritical fluid drying, Int J Pharm, 346 (2008) 102-108.

[3]   O. Nuchuchua, H. A. Every, G. W. Hofland, W. Jiskoot, Scalable organic solvent free supercritical fluid spray drying process for producing dry protein formulations, Eur J Pharm Biopharm, 88 (2014) 919-930.

[4]   N. Jovanović, A. Bouchard, G. W. Hofland, G. Witkamp, D. J. A. Crommelin, W. Jiskoot, Distinct effects of sucrose and trehalose on protein stability during supercritical fluid drying and freeze-drying, Eur J Pharm Sci, 27 (2006) 336-345.

[5]   S. P. Cape, J. A. Villa, E. T. S. Huang, T-H Yang, J. F. Carpenter, R. E. Sievers, Preparation of active proteins, vaccines and pharmaceuticals as fine powders using supercritical or near-critical fluids, Pharm Res, 25 (2008) 1967-1990.

[6]   U. B. Hendgen-Cotta, M. Kelm, T. Rassaf, *Myoglobin functions in the heart,* Free Radical Bio Med, 73 (2014) 252-259.

[7]   M. P. Richards, Redox Reactions of Myoglobin. Antioxid Redox Signal, 18 (2013) 2342-2351.

[8]   E. Breslow, F. R. N. Gurd, Reactivity of sperm whale metmyoglobin towards hydrogen ions and p-nitrophenyl acetate, J Biol Chem, 237 (1962) 371-381.

[9]   F.W. Teale, Cleavage of the haem-protein link by acid methylethylketone, Biochim Biophys Acta, 35 (1959) 543.

[10]   L. Tofani, A. Feis, R. E. Snoke, D. Berti, P. Baglioni, G. Smulevich, Spectroscopic and interfacial properties of myoglobin/surfactant complexes, Biophys J, 87 (2004) 1186-1195.

[11]   N. A. Nicola, E. Minasian, C. A. Appleby, S. J. Leach, Circular dichroism studies of myoglobin and leghemoglobin, Biochemistry, 14 (1975) 5141-5149.

[12]   D. Puett, The equilibrium unfolding parameters of horse and sperm whale myoglobin. Effects of guanidine hydrochloride, urea, and acid. J Biol Chem, 248 (1973) 4623-4634.

[13]   B. Meyssami, M. O. Balaban, A. A. Teixeira, Prediction of pH in Model Systems Pressurized with Carbon-Dioxide. Biotechnology Progress, 8 (1992) 149-154.

[14]   K. L. Toews, R. M. Shroll, C. M. Wai, N. G. Smart, pH-defining equilibrium between water and supercritical CO_2. Influence on SFE of organics and metal chelates, Anal Chem, 67 (1995) 4040-4043.

[15]   Z. Yu, A. S. Garcia, K. P. Johnston, R. O. Williams 3rd, Spray freezing into liquid nitrogen for highly stable protein nanostructured microparticles, Eur J Pharm and Biopharm, 58 (2004) 529-537.

[16]   Z. S. Yu, K. P. Johnston, R.O. Williams III, Spray freezing into liquid versus spray-freeze drying: Influence of atomization on protein aggregation and biological activity. Eur J Pharm Sci, 27 (2006) 9-18.

[17]   S. C. Harrison, E. R. Blout, Reversible conformational changes of myoglobin and apomyoglobin, J Biol Chem, 240 (1965) 299-303.

[18]   M. Momenteau, M. Rougee, B. Loock, Five-coordinate iron-porphyrin as a model for the active site of hemoproteins. Characterization and coordination properties, Eur J Biochem, 71 (1976) 63-76.

[19]   M. C. Hsu, R. W. Woody, The origin of the heme Cotton effects in myoglobin and hemoglobin, J Am Chem Soc, 93 (1971) 3515-3525.

[20]   M. Nagai, Y. Nagai, K. Imai, S. Neya, Circular dichroism of hemoglobin and myoglobin, Chirality, 26 (2014) 438-442.

[21]   M. S. Hargrove, D. Barrick, J. S. Olson, The association rate constant for heme binding to globin is independent of protein structure. Biochemistry, 35 (1996) 11293-11299.

[22]   A. N. Schechter, C. J. Epstein, Spectral studies on the denaturation of myoglobin, J Mol Biol, 35 (1968) 567-89.

[23]   W. Doster, R. Gebhardt, High pressure - unfolding of myoglobin studied by dynamic neutron scattering, Chem Phys, 292 (2003) 383-387.

[24]   G. W. Hofland, M. van Es, L. A. M. van der Wielen, G. Witkamp, Isoelectric precipitation of casein using high-pressure CO_2, Ind Eng Chem Res, 38 (1999) 4919-4927.

[25]   J. T. Sage, D. Morikis, P. M. Champion, Spectroscopic studies of myoglobin at low pH: heme structure and ligation, Biochemistry, 30 (1991) 1227-1237.

[26]   V. Palaniappan, D. F. Bocian, Acid-induced transformations of myoglobin - characterization of a new equilibrium heme-pocket intermediate, Biochemistry, 33 (1994) 14264-14274.

[27]   M. S. Hargrove, E. W. Singleton, M. L. Quillin, L. A. Ortiz, G. N. Jr. Philips, J. S. Olson, A. J. Mathews, His(64)(E7) --> Tyr apomyoglobin as a reagent for measuring rates of hemin dissociation, J Biol Chem, 269 (1994) 4207-4214.

[28]   M. S. Hargrove, J. S. Olson, The stability of holomyoglobin is determined by heme affinity, Biochemistry, 35 (1996) 11310-11318.

[29]   H. Ishikawa, M. Shimoda, A. Yonekura, K. Mishima, K. Matsumoto, Y. Osajima, Irreversible unfolding of myoglobin in an aqueous solution by supercritical carbon dioxide, J Agric Food Chem, 48 (2000) 4535-4539.

[30]   A. Bouchard, N. Jovanović, G. W. Hofland, W. Jiskoot, E Mendes, D. J. A. Crommelin, G. Witkamp, Supercritical fluid drying of carbohydrates: selection of suitable excipients and process conditions. Eur J Pharm Biopharm, 68 (2008) 781-794.

CHAPTER 5

The combined effects of carbon dioxide-water interface and pH shift on myoglobin stability

O Nuchuchua[1], B Öztürk[1], H A Every[2], and W Jiskoot[1]

[1] Division of Drug Delivery Technology, Cluster BioTherapeutics, Leiden Academic Centre for Drug Research (LACDR), Leiden University, The Netherlands
[2] FeyeCon Development & Implementation B.V., Weesp, The Netherlands

Abstract

The aim of this study was to investigate the effects of the CO_2/water interface and pH shift on heme destabilization and aggregation of myoglobin. The studies were carried out by bubbling either gaseous CO_2 or N_2 into solutions of myoglobin in pure water. The starting pH values of the myoglobin solutions were in the range of 4.0 to 7.0, and the pH was monitored during the bubbling process. CO_2 gas bubbling resulted in a decrease of the pH of the myoglobin solutions, except for the solution with a starting pH of 4.0. Changes in the heme binding and the secondary structure, as detected by changes in the UV/Vis absorption as well as the near- and far-UV/Vis circular dichroism (CD) spectra, were observed when the pH of the myoglobin solution was (shifted to) below 4.5. However, the heme still remained in the heme pocket in myoglobin, as reflected by no change in the intensity of the protein fluorescence signal. Flow imaging microscopy showed that after CO_2 bubbling, the solutions prepared at pH 6.2-7.0 exhibited amorphous sub-visible particles of myoglobin aggregates while the solutions with a starting pH of 4.0-5.3 gave fiber-like particles. Moreover, more myoglobin aggregates were observed when the solution starting pH was 6.2-7.0 compared to the solutions prepared at pH 4.0-5.3. In contrast, N_2 gas bubbling did not influence the pH and heme binding but still resulted in myoglobin aggregation. From this, it can be concluded that the gas bubbling induced myoglobin aggregation due to the creation of the gas-liquid interface, independent of the gas that was used. However, only CO_2 bubbling resulted in a pH shift, which caused changes in the heme binding and enhanced the formation of sub-visible myoglobin aggregates.

1.   Introduction

Proteins are structurally unstable, and the physical and chemical degradation processes that occur during purification, processing and storage [1-5] can lead to denaturation and aggregation of the native protein [6, 7]. In particular, the air/water interface that forms during agitation/stirring or atomization during spray drying exposes the protein to the hydrophobic air environment [8]. When proteins come in contact with the air/water interface [9], the hydrophobic components reorient towards the air phase, thus adopting a non-native protein structure that can readily aggregate [10-18]. For example, Yu et al. [19] observed the deactivation of lysozyme upon atomizing lysozyme formulations in air, whereas the activity was preserved when lysozyme formulations were sprayed into water. Similarly, another research study on spray lyophilization of recombinant human interferon-γ showed that the atomization and lyophilization caused the aggregation of the protein [20].

In previous studies on carbon dioxide (CO_2) spray drying of protein formulations [21, 22], protein aggregates in the sub-visible size range and/or the presence of insoluble residues in reconstituted solutions of polyclonal and monoclonal antibodies, myoglobin, α-chymotrypsinogen A, lysozyme, α-lactalbumin were observed. In addition, a comprehensive study of myoglobin exposed to the different CO_2 spray drying processing conditions showed that acidification by CO_2, in combination with the atomization and drying steps, led to partial heme loss and aggregation of myoglobin [23]. Briefly, a shift to a lower pH was observed for myoglobin solutions (pH 6.2) when incubated with CO_2 under pressure, dropping to pH 5.0 or lower. Under these conditions, the heme was destabilized and myoglobin aggregates were formed, but no release of the heme was observed. However, when spraying the same formulation into high pressure CO_2, a loss of heme was found. From these results, it was concluded that several factors in the CO_2 spray drying process, such as the shift in pH, the CO_2/water interface and the hydrophobicity of pressurized CO_2, could possibly contribute to heme loss and the aggregation of myoglobin [23].

As it is difficult to individually monitor the influence of these three parameters during the CO_2 spray drying process, it was proposed to investigate the effect of the CO_2/water interface and the pH shift on the heme destabilization and aggregation of myoglobin by bubbling myoglobin solutions with CO_2. This bubbling method allows for rapid regeneration of the gas/water interface, when compared to other techniques such as stirring [10]. To exclude any potential influence of formulation excipients, 5 mg/ml myoglobin solutions were prepared in

water at different pH values in the range of 4.0-7.0. During bubbling, the pH was monitored *in situ*. Myoglobin's structural integrity was observed by UV/Vis spectroscopy, fluorescence spectroscopy, circular dichroism, size-exclusion chromatography, and flow imaging microscopy analysis. In order to separate the influence of pH and the gas/water interface on the myoglobin integrity, N_2 gas was used as a control, as it does not influence the pH but shows only the effect of the gas/water interface on myoglobin.

2.   Materials and Methods

2.1 Preparation of myoglobin solution

Firstly, 5 mg/ml myoglobin (Sigma-Aldrich, St. Louis, USA) was dissolved in pure water, giving a pH of 8.4, and then titrated with 0.2 M HCl to determine the amount of acid needed to achieve the desired pH. The pH was measured *in situ* while adding the acid solution (SevenCompact™ pH/Ion S220, Mettler-Toledo AG, Schwerzenbach, Switzerland). In this study, the pH values of the solutions were 4.0, 4.5, 5.3, 6.2, and 7.0. Once the equivalent volume of acid solution was known, new solutions were prepared where the acid was mixed into the water prior to dissolving 5 mg/ml myoglobin, in order to obtain the correct pH while avoiding exposure of myoglobin to extremely low pH values. All myoglobin solutions were filtered through a 0.22 µm cellulose filter before starting the bubbling experiments, resulting in a final myoglobin concentration of about 3.5 mg/ml.

2.2 Experimental set-up

For the bubbling experiments, a 50 ml three-neck round-bottom flask (Z334545-1EA, Sigma-Aldrich, St. Louis, USA) was filled with 10 ml of myoglobin solution and placed in a water bath controlled at a temperature of 25 °C. Nitrogen or carbon dioxide gas was introduced into the myoglobin solution at a constant flow rate of 1.7 litre per hour for 60 minutes, whereas a non-bubbled solution incubated for the same time period was used as a reference control solution. The pH was measured *in situ* and recorded every 5 seconds by a SevenCompact™ pH/Ion S220 (Mettler-Toledo AG, Schwerzenbach, Switzerland). The experimental set-up is shown in Fig. 1.
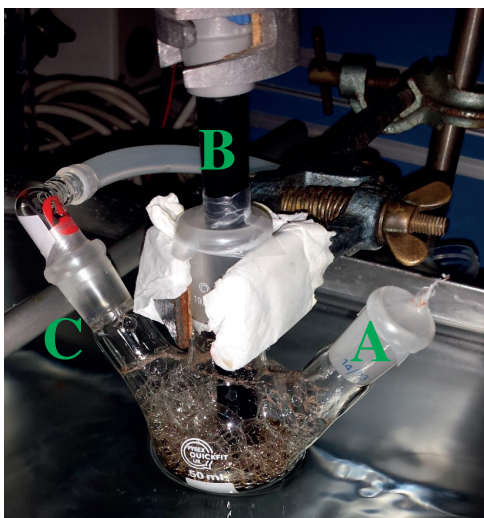
Fig. 1 The bubbling apparatus shows A) N_2 or CO_2 gas, B) pH probe, and C) gas outlet. The experiments were carried out at a gas flow of 1.7 l/h for an hour at 25°C.

2.3 Protein analysis

2.3.1   Protein content and heme binding

Samples of the myoglobin solutions were directly diluted to a concentration of 0.1 mg/ml myoglobin in 10 mM citrate buffer with the same pH as the myoglobin solution after 60 minutes bubbling. The diluted protein solution was filtered through a 0.22 μm pore filter prior to analysis. The protein content was determined by a UV spectrophotometer (Agilent 8453, Agilent Technologies, Santa Clara, USA). The spectra were collected from 190 nm to 1000 nm. The myoglobin concentration was calculated using the molar extinction coefficient of 3.45×10^4 $M^{-1}cm^{-1}$ at 280 nm [24]. The absorbance ratio between 409 and 280 nm (A_{409}/A_{280}) from each spectrum indicated the heme group binding to the proximal histidine in the heme pocket of myoglobin [22]. The percentages of protein content recovery of the treated myoglobin were compared to those of the untreated liquid myoglobin formulation at 25°C according to equation 1:

$$Protein\ recovery(\%) = \left[\frac{A280\ (processed)}{A280\ (nonprocessed)}\right] \times 100 \qquad (Eq.\ 1)$$

2.3.2   Circular dichroism (CD) spectroscopy

The structure of myoglobin was observed by measurements of far-UV CD (190-250 nm) and near-UV/Vis (350-450 nm) CD spectroscopy (J-810 Spectropolarimeter, JASCO Inc., Easton, USA). Analyses were performed at 25 °C. The parameters were set at a sensitivity of 100 mdeg, a data pitch of 10 nm, a bandwidth of 2 nm, and a scanning speed of 100 nm/min. Samples were diluted to 0.1 mg/ml myoglobin by adding 10 mM citrate with the same pH as the myoglobin solution after bubbling. The samples were placed in a 0.1 and 1 cm quartz cuvette for far-UV CD and near-UV/Vis CD, respectively. CD spectra of six sequential measurements were averaged and corrected for the blank. The CD signals were converted to molar ellipticity per amino acid residue ($[\theta]$, deg cm^{2}dmol^{-1}). The fraction of α-helix (f_H) was estimated by using Eq. 2, where $[\theta]_{222}$ is the molar ellipticity per amino acid residue at 222 nm [25]:

$$f_H = ([\theta]_{222} - 3{,}000)/(-36{,}000 - 3{,}000) \qquad \text{(Eq. 2)}$$

2.3.3   High performance size-exclusion chromatography

Samples of 50 µl of 1 mg/ml myoglobin (Mb) in 10 mM citrate pH 6.2 filtered through a 0.22 µm pore filter were analyzed by high performance size-exclusion chromatography (HP-SEC) with a Discovery® BIO Gel Filtration column (300 Å pore size) (Sigma-Aldrich, St. Louis, USA). The mobile phase, consisting of 150 mM phosphate buffer at a pH of 7.0 filtered through a 0.1 µm pore filter prior to use, had a flow rate of 0.7 ml/min. The UV and fluorescence chromatograms were recorded by a UV detector (Agilent 1100 VWD, Santa Clara, USA) and a fluorescence detector (Agilent 1200 FLD, Santa Clara, USA). The fluorescence emission intensity (I) was collected at 325, 337 and 350 nm with the excitation at 295 nm. For the same sample, the peak area of the fluorescence signal was compared to that of protein absorption (280 nm), and shown in terms of I/A_{280}. The I/A_{280} value of 1.19 for apomyoglobin (free-heme, apoMb) was used as a reference, as observed in previous study [23]. The amount of apomyoglobin was estimated by fluorescence data, as shown in Eq. 3. In addition, the peak area of myoglobin monomers was used to calculate the monomer recovery of the bubbled myoglobin, as compared to that of the non-bubbled sample.

Estimated apomyoglobin (%)

$$= \left[\frac{\text{I/A280 of bubbled Mb} - \text{I/A280 of nonbubbled Mb}}{\text{I/A280 of apoMb} - \text{I/A280 of nonbubbled Mb}} \right] \times 100$$

(Eq. 3)

2.3.4 *Flow imaging microscopy*

Sub-visible microparticles were analyzed by flow imaging microscopy using an MFI5200 instrument (Protein Simple, California, USA). The measurements were controlled by MVAS software version 1.3. One milliliter of undiluted myoglobin solution was introduced into a flow-cell with the dimensions of 100 and 1016 µm in depth and diameter, respectively. The sample stream, at a flow rate of 6 ml/min, passed through a flow cell illuminated by a blue LED. Images of the particles were captured by an optical camera. Pictures were obtained with a resolution of 1280x1024 pixels. The data were also analyzed by MVAS software. Total particle concentrations are reported for particle sizes larger than 1, 5, 10 and 25 µm. Measurements were made for samples both before and after bubbling.

3. Results

In this study, CO_2 and N_2 gas were bubbled into a myoglobin solution to investigate the heme-binding and aggregation of myoglobin, as a function of the pH and the presence of the gas/water interface.

3.1 *pH during bubbling of the myoglobin solution*

During the CO_2 gas bubbling experiments, changes in pH were observed. While the pH of the myoglobin solution prepared at pH 4.0 remained practically the same, the solutions with a starting pH of 4.5 and higher shifted to lower pH values after three minutes of CO_2 bubbling (Fig. 2). The myoglobin formulations prepared at pH 5.3, 6.2 and 7.0 showed a fast drop in pH within the first few minutes to 4.6, 4.8 and 5.0, respectively, and remained at these pH values until the end of the CO_2 bubbling process. In contrast, when N_2 gas bubbles were introduced into the myoglobin solutions, the original pH values of each of the myoglobin formulations did not change, as seen in Fig. 2. Thus, it is apparent that during the bubbling process, CO_2 dissolves into the water to form carbonic acid, causing a pH shift. N_2, however, does not react with water, and consequently has no influence on the solution pH.
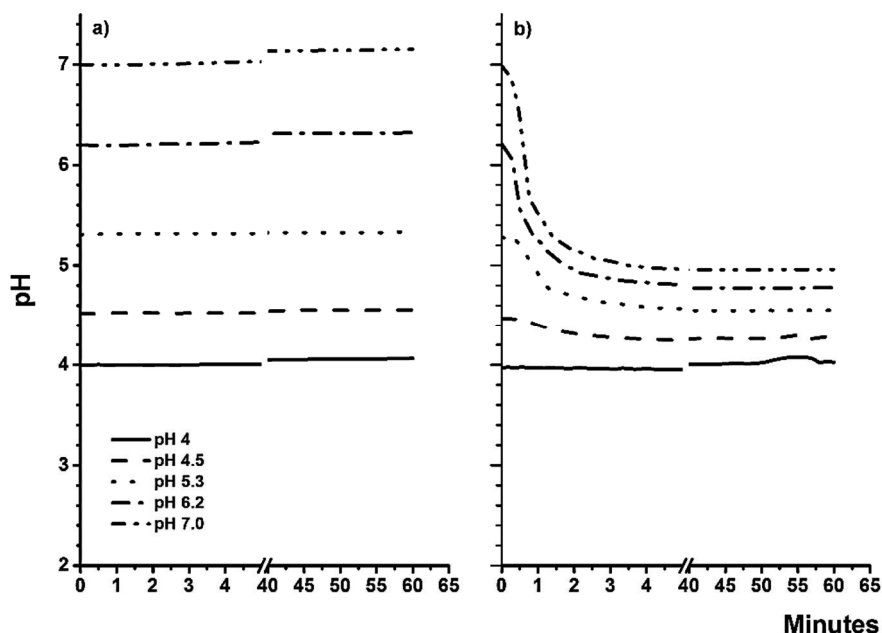
Fig. 2 *In situ* pH measurements of 5 mg/ml myoglobin solutions at pH 4-7 during nitrogen (a) and carbon dioxide (b) bubbling at a flow rate of 1.7 l/h. The experiments were carried out for an hour.

3.2 Heme binding and secondary structure of myoglobin upon gas bubbling

As the pH is reduced during CO_2 bubbling, it is possible that this affects the integrity of the protein. For the non-bubbled myoglobin solutions, the heme binding in myoglobin was studied over the pH range 4.0 - 7.0. Prior to bubbling, the solutions with a starting pH of 5.3 and higher exhibited very similar A_{409}/A_{280} ratios, molar ellipticities at 409 nm and fluorescence signals, suggesting that the myoglobin structure is not affected by the starting pH and is similar to the native form (Table 1 and Figures 3, 4 and 5). For the non-bubbled solution with a starting pH of 4.5, however, a slight change in the structure was observed, with a reduction in the A_{409}/A_{280} and alpha-helix fraction (Table 1). Moreover, a small increase in the fluorescence signal was also detected (Fig 5a), indicating that there is less quenching by the heme. The CD data, however, was very similar for all non-bubbled solutions with a starting pH of 4.5 and higher (Fig. 3a and Fig. 4a). These results suggest that the heme binding changes as a function of pH, with the changes starting to occur around pH 4.5.

For the non-bubbled solution with a starting pH of 4.0, the results are very different compared to the other starting solutions. There is a clear change in the heme binding to the proximal histidine, as observed by a reduction of both the A_{409}/A_{280} ratio (Table 1) and the molar ellipticity at 409 nm (Fig. 3). Furthermore, the secondary structure of myoglobin was perturbed, as observed by a decrease in the negative CD band representing the a-helix structure (Fig. 4 and Table 1). Moreover, an increase in the fluorescence signal indicates less heme quenching of myoglobin's intrinsic fluorescence (Fig. 5a). After bubbling this same solution with CO_2, the structure of myoglobin showed no further changes. Similar results were also found after N_2 bubbling at pH 4.0 (data not shown). These results confirm that under these conditions, the low pH, rather than the exposure to the gas/water interface, is the main factor behind the structural changes observed in the myoglobin structure. The behaviour is also consistent with what was previously observed by Ishikawa et al. [26] in a similar bubbling study. Moreover, they also saw that the secondary structure of myoglobin at pH 4.0 is reversibly folded when the pH is brought to neutral.

Upon bubbling the myoglobin solution with a starting pH of 4.5, the pH shifted to 4.3. This drop in pH led to similar changes in the myoglobin structure and heme binding as was observed at pH 4.0, as mentioned above. However, under these conditions (pH 4.3), the heme remained in the heme pocket after bubbling, as there was no change in the intrinsic fluorescence emission signal when compared to the fluorescence intensity of the non-bubbled myoglobin solution (Fig. 5). These results were similar to those of a non-bubbled myoglobin solution prepared in 10 mM citrate buffer at pH 4.3 (data not shown). In contrast, N_2 gas bubbling at pH 4.5 was less detrimental to myoglobin's structure, although a slight decrease in the A_{409}/A_{280} ratio was observed (Table 1). This suggests that for the solution with pH 4.5, the changes in the myoglobin structure after bubbling with CO_2 are again caused by the slight but significant acidification.

Solutions with pH 5.3 and higher showed a substantial reduction in pH upon CO_2 bubbling. However, the pH shift did not measurably affect the myoglobin structure and the heme binding (Table 1 and Fig. 5). Similarly, N_2 gas bubbling did not change the myoglobin structure when compared to the non-bubbled solutions. Moreover, for the solutions with pH values in the range of 4.5 to 7.0, the N_2 bubbling had almost no effect on the ratio of A_{409}/A_{280} (Table 1), secondary structure (Table 1), molar ellipticity at 409 nm (data not shown), and intrinsic fluorescence intensity (data not shown). So, the N_2 gas bubbling does not influence the pH of the solutions and the myglobin structure.
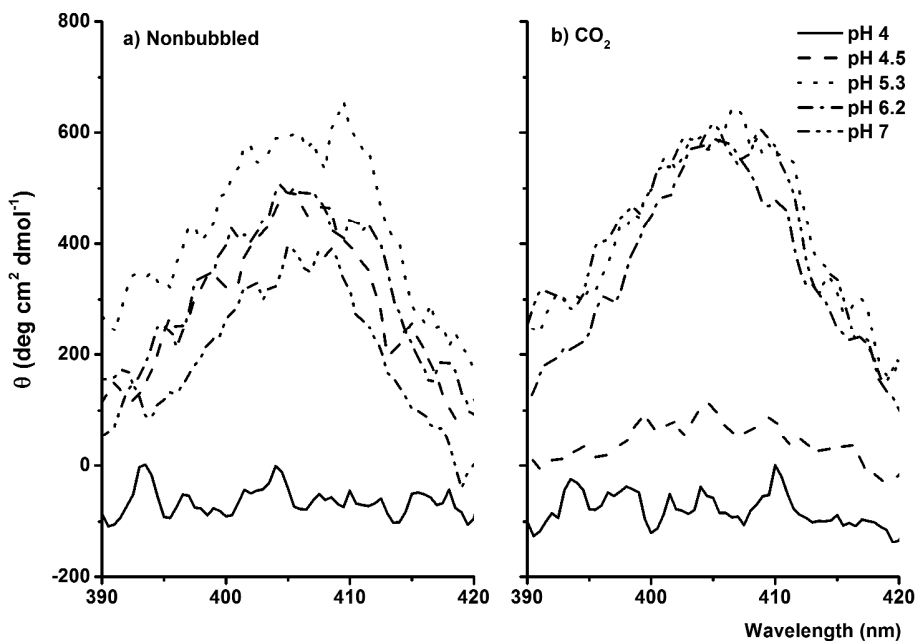
Fig. 3 Near-UV/Vis CD spectra of the myoglobin solutions at pH 4-7 before (a) and after one-hour CO_2 bubbling (b) at a flow rate of 1.7 l/h.
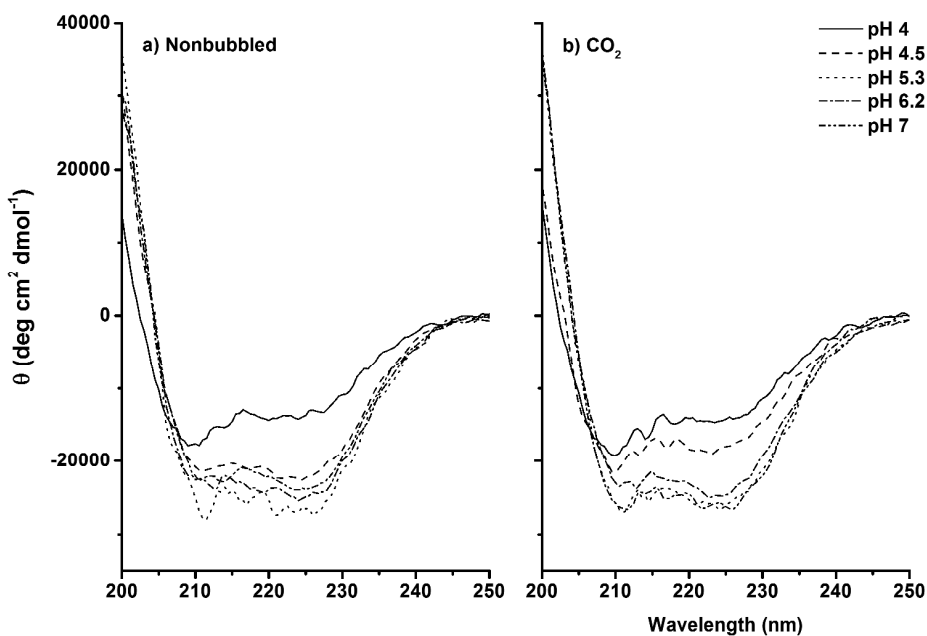

Fig. 4 Far-UV CD spectra of the myoglobin solutions at pH 4-7 before (a) and after CO_2 bubbling (b) at a flow rate of 1.7 l/h.
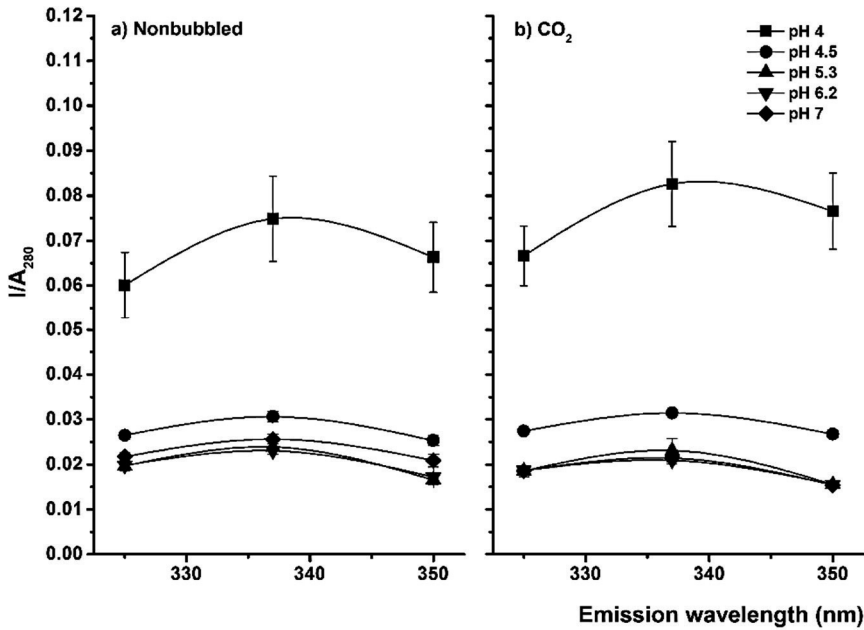
Fig. 5 Intrinsic fluorescence emission intensity of the myoglobin solutions at pH 4-7 before (a) and after CO_2 bubbling (b) at a flow rate of 1.7 l/h.

Table 1. UV/Vis absorption ratio at 409 and 280 nm (A_{409}/A_{280}) and a-helix fraction (f_H) derived from the far-UV CD signal at 222 nm of myoglobin (non-bubbled, N_2 and CO_2 gas bubbling).

5 mg/ml myoglobin	A_{409}/A_{280}[a]			f_H (222 nm)[b]		
	Non-bubbled	N_2	CO_2	Non-bubbled	N_2	CO_2
pH 4	1.29 ± 0.06	1.26 ± 0.05	1.18 ± 0.03	0.43 ± 0.02	0.48 ± 0.06	0.50 ± 0.02
pH 4.5	4.87 ± 0.14	4.97 ± 0.04	2.61 ± 0.03	0.65 ± 0.01	0.69 ± 0.01	0.55 ± 0.02
pH 5.3	5.78 ± 0.10	5.88 ± 0.04	5.81 ± 0.15	0.75 ± 0.02	0.76 ± 0.01	0.73 ±0.01
pH 6.2	5.58 ± 0.04	5.61 ± 0.01	5.47 ± 0.23	0.70 ± 0.04	0.71 ± 0.05	0.70 ± 0.06
pH 7.0	5.23 ± 0.09	5.24 ± 0.01	5.53 ± 0.04	0.67 ± 0.04	0.71 ± 0.02	0.75 ± 0.03

[a] Data were obtained from the ratio of the absorbance at 409 and 280 nm by UV/Vis spectroscopy (see methods section).
[b] The α-helix fraction of myoglobin before and after N_2 and CO_2 bubbling with a gas flow rate of 1.7 l/h (see eq. 2 in the methods section).

3.3 Myoglobin aggregation upon gas bubbling

Bubbling exposes the protein at the gas/water interface, which may lead to denaturation, and correspondingly aggregation, of the protein. Bubbling with any gas will continuously renew this interface, thus it is hypothesized that both N_2 and CO_2 bubbling will lead to protein aggregation. Indeed, the concentration of sub-visible particles increased after N_2 bubbling and showed similar values over the pH range studied (Fig. 6). Correspondingly, the CO_2-bubbled myoglobin solution prepared at pH 4.0-5.3 showed a similar increase in the particle concentration when compared to the N_2-bubbled solutions prepared at pH 4.0-7.0. For all these solutions, the morphology of the aggregates in the range 25-40 μm was fibril-like. In contrast, CO_2-bubbling of myoglobin solutions prepared at pH 6.2-7.0 showed a 7-fold increase in the number of particles larger than 1 μm, as compared to the corresponding N_2-bubbled myoglobin solutions (Fig. 6). Moreover, the aggregates that formed during the CO_2 bubbling of these solutions were amorphous (see Table 2 and 3 for representative examples of particles). In all cases, the particles were irregular with an amorphous appearance, as commonly observed for proteinaceous particles [27, 28]. Furthermore, no gas bubble-like particles were observed. From these results it is clear that the particle formation is dependent on the gas/water interface and the pH shift.

HP-SEC of the samples showed no formation of myoglobin dimers or oligomers (data not shown). However, some monomer loss (up to 20%) was observed after N_2 and CO_2 bubbling, indicating the formation of insoluble aggregates (data not shown). Since there was no clear trend in the extent of monomer loss with respect to incubation pH and N_2 versus CO_2 bubbling, these results will not be discussed further.
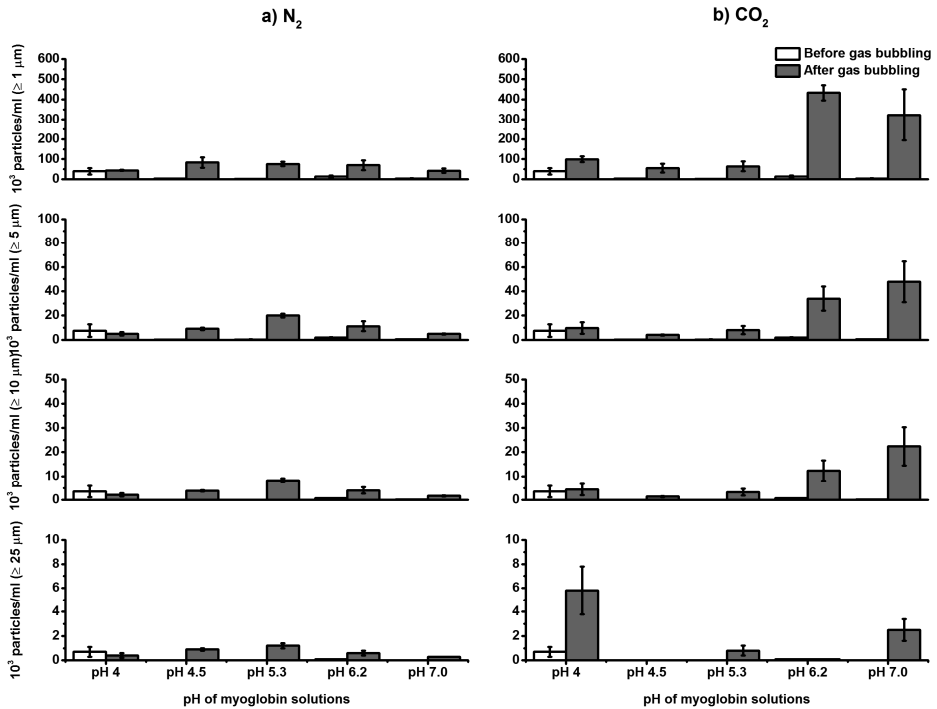
Fig. 6 Particle concentrations in myoglobin solutions at pH 4.0-7.0 measured by flow-imaging microscopy before and after N_2 (a) and CO_2 (b) bubbling at a flow rate of 1.7 l/h.
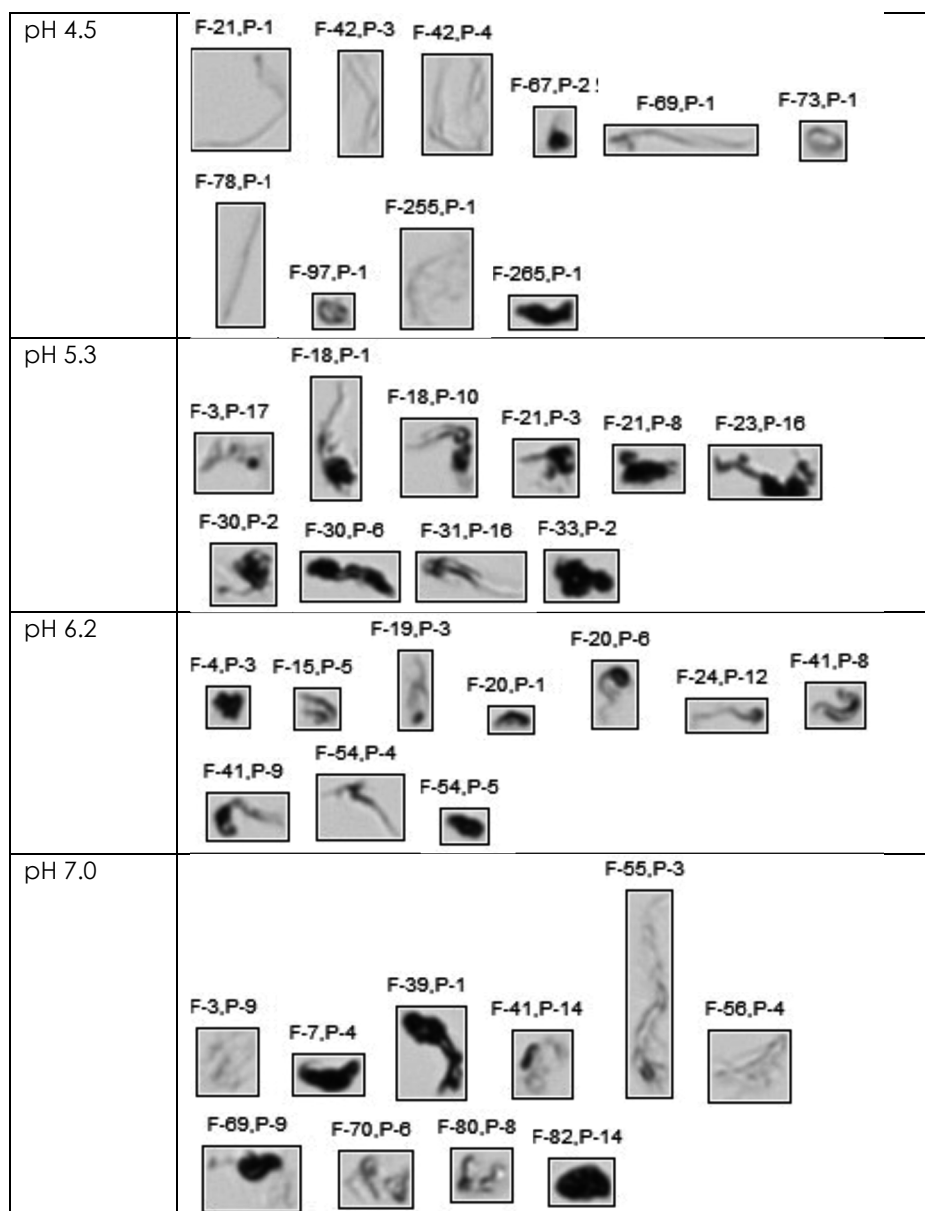
Table 2. Images of myoglobin aggregates captured by flow imaging microscopy for the myoglobin solutions at pH 4.0-7.0 after N_2 bubbling.

Original myoglobin solutions	Particle images (in range 25-40 um)
pH 4.0	

pH 4.5	
pH 5.3	
pH 6.2	
pH 7.0	

pH 4.5: F-21,P-1 F-42,P-3 F-42,P-4 F-67,P-2 F-69,P-1 F-73,P-1 F-78,P-1 F-97,P-1 F-255,P-1 F-265,P-1

pH 5.3: F-3,P-17 F-18,P-1 F-18,P-10 F-21,P-3 F-21,P-8 F-23,P-16 F-30,P-2 F-30,P-6 F-31,P-16 F-33,P-2

pH 6.2: F-4,P-3 F-15,P-5 F-19,P-3 F-20,P-1 F-20,P-6 F-24,P-12 F-41,P-8 F-41,P-9 F-54,P-4 F-54,P-5

pH 7.0: F-3,P-9 F-7,P-4 F-39,P-1 F-41,P-14 F-55,P-3 F-56,P-4 F-69,P-9 F-70,P-6 F-80,P-8 F-82,P-14

Table 3. Images of myoglobin aggregates captured by flow imaging microscopy for the myoglobin solutions at pH 4.0-7.0 after CO_2 bubbling.

Original myoglobin solutions*	Particle images (in range 25-40 um)
pH 4.0 (4.0)	
pH 4.5 (4.3)	
pH 5.3 (4.6)	

| pH 6.2 (4.8) | |
| pH 7.0 (5.0) | |
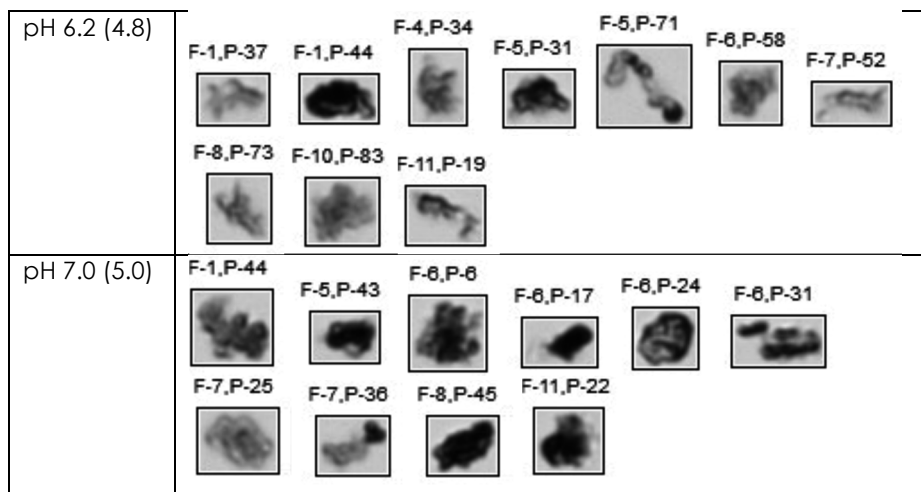
*The number in a bracket is the final pH of myoglobin solutions after CO_2 bubbling.

4.   Discussion

4.1 Effect of gas bubbling on the heme binding of myoglobin

In the atomization process in CO_2 spray drying [23], the CO_2 comes in contact with water at the surface of droplets (CO_2/water interface). As supercritical CO_2 is non-polar, the protein in the droplets will be exposed to the hydrophobic CO_2 at the droplet interface. Under these conditions, the protein may reorient, to expose the hydrophobic heme pocket of myoglobin towards to this surface, leading to protein unfolding at the droplet interface. In additional to this surface effect, the drying of the droplets occurs by the mass transfer of water into the CO_2 phase as well as the diffusion of CO_2 into the droplets. It is the latter that has been shown to cause acidification of the protein formulation, which also led to protein denaturation as shown by changes in the UV-Vis and CD spectra [23]. However, given that the CO_2 spray drying process takes place in a sealed high pressure vessel, it is not possible to determine whether the CO_2/water interface or the acidification is the predominant factor influencing the resultant protein destabilization.

It was anticipated that the gas bubbling study with CO_2 and N_2 would help to differentiate the influence of these two factors on the destabilization and aggregation of myoglobin. Although this method uses the myoglobin solution as the bulk phase (in contrast to the supercritical CO_2 being the bulk phase in the case of the spray drying process), the bubbles will still create a gas/water interface that may be representative of the behaviour observed during spraying. Moreover,

the bubbling method has previously been shown to enhance the protein aggregation rate 40 times compared to stirring, due to rapid regeneration and renewal of interfaces [3]. Furthermore, bubbling with CO_2 was expected to result in the acidification of myoglobin solutions in a similar manner to what was observed during the high pressure spray drying process, as CO_2 reacts with the water to form carbonic acid. A similar pH shift has previously been observed for a milk solution (120 g in 1000 g water), where the pH was also found to decrease from 6.8 to about 5 when exposed to high pressure CO_2 under static conditions at 20-40 bar [29]. In contrast, the solutions exposed to N_2 bubbling were not expected to show any pH shift, as N_2 does not form an acid in water.

As anticipated, bubbling with N_2 resulted in no change in the pH, while bubbling with CO_2 showed a shift in pH to values lower than 5.0 for all the myoglobin solutions, except those with the starting pH of 4.0. However, only the myoglobin solution prepared at pH 4.5 showed a change in the a-helix and heme binding of myoglobin (as observed by UV/Vis and CD at the Soret band), which was due to the shift in pH to 4.3. These results suggest that the heme experiences partial dislocation or dissociation within the myoglobin upon reducing the pH [30-32]. For this same solution, however, no change in the fluorescence signal was observed after bubbling, suggesting that the heme remains within the heme pocket. Based on these observations, it would seem that myoglobin is in an acid-denatured state under low pH conditions, and that the structure resembles a molten globule [33-35]. Additionally, myoglobin may present as an intermediate form between the native heme-bound and heme-dissociated forms at pH below 4.5 [33, 36].

In contrast, the fluorescence data for the myoglobin solution with a starting pH of 4.0 indicates that there is a clear change in the heme binding (Fig. 5). In general, an increase in the fluorescence signal indicates that the myoglobin structure is less quenched by heme [33, 37-39]. This is also supported by the A_{409}/A_{280} ratio, which decreases when the heme binding to the proximal histidine at the heme pocket is changed [40, 41]. For the completely heme-free form of myoglobin (apomyoglobin) extracted by acid-methylethylketone [42], the ratio of fluorescence intensity to protein absorption (I/A_{280}) is higher than that of myoglobin [23]. It is often assumed that any increase in the fluorescence signal corresponds to a loss of heme. However, it has also been shown that the intermediate form of myoglobin, which allows solvent molecules (typically water) to access the tryrosyl residues of tryptophan, can also result in an increase in the fluorescence signal [33]. Moreover, Stiebler et al. [43] reported that about 0.5 nmol/ml of heme was soluble in acidified aqueous solution (0.5 M sodium acetate buffer pH 4.8), which would correspond to about 0.0005% of the total heme in the myoglobin

solutions before CO_2 bubbling. Taking all this into consideration, it appears that destabilization of the heme binding of myoglobin that occurs at pH 4 is most likely the result of the presence of the intermediate form of myoglobin. Moreover, it is expected that this acid denaturation will be reversible, as no heme will be lost from the myoglobin structure [44].

From this study, it can be concluded that if the pH is lower than 4.5 (either from the starting pH or induced by the formation of carbonic acid), the myoglobin undergoes acid denaturation that results in structural changes. In contrast, the gas/water interface has no influence the myoglobin structure.

4.2 Effect of gas bubbling on the formation of myoglobin aggregates

During the bubbling experiments, aggregation of myoglobin was observed from an increase in the sub-visible (micron-size) particle concentration. The results were independent of the bubbling gas and the pH of the starting solution, suggesting that the gas/water interface induces aggregation. The mechanism of protein aggregation can be explained by the unfolding of the protein on the boundary between the gas and water, thereby forming a protein film. Xiao and Konermann [45] observed the unfolding of myoglobin on the surface of N_2 bubbles using hydrogen/deuterium exchange mass spectrometry. During sparging (bubbling), the non-polar residues of amino acids buried in myoglobin were exposed to the gas phase, resulting in an unfolded conformation of myoglobin. Moreover, Wiesbauer et al. [10] showed that after air bubbling, the exposure of the hydrophobic surface of recombinant human growth hormone (rhGH) resulted in precipitation, as detected by staining the insoluble aggregates with the hydrophobic dye ANSA (8-anilino-1-naphthalenesulfonic acid). The aggregates of rhGH also showed an increase in β-sheet structure, as observed by Fourier-transform infrared spectroscopy.

As N_2 does not influence the pH of the solution, the N_2 bubbling tests show the direct effect of the gas/water interface on the formation of aggregates. As shown in the data from flow imaging microscopy (Fig. 6), the concentration of sub-visible particles increased after N_2 bubbling, with a similar particle concentration observed in all myoglobin solutions, independent of the pH. The morphology of the sub-visible aggregates of myoglobin is elongated, similar in appearance to protein fibrils. This could be a result of an increase in intermolecular interactions, which has been observed in the case of rhGH aggregates induced by air bubbling [10].

In a similar manner to N_2, the CO_2 bubbling also induces sub-visible particle formation, but the associated pH shift with CO_2 bubbling appears to influence the morphology of sub-visible myoglobin aggregates. For the myoglobin solutions with an original pH of 4.0-5.3, the particle morphologies and concentration are similar to the results obtained for the N_2-bubbled solutions; fibril-like microparticles are present, which may also be the result of intermolecular interactions in myoglobin induced by the influence of the gas/water interface, as mentioned above. For the myoglobin solutions with a starting pH 6.2-7.0, however, the particles are agglomerated and non-uniform, which is likely to be related to combined effects of a lowering in the pH of the solutions in addition to exposure to the gas/water interface.

In conclusion, bubbling myoglobin solutions with N_2 or CO_2 results in the formation of fibrillar micron-sized aggregates when there is no shift in the pH. However, non-uniform and amorphous aggregates in the micron-size range are produced when the bubbling is combined with a large shift in the pH of the solution.

4.3 CO_2 bubbling and spray drying studies on myoglobin destabilization

During the CO_2 bubbling experiments, changes in the secondary structure and heme binding of myoglobin begin to occur when the resultant pH is decreased to 4.3. In contrast, the CO_2 spray dried myoglobin formulation exhibited changes in the heme binding but not in the secondary structure [23]. Upon reconstitution of the spray dried myoglobin powder, the resultant pH was about 5.0, which would suggest that the pH during CO_2 spray drying most likely reaches a value of 5.0 or lower. However, given that the secondary structure does not change during drying, the conditions required for acid-denaturation apparently had not been met.

From the bubbling experiments, the drop in pH that led to changes in the heme-binding and secondary structure within myoglobin. In the case of the CO_2 spray drying experiments, the size of atomized droplets is much smaller than the bubbles and thus the pH of the droplets is expected to rapidly decrease. At the same time however, the atomized droplets are also undergoing the drying process, which will decrease the mobility of the myoglobin molecule and its ability to unfold. Based on the results from the CO_2 spray drying experiments, it appears that the time for drying is shorter than the time for acidification, thereby minimizing the acid denaturation and thus preserving the secondary structure of myoglobin [46].

With regards to the bubbling experiments, only the solutions with a pH of 4.0 showed an increase in the fluorescence signal, which is thought to be indicative of the presence of an intermediate form of myoglobin rather than the loss of heme [47]. In the case of CO_2 spray drying, however, a greater increase in the fluorescence signal for myoglobin was observed, corresponding to about 10% loss of heme [23]. Moreover, the secondary structure was comparable to the non-processed myoglobin formulations [23]. Although the mechanism by which the heme is lost during CO_2 spray drying is not entirely clear, it is most likely the combination of the lowering of the pH and the solvent properties of supercritical CO_2. During $scCO_2$ spray drying, the liquid-like densities of supercritical CO_2 (750 kg/m^3 at 120 bar and 37°C, in contrast to acetone, which has a density of 791 kg/m^3) may enable it to function in a similar way to the organic solvent in the removal of heme [48]. Moreover, as the greatest exposure of heme to CO_2 occurs at the droplet surface, the partial heme loss from myoglobin is expected to primarily take place at the CO_2/water interface of the myoglobin droplets, where the water is more rapidly acidified. In the case of the bubbling study, however, the CO_2 is present as a gas (density ~2 kg/m^3), and therefore, cannot act as a solvent. Furthermore, no other organic solvent is present to assist with the removal of the heme, which remains embedded in the hydrophobic heme cavity [49, 50].

In addition, it should also be noted that the aggregation of myoglobin upon spray drying is about 5-fold greater than in the CO_2 bubbling experiment, when comparing the total sub-visible particle concentration of the reconstituted myoglobin formulation dried at 130 bar and 25°C [23] to that of the gas bubbled solution (starting pH 6.2) at 25°C. The exposure to CO_2 during spray drying will be substantially greater than in the case of the bubbling experiments, as CO_2 is the continuous phase in the case of CO_2 spray drying, while the myoglobin solution is the continuous phase in the bubbling experiments. Moreover, there will also be differences in the interface area, CO_2 exposure time and regeneration of CO_2 for the atomized myoglobin droplets when compared to the gas bubbles. Aside from myoglobin, other proteins, such as lysozyme, monoclonal antibodies, α-chymotrypsinogen A, and α-lactalbumin, also showed a significant increase in the number of sub-visible particles after the spray drying process [21]. Overall, it can be concluded that the CO_2 spray drying process increases the likelihood that the protein is exposed to the CO_2, leading to unfolding of the protein structure at the droplet surface and consequently aggregation of the protein.

5.   Conclusion

In order to understand the influence of the gas/water interface on the aggregation of myoglobin, a series of gas bubbling tests were conducted for myoglobin solutions over a pH range of 4.0-7.0. For the solutions with a starting pH of 4.0, changes in the secondary structure and heme binding were observed, even in the absence of gas bubbling. From this, it can be concluded that the pH alone plays a role in destabilizing the myoglobin structure. This was confirmed by the nitrogen gas bubbling tests, which does not affect the pH of the solutions, the secondary structure or the heme binding site of myoglobin. However, N_2 bubbling does cause the formation of fibrillar sub-visible myoglobin aggregates over the entire pH range studied. Conversely, CO_2 bubbling causes a shift in pH for the solutions over the starting pH range of 4.5-7. Yet, changes in the myoglobin secondary structure and the heme binding were only found when the CO_2 bubbling shifts the pH of the solution to 4.3, again supporting the conclusion that there is a critical pH below which the myoglobin is destabilized. However, no heme loss was observed during the CO_2 gas bubbling due to the absence of the organic solvent needed for heme extraction. While sub-visible aggregates were observed for all the CO_2 bubbling tests, the combination of the gas/water interface and the pH shift influence the morphology of the aggregates. For the starting solutions in the pH range of 4.0-5.3, the effect of CO_2/water interface on myoglobin aggregation is similar to that of the N_2/water interface, as fibril-like sub-visible aggregates are formed with a similar concentration. For the solutions prepared at pH 6.2-7.0, however, the CO_2/water interface in combination with the CO_2 acidification resulted in the formation of non-uniform myoglobin aggregates. From these results, it can be concluded that the myoglobin aggregation is largely influenced by the gas/water interface, but that the morphology of the aggregates is also dependent on the extent to which the pH shifts.

References

[1]   E.Y. Chi, S. Krishnan, T.W. Randolph, J. F. Carpenter, Physical stability of proteins in aqueous solution: Mechanism and driving forces in nonnative protein aggregation, Pharm Res, 20 (2003) 1325-1336.

[2]   M.E.M. Cromwell, E. Hilario, F. Jacobson, Protein aggregation and bioprocessing, AAPS J, 8 (2006) E572-579.

[3]   C.N. Pace, Conformational stability of globular proteins, Trends Biochem Sci, 15 (1990) 14-7.

[4]   W. Wang, Instability, stabilization, and formulation of liquid protein pharmaceuticals. Int J Pharm, 185 (1999) 129-88.

[5]   J.K. Towns, Moisture content in proteins: its effects and measurement. J Chromatogr A, 705 (1995) 115-27.

[6]   S. Ohtake, Y. Kita, T. Arakawa, Interactions of formulation excipients with proteins in solution and in the dried state. Adv Drug Deliv Rev, 63 (2011) 1053-73.

[7]   A.S. Rosenberg, Effects of protein aggregates: an immunologic perspective, AAPS J, 8 (2006) E501-507.

[8]   J.S. Bee, T.W. Randolph, J.F. Carpenter, S.M. Bishop, M.N. Dimitrova, Effects of surfaces and leachables on the stability of biopharmaceuticals. J Pharm Sci, 100 (2011) 4158-70.

[9]   J.S. Bee, J. L. Stevenson, B. Mehta, J. Svitel, J. Pollastrini, R. Platz, E. Freund, J.F. Carpenter, T.W. Randolph, Response of a concentrated monoclonal antibody formulation to high shear. Biotechnol Bioeng, 103 (2009) 936-43.

[10]   J. Wiesbauer, R. Prassl, B. Nidetzky, Renewal of the air-water interface as a critical system parameter of protein stability: aggregation of the human growth hormone and its prevention by surface-active compounds. Langmuir, 29 (2013) 15240-50.

[11]   S. Rudiuk, L. Cohen-Tannoudji, S. Huille, C. Tribet, Importance of the dynamics of adsorption and of a transient interfacial stress on the formation of aggregates of IgG antibodies, Soft Matter, 8 (2012) 2651-2661.

[12]   D.E. Graham, M.C. Phillips, Proteins at Liquid Interfaces: 1. Kinetics of Adsorption and Surface Denaturation, J Colloid Interface Sci, 70 (1979) 403-414.

[13]   T.L. Donaldson, E.F. Boonstra, J.M. Hammond, Kinetics of Protein Denaturation at Gas-Liquid Interfaces, J Colloid Interface Sci, 74 (1980) 441-450.

[14]   J.R. Clarkson, Z.F. Cui, R.C. Darton, Protein denaturation in foam - I. Mechanism study, J Colloid Interface Sci, 215 (1999) 323-332.

[15]   M. Cornec, D. Cho, G. Narsimhan, Adsorption dynamics of alpha-lactalbumin and beta-lactoglobulin at air-water interfaces, J Colloid Interface Sci, 214 (1999) 129-142.

[16]   J.B. Hedges, S. Vahidi, X. Yue, L. Konermann, Effects of Ammonium Bicarbonate on the Electrospray Mass Spectra of Proteins: Evidence for Bubble-Induced Unfolding, Anal Chem, 85 (2013) 6469-6476.

[17]   A. Prins, K. Vantriet, Proteins and Surface Effects in Fermentation - Foam, Antifoam and Mass-Transfer, Trends Biotechnol, 5 (1987) 296-301.

[18]   P.J. Wilde, Interfaces: their role in foam and emulsion behavior, Curr. Opin. Colloid Interface Sci., 5 (2000) 176-181.

[19]   Z. Yu, K.P. Johnston, R.O. Williams 3rd, Spray freezing into liquid versus spray-freeze drying: influence of atomization on protein aggregation and biological activity, Eur J Pharm Sci, 27 (2006) 9-18.

[20]   S.D. Webb, S.L. Golledge, J.L. Cleland, J.F. Carpenter, T.W. Randolph, Surface adsorption of recombinant human interferon-gamma in lyophilized and spray-lyophilized formulations, J Pharm Sci, 91 (2002) 1474-87.

[21]   O. Nuchuchua, H.A. Every, G.W. Hofland, W. Jiskoot, Scalable organic solvent free supercritical fluid spray drying process for producing dry protein formulations. Eur J Pharm Biopharm, 88 (2014) 919-930.

[22]   N. Jovanović, A. Bouchard, G. W. Hofland, G. Witkamp, D. J. A. Crommelin, W. Jiskoot, Distinct effects of sucrose and trehalose on protein stability during supercritical fluid drying and freeze-drying, Eur J Pharm Sci, 27 (2006) 336-345.

[23]   O. Nuchuchua, H.A. Every, G.W. Hofland, W. Jiskoot, Critical processing parameters of carbon dioxide spray drying for the production of dried protein formulations: A study with myoglobin, Eur J Pharm Biopharm, 103 (2016) 200-9.

[24]   S.C. Harrison, E.R. Blout, Reversible Conformational Changes of Myoglobin and Apomyoglobin, J Biol Chem, 240 (1965) 299-303.

[25]   J.D. Morrisett, J.S.K. David, H.J. Pownall, A.M. Gotto Jr, Interaction of an apolipoprotein (apoLP-alanine) with phosphatidylcholine. Biochemistry, 12 (1973) 1290-9.

[26]   H. Ishikawa, M. Shimoda, A. Yonekura, K. Mishima, K. Matsumoto, Y. Osajima, Irreversible unfolding of myoglobin in an aqueous solution by supercritical carbon dioxide, J Agric Food Chem, 48 (2000) 4535-9.

[27]   S. Zölls, D. Weinbuch, M. Wiggenhorn, G. Winter, W. Friess, W. Jiskoot, A. Hawe, Flow imaging microscopy for protein particle analysis--a comparative evaluation of four different analytical instruments, AAPS J, 15 (2013) 1200-11.

[28]   D.K. Sharma, D. King, P. Oma, C. Merchant, Micro-flow imaging: flow microscopy applied to sub-visible particulate analysis in protein formulations, AAPS J, 12 (2010) 455-64.

[29]   G.W. Hofland, M. van Es, L.A.M. van der Wielen, G. Witkamp, Isoelectric precipitation of casein using high-pressure CO_2. Industrial & Engineering Chemistry Research, 38 (1999) 4919-4927.

[30]   M. Momenteau, M. RougÉE, B. Loock, Five-Coordinate Iron-Porphyrin as a Model for the Active Site of Hemoproteins Characterization and Coordinating Properties, Eur J Biochem, 71 (1976) 63-76.

[31]   M.C. Hsu, R.W. Woody, The origin of the heme Cotton effects in myoglobin and hemoglobin, J Am Chem Soc, 93 (1971) 3515-25.

[32]   M. Nagai, Y. Nagai, K. Imai, S. Neya, Circular dichroism of hemoglobin and myoglobin, Chirality, 26 (2014) 438-42.

[33]   G. Irace, E. Bismuto, F. Savy, G. Colonna, Unfolding pathway of myoglobin: molecular properties of intermediate forms, Arch Biochem Biophys, 244 (1986) 459-69.

[34]   Y. Wang, D. Shortle, The equilibrium folding pathway of staphylococcal nuclease: identification of the most stable chain-chain interactions by NMR and CD spectroscopy, Biochemistry, 34 (1995) 15895-905.

[35]   I. Nishii, M. Kataoka, F. Tokunaga, Y. Goto, Cold denaturation of the molten globule states of apomyoglobin and a profile for protein folding, Biochemistry, 33 (1994) 4903-9.

[36]   K. Matsuo, Y. Sakurada, R. Yonehara, M. Kataoka, K. Gekko, Secondary-structure analysis of denatured proteins by vacuum-ultraviolet circular dichroism spectroscopy, Biophys J, 92 (2007) 4088-96.

[37]   Z. Gryczynski, J. Lubkowski, E. Bucci, Heme-protein interactions in horse heart myoglobin at neutral pH and exposed to acid investigated by time-resolved fluorescence in the pico- to nanosecond time range, J Biol Chem, 270 (1995) 19232-7.

[38]   M.S. Hargrove, D. Barrick, J.S. Olson, The association rate constant for heme binding to globin is independent of protein structure, Biochemistry, 35 (1996) 11293-9.

[39]   A.N. Schechter, C.J. Epstein, Spectral studies on the denaturation of myoglobin, J Mol Biol, 35 (1968) 567-89.

[40]   M.P. Richards, Redox reactions of myoglobin, Antioxid Redox Signal, 18 (2013) 2342-51.

[41]   E. Breslow, F.R. Gurd, Reactivity of sperm whale metmyoglobin towards hydrogen ions and p-nitrophenyl acetate, J Biol Chem, 237 (1962) 371-81.

[42]   F.W. Teale, Cleavage of the haem-protein link by acid methylethylketone, Biochim Biophys Acta, 35 (1959) 543.

[43]   R. Stiebler, A.N. Hoang, T.J. Egan, D.W. Wright, M.F. Oliveira, Increase on the initial soluble heme levels in acidic conditions is an important mechanism for spontaneous heme crystallization in vitro, PLoS One, 5 (2010) e12694.

[44]   J.T. Kindt, A. Woods, B.M. Martin, R.J. Cotter, Y. Osawa, Covalent alteration of the prosthetic heme of human hemoglobin by BrCCl3. Cross-linking of heme to cysteine residue 93, J Biol Chem, 267 (1992) 8739-43.

[45]   Y.M. Xiao, L. Konermann, Protein structural dynamics at the gas/water interface examined by hydrogen exchange mass spectrometry, Protein Sci, 24 (2015) 1247-1256.

[46]   M.C. Manning, K. Patel, R.T. Borchardt, Stability of protein pharmaceuticals, Pharm Res, 6 (1989) 903-18.

[47]   J.A. Hyatt, Liquid and Supercritical Carbon-Dioxide as Organic-Solvents, J Org Chem, 49 (1984) 5097-5101.

[48]   E. Bismuto, G. Colonna, G. Irace, Unfolding pathway of myoglobin. Evidence for a multistate process, Biochemistry, 22 (1983) 4165-70.

[49]   J.T. Sage, D. Morikis, P.M. Champion, Spectroscopic studies of myoglobin at low pH: heme structure and ligation. Biochemistry, 30 (1991) 1227-37.

CHAPTER 6

Formulation optimization in supercritical CO$_2$ spray drying for production of dry protein formulations: a case study with myoglobin

O Nuchuchua[1], H A Every[2], W Jiskoot[1]

[1] Division of Drug Delivery Technology, Cluster BioTherapeutics, Leiden Academic Centre for Drug Research (LACDR), Leiden University, The Netherlands

[2] FeyeCon Development & Implementation B.V., Weesp, The Netherlands

Abstract

It was observed previously that supercritical CO_2 ($scCO_2$) spray drying causes the destabilization of myoglobin resulting in heme loss and myoglobin aggregation. This destabilization was found to be induced by a drop in pH during the spray drying process, from which it was concluded that the excipients were ineffective in this formulation (1:10 weight ratio of myoglobin to trehalose in 10 mM phosphate buffer pH 6.2). Therefore, the aim of this study was to investigate the effect of formulation excipients (i.e., trehalose, buffers, polysorbate 80) on their ability to maintain myoglobin integrity during $scCO_2$ spray drying. Myoglobin formulations were prepared at a starting pH of 6.2. The myoglobin integrity was evaluated after reconstitution of the dried formulations. It was found that while trehalose was unable to control the pH of myoglobin formulations, it did result in a significant decrease of heme loss. By using of 50-150 mM phosphate buffer, 10 mM citrate, or 25 mM histidine in the myoglobin/trehalose formulations, the pH was maintained at 6.2 during $scCO_2$ spray drying, resulting in a full retention of the heme in myoglobin, as observed by UV/Vis, circular dichroism and fluorescence spectroscopy. Myoglobin aggregation, in terms of monomer loss and sub-visible particle formation, decreased when the pH of myoglobin/trehalose formulations was stable, except in the case of citrate buffer. The addition of a surfactant, polysorbate 80, did not help to minimize the myoglobin aggregation. Interestingly, the formulation without any buffer or surfactant but with a high concentration of myoglobin was self-buffering, which led to the stabilization of heme binding and a significant reduction in myoglobin aggregation. From this study, it can be concluded that a carefully selected formulation excipients help to maintain the protein integrity during $scCO_2$ spray drying.

1. Introduction

Supercritical carbon dioxide ($scCO_2$) can be used as an atomizing gas and drying medium in a spray drying process to prepare dried protein formulations. $ScCO_2$ spray drying methods have previously been used to prepare several dried protein formulations with lysozyme, a-lactalbumin, a-chymotrypsinogen A, myoglobin, monoclonal and polyclonal immunoglobulin [1-4]. However, for a myoglobin formulation consisting of 5 mg myoglobin and 50 mg trehalose in 10 mM phosphate buffer at pH 6.2, heme loss and myoglobin aggregation were found after CO_2 spray drying [5]. Further evaluation of the product showed that the pressurized CO_2 caused significant acidification of the myoglobin formulation, with the pH decreasing from 6.2 to about 5.0. Subsequently, the acidification led to a partial removal of the heme during spray drying, as was evident from analyzing the reconstituted dried myoglobin formulations in water. Based on these results, it appears that the myoglobin formulation is lacking sufficient buffering capacity of the phosphate buffer to maintain the pH during spraying.

In a previous study, $scCO_2$ spray-dried IgG formulations (originally consisting of 10 mM phosphate or citrate pH 5 and 6.2) that were treated with N_2 gas maintained the original pH of the protein formulations upon reconstitution [2, 6]. However, aggregation of IgG was still observed, as detected by a decrease in the monomer content and an increase in the amount of dimers and oligomers [2]. This implies that while treating the powdered product with N_2 gas helps to eliminate any residual CO_2 (and correspondingly acidity upon reconstitution), it cannot reverse the detrimental effect of pH on protein integrity that occurs during the spray drying process. Ideally, a protein formulation should contain a proper buffering agent to resist any changes in the pH of formulations during processing, which may not only cause physical degradation, such as unfolding and aggregation, but also chemical degradation, such as deamination, oxidation and proteolysis [7-10]. Therefore, the first aim of this study is to evaluate the effect of different buffer agents on their ability to stabilize myoglobin during $scCO_2$ spray drying.

It has also been shown that the use of sugars, such as trehalose and sucrose, help to preserve the a-helix structure in lysozyme after reconstitution, as compared to the sugar-free formulation [3]. For myoglobin, a previous study showed markedly changes in the heme binding of the $scCO_2$-dried myoglobin formulation when the myoglobin was formulated with trehalose, as compared to the trehalose-free myoglobin formulation [1]. Thus sugars appear to have a stabilizing effect on the protein during $scCO_2$ spray drying. The second aim of this

study is to evaluate further the role of trehalose in stabilizing myoglobin during $scCO_2$ spray drying.

In a spray drying process, the atomization creates gas/water interfaces, leading to protein inactivation and/or aggregation [11, 12]. Nonionic surfactants (e.g., polysorbate 20, polysorbate 80) are generally used as biopharmaceutical excipients, in order to decrease the absorption of proteins at this gas/water interface [13, 14]. In case of a hot air spray-dried lactate dehydrogenase (LDH) formulation, the loss of LDH activity, unfolding and aggregation that occurred during atomization was decreased when 0.05%wt polysorbate 80 was present in the formulation [15]. Furthermore, the surface of dried LDH particles prepared with 0.1%wt polysorbate 80 was smoother than the formulation without the surfactant, due to a decrease in the surface tension of the LDH formulation [15]. A similar result was also observed when polysorbate 20 was added to a recombinant human growth hormone formulation [16]. From a previous study of CO_2 gas bubbling in myoglobin solutions, it has become clear that the CO_2/water interface influences both the morphology and concentration of sub-visible myoglobin aggregates (see Chapter 5). Similar results were seen after $scCO_2$ spray drying, from which it was concluded that the CO_2/water interface leads to myoglobin aggregation. In order to decrease the surface-induced protein aggregation during $scCO_2$ spray drying, a surfactant can be added to act as a barrier at the CO_2/water interface. Thus, the third aim of this study is to evaluate the influence of a surfactant, polysorbate 80, on reducing protein aggregation during $scCO_2$ spray drying.

In all cases, the dried myoglobin formulations were freshly prepared and reconstituted in water on the production day. The myoglobin structure and aggregation were examined by UV-Vis, fluorescence and circular dichroism spectroscopy, as well as size-exclusion chromatography and flow-imaging microscopy.

2. Materials and methods

2.1 Materials

All chemicals, salt-free myoglobin from equine skeletal muscle, trehalose dihydrate, sodium phosphate monobasic dihydrate, sodium phosphate dibasic dihydrate, citric acid monohydrate, tris base (Trizma base®), histidine and polysorbate 80, were purchased from Sigma-Aldrich, St. Louis, USA.

2.2 Preparation of liquid myoglobin formulations

Liquid formulations for the $scCO_2$ spray drying experiments were prepared at pH 6.2 and 8.2, as shown in Table 1 and 2. To study the buffering capacity of buffers in the $scCO_2$ spray drying system, 55 mg/ml trehalose solutions were prepared in water, 10-150 mM phosphate buffer, 10 mM citrate buffer, 25 mM histidine buffer or 10-150 mM Tris buffer (formulations T1-T12). Furthermore, in order to study effects of trehalose and buffer salts on myoglobin integrity, 5 mg/ml myoglobin with and without 50 mg/ml trehalose were prepared in pure water, 10-150 mM phosphate, 10 mM citrate and 25 mM histidine (shown as formulations M1-M2, and MT1-MT6). Solutions consisting of 5 and 20 mg/ml myoglobin with a 1:10 (w/w) myoglobin:trehalose ratio in water (formulations MT1 and MT10), were used to observe the self-buffering and self-stabilizing properties of myoglobin. Finally, the effect of the surfactant on myoglobin aggregation was studied by adding 0.002% - 0.050% w/v polysorbate 80 in 25 mM histidine pH 6.2 (formulations MT7-MT9).

In all cases, the pH of the formulations slightly increased when myoglobin was dissolved in water with a starting pH 6.2. To adjust the pH of the myoglobin formulations, the solutions were titrated with 0.2 M HCl to determine the amount of acid needed to achieve the working pH. Later, new myoglobin formulations were prepared by adding the required amount of the acid solution into the aqueous solutions prior to dissolving the myoglobin. As myoglobin did not completely dissolve, the liquid formulations were filtered through a 0.22-μm pore cellulose acetate filter (Millex®-GV, Cork, Ireland) before starting the spray drying experiments. After filtration, the myoglobin concentrations were reduced to about 70% of the starting concentration in the non-filtrated formulations.

Table 1 pH of CO_2 spray dried formulations of trehalose (55 mg/ml) after reconstituting in water.

Formulation	Solution composition and pH	pH after reconstitution
T1	**Water, pH 6.2**	3.96 ± 0.23
	Phosphate buffer, pH 6.2	
T2	10 mM	3.65 ± 0.30
T3	50 mM	5.69 ± 0.03
T4	75 mM	6.09 ± 0.04
T5	100 mM	6.10 ± 0.04
T6	150 mM	6.24 ± 0.05
	Phosphate buffer, pH 8.2	
T7	10 mM	6.50 ± 0.01
T8	150 mM	6.97 ± 0.01
	Citrate buffer, pH 6.2	
T9	10 mM	5.99 ± 0.01
	Histidine, pH 6.2	
T10	25 mM	5.92 ± 0.04
	Tris base, pH 8.2	
T11	10 mM	6.38 ± 0.02
T12	150 mM	7.25 ± 0.02

Table 2 Analysis of reconstituted myoglobin formulations (with and without trehalose) in terms of reconstituting pH, % recovery of A_{409}/A_{280}, % recovery of α-helix fraction (f_H), % protein recovery and % loss of myoglobin monomer.

Formulation	Formulation composition, pH	pH after reconstitution[a]	% A_{409}/A_{280} recovery[b]	% recovery of α-helix fraction (f_H)[c]	% protein recovery[e]	% loss of myoglobin monomer[f]
5 mg/ml myoglobin, pH 6.2						
M1	Water pH 6.2	4.35 ± 0.12	66.8 ± 2.2	100.4 ± 3.2	93.7 ± 4.7	13.3 ± 0.2
M2	10 mM phosphate buffer pH 6.2	3.51 ± 0.13	62.3 ± 0.3	111.0 ± 1.1	71.0 ± 5.6	42.6 ± 1.9
5 mg/ml myoglobin with 50 mg/ml trehalose, pH 6.2						
MT1	Water	4.20 ± 0.34	91.8 ± 3.0	97.6 ± 0.6	104.9 ± 3.0	-0.4 ± 1.8
MT2	10 mM phosphate buffer*	5.12 ± 0.06	89.9 ± 3.3	102.1 ± 2.4	79.5 ± 1.6	24.7 ± 2.8
MT3	50 mM phosphate buffer	6.28 ± 0.06	101.4 ± 0.9	110.0 ± 2.6	85.7 ± 5.3	9.9 ± 2.2
MT4	150 mM phosphate buffer	6.35 ± 0.02	99.8 ± 0.2	97.7 ± 0.9	100.2 ± 4.0	-0.6 ± 1.0
MT5	10 mM citrate buffer	6.26 ± 0.05	97.3 ± 0.8	102.0 ± 1.6	84.5 ± 1.0	17.4 ± 0.3
MT6	25 mM histidine	6.08 ± 0.06	100.4 ± 2.1	n/a	93.7 ± 1.6	10.0 ± 4.6
MT7	25 mM histidine + 0.002% w/w polysorbate 80	5.99 ± 0.06	99.9 ± 0.6	n/a	95.2 ± 1.0	2.4 ± 1.5
MT8	25 mM histidine + 0.005% w/w polysorbate 80	5.98 ± 0.01	100.3 ± 0.4	n/a	95.2 ± 3.2	8.4 ± 0.4
MT9	25 mM histidine + 0.05% w/w polysorbate 80	5.99 ± 0.00	100.2 ± 0.7	n/a	95.9 ± 0.2	6.6 ± 0.1

20 mg/ml myoglobin with 200 mg/ml trehalose, pH 6.2

MT10	Water	5.06 ± 0.01	101.5 ± 0.5	98.3 ± 1.9	104.4 ± 6.2	-7.45 ± 0.42

[a] Powdered products were reconstituted in water (see methods).

[b] Data were obtained from the ratio of the absorbances at 409 nm (A_{409}) and 280 nm (A_{280}) by UV/Vis spectroscopy (see methods).

[c] Data were obtained from the molar ellipticity at 222 nm (see methods).

[d] Data were obtained from the molar ellipticity at 409 nm (see methods).

[e] Data were obtained from the absorbance at 280 nm by UV/Vis spectroscopy (see methods).

[f] Data were obtained from size-exclusion chromatography with UV detection (see methods).

*See the reference [5] or the chapter 4.

n/a = not applicable

2.3 Spray drying conditions

For all formulations, the $scCO_2$ spray drying was operated at 130 bar and 37°C in a 4-litre spray drying module (F54250S model from Separex, Champigneulles, France). The drying vessel was filled with the pressurized CO_2 and brought to the desired temperature and pressure before feeding in the liquid myoglobin formulation via a high-pressure syringe pump maintained at 25 °C (TELEDYNE ISCO, Lincoln, USA). The protein solution was atomized by pressurized CO_2 stream through a coaxial converging nozzle (Spraying Systems Co. B.V., Ridderkerk, The Netherlands). The diameter of the nozzle orifices were 0.16 cm and 0.04 cm for the CO_2 and the liquid, respectively. The protein solution (about 8 ml) and CO_2 flow rates were kept constant at 0.2 ml/min and 500 g/min, respectively. The spraying time was 40 minutes, followed by 30 minutes post-drying with fresh CO_2, to remove any residual moisture from the vessel and consequently the product [4]. After depressurization, the dried myoglobin formulations were collected from a paper filter (Whatman® qualitative filter paper, Grade 1, 25 mm diameter, Diegem, Belgium). Each experimental condition was tested at least twice.

2.4 Protein analysis

2.4.1 Sample preparation for myoglobin analysis

To achieve a desired protein and trehalose concentration of 53.5 mg/ml and 55 mg/ml of the dried myoglobin/trehalose formulations and the dried trehalose formulations were reconstituted in 1 ml of water by taking into account the solid content of myoglobin after filtration, trehalose and buffer salts along with the residual water content [3]. The powdered products were dissolved overnight at room temperature to complete the dissolution. The reconstituted solutions were subsequently diluted with their original aqueous-based medium without myoglobin (see Table 1 and Table 2). However, the dilution of the samples MT7 to MT9 (histidine with polysorbate 80) was carried out in 25 mM histidine without the surfactant. The diluted samples were filtered through a 0.22-µm pore cellulose acetate filter (Millex®-GV, Cork, Ireland) before protein structural analysis by UV/Vis, circular dichroism and fluorescence spectroscopy. The sample concentrations for each analysis are mentioned below.

2.4.2 Protein and bound heme recovery

The protein solutions were diluted to approximately 0.1 mg/ml prior to measurement. The protein content was determined by using a UV spectrophotometer (Agilent 8453, Agilent Technologies, Santa Clara, USA). The spectra were collected from 190 nm to 1000 nm. The myoglobin concentration was calculated using a molar extinction coefficient of 3.45×10^4 $M^{-1}cm^{-1}$ at 280 nm [16]. The absorbance ratio between 409 and 280 nm (A_{409}/A_{280}) from each spectrum represents the retention of the heme group bound to the proximal histidine in the heme pocket of myoglobin [17]. The percentages of protein content recovery of the treated myoglobin were compared to those of each untreated liquid myoglobin formulation at 25°C (see Eq. 2).

$$Protein\ recovery(\%) = \left[\frac{A_{280}\ (processed)}{A_{280}\ (nonprocessed)}\right] \times 100 \qquad (Eq.\ 2)$$

2.4.3 Circular dichroism spectroscopy

In order to study the structure of myoglobin, far-UV (190-250 nm) and near-UV/Vis (350-450 nm) CD spectroscopy measurements (J-810 Spectropolarimeter, JASCO Inc., Easton, USA) were performed at 25 °C. The parameters were set at a sensitivity of 100 mdeg, with a data pitch of 10 nm, a bandwidth of 2 nm, and a scanning speed of 100 nm/min. Samples were freshly prepared with a myoglobin concentration of 0.1 mg/ml and placed in a 0.1-cm and 1-cm quartz cuvette for far-UV CD and near-UV/Vis CD measurements, respectively. CD spectra of six sequential measurements were averaged and corrected for the blank. The CD signals were converted to molar ellipticity per amino acid residue ($[\theta]$, deg cm^2 $dmol^{-1}$). The fraction of α-helix (f_H) was estimated by using Eq. 3 [17], where $[\theta]_{222}$ is the molar ellipticity per amino acid residue at 222 nm. The signals of the samples were compared to that of untreated solution and shown as % recovery at the α-helix fraction at 222 nm.

$$f_H = ([\theta]_{222} - 3{,}000)/(-36{,}000 - 3{,}000) \qquad (Eq.\ 3)$$

2.4.4 High performance size-exclusion chromatography (HP-SEC)

Samples of 50 µl of 1 mg/ml protein concentration were analyzed by HP-SEC with a Discovery® BIO Gel Filtration column (300 Å pore size)

(Sigma-Aldrich, St. Louis, USA). The mobile phase consisted of 150 mM phosphate buffer, pH 7.0, and was filtered through a 0.2-µm filter prior to use. The flow rate was set at 0.7 ml/min. The chromatograms were recorded by a UV detector (Agilent 1100 VWD, Santa Clara, USA) and a fluorescence detector (Agilent 1200 FLD, Santa Clara, USA). The absorbance of each spectrum at a wavelength of 280 nm was used to calculate the percentages of myoglobin monomer, aggregates, and fragments relative to that of the untreated samples. The fluorescence emission intensity was collected at 350 nm with the excitation at 295 nm. For each chromatogram, the total peak area of the fluorescence signal intensity was compared to the absorbance at 280 nm, and shown as I_{350}/A_{280}. Apomyoglobin, which lacks the heme group, was used as a control [5].

2.4.5 Flow imaging microscopy

The presence of sub-visible microparticles was determined by flow imaging microscopy using an MFI5200 instrument (Protein Simple, California, USA). The measurements were controlled and the data analyzed by MVAS software version 1.3. Prior to analysis, the formulations were diluted to a myoglobin concentration of 1 mg/ml (no filtration). One milliliter of solution was introduced at a flow rate of 6 ml/min into a flow cell with the dimensions of 100 and 1016 µm in depth and diameter, respectively, illuminated by a blue LED. Images of the particles were captured by an optical camera. Pictures were obtained with a resolution of 1280x1024 pixels. Total particle concentrations are reported for particle sizes larger than 1 µm.

3. Results

3.1 Formulations

In order to evaluate the effect of the formulations on the ability to stabilize myoglobin during $scCO_2$ spray drying, three different systems have been studied; trehalose only formulations (T1-T12), myoglobin only formulations (M1-M2) and myoglobin/trehalose formulations (MT1-MT10), as shown in Table 1 and 2. The role of excipients in maintaining the pH during spraying (which is thought to contribute to protein stabilization) was investigated by first studying the formulations in water only (T1, M1, MT1), and then by adding buffer (10-150 mM phosphate buffer, 10 mM citrate buffer or 25 mM histidine buffer) at pH 6.2. For the trehalose only formulations, tests were also conducted using 10-150 mM phosphate and Tris buffer at pH 8.2. In the case of the histidine buffer, the surfactant,

polysorbate 80, was added in different concentrations (0.002-0.050%) to evaluate whether changing the surface tension influences the protein stability during spray drying. Finally, the self-buffering capacity of myoglobin was studied as a function of concentration (MT1 compared to MT10).

3.2 pH upon reconstitution

During $scCO_2$ spray drying, the pH of the myoglobin solutions decreased due to the reaction between CO_2 and water in the droplets to form carbonic acid. Dried myoglobin formulations (starting pH 6.2) gave a final pH of about 5.0 after reconstituting in water [5]. An investigation into the effect of buffer agents (e.g. buffer salts and self-buffering protein) on the ability to control the pH of myoglobin formulations in the $scCO_2$ spray drying system was carried out for the above-mentioned formulations.

For the trehalose only formulations (Table 1), the trehalose alone cannot control the pH during spraying. The reconstitution of dried trehalose gave a pH of about 4.0 instead of pH 6.2 (see formulation T1). For the formulations containing phosphate buffer, a lack of buffer control of the pH was seen in cases of 10 and 50 mM phosphate buffer at pH 6.2 (T2 and T3). However, increasing the concentration of phosphate buffer up to 150 mM at pH 6.2 resulted in the gradual stabilization of the pH, as shown in the formulations T2-T6. In contrast, phosphate buffer at pH 8.2 over the concentration range 10-150 mM (formulations T7 and T8) did not show sufficient buffering capacity to maintain the original pH after $scCO_2$ spray drying. Therefore, phosphate buffer at pH 6.2 was used to prepare myoglobin/trehalose formulations, while the phosphate buffer at pH 8.2 was excluded in the further study.

In order to investigate whether other buffers allow for better pH control, particularly at low buffer concentrations, tests were also performed using citrate, histidine, and Tris base, as these buffers have pKa values close to the starting pH values of 6.2 [18] and 8.2 (T9-T12). As shown in Table 1, both citrate and histidine were able to control the pH of the formulations to values near pH 6.0. However, the Tris base did not maintain the original pH 8.2 over the concentration range studied. In actual fact, this study showed that neither phosphate buffer nor Tris could maintain the pH of the formulations at 8.2 during the $scCO_2$ drying process. Consequently, only the buffers with pH 6.2 were used for further investigation.

For myoglobin formulations without trehalose at a starting pH 6.2 (M1-M2), myoglobin alone lacked sufficient buffering capacity, as the pH of the formulations was about 3.5-4.4 after reconstitution. However, for the myoglobin/trehalose formulations (MT2-MT9), the addition of 50-150 mM phosphate buffer resulted in a stable pH at 6.2 after scCO$_2$ spray drying. Moreover, 10 mM citrate (MT5) was also able to maintain the pH around 6.2 while 25 mM histidine (MT6) showed a slight decrease in pH for the reconstituted formulation. However, adding a surfactant (0.002-0.050% polysorbate 80) did not influence the buffering capacity of 25 mM histidine. For the formulations prepared at a high concentration (20 mg/ml, MT10), myoglobin exhibited self-buffering capacity as shown by a higher reconstituting pH (pH 5.0), in contrast to the reconstituted formulation with only 5 mg/ml myoglobin (pH 4.2). All results are summarized in Table 2.

3.3 UV/Vis spectra of myoglobin

When analyzing the UV/Vis spectra of myoglobin, a decrease in the ratio of A_{409}/A_{280} reflects changes in the heme-binding [5, 19]. As seen in Table 2, myoglobin alone prepared in water and 10 mM phosphate buffer (formulations M1 and M2) showed a significant decrease in the A_{409}/A_{280} ratio. Upon adding trehalose, a higher A_{409}/A_{280} ratio was observed for both the formulations in water and 10 mM phosphate buffer (formulations MT1 and MT2). In contrast, the A_{409}/A_{280} ratio was fully preserved when myoglobin was formulated with high concentrations of phosphate buffer, citrate and histidine with and without polysorbate 80. Similarly, the ratio was also maintained at 100% when myoglobin was prepared in water with a concentration of 20 mg/ml.

3.4 Circular dichroism (CD)

Far-UV CD spectroscopy, which was used to monitor the secondary structure of myoglobin, showed similar spectra when comparing the untreated and dried myoglobin formulations (data not shown). The results are presented as %recovery of the estimated myoglobin α-helix fraction at 222 nm, with values close to 100% for all formulations (Table 1). For the formulations containing 25 mM histidine (with and without a surfactant), an interference in the far-UV CD signal was observed due to the chirality of histidine [20, 21].

From the CD spectra, changes in the heme binding are observed as a shift and/or decrease in the molar ellipticity at the Soret band (409 nm) [22, 23]. For the myoglobin formulations without trehalose (Fig. 1a), a significant decrease in the molar ellipticity at 409 nm was observed after spray drying when compared to the untreated solutions. However, the addition of trehalose helped to stabilize the heme in the spray dried myoglobin formulations (Fig. 1b), as shown by an increase in the molar ellipticity at 409 nm relative to both the trehalose-free formulations.

A comparison of the Soret band for the different buffers and buffer concentrations is shown in Fig 2. For the 5 mg/ml myoglobin/trehalose solutions prepared in water (MT1) and 10 mM phosphate buffer (MT2), the results show that there is a slight decrease in the signals after spray drying. For the other formulations with the various buffers and 20 mg/ml myoglobin, the signals are relatively stable compared to the untreated formulations (Fig. 2). However, adding the surfactant to the formulations (MT7-MT9) resulted in a slight decrease in the molar ellipticity after spray drying (Fig. 3).
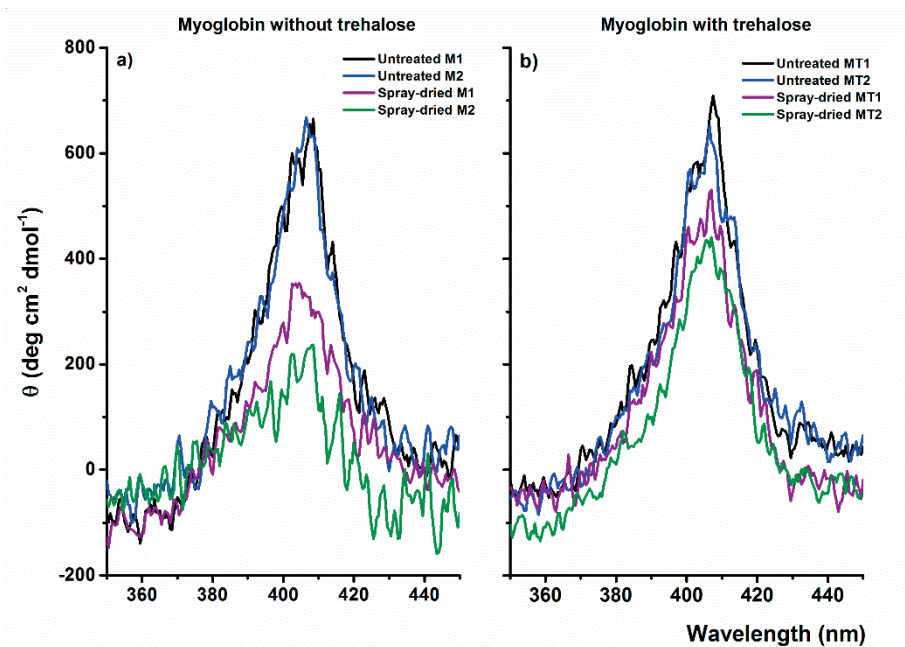
Fig. 1   Near/Vis-CD spectra at the Soret band (409 nm) of myoglobin without trehalose (a) and with trehalose (b). Spray-dried myoglobin formulations were conducted at 130 bar and 37 °C. M1 = myoglobin in water, M2 = myoglobin in 10 mM phosphate buffer, MT1 = myoglobin/trehalose in water and MT2 = myoglobin/trehalose in 10 mM phosphate buffer. All untreated solutions were freshly prepared at pH 6.2. For formulation compositions, see Table 2.
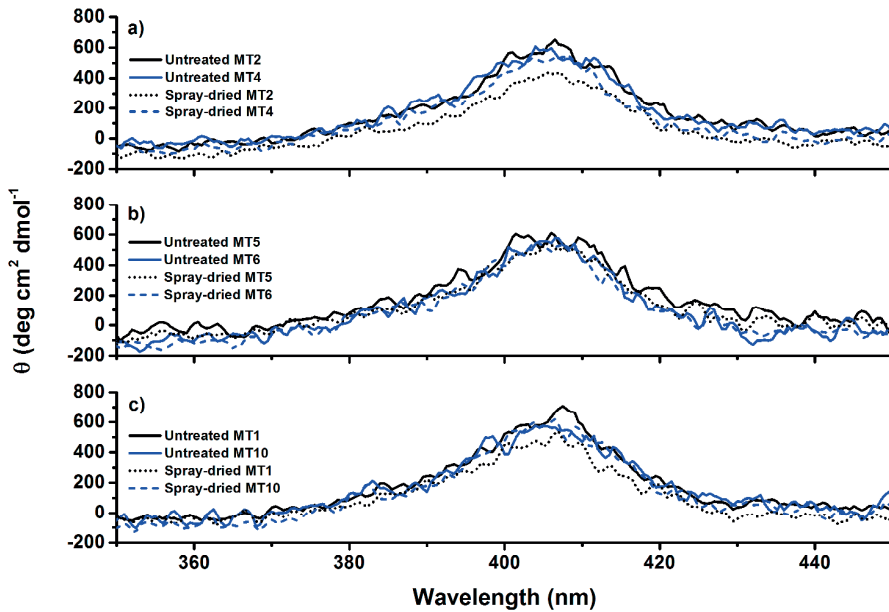
Fig. 2 Near/Vis-CD spectra at the Soret band (409 nm) of untreated myoglobin with trehalose and scCO$_2$ spray-dried myoglobin with trehalose, prepared in (a) phosphate buffer, (b) citrate and histidine, and (c) buffer-free solution. Spray-dried myoglobin formulations were conducted at 130 bar and 37 °C. MT2 and MT4 = myoglobin/trehalose in 10 and 150 mM phosphate buffer, MT5 = myoglobin/trehalose in 10 mM citrate, MT6 = myoglobin/trehalose in 25 mM histidine, MT1 and MT10 = 5 and 20 mg/ml myoglobin with 50 and 200 mg/ml, respectively, of trehalose in water. All untreated solutions were freshly prepared at pH 6.2. For formulation compositions, see Table 2.
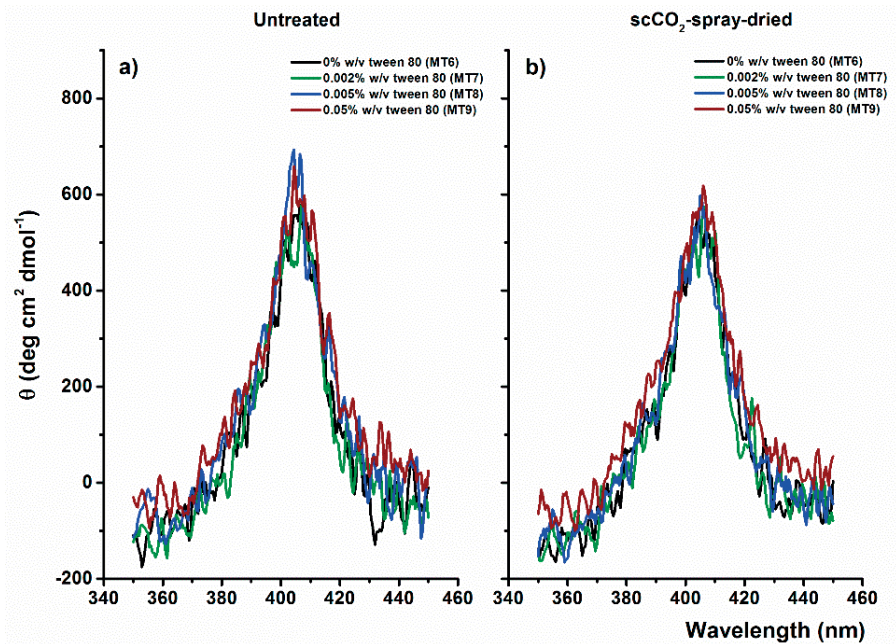
Fig. 3 Near/Vis-CD spectra at the Soret band (409 nm) of untreated formulations (a) and scCO₂ spray-dried myoglobin/trehalose formulations (b). Spray-dried myoglobin formulations (MT6-MT9 in 25 mM histidine, pH 6.2) contained 0-0.05% polysorbate 80 were prepared at 130 bar and 37 °C. For formulation compositions, see Table 2.

3.5 Intrinsic tryptophan fluorescence emission intensity

The tryptophan fluorescence signal is highly quenched when heme is bound in the heme pocket [24, 25], and consequently, native myoglobin gives a low fluorescence signal. In the absence of any change in the myoglobin secondary structure, an increase in the fluorescence emission intensity is most likely due to the loss of heme to form apomyoglobin [5]. The fluorescence data, presented as the ratio of the fluorescence emission signal at 350 nm to protein absorption at 280 nm (I_{350}/A_{280}), is shown in Fig. 4. For the myoglobin-only formulations in water and 10 mM phosphate buffer pH 6.2 (formulations M1 and M2), a significant increase in the fluorescence signal was observed after spray drying. Adding trehalose results in a reduction in fluorescence signal, but the I_{350}/A_{280} ratios were still slightly higher than those of the untreated formulations (formulations MT1 and MT2). All other formulations showed no change in the heme binding as the I_{350}/A_{280} ratio was low in all cases. However, it seemed that the structure of myoglobin was even more

quenched by heme in the presence of histidine, as a decrease in the fluorescence signals were observed in formulations MT6-MT9.
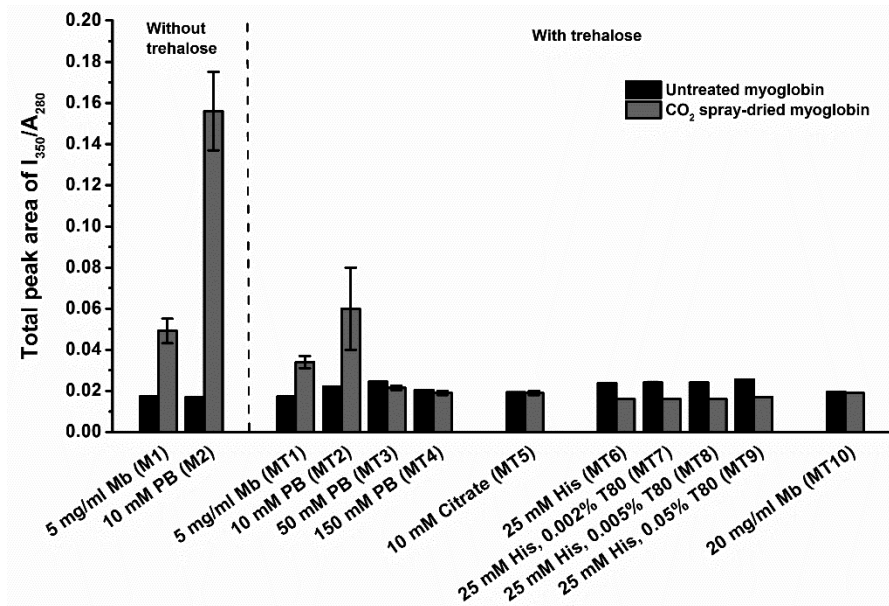

Fig. 4 The relative total peak area of the fluorescence emission signal at 350 nm to protein absorption at 280 nm (I_{350}/A_{280}) for reconstituted spray dried myoglobin formulations with half an hour post drying produced at 130 bar and 37 °C. Formulations M1-M2 are 5 mg/ml myoglobin in water and 10 mM phosphate pH 6.2. Formulations MT1-MT9 are 5 mg/ml myoglobin with 50 mg/ml trehalose. Formulation MT10 is 20 mg/ml myoglobin with 200 mg/ml trehalose.

3.6 Myoglobin aggregation

In a previous study [5], the untreated myoglobin solutions showed 1% of dimer and 99% of monomer according to HP-SEC. After scCO$_2$ spray drying, the dimer (2.5-7.5%) and small fragments (0.5-2.0%) were present in the reconstituted solution of spray-dried myoglobin formulations. However, in this present study, neither dimers/oligomers nor small fragments of myoglobin in any formulation before and after spray drying were detected by HP-SEC (data not shown). Yet, a loss in the monomer content was still observed (Table 1), which may be correlated with the formation of insoluble aggregates (removed by filtration). Myoglobin without trehalose in 10 mM phosphate buffer pH 6.2 (formulation M2) showed the highest loss in monomer content, while the formulation with trehalose (formulation MT2) helped to reduce the

monomer loss. Myoglobin aggregation still occurred when citrate and histidine buffers were used. However, a reduction in the extent of aggregation was found when the concentration of phosphate buffer was increased (50-150 mM) or when a high protein concentration (20 mg/ml myoglobin) was used.

In line with the formation of insoluble aggregates, sub-visible particles (≥ 1 µm) were detected in the different formulations (Fig. 5). Adding trehalose to the myoglobin-only formulation resulted in a substantial reduction in the number of sub-visible particles (cf. M1 and MT1). Similarly, the use of a buffer also reduced the presence of sub-visible particles, independent of the type of buffer. Moreover, a decrease in the sub-visible particle content was also observed upon increasing the phosphate buffer or myoglobin concentration.
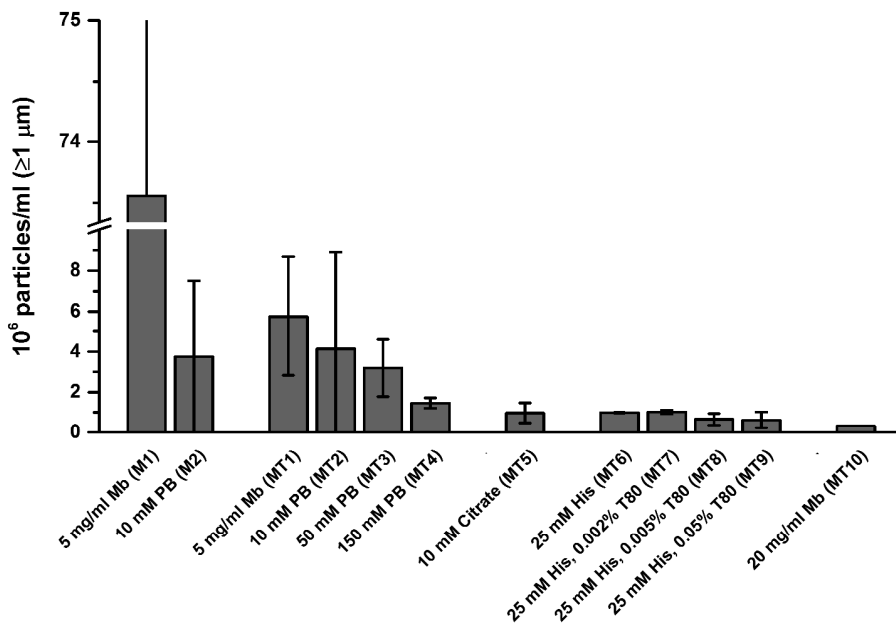

Fig. 5 Particle concentrations larger than 1 µm in the reconstituted scCO$_2$ spray dried myoglobin formulations (produced at 130 bar and 37 °C with half an hour post drying) observed by flow imaging microscopy. Volume refers to that of undiluted (reconstituted) liquid myoglobin formulation. Formulations M1-M2 are 5 mg/ml myoglobin in water and 10 mM phosphate pH 6.2. Formulations MT1-MT9 are 5 mg/ml myoglobin with 50 mg/ml trehalose. Formulation MT10 is 20 mg/ml myoglobin with 200 mg/ml trehalose.

4. Discussion

In a previous study [5], it was shown that 10 mM phosphate buffer at pH 6.2 (formulation MT2) lacked sufficient buffering capacity to stabilize myoglobin during $scCO_2$ spray drying, resulting in the partial loss of heme due to CO_2 acidification of the sprayed solution. In this current work, the effect of excipients (i.e., trehalose, buffer species, and surfactant) and myoglobin concentration on the stability of myoglobin during $scCO_2$ spray drying has been studied.

4.1 Effect of trehalose during CO_2 spray drying

Trehalose is an osmolyte that can form H-bonds with a protein molecule, helping to stabilize the protein when it is subjected to chemical and/or thermal stress, or dehydration [26-28]. During freeze-drying, trehalose also helps to prevent freeze damage of proteins from ice crystal formation [27, 28]. It was hoped that trehalose would also assist in stabilizing myoglobin during CO_2 spray drying, where the atomized protein formulation is exposed to a hydrophobic environment and acidification by pressurized CO_2. However, previous tests showed that changes in the myoglobin structure and aggregation still occurred, even for a formulation containing a 10:1 trehalose to protein ratio [5]. Yet, when comparing the myoglobin stability for formulations with (MT1 and MT2) and without (M1 and M2) trehalose, the trehalose clearly helps to stabilize the myoglobin structure (Table 2 and Fig. 1), and decreases the formation of myoglobin aggregates (Table 2 and Fig. 5). As expected, however, trehalose alone did not stabilize the pH of the formulation (Table 1 and Table 2), as it is not a buffer.

4.2 Effect of phosphate buffer at pH 6.2 during CO_2 spray drying

It was previously observed that myoglobin/trehalose formulations containing 10 mM phosphate buffer pH 6.2, were acidified during CO_2 spray drying [5], which induced instability in the heme-binding and myoglobin aggregation. From these results, it was concluded that controlling the pH is crucial for stabilizing the myoglobin and ensuring that the functionality is maintained.

Phosphate buffer has pKa values of 2.2, 7.2 and 12.4. In fact, a buffer solution is typically used to control the pH of a solution within a range of the pKa ± 1, and is most effective when the working pH is equal to the pKa of a buffer (Fig. 6). As the phosphate buffer at pH 6.2 used for the myoglobin formulations is on the limit of the effective operating pH

range, it had a low buffering capacity. Furthermore, the pH of the formulations was shifted out of the buffering range (Table 1 and 2) during the CO_2 spray drying process, thereby rendering this buffer completely ineffective.
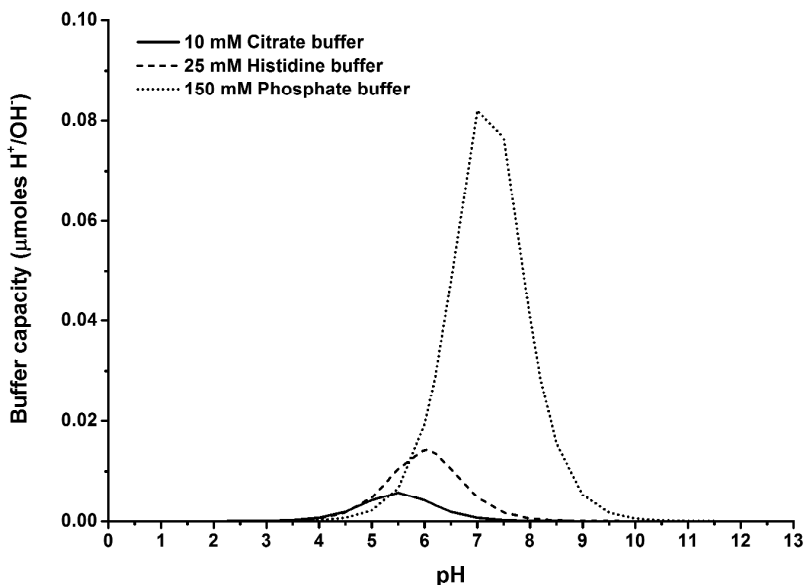

Fig. 6 Buffer capacities of 10 mM citrate buffer, 25 mM histidine buffer and 150 mM phosphate buffer at pKa 5.5, 6.0, and 7.2, respectively, calculated from Van Slyke [18, 38].

Aside from the pH range (relative to the pKa), the buffering capacity of a specific buffer is also dependent on its concentration. The effect of increasing the concentration of phosphate buffer at pH 6.2 on the ability to stabilize the pH during CO_2 spray drying is shown in Table 1 and Table 2 for trehalose and myoglobin formulations, respectively. For all the phosphate buffer formulations studied, only 150 mM phosphate buffer showed a complete stabilization of the pH, for both the trehalose-only formulation (T6) and the myoglobin/trehalose formulation (MT4). For the MT4 formulation, the heme binding of myoglobin was also fully preserved, as observed by 100% recovery of A_{409}/A_{280} ratio (Table 2) and molar ellipticity at the Soret band (Fig. 2), and the constant fluorescence signal (Fig. 4). Moreover, maintaining the pH of the formulation markedly decreased the formation of myoglobin aggregates, with 100% of the

myoglobin and monomers recovered (Table 2), as well as a significant decrease in the sub-visible particle concentration when compared to the myoglobin/trehalose formulations with 10 to 50 mM phosphate buffer. From these results, it can be concluded that a high concentration of phosphate buffer can stabilize the pH of the myoglobin formulation during $scCO_2$ spray drying, even if the pH is near the limit of the effective buffering range.

While using high phosphate buffer concentrations has positive effects on the myoglobin integrity, there are several negative aspects to consider when using such high concentrations. From a processing perspective, the high concentration of phosphate buffer caused the $scCO_2$ spray-dried protein formulations to be very hygroscopic. This not only made it difficult to collect the powdered samples, but also means that the residual water content may be higher than the recommended 3% for dried protein formulations [4]. Moreover, the use of high phosphate buffer concentrations may also have a negative effect on the protein integrity during storage, e.g., by causing crystallization of powdered protein formulations [29]. Furthermore, such high concentrations may also lead to hypertonicity, which can cause undesirable local tissue irritations upon administration [30]. For these reasons, the use of high salt concentrations is not recommended for protein formulations.

4.3 Effect of other buffers during CO_2 spray drying

In this current study, the stability of the heme binding and the degree of myoglobin aggregation were also investigated in citrate and histidine buffer solutions at pH 6.2. Citrate is composed of tri-carboxylic groups with the pKa at 3.1, 4.4 and 5.5, leading to a large buffering capacity over the pH range 2.5-6.5 [18]. Histidine has different pKa values, at 1.8, 6.0 and 9.3 from the carboxylic group, pyrrole NH, and ammonium group, respectively [18], and is used for pH control of parenteral formulations in a pH range of 5.5-6.5 [31]. These buffer salts are generally used to cover the working pH range of about 3.0-8.0. However, the choice of a buffer as a protein excipient will vary depending on the formulation, as different buffer ions can have an effect on the chemical and conformational stabilization (or perhaps destabilization) of proteins. For instance, in a study by Zheng and Janis [32], the deamination of asparagine (Asn55) in humanized monoclonal antibody was much higher in phosphate buffer than in citrate buffer. From the research of Jovanovic et al. [2], CO_2 spray-drying of immunoglobulin G (IgG) in 10 mM acetate pH 5.0 resulted in about 50%

loss of the protein, whereas almost 100% of the IgG was recovered when formulated with 10 mM citrate and phosphate pH 5.0-6.2.

In the current study, it was found that the pH of the CO_2 spray dried myoglobin/trehalose formulation was maintained when 10 mM citrate pH 6.2 was used. This is due to the broad buffering capacity range of the citrate [18]. Although the heme binding was maintained, the citrate buffer did cause marked myoglobin aggregation, as seen by a loss of monomers and total protein content. This aggregation could be the result of the Hofmeister salting-out effect during the drying process, where specific anions can lead to protein precipitation. The effect is typically greater in the case of multivalent anions, such as citrate [33]. Moreover, the salting-out is likely to be exacerbated during $scCO_2$ spray drying, as the citrate concentration in the atomized myoglobin formulations will increase during drying, which might lead to precipitation of the protein.

Histidine at a concentration of 25 mM at pH 6.2 (formulation MT6) was also shown to be effective in maintaining the pH of the myoglobin formulation during the $scCO_2$ drying process. Moreover, it appeared to have some favourable effect on the myoglobin structure, as a decrease in the myoglobin fluorescence signal was observed, which suggests that there is greater quenching by the heme (Fig. 1). This may indicate that the histidine can help to stabilize the heme binding. Moreover, histidine decreased the aggregation of dried myoglobin, as compared to a myoglobin with 10 mM phosphate buffer pH 6.2 (formulation MT2) [5]. In lyophilization, histidine has also been shown to lower the aggregation of recombinant factor VIII-SQ [34] and human anti-IL8 monoclonal antibody [31].A histidine concentration lower than 25 mM was not tested, because the final pH of the dried formulation MT6 had slightly dropped as compared to the dried formulation MT5 with 10 mM citrate.

When comparing these results to those of the phosphate buffer at pH 6.2, it can be concluded that the protein formulations with a working pH closed to the pKa of buffer agents (e.g., citrate and histidine) give the greatest buffering effect [18]. Consequently, these buffers can be used at a low concentration, as shown for histidine and citrate in the present study. Histidine was the best choice for controlling the pH of myoglobin formulations during $scCO_2$ spray drying, as unlike citrate it was found to be effective in stabilizing the protein structure and decreasing the protein aggregation.

4.4 Effect of protein concentration during CO_2 spray drying

In the absence of any buffer excipients, a comparison of the powders with and without protein showed that the solution pH after reconstitution was higher for the protein-containing formulation (MT2) than for the formulation without protein (T2). A similar behaviour was also observed upon increasing the myoglobin concentration from 5 mg/ml to 20 mg/ml (cf MT1 and MT10), with the higher concentration formulation exhibiting a higher pH after reconstitution. These results demonstrate the self-buffering effect of myoglobin. Aside from minimizing the pH shift, this self-buffering effect also resulted in the self-stabilization of myoglobin, as seen by an increase in the heme recovery, monomer and total protein content when the myoglobin formulation was prepared in water (formulation MT10) as compared to myoglobin in 10 mM phosphate buffer (formulation MT2). The self-buffering effect of the myoglobin formulations is due to the ionizable amino acid residues in the polypeptide. In a previous study [30], the buffering capacity of monoclonal antibody (mAb) in the pH range of 5.0-6.0 was determined by acid/base titration. From these tests, it was found that 50 mg/ml mAb in water is equivalent to 6 mM citrate or 14 mM histidine, while 220 mg/ml mAb corresponds to 30 mM citrate or 50 mM histidine [18]. It was anticipated that an increase in the myoglobin concentration to values higher than 20 mg/ml would maintain the pH of the protein formulation even closer to the original pH 6.2. However, this has not been further studied due to the limited solubility of myoglobin under the formulation conditions tested (data not shown).

Aside from minimizing the pH drop, the 20 mg/ml myoglobin formulation in water at pH 6.2 also showed a decrease in the myoglobin aggregation, even in the absence of buffer salts. Aggregate formation has been previously shown to be influenced by the CO_2/water interface which forms during CO_2 spray drying (see Chapter 5). The amphiphilic structure of proteins can act as a natural surfactant, forming an active barrier on the surface of bubbles and foams [35]. Therefore, it is anticipated that myoglobin behaves as a surfactant on the atomized droplets during $scCO_2$ spray drying. An increase in the concentration of myoglobin would help to decrease the exposure of the hydrophobic components of myoglobin (e.g., heme) to the hydrophobic CO_2 environment and 2) to reduce the surface tension at the surface of atomized droplets, resulting in heme stabilization and reduction of myoglobin aggregation during the CO_2 spray drying process.

These experiments suggest that it is possible to develop buffer free protein formulations that assist in stabilizing the protein during CO_2 spray drying. By working with such self-buffering protein formulations,

potentially adverse interactions between the protein and buffer salts are avoided. However, achieving the desired self-buffering capacity for a specific protein requires finding the right protein concentration [18]. In any case, each protein is expected to have a specific self-buffering capacity due to the difference in amino acids present in the primary structure. Therefore, before developing a buffer-free formulation for $scCO_2$ spray drying, the self-buffering capacity of a protein should be observed at the intended working concentrations and pH. Working with higher concentrations of protein may present challenges in solution preparation, as was seen in case of myoglobin and in general with monoclonal antibodies [36]. Moreover, for highly potent proteins that are dosed in the microgram range, such as cytokines and epoetin, high-concentration formulations are no option. These cases would necessitate the use of classical buffers.

4.5 Effects of surfactant

From the formulations investigated in this study, myoglobin formulated with trehalose in 25 mM histidine at pH 6.2 (formulation MT6) showed the best results in terms of maintaining both the pH and myoglobin integrity. However, despite the observation that the reconstituted pH was close to the original pH, this formulation also exhibited some aggregation after CO_2 spray drying. It was previously reported that myoglobin aggregation most likely occurs during $scCO_2$ spray drying due to exposure of the protein at the interface between the atomized myoglobin droplets and the pressurized CO_2 [5]. Based on these results, it was hypothesized that adding a surfactant to this formulation will act as a barrier between the water phase and the CO_2, thus limiting the exposure of the myoglobin to the CO_2. By doing so, the myoglobin is expected to remain in a hydrophilic environment, thereby inhibiting the protein unfolding that leads to aggregation. In this study, polysorbate 80 was included in the 25 mM histidine formulation (MT6) in order to prevent surface-induced protein aggregation (formulations MT7-9).

In biopharmaceutics, nonionic surfactants such as polysorbate 20 and polysorbate 80 are generally used to stabilize protein formulations in a solution [37]. However, in this current study, the addition of polysorbate 80 resulted in almost no improvement in the myoglobin monomer recovery when compared to the formulation without surfactant (Table 2). Moreover, even at the highest polysorbate concentration tested there was neither a reduction in the total sub-visible particle concentration (Fig. 5) nor an increase in the total

myoglobin content after spray drying (Table 1). From these results, it can be concluded that the surfactant is ineffective under these conditions, which may be related to the surfactant concentration, the choice of buffer excipients and the $scCO_2$ spray drying conditions. It has previously been observed that nonionic biocompatible surfactants, like polysorbate 80, can be used to prepare CO_2/water and water/CO_2 nano- and microemulsions, but require relatively high surfactant concentrations (typically 0.5-1.0%wt. exceeding polysorbate concentrations up to max. 0.1%wt typically used in protein formulations), depending on the pressure and temperature, stirring rate, water and salt concentrations [38].

5. Conclusion

We investigated the role of the formulation excipients on stabilizing myoglobin during $scCO_2$ spray drying. In particular, the excipients used in the formulation should maintain the heme and overall structure of myoglobin while minimizing aggregation. While trehalose helped to retain the heme within the binding pocket, it was unable to prevent the acidification of the myoglobin solutions during spraying, which resulted in some heme loss and myoglobin aggregation. Heme stabilization in myoglobin was achieved when the pH of protein formulations was maintained at pH 6.2, by using a high concentration of phosphate buffer or a low concentration of citrate or histidine buffer. Furthermore, the phosphate and histidine buffers, but not the citrate buffer, reduced myoglobin aggregation. In the absence of classical buffers, myoglobin presented self-buffering and self-stabilizing properties at high concentration. The addition of polysorbate 80 to the myoglobin formulation did not have a significant effect on reducing myoglobin aggregation. From this study, it can be concluded that excipients are required to protect the protein against process-induced damage during $scCO_2$ spray drying.

References

[1]   N. Jovanović, A. Bouchard, G. W. Hofland, G. Witkamp, D. J. A. Crommelin, W. Jiskoot, Distinct effects of sucrose and trehalose on protein stability during supercritical fluid drying and freeze-drying, Eur J Pharm Sci, 27 (2006) 336-345.

[2]   N. Jovanović, A. Bouchard, G. W. Hofland, D. J. Crommelin, W. Jiskoot, Stabilization of IgG by supercritical fluid drying: optimization of formulation and process parameters, Eur J Pharm Biopharm, 68 (2008) 183-190.

[3]   N. Jovanović, A. Bouchard, M. Sutter, M. V. Speybroeck, G. W. Hofland, G. Witkamp, D. J. A. Crommelin, W. Jiskoot, Stable sugar-based protein formulations by supercritical fluid drying, Int J Pharm, 346 (2008) 102-108.

[4]   O. Nuchuchua, H. A. Every, G. W. Hofland, W. Jiskoot, Scalable organic solvent free supercritical fluid spray drying process for producing dry protein formulations, Eur J Pharm Biopharm, 88 (2014) 919-930.

[5]   O. Nuchuchua, H.A. Every, G.W. Hofland, W. Jiskoot, Critical processing parameters of carbon dioxide spray drying for the production of dried protein formulations: A study with myoglobin, Eur J Pharm Biopharm, 103 (2016) 200-9.

[6]   A. Bouchard, N. Jovanović, G.W. Hofland, W. Jiskoot, E. Mendes, D.J.A. Crommelin, G.J. Witkamp, Supercritical fluid drying of carbohydrates: Selection of suitable excipients and process conditions, Eur J Pharm Biopharm, 68 (2008) 781-794.

[7]   N. P. Bhatt, K. Patel, R.T. Borchardt, Chemical pathways of peptide degradation. I. Deamidation of adrenocorticotropic hormone, Pharm Res, 7 (1990) 593-599.

[8]   C. Oliyai, R.T. Borchardt, Chemical pathways of peptide degradation. IV. Pathways, kinetics, and mechanism of degradation of an aspartyl residue in a model hexapeptide, Pharm Res, 10 (1993) 95-102.

[9]   C. Oliyai, R.T. Borchardt, Chemical pathways of peptide degradation. VI. Effect of the primary sequence on the pathways of degradation of aspartyl residues in model hexapeptides, Pharm Res, 11 (1994) 751-758.

[10]   K. Patel, R.T. Borchardt, Chemical pathways of peptide degradation. II. Kinetics of deamidation of an asparaginyl residue in a model hexapeptide, Pharm Res, 7 (1990) 703-711.

[11]   D.E. Graham, M.C. Phillips, Proteins at Liquid Interfaces .1. Kinetics of Adsorption and Surface Denaturation, Journal of Colloid and Interface Science, 1979. **70**(3): p. 403-414.

[12]   Z. Yu, K.P. Johnston, R.O. Williams 3rd, Spray freezing into liquid versus spray-freeze drying: influence of atomization on protein aggregation and biological activity, Eur J Pharm Sci, 27 (2006) 9-18.

[13]   S. Ohtake, Y. Kita, T. Arakawa, Interactions of formulation excipients with proteins in solution and in the dried state. Adv Drug Deliv Rev, 63 (2011) 1053-73.

[14]   L. S. Jones, N. B. Bam, T. W. Randolph, Surfactant-stabilized protein formulations: A review of protein-surfactant interactions and novel analytical methodologies (Chapter 12) in Therapeutic Protein and Peptide Formulation and Delivery, 1997, 206–222.

[15]   M. Adler, G. Lee, Stability and surface activity of lactate dehydrogenase in spray-dried trehalose. J Pharm Sci, 88 (1999) 199-208.

[16]   Y.F. Maa, P.A.T. Nguyen, S.W. Hsu, Spray-drying of air-liquid interface sensitive recombinant human growth hormone, J Pharm Sci, 87 (1998) 152-159.

[17]   J.D. Morrisett, J.S.K. David, H.J. Pownall, A.M. Gotto Jr, Interaction of an apolipoprotein (apoLP-alanine) with phosphatidylcholine. Biochemistry, 12 (1973) 1290-1299.

[18]   A.R. Karow, S. Bahrenburg, P. Garidel, Buffer Capacity of Biologics-From Buffer Salts to Buffering by Antibodies, Biotechnol Prog, 29 (2013) 480-492.

[19]   M. Momenteau, M. RougÉE, B. Loock, Five-Coordinate Iron-Porphyrin as a Model for the Active Site of Hemoproteins Characterization and Coordinating Properties, Eur J Biochem, 71 (1976) 63-76.

[20]   E. Peggion, A. Cosani, M. Terbojevich, Solution properties of synthetic polypeptides. Assignment of the conformation of poly(L-tyrosine) in water and in ethanol-water solutions. Macromolecules, 7 (1974) 453-459.

[21]   H. Yamamoto, A. Nakazawa, T Hayakawa, Circular-dichroism studies of complexes of sequential histidine polypeptides with methyl-orange, In. J Biol Macromolec, 7 (1985) 167-172.

[22]   M.C. Hsu, R.W. Woody, The origin of the heme Cotton effects in myoglobin and hemoglobin, J Am Chem Soc, 93 (1971) 3515-25.

[23]   M. Nagai, Y. Nagai, K. Imai, S. Neya, Circular dichroism of hemoglobin and myoglobin, Chirality, 26 (2014) 438-442.

[24]   M. S. Hargrove, D. Barrick, J.S. Olson, The association rate constant for heme binding to globin is independent of protein structure, Biochemistry, 35 (1996) 11293-11299.

[25]   A. N. Schechter, C. J. Epstein, Spectral studies on the denaturation of myoglobin, J Mol Biol, 35 (1968) 567-589.

[26]   T. Arakawa, S.N. Timasheff, Stabilization of protein structure by sugars, Biochemistry, 21 (1982) 6536-6544.

[27]   N. K. Jain, I. Roy, Trehalose and protein stability, Curr Protoc Protein Sci, 2010, Chapter 4: p. Unit 4 9.

[28]   N. K. Jain, I. Roy, Effect of trehalose on protein structure, Protein Sci, 18 (2009) 24-36.

[29]   A. Pyne, K. Chatterjee, R. Suryanarayanan, Solute crystallization in mannitol-glycine systems--implications on protein stabilization in freeze-dried formulations, J Pharm Sci, 92 (2003) 2272-2283.

[30]   M. Robinson, A. L. Hemming, J. A. Regnis, A. G. Wong, D. L. Bailey, G. J. Bautovich, M. King, P. T. Bye, Effect of increasing doses of hypertonic saline on mucociliary clearance in patients with cystic fibrosis, Thorax, 52 (1997) 900-3.

[31]   B. Chen, R. Bautista, K. Yu, G. A. Zapata, M. G. Mulkerrin, Influence of histidine on the stability and physical properties of a fully human antibody in aqueous and solid forms, Pharm Res, 20 (2003) 1952-1960.

[32]   J. Y. Zheng, L. J. Janis, Influence of pH, buffer species, and storage temperature on physicochemical stability of a humanized monoclonal antibody LA298, Int J Pharm, 308 (2006) 46-51.

[33]   M. G. Cacace, E. M. Landau, J. J. Ramsden, The Hofmeister series: salt and solvent effects on interfacial phenomena, Q Rev Biophys, 30 (1997) 241-277.

[34]   T. Osterberg, A. Fatouros, M. Mikaelsson, Development of freeze-dried albumin-free formulation of recombinant factor VIII SQ, Pharm Res, 14 (1997) 892-898.

[35]   A. Cooper, M. W. Kennedy, Biofoams and natural protein surfactants, Biophys Chem, 151 (2010) 96-104.

[36]   S. J. Shire, Z. Shahrokh, J. Liu, Challenges in the development of high protein concentration formulations, J Pharm Sci, 93 (2004), 1390-1402.

[37]   T. W. Randolph, L. S. Jones, Surfactant-protein interactions, Pharm Biotechnol, 13 (2002) 159-175.

[38]   D. D. V. Slyke, On the measurement of buffer values and on the relationship of buffer value to the dissociation constant of the buffer and the concentration and reaction of the buffer solution, J Biol Chem, 52 (1922) 525.

CHAPTER 7

Summary and prospective

Supercritical carbon dioxide ($scCO_2$) processing technologies are a broad and diverse array of techniques that can be used to engineer nano- and microparticles for a variety of pharmaceutical applications, such as allowing the use of less invasive administration routes, improving drug stability, controlling the release of drug, increasing bioavailability and/or selectively targeting of particular tissues or cell types [1-3]. In each case, the $scCO_2$ can be used in different ways, for example as a solvent or anti-solvent, in order to obtain particles with the desired drug delivery profile and therapeutic efficacy [4-6]. As the functionality of the resultant nano-/microparticles is often related to the particle characteristics (such as the efficiency of the drug loading, particle size and morphology), it is necessary to provide proper particle characterization, in order to obtain crucial data for the development and optimization of the production process and the product. A review of these characterization techniques is presented in **Chapter 2**.

Supercritical carbon dioxide spray drying is a dehydration technique, which has been proposed as an alternative for freeze-drying and conventional spray-drying, to prepare dried therapeutic protein formulations and other biologics at ambient temperature, thereby avoiding thermal denaturation [7]. As the solubility of water in CO_2 is low, organic solvents, such as ethanol and acetone, were often introduced as co-solvents, to enhance the water evaporation. However, the use of co-solvents can lead to destabilization and aggregation of proteins [8]. Preliminary tests in the absence of a co-solvent resulted in up to 10%wt residual water content in the protein formulation after $scCO_2$ spray drying [9]. Yet, according to Title 21 of the Code of Federal Regulations for Food and Drugs (1990), the maximum residual moisture content in freeze-dried protein formulations should be no greater than 3%wt, in order to preserve the protein integrity during storage. Therefore, one of many challenges in $scCO_2$ spray drying is finding suitable conditions to prepare stable dried protein formulations similar to freeze-dried products, with less than 3%wt of residual water content without the need for organic solvents. In **Chapter 3**, it is shown that the residual water content in $scCO_2$ spray dried powders is related to the processing parameters. The experiments were carried out for lysozyme/trehalose formulations at 1:0, 1:4 and 1:10 weight ratios. To decrease the residual water content, the relative humidity in the high pressure CO_2 drying medium should be controlled by using a high CO_2 to solution flow rate ratio and low solution volume. Under these conditions, the resulting dried protein formulation had a residual water content of about 2.5%wt. However, the use of low solution flow rate and volume limits the production capacity of the $scCO_2$ spray drying process. In **Chapter 3** also the scalability of $scCO_2$ spray drying is examined by maintaining a

constant gas (CO_2) to liquid flow rate ratio (GLR) on a pilot-scale unit. When using the same GLR value in 4- and 10-litre drying vessels of the $scCO_2$ spray dryers, the final powdered products had comparable quality in terms of the droplet size, residual water content, protein structure and activity and particle size and morphology.

From the results obtained in **Chapter 3**, the best conditions were used to prepare $scCO_2$ spray dried formulations of other proteins. While the protein integrity for polyclonal and monoclonal antibodies, a-chymotrypsinogen A, lysozyme and a-lactalbumin was maintained after drying, the 1:10 myoglobin/trehalose formulation showed heme destabilization and myoglobin aggregation, which most likely was process induced. Parameters related to the $scCO_2$ spray drying process, such as pressure, temperature, high pressure CO_2 and spray drying, were individually studied, in order to assess their influence on heme binding destabilization and myoglobin aggregation. In the range of 65-130 bar and 25-50°C, pressure and temperature alone did not influence the myoglobin integrity. However, the results showed that myoglobin instability was induced by exposure to pressurized CO_2. Furthermore, the pH of the myoglobin formulation was found to decrease from 6.2 to about 5.0, leading to a partial loss of heme during spray drying. This study is presented in **Chapter 4**. The changes in myoglobin structure were monitored by UV-Vis spectroscopy, circular dichroism spectroscopy and size-exclusion chromatography. However, the nature of the interaction between CO_2 and myoglobin was not investigated. Consequently, it is not known whether the pressurized CO_2 only causes physical instability of the myoglobin structure, or whether there is actually a chemical reaction occurring between them. For this, the chemical modification of proteins should be observed in order to better understand the mechanisms by which the myoglobin integrity is affected by $scCO_2$, e.g., by using mass spectroscopy in combination with Fourier transform infrared spectroscopy (FTIR) spectroscopy [10].

During spray drying, atomization results in the formation of droplets and correspondingly a gas/water interface. Protein molecules can adsorb at the interface, leading to reorientation of the protein structure that results in protein destabilization and aggregation [11, 12]. However, the critical parameter study of the CO_2 spray drying process as described in **Chapter 4** was not able to directly show the influence of atomization on myoglobin instability. For this reason, a gas bubbling study was conducted, as a means to evaluate the influence of CO_2/water interface and acidification by CO_2 on myoglobin integrity. **Chapter 5** shows a series of CO_2 and N_2 gas bubbling tests on myoglobin solutions over a range of pH 4.0-7.0. CO_2 gas bubbling decreased the pH of the myoglobin solutions prepared at starting pH 4.5-7.0. However,

changes in the secondary structure of myoglobin were only found when the myoglobin solution had a final pH of 4.3, although no loss of heme was observed. In case of myoglobin solutions with a starting pH of 4.0-5.3, the effect of CO_2/water interface resulted in the formation of sub-visible myoglobin aggregates (1-100 μm diameter) with a fiber-like morphology. For the myoglobin solutions with a starting pH of 6.2 and 7.0, however, the CO_2/water interface in combination with the CO_2 acidification resulted in sub-visible aggregates with a highly irregular morphology. Moreover, the concentration of the aggregates was five times higher than what was observed for the solutions with the low starting pH. In contrast, N_2 gas bubbling did not affect the pH of the solutions, and consequently there was no change in the secondary structure and the heme binding site of myoglobin. However, N_2 bubbling also led to the formation of fiber-like myoglobin aggregates, but in this case, they were observed over the entire pH range studied. From these results, it was concluded that the gas/water interface induces the formation of aggregates, while the gas/water interface in combination with the drop in pH results in conformational changes and changes in the particle morphology.

The effects observed in the CO_2 bubbling study are not entirely comparable to those occurring at the gas/water interface formed during CO_2 spray drying, due to the different properties of gaseous and supercritical CO_2 as well as the difference in processing conditions. However, the bubbling method still suggests that heme destabilization is induced by acidification, whereas myoglobin aggregation can be caused by exposure of the protein to the CO_2/water interface and the CO_2 acidification, depending on the starting pH of the protein solutions. Moreover, this protein instability appears to be a surface-induced process, which is most likely enhanced in pressurized CO_2. Furthermore, the pH shift also suggests that the protein formulation needs a buffer agent to control the pH of the formulation upon exposure to CO_2. In this study, protein aggregation was evaluated in terms of the sub-visible particles and morphology by flow-imaging microscopy and the partial loss of monomer and protein by UV/Vis and size-exclusion chromatography. However, in order to intrinsically understand the mechanism of protein aggregation, the molecular interactions that lead to aggregation should be investigated. For example, the secondary structure of protein aggregates can be studied by FTIR [13].

In order to understand the role of the formulation in stabilizing myoglobin, a series of tests were conducted using different excipients. **Chapter 6** shows effects of sugar (trehalose), buffer agents (phosphate, citrate and histidine) and a surfactant (Tween 80) on the heme binding and aggregation of myoglobin during CO_2 spray drying. The heme was

stabilized in the myoglobin structure when trehalose was added to the myoglobin formulations. The pH of the myoglobin/trehalose formulations was maintained at pH 6.2 after CO_2 spray drying when introducing buffer salts such as 50-150 mM phosphate, 10 mM citrate and 25 mM histidine, with full recovery of the heme observed. Myoglobin aggregation was gradually reduced with an increasing concentration of phosphate buffer. Moreover, a high concentration of myoglobin exhibited self-buffering properties, leading to the stabilization of heme and a significant reduction in myoglobin aggregation. The use of the surfactant was hypothesized to act as a barrier at the interface of the high pressure CO_2 and atomized protein droplets, thereby minimizing protein adsorption at the interface that leads to protein aggregation. However, Tween 80 did not show any significant effect in reducing myoglobin aggregation. As discussed in **Chapter 5**, it is likely that the pressurized CO_2/water interface is not the same as the interface between gaseous CO_2 and water observed in the gas bubbling study, from which it may be inferred that the surfactant will not have the same effect in the supercritical CO_2 environment as it does under atmospheric conditions. Moreover, polysorbates have been shown to be unstable under certain conditions, undergoing autoxidation, side-chain cleavage, formation of short-chain acids upon exposure to changes in pH and temperature, as well as light exposure [14-16]. It is possible that one or more of these factors may influence the surfactant properties of Tween 80 during $scCO_2$ spray drying.

As shown in **Chapter 6**, it was of key importance to avoid significant acidification and exposure of the myoglobin to the hydrophobic CO_2 during $scCO_2$ spray drying, in order to stabilize the heme binding in myoglobin and to reduce myoglobin aggregation [17]. The integrity of myoglobin was preserved by adding trehalose and a suitable buffer agent. While it is anticipated that other proteins may also be destabilized during $scCO_2$ spray drying, it should not be assumed that the formulation that was used to stabilize myoglobin will be applicable in all cases. Given the diversity of proteins, the choice of the pH and the use of stabilizing agents (e.g., disaccharides, polyols, buffers and surfactants) should be tailored for each specific protein. Moreover, it is anticipated that working with a high protein concentration may allow for buffer-free protein formulations. However, the self-buffering capacity of each individual protein should be fundamentally studied, in order to understand what protein concentration is needed to maintain the pH during $scCO_2$ spray drying. The self-buffering property of proteins can be observed by following a similar experimental approach as outlined in a study by Karow et al. [18]. By acid-base titration, the buffering capacity of proteins at any working pH can be investigated in terms of the

equivalent amount of hydrogen or hydroxide ions used for changing one unit of the starting pH of a protein solution.

In general, $scCO_2$ spray drying is a promising process for preparing stable dried protein formulations for research and commercial purposes. Similar to other drying techniques, care should be taken to choose the appropriate processing conditions and formulation (**Chapter 3, 4 and 6**). Although only proteins were studied in this thesis, it is anticipated that the $scCO_2$ spray drying technique is also applicable to peptides, genetic materials (DNA and RNA) and vaccines. Moreover, $scCO_2$ spray drying could be used as a technique to engineer a broad range of different types of drug delivery systems, such as particles with core-shell structures, tunable matrix compositions, and hierarchical structures, such as microparticles decorated with nanoparticles [19].

References

[1]   O.C. Farokhzad, R. Langer, Impact of nanotechnology on drug delivery, ACS Nano, 3 (2009) 16-20.

[2]   A.H. Chow, H.H. Tong, P. Chattopadhyay, B.Y. Shekunov, Particle engineering for pulmonary drug delivery, Pharm Res, 24 (2007) 411-437.

[3]   M. Manzano, M. Manzano, V. Aina, C.O. Areán, F. Balas, V. Cauda, M. Colilla, M.R. Delgado, M. Vallet-Regí, Studies on MCM-41 mesoporous silica for drug delivery: Effect on particle morphology and amine functionalization, Chem Eng J, 137 (2008) 30-37.

[4]   A. Tabernero, E.M. Martín del Valle, M.A. Galán, Supercritical fluids for pharmaceutical particle engineering: Methods, basic fundamentals and modeling. Chem Eng Process, 60 (2012) 9-25.

[5]   E. Reverchon, R. Adami, G. Caputo, I. De Marco, Spherical microparticles production by supercritical antisolvent precipitation: Interpretation of results. J Supercrit Fluids, 47 (2008) 70-84.

[6]   E. Reverchon, Supercritical antisolvent precipitation of micro- and nano-particles. J Supercrit Fluids, 15 (1999) 1-21.

[7]   N. Jovanović, A. Bouchard, G.W. Hofland, G-J Witkamp, D.J. Crommelin, W. Jiskoot, Stabilization of proteins in dry powder formulations using supercritical fluid technology, Pharm Res, 21 (2004) 1955-69.

[8]   N. Jovanović, A. Bouchard, M. Sutter, M. V. Speybroeck, G. W. Hofland, G. Witkamp, D. J. A. Crommelin, W. Jiskoot, Stable sugar-based protein formulations by supercritical fluid drying, Int J Pharm, 346 (2008) 102-108.

[9]   O. Nuchuchua, H. A. Every, G. W. Hofland, W. Jiskoot, Scalable organic solvent free supercritical fluid spray drying process for producing dry protein formulations, Eur J Pharm Biopharm, 88 (2014) 919-930.

[10]   S. Kamat, G. Critchley, E.J. Beckman, A.J. Russell, Biocatalytic Synthesis of Acrylates in Organic-Solvents and Supercritical Fluids .3. Does Carbon-Dioxide Covalently Modify Enzymes?, Biotechnol Bioeng, 46 (1995) 610-620.

[11]   Z. Yu, K.P. Johnston, R.O. Williams 3rd, Spray freezing into liquid versus spray-freeze drying: influence of atomization on protein aggregation and biological activity, Eur J Pharm Sci, 27 (2006) 9-18.

[12]   S.D. Webb, S.L. Golledge, J.L. Cleland, J.F. Carpenter, T.W. Randolph, Surface adsorption of recombinant human interferon-gamma in lyophilized and spray-lyophilized formulations, J Pharm Sci, 91 (2002) 1474-1487.

[13]   A. Natalello, S.M. Doglia, Insoluble protein assemblies characterized by fourier transform infrared spectroscopy, Methods Mol Biol, 1258 (2015) 347-69.

[14]   M. Donbrow, E. Azaz, A. Pillersdorf, Autoxidation of polysorbates, J Pharm Sci, 67 (1978) 1676-81.

[15]   R.S. Kishore, A. Pappenberger, I.B. Dauphin, A. Ross, B. Buergi, A. Staempfli, H.C. Mahler, Degradation of polysorbates 20 and 80: studies on thermal autoxidation and hydrolysis, J Pharm Sci, 100 (2011) 721-31.

[16]   M. Agarkhed, C. O'Dell, M.C. Hsieh, J. Zhang, J. Goldstein, A. Srivastava, Effect of polysorbate 80 concentration on thermal and photostability of a monoclonal antibody. AAPS Pharm Sci Tech, 14 (2013) 1-9.

[17]   O. Nuchuchua, H.A. Every, W. Jiskoot, Critical processing parameters of carbon dioxide spray drying for the production of dried protein formulations: A study with myoglobin, Eur J Pharm Biopharm, 103 (2016) 200-9.

[18]   A.R. Karow, S. Bahrenburg, P. Garidel, Buffer Capacity of Biologics-From Buffer Salts to Buffering by Antibodies, Biotechnol Prog, 29 (2013) 480-492.

[19]   W. Liu, X.D. Chen, C. Selomulya, On the spray drying of uniform functional microparticles, Particuology, 22 (2015) 1-12.

Nederlandse samenvatting

Superkritische koolstofdioxide (scCO$_2$) procestechnologieën bestaan uit een breed scala aan technieken die gebruikt kunnen worden om nano- en microdeeltjes te verwerken voor verschillende farmaceutische toepassingen. Voorbeelden hiervan zijn het gebruik van minder invasieve toedieningsroutes, het verbeteren van de stabiliteit van geneesmiddelen, het reguleren van de afgifte van het geneesmiddel, het verbeteren van de biologische beschikbaarheid en/of het selectief *targeten* van een bepaald type weefsel of cel [1-3]. Voor elke toepassing kan de scCO$_2$ op verschillende manieren worden gebruikt, bijvoorbeeld als oplosmiddel of als anti-oplosmiddel om zodoende deeltjes te verkrijgen met het gewenste geneesmiddelafgifteprofiel en therapeutische werking [4-6]. Het is noodzakelijk om de deeltjes op een juiste wijze te karakteriseren om zodoende noodzakelijke data te verkrijgen voor de ontwikkeling en de optimalisatie van het productieproces en het product. De functionaliteit van de verkregen nano-/microdeeltjes zijn namelijk vaak gerelateerd aan de kenmerken van het deeltje. Een overzicht van analytische technieken voor het karakteriseren van zulke deeltjeskenmerken wordt gegeven in **Hoofdstuk 2**.

scCO$_2$ sproeidrogen is een alternatieve dehydratietechniek, in plaats van vriesdrogen en conventioneel sproeidrogen, om gedroogde therapeutische eiwitformuleringen te bereiden. scCO$_2$ sproeidrogen gebeurt bij een relatief lage temperatuur, waardoor thermische denaturatie voorkomen wordt [7]. Vanwege de lage oplosbaarheid van water in scCO$_2$ worden organische oplosmiddelen, zoals ethanol en aceton, vaak geïntroduceerd als co-oplosmiddel om verdamping te bevorderen . Echter, het gebruik van een co-oplosmiddel kan leiden tot destabilisatie en aggregatie van eiwitten [8]. Uit onderzoek blijkt dat scCO$_2$ sproeidrogen zonder co-oplosmiddel resulteert in de aanwezigheid van maximaal 10 wt% residueel water (restvocht) in de gedroogde eiwitformulering [9]. Echter, volgens paragraaf 21 van de Code of Federal Regulations for Food and Drugs (1990) zou het maximale aanwezige vochtgehalte niet hoger moeten zijn dan 3 wt% in gevriesdroogde eiwitformuleringen om te voorkomen dat de eigenschappen van het eiwit veranderen bij opslag. Een van de vele uitdagingen bij scCO2 sproeidrogen is het vinden van geschikte omstandigheden voor de bereiding van stabiele gedroogde eiwitformuleringen met minder dan 3 wt% restvocht zonder

gebruikmaking van organische oplosmiddelen. **Hoofdstuk 3** geeft weer dat het restvochtgehalte in $scCO_2$ gesproeidroogd poeder gerelateerd is aan de procesparameters in zo'n co-oplosmiddelvrij proces. Deze experimenten zijn uitgevoerd voor lysozym/trehalose-formuleringen bij 1:0, 1:4 en 1:10 gewichtsverhoudingen. De relatieve luchtvochtigheid in het hogedruk CO_2 droogmedium kon beperkt worden door een hoge verhouding te kiezen van de toevoersnelheid van het gas (CO_2) t.o.v. die van

de te drogen oplossing (GLR = gas liquid ratio) en door het volume van deze oplossing laag te houden. Hiermee kon het restvochtgehalte in de verkregen gedroogde eiwitformulering beperkt worden tot ongeveer 2.5 wt%. Het gebruik van een lage toevoersnelheid en een klein volume beperkt echter de capaciteit van het $scCO_2$ sproeidroogproces. In **Hoofdstuk 3** is daarom ook de schaalbaarheid van $scCO_2$ sproeidrogen onderzocht. Door gebruikmaking van dezelfde GLR waarde in 4- en 10-liter droogvaten van de $scCO_2$ sproeidrogers, waren de gedroogde eindproducten vergelijkbaar wat betreft druppelgrootte, restvochtgehalte en andere producteigenschappen (eiwitstructuur- en activiteit, deeltjesgrootte en morfologie van de gedroogde poeders).

Uit de resultaten, verkregen in **Hoofdstuk 3,** zijn de beste condities geselecteerd voor de bereiding van $scCO_2$ gesproeidroogde formuleringen van andere eiwitten. De eigenschappen van polyklonale en monoklonale antilichamen, a-chymotrypsinogeen A, lysozym en a-lactalbumine waren behouden na het drogen in aanwezigheid van trehalose (gewichtsverhouding eiwit/trehalose 1:10). De 1:10 myoglobin/trehalose-formulering liet echter destabilisatie van de binding van de heemgroep en myoglobine-aggregatie zien, hoogstwaarschijnlijk als gevolg van het droogproces. Om dit te onderzoeken zijn aan het $scCO_2$ sproeidroogproces gerelateerde parameters, zoals druk, temperatuur, hoge druk CO_2 en sproeidrogen afzonderlijk onderzocht. Tussen 65-130 bar en 25-50 °C bleken de parameters druk en temperatuur onafhankelijk van elkaar geen invloed te hebben op de eigenschappen van myoglobine. Deze resultaten tonen aan dat de myoglobine-instabiliteit vermoedelijk is veroorzaakt door de blootstelling aan CO_2 onder druk. Verder nam de pH van de formulering af van 6.2 naar 5.0, wat leidde tot een gedeeltelijk verlies van de heemgroep tijdens het sproeidrogen. Dit onderzoek is beschreven in **Hoofdstuk 4**. De verandering in de myoglobinestuctuur is onderzocht met UV-VIS spectroscopie, circulair dichroisme spectroscopie en size-exclusion chromatografie. Echter, de aard van de interactie tussen CO_2 en myoglobine is niet onderzocht. Hierdoor is het onbekend of CO_2 onder druk alleen fysische instabiliteit van de myoglobinestructuur veroorzaakt, of dat er een chemische reactie

optreedt. Om dit te onderzoeken zouden de eventuele chemische modificaties van het eiwit als gevolg van blootstelling aan $scCO_2$ geanalyseerd moeten worden, bijvoorbeeld door gebruikmaking van massaspectroscopie in combinatie met infraroodspectroscopie [10].

Tijdens sproeidrogen, leidt atomisering tot de vorming van druppels en overeenkomstig een gas/water-grensvlak. Eiwitmoleculen kunnen adsorberen aan het grensvlak, wat leidt tot de heroriëntatie van de eiwitstructuur wat resulteert in eiwitdestabilisatie en -aggregatie [11, 12]. Echter, het parameteronderzoek van het $scCO_2$ sproeidroogproces, zoals beschreven in **Hoofdstuk 4,** heeft niet direct de invloed van de atomisering op myoglobine-instabiliteit rechtstreeks aangetoond. Om deze reden is onderzocht in hoeverre het CO_2/water-grensvlak en de verzuring door CO_2 de myoglobinestructuur beïnvloeden. **Hoofdstuk 5** beschrijft een reeks van testen waarbij CO_2- en N_2-gasbellen doorgevoerd zijn door myoglobine-oplossingen met diverse initiële pH-waarden tussen 4.0-7.0. De CO_2-gasbellen verlaagden de pH van de oplossingen met initiële pH-waarden tussen 4.5-7.0. Veranderingen in de secundaire structuur van myoglobine werden alleen gevonden wanneer de myoglobine-oplossing een eind pH had van 4.3. Onder alle onderzochte omstandigheden bleef de heemgroep gebonden aan het eiwit. Bij myoglobine-oplossingen met een initiële pH van 4.0-5.3 resulteerde het doorvoeren van CO_2-gasbellen in de vorming van sub-zichtbare myoglobine-aggregaten (1-100 μm diameter) met een vezelachtige morfologie. Bij de myoglobine-oplossingen met een initiële pH van 6.2 en 7.0 resulteerde het CO_2/water-grensvlak, in combinatie met de door CO_2 veroorzaakte verzuring, in sub-zichtbare aggregaten met een zeer onregelmatige morfologie. Bovendien was de concentratie van de aggregaten vijf keer zo hoog als voor de oplossingen met de lage start pH. Daarentegen vertoonden de N_2-gasbellen geen invloed op de pH van de oplossingen, waardoor geen verandering in de secundaire structuur en de heembinding van myoglobine optrad. Echter de N_2-gasbellen leidden wel tot de vorming van vezelachtige myoglobine-aggregaten over het gehele bestudeerde pH-traject. Uit deze resultaten kan geconcludeerd worden dat het gas/water-grensvlak leidt tot de vorming van aggregaten, terwijl het gas/water-grensvlak in combinatie met de daling van de pH leidt tot conformationele veranderingen en wijzigingen in de deeltjesmorfologie.

Om de rol van de formulering bij het stabiliseren van myoglobine te begrijpen, is een serie testen uitgevoerd met diverse hulpstoffen. **Hoofdstuk 6** toont effecten van suiker (trehalose), buffers (fosfaat, citraat en histidine) en een oppervlakte-actieve stof (polysorbaat 80) op de

heembinding en aggregatie van myoglobine gedurende $scCO_2$ sproeidrogen. De pH van de myoglobine/trehalose-formuleringen is constant gehouden op 6.2 na $scCO_2$ sproeidrogen bij de introductie van bufferzouten, zoals 50-150 mM fosfaat, 10 mM citraat en 25 mM histidine, waarbij de binding van de heemgroep volledig behouden bleef. Aggregatie van myoglobine werd geleidelijk gereduceerd met een toenemende concentratie fosfaatbuffer. Bovendien bleek een hoge concentratie myoglobine zelf-bufferende eigenschappen te vertonen, leidend tot de stabilisatie van de heembinding en een significante vermindering van myoglobine-aggregatie. Tegen de verwachting in bleek polysorbaat 80 geen significante bescherming te bieden tegen de aggregatie van myoglobine. Wellicht dat polysorbaat 80 in de $scCO_2$-omgeving niet hetzelfde effect heeft als onder atmosferische omstandigheden. Bovendien is aangetoond dat polysorbaten instabiel zijn onder bepaalde omstandigheden: ze ondergaan auto-oxidatie en fragmentatie bij blootstelling aan veranderingen in pH en temperatuur, en de blootstelling aan licht [13-15]. Het is mogelijk dat één of meer van deze factoren de eigenschappen van polysorbaat 80 kunnen beïnvloeden tijdens $scCO_2$ sproeidrogen.

Zoals weergegeven in **Hoofdstuk 6**, is het van groot belang om significante verzuring en blootstelling van het myoglobine aan de hydrofobe CO_2 gedurende het $scCO_2$ sproeidroogproces te voorkomen, om daarmee de heembinding in myoglobine te stabiliseren en myoglobine-aggregatie te verminderen [16]. De eigenschappen van myoglobine kunnen worden behouden door de toevoeging van trehalose en een geschikte buffer. Hoewel wordt verwacht dat andere eiwitten kunnen destabiliseren tijdens $scCO_2$ sproeidrogen, mag niet worden aangenomen dat de formulering die gebruikt werd om myoglobine te stabiliseren in alle gevallen toepasbaar is. Gezien de diversiteit van eiwitten, moet de keuze van de pH en het gebruik van stabiliserende hulpstoffen worden aangepast voor elk specifiek eiwit. Bovendien is de verwachting dat het werken met een hoge eiwitconcentratie het mogelijk maakt om buffer-vrije eiwitformuleringen te gebruiken. De zelf-bufferende capaciteit dient echter voor elk eiwit te worden onderzocht bij de gewenste pH, om te kunnen begrijpen welke eiwitconcentratie nodig is om de pH tijdens $scCO_2$ sproeidrogen te handhaven, bijvoorbeeld zoals beschreven in een studie van Karow et al. [17].

Op basis van dit proefschrift kan gesteld worden dat $scCO_2$ sproeidrogen een veelbelovende techniek voor het bereiden van stabiele gedroogde eiwitformuleringen voor commerciele en onderzoeksdoeleinden. Vergelijkbaar met andere droogtechnieken

moet erop gelet worden dat de juiste procescondities en formuleringen gekozen worden (**Hoofdstuk 3,4 en 6**). Hoewel in dit proefschrift alleen eiwitten bestudeerd zijn, kan $scCO_2$ sproeidrogen ook toegepast worden op peptiden, genetisch materiaal (DNA en RNA) en vaccins. Bovendien kan $scCO_2$ sproeidrogen worden gebruikt als een techniek om een groot aantal verschillende geneesmiddelafgiftesystemen te ontwikkelen [18].

Referenties

[1]   O.C. Farokhzad, R. Langer, Impact of nanotechnology on drug delivery, ACS Nano, 3 (2009) 16-20.

[2]   A.H. Chow, H.H. Tong, P. Chattopadhyay, B.Y. Shekunov, Particle engineering for pulmonary drug delivery, Pharm Res, 24 (2007) 411-437.

[3]   M. Manzano, M. Manzano, V. Aina, C.O. Areán, F. Balas, V. Cauda, M. Colilla, M.R. Delgado, M. Vallet-Regí, Studies on MCM-41 mesoporous silica for drug delivery: Effect on particle morphology and amine functionalization, Chem Eng J, 137 (2008) 30-37.

[4]   A. Tabernero, E.M. Martín del Valle, M.A. Galán, Supercritical fluids for pharmaceutical particle engineering: Methods, basic fundamentals and modeling. Chem Eng Process, 60 (2012) 9-25.

[5]   E. Reverchon, R. Adami, G. Caputo, I. De Marco, Spherical microparticles production by supercritical antisolvent precipitation: Interpretation of results. J Supercrit Fluids, 47 (2008) 70-84.

[6]   E. Reverchon, Supercritical antisolvent precipitation of micro- and nano-particles. J Supercrit Fluids, 15 (1999) 1-21.

[7]   N. Jovanović, A. Bouchard, G.W. Hofland, G-J Witkamp, D.J. Crommelin, W. Jiskoot, Stabilization of proteins in dry powder formulations using supercritical fluid technology, Pharm Res, 21 (2004) 1955-69.

[8]   N. Jovanović, A. Bouchard, M. Sutter, M. V. Speybroeck, G. W. Hofland, G. Witkamp, D. J. A. Crommelin, W. Jiskoot, Stable sugar-based protein formulations by supercritical fluid drying, Int J Pharm, 346 (2008) 102-108.

[9]   O. Nuchuchua, H. A. Every, G. W. Hofland, W. Jiskoot, Scalable organic solvent free supercritical fluid spray drying process for producing dry protein formulations, Eur J Pharm Biopharm, 88 (2014) 919-930.

[10]   S. Kamat, G. Critchley, E.J. Beckman, A.J. Russell, Biocatalytic Synthesis of Acrylates in Organic-Solvents and Supercritical Fluids .3. Does Carbon-Dioxide Covalently Modify Enzymes?, Biotechnol Bioeng, 46 (1995) 610-620.

[11]   Z. Yu, K.P. Johnston, R.O. Williams 3rd, Spray freezing into liquid versus spray-freeze drying: influence of atomization on protein aggregation and biological activity, Eur J Pharm Sci, 27 (2006) 9-18.

[12]   S.D. Webb, S.L. Golledge, J.L. Cleland, J.F. Carpenter, T.W. Randolph, Surface adsorption of recombinant human interferon-gamma in lyophilized and spray-lyophilized formulations, J Pharm Sci, 91 (2002) 1474-1487.

[13]   A. Natalello, S.M. Doglia, Insoluble protein assemblies characterized by fourier transform infrared spectroscopy, Methods Mol Biol, 1258 (2015) 347-69.

[14]   M. Donbrow, E. Azaz, A. Pillersdorf, Autoxidation of polysorbates, J Pharm Sci, 67 (1978) 1676-81.

[15]   R.S. Kishore, A. Pappenberger, I.B. Dauphin, A. Ross, B. Buergi, A. Staempfli, H.C. Mahler, Degradation of polysorbates 20 and 80: studies on thermal autoxidation and hydrolysis, J Pharm Sci, 100 (2011) 721-31.

[16]   M. Agarkhed, C. O'Dell, M.C. Hsieh, J. Zhang, J. Goldstein, A. Srivastava, Effect of polysorbate 80 concentration on thermal and photostability of a monoclonal antibody. AAPS Pharm Sci Tech, 14 (2013) 1-9.

[17]   O. Nuchuchua, H.A. Every, W. Jiskoot, Critical processing parameters of carbon dioxide spray drying for the production of dried protein formulations: A study with myoglobin, Eur J Pharm Biopharm, 103 (2016) 200-9.

[18]   A.R. Karow, S. Bahrenburg, P. Garidel, Buffer Capacity of Biologics-From Buffer Salts to Buffering by Antibodies, Biotechnol Prog, 29 (2013) 480-492.

[19]   W. Liu, X.D. Chen, C. Selomulya, On the spray drying of uniform functional microparticles, Particuology, 22 (2015) 1-12.

CURRICULUM VITAE

Onanong Nuchuchua was born on the 28th of March 1982 in Bangkok, Thailand.

In 2004, she completed her Bachelor studies in Biochemistry with 2nd class Honors at Chulalongkorn University, Thailand. In 2007, she obtained a Master's degree in Biomedicinal Chemistry at the Faculty of Pharmaceutical Sciences, Chulalongkorn University, Thailand. After graduation, she started her scientific carrier as a research assistant at the National Nanotechnology Centre, National Science and Technology Development Agency, Thailand.

Subsequently, in 2011, she was awarded the Royal Thai Government Scholarship to perform her PhD study at the Division of Drug Delivery Technology, Leiden Academic Center for Drug Research, Leiden University, The Netherlands. The topic of her PhD project is "**Supercritical carbon dioxide spray drying for the production of stable dried protein formulations**" under the supervision of Prof. Dr. Wim Jiskoot and Dr. Hayley A. Every.

After obtaining her PhD degree, she will continue working as a researcher at the National Nanotechnology Centre, National Science and Technology Development Agency, Thailand.

LIST OF PUBLICATIONS

[1]   **O. Nuchuchua**, H.A. Every, G.W. Hofland, W. Jiskoot, Scalable organic solvent free supercritical fluid spray drying process for producing dry protein formulations, European Journal of Pharmaceutics and Biopharmaceutics, Volume 88, Issue 3, November 2014, Pages 919-930

[2]   **O. Nuchuchua**, H.A. Every, W. Jiskoot, Critical processing parameters of carbon dioxide spray drying for the production of dried protein formulations: A study with myoglobin, European Journal of Pharmaceutics and Biopharmaceutics, Volume 103, June 2016, Pages 200-209

[3]   **O. Nuchuchua**, R. Nejadnik, S.C. Goulooze, N. Jovanović Lješković, H.A. Every, W. Jiskoot, Characterization of particles for drug delivery produced by supercritical carbon dioxide technologies, 2016 (Manuscript submitted)

[4]   **O. Nuchuchua**, B. Öztürk, H.A. Every, W. Jiskoot, The combined effects of carbon dioxide-water interface and pH shift on myoglobin stability, 2016 (Manuscript in preparation)

[5]   **O. Nuchuchua**, H.A. Every, W. Jiskoot, Formulation optimization in supercritical CO_2 spray drying for production of dry protein formulations, 2016 (Manuscript in preparation)